FLEXURAL BEHAVIOR OF NSM FRP STRENGTHENED REINFORCED CONCRETE BEAMS UNDER SUSTAINED LOADING

Mohamed Abdalla Mohamed Mohamed Moawad

DOCTORAL THESIS

FLEXURAL BEHAVIOR OF NSM FRP STRENGTHENED REINFORCED CONCRETE BEAMS UNDER SUSTAINED LOADING

Mohamed Abdalla Mohamed Mohamed Moawad

2020

DOCTORAL THESIS

FLEXURAL BEHAVIOR OF NSM FRP STRENGTHENED REINFORCED CONCRETE BEAMS UNDER SUSTAINED LOADING

Mohamed Abdalla Mohamed Mohamed Moawad

2020

DOCTORAL PROGRAM IN TECHNOLOGY

Supervised by:

Dr. Lluís Torres Llinàs
University of Girona

Dr. Cristina Barris Peña
University of Girona

Dr. Marta Baena Muñoz
University of Girona

A thesis submitted for the degree of Doctor of Philosophy by the University of Girona

IN THE NAME OF ALLAH

Acknowledgment

I would like to express my gratitude to my supervisors, Dr. Lluís Torres Llinàs, Dr. Cristina Barris Peña and Dr. Marta Baena Muñoz, for the indefatigable help and for the key contributions that have allowed the development of the present thesis.

Of course, I am grateful to all members of the research group AMADE of the University of Girona for the help and nice moments that I have received from each one.

I would also like to acknowledge the support and the help from my home Department of Materials Engineering at Zagazig University.

I would also like to thank my family for the support they provided me through my entire life and in particular, I must acknowledge my parents, my wife's parents, my wife, my sons Abdullah and Abdurrahman and my daughter Fatema Azzahraa for their support and being without me for a long time throughout my stay in Girona.

Funding

The work contained in this Ph.D. thesis was conducted in the AMADE research group, Department of Mechanical Engineering and Industrial Construction, at the University of Girona Spain. The work was supported by the Spanish Government (Ministerio de Economía y Competitividad) Project Ref. BIA2013-46944-C2-2-P and by the University of Girona with the grant IFUdG2015/38.

Universitat de Girona

To whom it might concern,

Dr. Lluís Torres Llinàs, Professor at the Universitat de Girona of the Department of Enginyeria Mecànica i de la Construcció Industrial, Dr. Cristina Barris Peña, Associate Professor at the Universitat de Girona of the Department of Enginyeria Mecànica i de la Construcció Industrial, and Dr. Marta Baena Muñoz, Associate Professor at the Universitat de Girona of the Department of Enginyeria Mecànica i de la Construcció Industrial,

CERTIFY that,

The study entitled FLEXURAL BEHAVIOR OF NSM FRP STRENGTHENED REINFORCED CONCRETE BEAMS UNDER SUSTAINED LOADING has been carried out under their supervision by Mohamed Abdalla Mohamed Mohamed Moawad,

Girona, 20 April 2020,

Dr. Lluís Torres Llinàs
University of Girona

Dr. Cristina Barris Peña
University of Girona

Dr. Marta Baena Muñoz
University of Girona

List of Publications

- M. Moawad, L. Torres, C. Barris, M. Baena, M. Emara, Flexural Behavior of NSM FRP Strengthened RC Beams under Sustained Loading, in the 19th International Conference on Composite Structures (ICCS19), Porto, Portugal, 5-9 September 2016.

- M. Moawad, L. Torres, C. Barris, M. Baena, M. Emara, R. Perera, Time-Dependent Deformations of NSM CFRP Strengthened RC Beams, in the 7th International Conference on Structures (ACHE), A Coruña, Spain, 20-22 June 2017.

- M. Moawad, L. Torres, C. Barris, M. Baena, M. Emara, R. Perera, Sustained Loading Effects on NSM Strengthened RC Beams with Different CFRP Ratios, in the 8th International Conference on Advanced Composites in Construction (ACIC), Sheffield, UK, 5-7 September 2017.

List of Abbreviations

Abbreviation	Description
a	Crack length
A_f	Area of carbon fiber reinforced polymer
AFRP	Aramid fiber reinforced polymer
a_{max}	Maximum crack length
a_{mean}	Mean crack length
a_{min}	Minimum crack length
A_s	The tension steel reinforcement area
$A_{s'}$	Compression steel reinforcement area
a_{SD}	Standard deviation of crack length
CC	Concrete crushing
CFRP	Carbon fiber reinforced polymer
E_a	Elastic modulus of adhesive material
$E_{a,\varepsilon=0.15\%}$	Secant modulus of adhesive material at tensile strain of 15%
EB	Externally-bonded
EBR	Externally bonded reinforcement
E_c	Concrete modulus of elasticity
ECs	Cover concrete separation at CFRP strip end
E_f	Elastic modulus of CFRP strip
E_s	Elastic modulus of the steel bar
E_u	The area under load-deflection curve up to ultimate load
E_y	The area under load-deflection curve up to yield point
$f_{a.u}$	Ultimate tensile strength of adhesive material
f_c	Concrete strength
f_{ck}	Characteristic compressive strength
f_{ct}	Concrete tensile strength
$f_{ct,sp}$	Splitting tensile strength of concrete
$f_{f.u}$	Ultimate tensile strength of CFRP strip
FR	Rupture of CFRP strip
FRP	Fiber reinforced polymers
f_{us}	Ultimate strength of the steel bar
f_{ys}	Yield strength of the steel bar
GFRP	Glass fiber reinforced polymer
ICs	Intermediate flexural crack induced concrete cover separation
ID	Identification
L	Length of the concrete cylinder
L_b	Bonded length

M_D/M_{cr}	The ratio between the applied moment at service design load to the cracking moment
M_s/M_{cr}	The ratio between the applied moment at sustained load to the cracking moment
NSM	Near surface mounted
Ø	Diameter of the concrete cylinder
P	The applied load
P_c	The constant load of captured crack pattern
P_{cr}	Cracking load of beam
P_D	Service design load
P_s	Sustained load
P_u	Load carrying capacity of beam
P_y	Yield load of beam
RC	Reinforced concrete
s	Crack spacing
$S1$	End slip of CFRP strip at one of its two ends
$S1_u$	End slip of CFRP strip at one of its two ends at ultimate load
$S1_y$	End slip of CFRP strip at one of its two ends at yield load
$S2$	End slip of CFRP strip at the other end
$S2_u$	End slip of CFRP strip at the other end at ultimate load
$S2_y$	End slip of CFRP strip at the other end at yield load
Sf	Strain gage for CFRP strips
SG	Strain gage for steel and concrete
s_{max}	Maximum crack spacing
s_{mean}	Mean crack spacing
s_{min}	Minimum crack spacing
s_{SD}	Standard deviation of crack spacing
t	Loading time
T_g	Glass transition temperature
t_o	Concrete cylinder age at the start of loading
TR	Displacement transducer
δ	Mid-span deflection
δ_{cr}	Cracking deflection of beam
δ_D	Deflection of beam at its service design load
δ_i	Instantaneous deflection due to sustained loading of beam
δ_{max}	Maximum deflection of beam
δ_o	Initial deflection of beam
δ_r	Permanent deflection of beam after removing the sustained load
$\delta_{r,o}$	Permanent deflection of beam after two loading/unloading cycles
δ_T	Total deflection of beam with time
$\delta_{T,e}$	Total deflection of beam at the end of the loading period

δ_{td}	Time dependent deflection of beam
δ_u	Deflection of beam at the ultimate load
δ_y	Yield deflection of beam
ε_1	Concrete compressive strain of $50x10^{-6}$
ε_2	The corresponding strain to 40% of the concrete strength
$\varepsilon_{a,u}$	Ultimate tensile strain of adhesive material
ε_c	Concrete strain at mid-span section of beam
$\varepsilon_c(t, t_o)$	Total concrete strain
$\varepsilon_{c, cr}$	Concrete strain at cracking load
$\varepsilon_{c, D}$	Concrete strain of beam at its service design load
$\varepsilon_{c, r,o}$	Permanent concrete strain of beam after two loading/unloading cycles
$\varepsilon_{c, u}$	Concrete strain at ultimate load
$\varepsilon_{c, y}$	Concrete strain at yield load
$\varepsilon_{ci}(t_o)$	Instantaneous concrete strain
$\varepsilon_{cs}(t, t_o)$	Concrete shrinkage strain
ε_f	Tensile strain of CFRP
$\varepsilon_{f,u}$	Ultimate tensile strain of CFRP strip
ε_{f1}	Tensile strain of CFRP at mid-span section of beam
$\varepsilon_{f1, cr}$	Tensile strain of CFRP at cracking load
$\varepsilon_{f1, D}$	CFRP tensile strain of beam at its service design load
$\varepsilon_{f1, r,o}$	Permanent CFRP tensile strain of beam after two loading/unloading cycles
$\varepsilon_{f1, u}$	Tensile strain of CFRP at ultimate load
$\varepsilon_{f1, y}$	Tensile strain of CFRP at yield load
$\varepsilon_{free}(t)$	Average free strain of the aged resin specimens
$\varepsilon_r(t)$	Total strain of resin
$\varepsilon_{r,a}$	Strain of resin after removing creep pressure
$\varepsilon_{r,i}$	Instantaneous strain of resin
ε_s	Tension steel strain at mid-span section of beam
$\varepsilon_{s, cr}$	Tension steel strain at cracking load
$\varepsilon_{s, D}$	Tension steel strain of beam at its service design load
$\varepsilon_{s, r,o}$	Permanent tension steel strain of beam after two loading/unloading cycles
$\varepsilon_{s, u}$	Tension steel strain at ultimate load
$\varepsilon_{s, y}$	Tension steel strain at yield load
μ_D	Displacement ductility index
μ_E	Deformability factor
ρ	Tension steel ratio
ρ'	Compression steel ratio
σ_1	The concrete compressive stress corresponding to concrete strain of $50x10^{-6}$

σ_2	The concrete compressive stress equal 40% of the concrete strength
σ_{co}	Instantaneous maximum concrete compressive stress at the top of mid-span section
$\varphi(t, t_o)$	Concrete creep coefficient
$\varphi_r(t)$	Creep coefficient of resin
ω	Crack width
ω_c	Crack width at constant load
ω_D	Crack width of beam at its service design load
$\omega_{r,o}$	Permanent crack width of beam after two loading/unloading cycles
ω_u	Crack width at ultimate load
ω_y	Crack width at yield load

Contents

List of Figures

List of Tables

Abstract

Fiber Reinforced Polymers (FRP) are being used extensively all over the world, either for reinforcing new concrete structures or for the rehabilitation and strengthening of existing ones. The most common techniques for strengthening Reinforced Concrete (RC) structures using FRP materials are those usually known as Externally Bonded Reinforcement (EBR) and Near Surface Mounted (NSM) reinforcement. Recently, the interest in the NSM technique has increased due to several potential advantages, such as: less prone to debonding from the concrete substrate, does not require any surface preparation work except grooving, being the FRP reinforcements better protected by the concrete cover, and the aesthetics of a strengthened structure with NSM reinforcement is virtually unchanged. Although FRP-strengthening technology has attracted an increasing amount of research, there is still uncertainty about its long-term performance under the effect of sustained loading, which may restrict a broader application.

The main objective of this work is to study the long-term and residual flexural strength of NSM strengthened RC beams with Carbon FRP (CFRP) strips when subjected to sustained loading. To this end, an extensive experimental program was carried out to investigate the flexural behavior of RC members strengthened with NSM FRP reinforcement under long-term sustained loading. The studied parameters were CFRP area, tension steel reinforcement ratio, concrete type, sustained load level, ratio between compression and tension steel ratio, and loading history.

This work involved twenty-eight RC beams divided into two series, A and B, with two concrete batches of different compressive strength. In each series, some of the beams were strengthened with CFRP strips using the NSM strengthening technique and the others were un-strengthened. Series A was divided into two groups, A1 and A2, while series B was divided into three groups, B1, B2, and B3. The beams of the first group in each series, A1 and B1, were tested at age of 55 days to determine the short-term flexural behavior of un-strengthened and strengthened beams. Other groups, A2, B2, and B3, were subjected to long term test with different sequences. Each sequence

contained some of three stages. The first stage is a short term test for two loading/unloading cycles up to service design load to ensure that the beams are cracked under the service conditions, before sustained loading. The second stage is the application of sustained loading up to age of 345 days with a sustained load designed to obtain instantaneous maximum concrete compressive stress at the top of mid-span section lower than 40% of the concrete strength. The third stage is a short-term test under monotonic loading up to failure, after removing the sustained loads at age of 365 days to study the effect of the sustained loading on the residual flexural strength.

The experimental results are reported and discussed. It was found that the behavior of the pre-cracked beam was identical to that of virgin beam after the pre-cracking load and up to failure. Increasing the CFRP area increased the yield load and the load carrying capacity, magnified the slips of CFRP strip at its both ends and decreased the ductility and crack width of strengthened beams. The RC beam NSM strengthened with three CFRP strips of 2.8 mm thickness each achieved an increase of 79% and 129% in the yielding load and the load carrying capacity, respectively, and a decrease of 61% and of 68% in the maximum deflection and the ductility, respectively. Increasing of CFRP area enhanced the efficiency of NSM strengthening to control initial deflection. Increasing of CFRP area also aided the NSM strengthened beam to retain more deflection from its time dependent deflection. This happened in the virgin and preloaded beams. The preloading of the NSM strengthened beam with CFRP strips up to its design service load led to decrease its time dependent deflection under sustained loading compared to the un-strengthened beam. This was at the odds of the beams sustained loaded directly without preloading. The presence of the compression steel magnified the benefit of NSM CFRP strengthening in the reduction of initial deflections. The aged un-strengthened and strengthened beams showed decreases in the load carrying capacity and the maximum deflection compared to their corresponding young beams, despite the similarity of their failure modes. The sustained loading increased the tensile stresses in the concrete cover at the end of CFRP strip accelerating its separation from the beams. Therefore, the sustained loading did not change the load carrying capacity and the maximum deflection of either the un-strengthened beam and NSM strengthened beam failed due to concrete crushing or CFRP rupture.

Resum

Els materials compostos a base de polímers reforçats amb fibres (FRP, de l'anglès Fiber Reinforced Polymer) són cada vegada més emprats tant per a l'armat de noves estructures de formigó, com per al reforç d'estructures existents. Les tècniques més usuals per al reforç d'estructures de formigó armat (FA) mitjançant FRP consisteixen en la seva utilització com a reforç extern (EB, de l'anglès Externally Bonded) o en l'aplicació del material FRP inserit en el recobriment del formigó (NSM, de l'anglès Near-Surface Mounted). En els últims anys ha augmentat l'interès en la tècnica NSM a causa de diversos avantatges potencials com poden ser la menor tendència a la fallada per adherència entre laminat i formigó, la no necessitat de preparació de la superfície, amb excepció de la realització de la ranura, la millor protecció del material pel recobriment de formigó, i la pràctica no alteració estètica de l'estructura reforçada. Encara que el reforç amb FRP ha estat objecte d'un esforç creixent en recerca, queden encara aspectes per clarificar sobre el seu comportament a llarg termini sota càrregues mantingudes que poden restringir una aplicació més àmplia.

El principal objectiu d'aquest treball és l'estudi de la resistència a llarg termini i la resistència residual de bigues de FA reforçades amb FRP a base de fibres de carboni (CFRP, de l'anglès Carbon Fiber Reinforced Polymer) sotmeses a càrregues mantingudes. Amb aquesta finalitat s'ha portat a terme un ampli programa experimental per investigar el comportament a flexió d'elements de FA reforçats amb la tècnica NSM FRP sotmesos a càrrega mantinguda a llarg termini. Els paràmetres de l'estudi han estat l'àrea de CFRP, la quantia d'armadura d'acer, el tipus de formigó, el nivell de càrrega mantinguda, la proporció entre àrea d'armadura comprimida i traccionada i la història de càrrega.

En el treball s'han assajat i analitzat vint-i-vuit bigues de FA agrupades en dues sèries, A i B, corresponents a dos lots de formigó amb diferent resistència a compressió. A cada sèrie, algunes de les bigues van ser reforçades amb laminats de CFRP mitjançant la tècnica NSM FRP, mentre que altres espècimens es van mantenir sense reforçar. La sèrie A es va dividir en dos grups, A1 i A2, i la sèrie B en tres, B1, B2 i B3. Les bigues del primer grup de cada sèrie, A1 i B1, es van assajar a l'edat de 55 dies per tal d'establir el comportament a flexió amb càrrega instantània tant de les bigues sense reforçar

com de les reforçades. Els altres grups, A2, B2, i B3, es van assajar a llarg termini amb diferents seqüències, contenint alguna de les següents etapes o fases. La primera fase va consistir en un assaig instantani amb dos cicles de càrrega/descàrrega fins a la càrrega de servei, abans de l'aplicació de la càrrega mantinguda. La segona fase va consistir en l'aplicació de càrrega mantinguda fins a l'edat de 345 dies, amb un valor de carga calculat per a obtenir una tensió màxima instantània a la fibra superior de les bigues menor que el 40% de la resistència del formigó. La tercera fase va consistir en un assaig instantani amb càrrega monotònica fins a la ruptura a l'edat de 365 dies, un cop retirada la càrrega mantinguda, amb la finalitat d'estudiar l'efecte de l'acció de la càrrega mantinguda en la resistència residual a flexió.

En el treball s'han reportat i discutit els resultats experimentals. S'ha vist que el comportament de la biga prefissurada va ser idèntic al de la biga original després de la prefissuració i fins a la ruptura. L'increment de l'àrea de CFRP va produir un augment de la càrrega de plastificació de l'acer i de la capacitat portant, va incrementar el lliscament dels laminats de CFRP en ambdós extrems i va disminuir la ductilitat i amplada de fissura de les bigues reforçades. Les bigues reforçades amb tres laminats de CFRP de 2,8 mm de gruix van arribar a increments del 79 % i del 129 % a la càrrega de plastificació de l'acer i a la capacitat portant, respectivament, i disminucions del 61 % i del 68 % a la fletxa màxima i a la ductilitat, respectivament. L'increment de l'àrea de CFRP va millorar l'eficiència del reforç NSM en el control de la fletxa inicial. Igualment, va contribuir a la retenció de part de la fletxa a llarg termini en les bigues reforçades, tan en les bigues amb precàrrega com en les originals. La precàrrega de les bigues reforçades amb NSM CFRP fins a la càrrega de servei va produir una disminució a la fletxa diferida amb càrrega mantinguda en comparació amb les bigues no reforçades. Aquest comportament no es correspon amb el de les bigues sense precàrrega prèvia. La presència d'armadura de compressió va incrementar l'efecte del reforç amb NSM FRP en la reducció de les fletxes inicials. Les bigues no reforçades guardades per a ser assajades a edats en correspondència amb el final dels assajos a llarg termini van mostrar disminucions de la capacitat portant i de la fletxa màxima en comparació amb les corresponents bigues assajades a edats més joves, malgrat que van mantenir modes de fallada similars. La càrrega mantinguda va incrementar les tensions de tracció al formigó del recobriment a l'extrem dels laminats de CFRP afavorint la seva separació de la biga. La càrrega mantinguda no va canviar la capacitat

portant i la fletxa màxima tant de les bigues no reforçades com de les reforçades amb NSM que van fallar per compressió del formigó o per ruptura del CFRP.

Resumen

Los materiales compuestos a base de polímeros reforzados con fibras (FRP, del inglés Fiber Reinforced Polymer) están siendo cada vez más usados tanto para el armado de nuevas estructuras de hormigón, como para el refuerzo de estructuras existentes. Las técnicas más comunes para el refuerzo de estructuras de hormigón armado (HA) mediante el empleo de los FRP consisten en su uso como refuerzo externo (EB, del inglés Externally Bonded) o en la aplicación del material FRP insertado en el recubrimiento del hormigón (NSM, del inglés Near-Surface Mounted). En los últimos años, el interés en la técnica NSM se ha visto incrementado debido a diversas ventajas potenciales como pueden ser la menor tendencia al despegue del hormigón, la ausencia de preparación de la superficie, con excepción de la realización de la ranura, la mejor protección del material por el recubrimiento de hormigón, y la práctica no alteración estética de la estructura reforzada. Aun cuando el refuerzo con los FRP ha sido objeto de un creciente esfuerzo en investigación, quedan todavía aspectos por clarificar acerca de su comportamiento a largo plazo bajo cargas mantenidas que pueden ser obstáculo para una aplicación más amplia.

El principal objetivo de este trabajo es el estudio de la resistencia a largo plazo y la resistencia residual de vigas de HA reforzadas con FRP a base de fibras de carbono (CFRP, del inglés Carbon Fiber Reinforced Polymer) sometidas a cargas mantenidas. Para ello se ha llevado a cabo un amplio programa experimental para investigar el comportamiento a flexión de elementos de HA reforzados con la técnica NSM FRP sometidos a carga mantenida a largo plazo. Los parámetros del estudio han sido el área de CFRP, la cuantía de armadura de acero, el tipo de hormigón, el nivel de carga mantenida, la proporción entre área de armadura comprimida y traccionada y la historia de carga.

En el trabajo se han ensayado y analizado veintiocho vigas de HA agrupadas en dos series, A y B, correspondientes a dos lotes de hormigón con diferente resistencia a compresión. En cada serie, algunas de las vigas fueron reforzadas con laminados de CFRP mediante la técnica NSM FRP, mientras que otros especímenes se mantuvieron sin reforzar. La serie A se dividió en dos grupos, A1 y A2, y la serie B en tres, B1, B2 i B3. Las vigas del primer grupo de cada serie, A1 y B1, se ensayaron a la edad de 55 días

para determinar el comportamiento a flexión con carga instantánea ya sea de las vigas sin reforzar como de las reforzadas. Los otros grupos, A2, B2, y B3, se ensayaron a largo plazo con diferentes secuencias, conteniendo alguna de las siguientes etapas o fases. La primera fase consistió en un ensayo instantáneo con dos ciclos de carga/descarga hasta la carga de servicio, antes de la aplicación de la carga mantenida. La segunda fase consistió en la aplicación de carga mantenida hasta la edad de 345 días, con un valor de carga calculado para obtener una tensión instantánea máxima en la fibra superior de las vigas menor que el 40% de la resistencia del hormigón. La tercera fase consistió en un ensayo instantáneo con carga monotónica hasta rotura a la edad de 365 días, una vez retirada la carga mantenida, con objeto de estudiar el efecto de la acción de la carga mantenida en la resistencia residual a flexión.

En el trabajo se han reportado y discutido los resultados experimentales. Se ha visto que el comportamiento de la viga prefisurada fue idéntico que el de la viga original después de la prefisuración y hasta la carga de rotura. El incremento del área de CFRP produjo un aumento de la carga de plastificación del acero y de la capacidad portante, incrementó el deslizamiento de los laminados de CFRP en ambos extremos y disminuyó la ductilidad y ancho de fisura de las vigas reforzadas. Las vigas reforzadas con tres laminados de CFRP de 2,8 mm de grosor alcanzaron incrementos del 79 % y del 129 % en la carga de plastificación del acero y en la capacidad portante, respectivamente, y disminuciones del 61 % y del 68 % en la flecha máxima y en la ductilidad, respectivamente. El incremento del área de CFRP mejoró la eficiencia del refuerzo NSM en el control de la flecha inicial. Asimismo, contribuyó a la retención de parte de la flecha a largo plazo en las vigas reforzadas, tanto en las vigas con precarga como en las originales. La precarga de las vigas reforzadas con NSM CFRP hasta la carga de servicio produjo una disminución en la flecha diferida con carga mantenida en comparación con las vigas no reforzadas. Este comportamiento no se corresponde con el de las vigas sin precarga previa. La presencia de armadura de compresión incrementó el efecto del refuerzo con NSM FRP en la reducción de las flechas iniciales. Las vigas no reforzadas guardadas para ser ensayadas a edades en correspondencia con el final de los ensayos a largo plazo mostraron disminuciones en la capacidad portante y en la flecha máxima en comparación con las correspondientes vigas ensayadas a las edades tempranas, aun cuando mantuvieron modos de fallo similares. La carga mantenida incrementó las tensiones de tracción en el hormigón del

recubrimiento en el extremo de los laminados de CFRP favoreciendo su separación de la viga. La carga mantenida no cambió la capacidad portante y la flecha máxima tanto de las vigas no reforzadas como de las reforzadas con NSM que fallaron por aplastamiento del hormigón o rotura del CFRP.

CHAPTER 1 INTRODUCTION

The economical effort in rehabilitation and maintenance will be increased in the next years, as a consequence of the increasing trend towards rehabilitation and strengthening of existing civil infrastructure and buildings in front of the budget addressed to new construction. Therefore, the strengthening of concrete structures during their service life is one of the essential difficulties that will have to tackle structural engineers globally. These concrete structures possibly will be insufficient as a result of the change of use, the increase of the applied loads, errors in design, corrosion, and environmental damage [1–3].

Reinforced Concrete (RC) structures can be strengthened/rehabilitated using different solution methods, such as steel or concrete jackets, external post-tensioning, externally-bonded (EB) steel plates, replacement of degraded members or the addition of new extra members. Although these traditional repairing methods can improve the strength, capacity and stiffness of deficient concrete structures, they may also increase the dead load of repaired structures and are time consuming. Thus, to repair or strengthen existing deficient structural concrete members, there is a necessity to find alternative materials or methods [4].

As an appropriate alternative, Fiber Reinforced Polymers (FRP) are being used extensively all over the world, either for reinforcing new concrete structures or for the rehabilitation and strengthening of existing ones [5–9]. FRP composites have lightweight, high tensile strength, resistance to corrosion, low thermal conductivity, remaining fatigue strength, availability in various forms, ease of installation, reduced mechanical fixing, reduced construction period, lower installation cost and reduced maintenance cost [10–12]. The most common techniques for strengthening RC structures using FRP materials are those usually known as Externally Bonded Reinforcement (EBR) and Near Surface Mounted (NSM) reinforcement [6,13–21]. Recently, researchers have shown an increased interest in the NSM technique due to several potential advantages, such as: less prone to debonding from the concrete substrate, does not require any surface preparation work except grooving, being the FRP reinforcements better protected by the concrete cover. This technique is then

suitable to strengthen the negative moment regions of beams and slabs, and the aesthetics of a strengthened structure with NSM reinforcement is virtually unchanged [15,22].

Although FRP-strengthening technology has been implemented in a large number of practical projects worldwide and has attracted an increasing amount of research, the existing uncertainty about its long-term performance under the effect of sustained loading may still restrict a broader application. The creep of the concrete member and potential creep of the strengthening system (mainly the adhesive, whose viscoelastic behavior is generally ignored) may affect bond and load carrying capacity over time, and cause deformation as well as redistribution of stresses. Understanding and clarifying these aspects, which highlight various modeling challenges, is required for an improved design of FRP strengthened members. Long-term effects and sustained loads, creep and shrinkage of concrete and creep of resin and FRP are expected to have an important influence on the flexural behavior of RC strengthened beams with NSM FRP reinforcement, causing larger deflections, cracks width and distance, end slips, redistributions of stresses and changes in mode of failure or failure load [23–26]. To this end, effects of time-dependent properties of materials (concrete, adhesive and FRP) on the behavior of the strengthened beam need to be assessed with the final aim of contributing to improve the design of FRP RC strengthened structures.

1.1 Objectives

The effect of sustained loading on the NSM FRP strengthened RC structures during the life-span of the structure is observed as an area of incomplete knowledge. Understanding and clarifying how the structure is affected by this type of external actions is a main requirement for an improved design of FRP strengthened members. The main objective of this work is to study the long-term and residual flexural behavior of NSM strengthened RC beams with carbon FRP (CFRP) strips when subjected to sustained loading, in terms of loads, deflections, end slips of CFRP strips, cracking, failure modes and strains of constitutive materials (steel, concrete and CFRP strips). The area of CFRP, steel reinforcement ratios, loading history, concrete type and load level will be the main parameters of the study.

In order to achieve this aim, the following tasks have been undertaken:

1- Review the research carried out on both short-term and long-term flexural behavior of NSM FRP strengthened RC beams to gain a better understanding of the behavior and the role of the different variables involved in that behavior.
2- Experimental investigation of the short-term flexural behavior of NSM CFRP strengthened RC beams including different CFRP areas, tensile reinforcement ratios and concrete types.
3- Experimental investigation of the long-term flexural behavior of NSM CFRP strengthened RC beams under sustained loading including different CFRP areas, tensile and compression reinforcement ratios, loading histories, concrete types and load levels.
4- Experimental investigation of the residual flexural behavior of NSM CFRP strengthened RC beams including different CFRP areas, tensile and compression reinforcement ratios, loading histories, concrete types and load levels.

1.2 Thesis layout

In order to achieve the aim of the current study, the thesis is structured as follows:

In CHAPTER 2, a survey of the previous literature on the strengthening techniques used for repairing and strengthening of RC structural elements is presented. First, an overview on FRP composite materials presenting manufacturing and products of FRP, mechanical properties of FRP materials and adhesives used with FRP in strengthening applications. Then, the relevant aspects of EB and NSM strengthening techniques are presented. A detailed review of bond between NSM FRP and concrete is presented after including failure modes of the bond between NSM FRP-concrete and parameters affecting the bond property. Then, a survey on the existing work on flexural behavior of NSM FRP strengthened RC members is presented including modes of failure. After that, creep of materials used in the NSM system (concrete, FRP, adhesive) is presented in detail. The effect of sustained loading on bond between NSM FRP-concrete is explained including a survey on its existing work. Finally, a detailed review of long-

term behavior of FRP strengthened RC members is presented including the existing work of EB and NSM FRP strengthened RC members under sustained loading.

In CHAPTER 3, details of the experimental program conducted in this research are presented. First, the test matrix of the specimens is provided followed by a fabrication description of the beams' specimens involving the RC beams preparation and the application of NSM strengthening technique. The instrumentation and test setup of short and long-term tests are after described. At the end, the materials characterization procedure, results and discussions are illustrated in detail.

In CHAPTER 4, the significant experimental results of short-term flexural tests and sustained loading of all beams are presented and discussed in detail.

Finally, the thesis is concluded in CHAPTER 5 in addition to some suggestions for future work.

CHAPTER 2 LITERATURE REVIEW

2.1 Introduction

This chapter presents a survey of the previous literature on the strengthening techniques used for repairing and strengthening of reinforced concrete (RC) structural elements. The relevant aspects of the externally bonded (EB) and near surface mounted (NSM) strengthening techniques are presented. An overview on FRP composite materials is carried out, presenting manufacturing and FRP products, mechanical properties of FRP materials and adhesives used with FRP in strengthening applications.

A detailed review of bond between NSM FRP and concrete is presented including failure modes of the bond among NSM FRP-concrete and parameters affecting the bond property. A survey on the existing work on flexural behavior of NSM FRP strengthened RC members is presented after including the observed modes of failure. Then, creep of materials used in NSM system (concrete, FRP, adhesive) is presented in detail. The effect of sustained loading on bond among NSM FRP-concrete is after detailed, including a survey on its existing work. Finally, a detailed review of long-term behavior of FRP strengthened RC members is presented including the existing work of EB and NSM FRP strengthened RC members under sustained loading.

2.2 Fiber Reinforced Polymers (FRP) Materials

The use of the composite materials presents several advantages, such as the easier and faster installation, and the smaller weight and higher durability than conventional steel reinforcement. The FRP is the most widely composite material used in huge variety of applications in structural engineering and construction applications such as FRP structures, FRP reinforced concrete, and repair and rehabilitation of structures (see some examples in Figure 2.1).

FRP consists of different types of fibers (carbon, glass, aramid and basalt) embedded in a polymer matrix (epoxy, vinylester, polyester) [27]. However a variety of products can be used as fibers, as for example fibers from polyethylene terephthalate (PET) bottles, which were used to increase the ductility of the concrete [28,29]. Other

researches were performed to assess the behavior of concrete specimens reinforced with rheoplastic mortars [30].

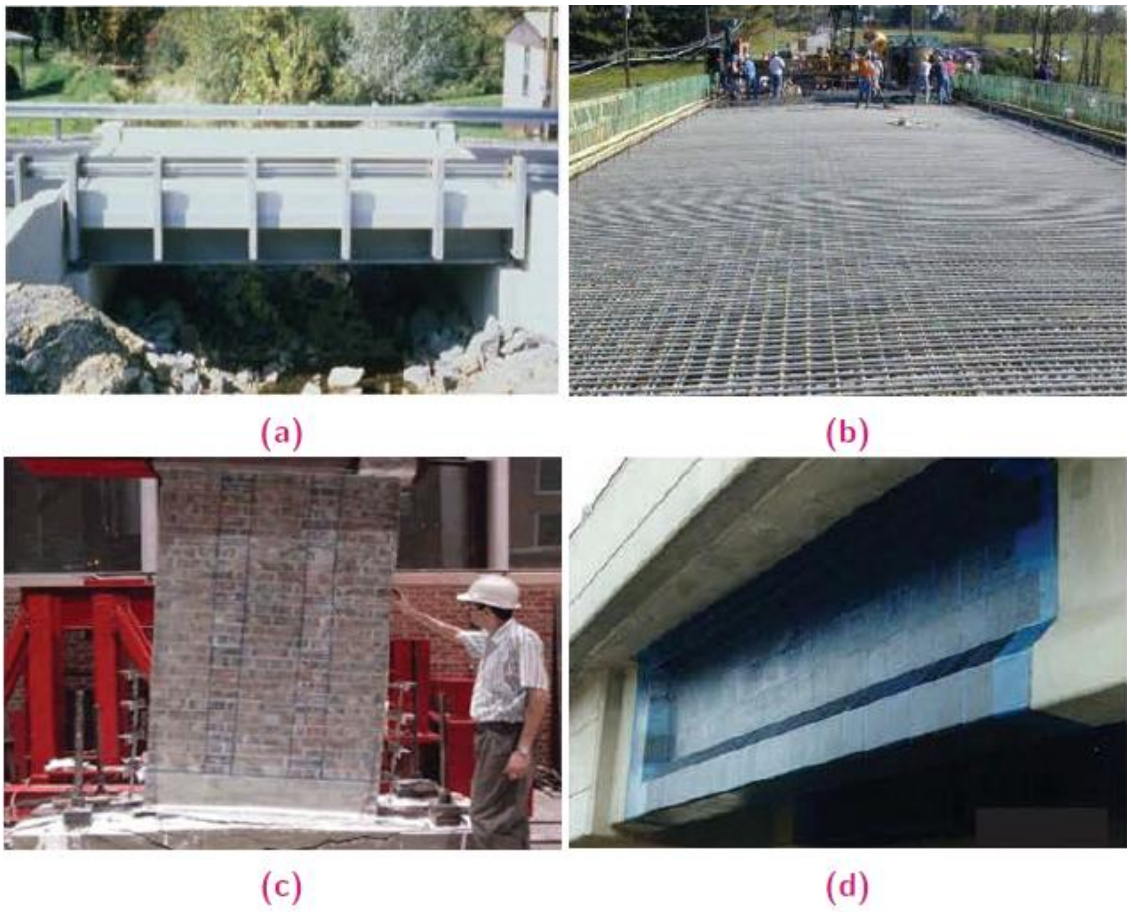

Figure 2.1 Applications of FRPs in Civil Engineering (a) A short-span FRP road bridge, (b) GFRP reinforcing bars placed in a concrete bridge deck, (c) Strengthening of clay brick masonry wall with EB GFRP sheets, and (d) Strengthening of RC bridge girder with CFRP sheets [11].

Unlike steel bars, the tensile strength of FRP bars cannot be considered constant and depends on the cross-sectional area. When a FRP bar is pulled in tension through the surface, a differential movement between the core and the surface fibers may occur and results in a non-uniform distribution of normal stresses through the cross section of the bar [31]. FRP bars are also manufactured with several surface treatments that affect greatly their bond behavior when used as NSM reinforcement [32]. Figure 2.2 shows surface treatment of some available FRP bars.

2.2.1 Manufacturing and products of FRP composites

Among a wide variety of techniques by which FRP components can be manufactured, three of them are of immediate interest to the structural engineering: (i) pultrusion,

which is used for manufacturing FRP composites with uniform cross-sectional shape such as FRP bars, rods, tendons, plates, and structural sections, (ii) wet lay-up, which is often used in structural rehabilitation applications where FRP sheets or fabrics are bonded to the exterior of RC, steel, aluminum, or timber members, and (iii) filament winding, which is an automated process in which raw fibers are drawn off spools, through a resin bath, and wound onto a rotating mandrel [11].

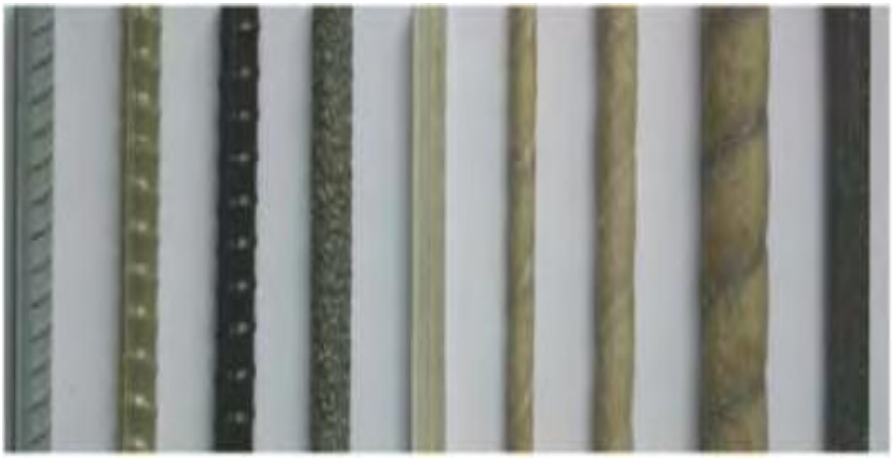

Figure 2.2 Surface treatments of some available FRP bars [27].

In FRP composites, the fibers may be placed in one direction (unidirectional) or may be woven or bonded in many directions (bi or multi-directional). Unidirectional composites are commonly employed for strengthening purposes. FRP composites can be produced in different shapes such as rebars, strips/laminates, plates, and profiles, as shown in Figure 2.3 [33].

FRP bars are mainly used either as internal reinforcement for RC structures or as NSM reinforcement for strengthening applications. A wide range of FRP bars is available in the market having several classifications based on different features such as type of fiber, cross sectional shape, surface texture and surface treatment. On the other hand, both FRP sheets and strips/laminates are mainly used for strengthening and rehabilitation of existing structures. The sheets are generally supplied in form of rolls as shown in Figure 2.3b. In the case of laminates and strips, the presence of the polymeric matrix provides stiffness to them (Figure 2.3a). Usually, the strips have thicknesses of about 1.0-1.5 mm, whereas the thickness of the sheets is about 10 times smaller. The advantages of the sheets are their high versatility and portability, while

the main drawback is that it is difficult to determine a priori the amount of epoxy required to be applied on the reinforcement.

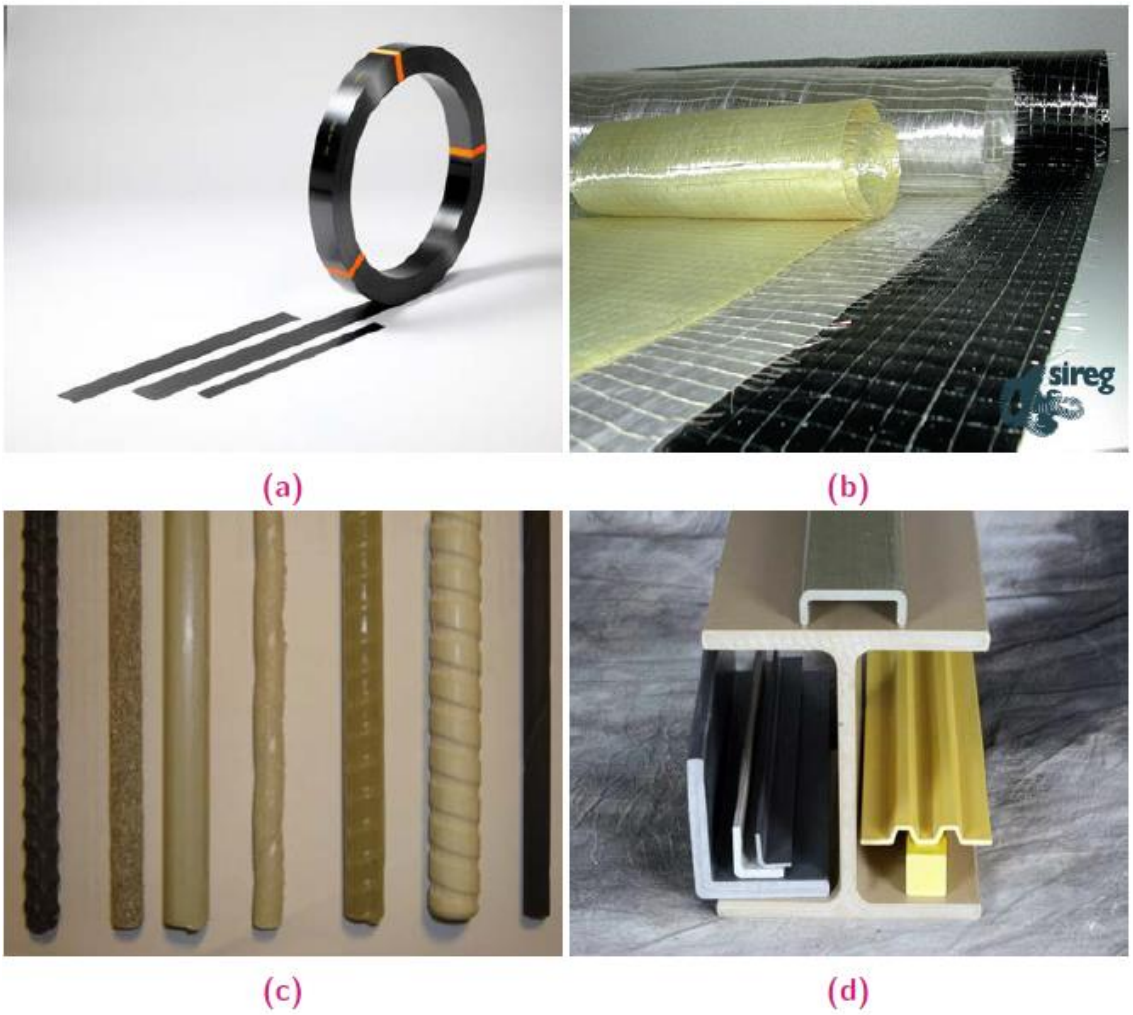

Figure 2.3 Different shapes of FRP composites; (a) Strips/laminates, (b) Sheets, (c) Bars and (d) Profiles [33].

Among various FRP shapes and cross sections available, strips (jointly with bars) are the most usual reinforcement shape used for NSM reinforcement systems, since they must be placed into a relatively narrow groove in the concrete cover. FRP strips are least prone to debonding from the concrete substrate [34]. Besides, the use of narrow strips maximizes the surface area to sectional area ratio for a given volume and thus minimizes the risk of debonding [15]. In case of using FRP strips, the normal stresses accompanying the tangential stresses in the adhesive act against both sides of the strip into the concrete substrate, thus effectively confining the strip and improving bond performance. On the contrary, when round FRP bars are used, the normal stresses act

outward in all directions, eventually causing the epoxy cover to split when the tensile strength of the adhesive is reached [35–37]. Higher local bond strength has been provided by NSM reinforcement with FRP strips compared to that provided by both NSM reinforcement with FRP rods and EB systems [37,38].

2.2.2 Mechanical properties of FRP materials

The modulus of elasticity of FRP commercial products is generally lower than that of steel and remains practically constant up to the failure point (elastic brittle behavior) unlike steel bars, for which a ductile behavior is expected and therefore considered in design codes. Due to the lower values of modulus of elasticity, deformations expected in FRP reinforced concrete structures are larger than that of steel reinforced concrete structures. These two differences in mechanical properties will affect bond behavior and therefore it is important to have them into consideration when developing design codes. Glass fiber reinforced polymer (GFRP) bars (having the lowest value of modulus of elasticity) are cheaper than the other types of FRP bars [39].

The tensile strength of FRP bars is higher than that of steel bars. For example, the tensile strength of GFRP bars can be more than twice the tensile strength of steel bars, whereas carbon fiber reinforced polymer (CFRP) and aramid fiber reinforced polymer (AFRP) bars can develop more than threefold, depending on the nature of fibers and matrix. A comparison of the tensile properties of FRP and steel bars is shown in Table 2.1 [39] and Figure 2.4 [40].

Table 2.1 Mechanical properties of FRP and steel materials [39].

FRP types	GFRP	CFRP	AFRP	Steel
Fiber content, weight%	50-80	65-75	60-70	-
Density, kg/m^3	1600-2000	1600-1900	1050-1250	7850
Tensile modulus, GPa	25-55	120-250	40-125	200
Tensile strength, MPa	400-1800	1200-2250	1000-1800	400

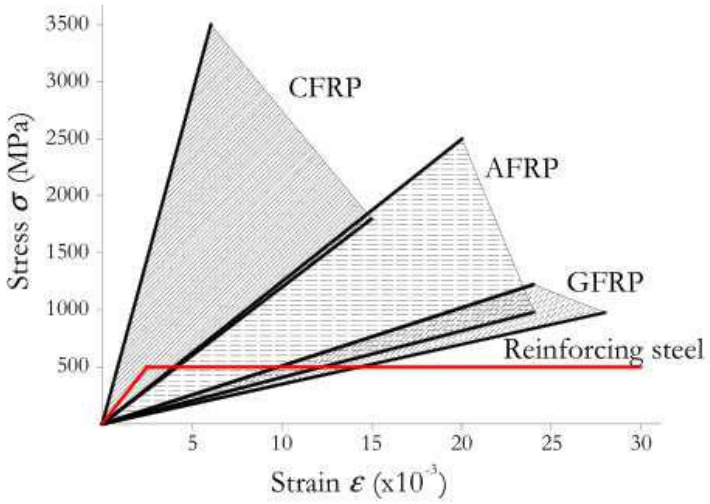

Figure 2.4 A comparison of the tensile properties of FRP and steel bars [40].

2.2.3 Adhesives used with FRP in strengthening applications

Adhesives play an important role for most industries, for both structural and nonstructural use. They are responsible for holding materials together and provide the following general advantages [41]:

- Increased speed of production
- Wider selection of materials combinations to suit production cost
- Local stress concentrations can be avoided
- Improved fatigue resistance when compared to welded structures

Five theories to describe mechanisms of adhesion are available: (i) Mechanical adhesion theory in which surfaces are held together by mechanical interlocking as a result of the penetration of adhesives into pores, cavities, voids and other surface irregularities on the surface of the substrate; (ii) Electrostatic adhesion theory in which the adhesion takes place due to electrostatic effects between the adhesive and the adherent; (iii) Diffusion adhesion theory in which the adhesion is developed through the interdiffusion of molecules in between the adhesive and the adherent (the molecules of both materials are mobile and soluble in each other); (iv) Wetting adhesion theory (also known as dispersive adhesion) which proposes that adhesion results from molecular contact between two materials and the surface forces that develop through the attraction between molecules of different charge (the Van der Waals forces) and (v) Chemical adhesion theory in which the adhesion is attributed to the formation of an adhesion bond to surface chemical forces. Hydrogen, covalent, and

ionic bonds formed between the adhesive and the adherents are stronger than the dispersion attractive forces [42,43].

Although a bonded joint is preferably loaded in shear, the adhesive layer can be subjected to various forces, based on the bonded joint design, such as tension, compression, shear, cleavage and peel (Figure 2.5) [42].

Structural adhesives are a common type of adhesives that are used for bonding several materials, such as metals, glass, ceramics, concrete, plastics and composites, providing a load-bearing joint [42]. Epoxy based and cement based adhesives are the most widely accepted structural adhesives used for strengthening RC structures with FRP [15]. Epoxy adhesives were first used in 1930 in Germany, USA and Switzerland [42]. They are based on polymeric materials and exhibit properties that are characteristic for polymers, as for example the change from relatively hard to elastic glass-like behavior to relatively rubbery behavior at a certain temperature. This phenomenon takes place at what is called as glass transition temperature, T_g. Being T_g a very important material property that depends on the polymer, its typical values for epoxies normally vary between 45˚C and 200˚C [42].

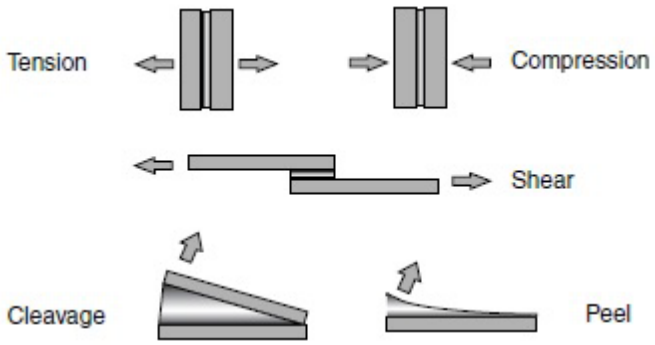

Figure 2.5 Different forces acting on a bonded joint [42].

Although epoxy-based adhesives have a wide range of mechanical and physical properties that make them the most efficient bonding material in building industry, their main drawback is that their properties can be affected when subjected to relatively low and high temperatures [15,42]. In those cases, cement-based adhesives can provide lower material cost and better resistance to high temperature. However, bond tests of NSM reinforcement have identified limitations for using cement-based adhesives due to their low bond strength [44].

2.3 FRP Strengthening techniques

The main strengthening techniques of RC structures using FRP materials are the externally bonded reinforcement, EB and the near surface mounted reinforcement, NSM as shown in Figure 2.6. The two techniques are explained in the following:

2.3.1 Externally bonded strengthening technique

The EB technique is the method of bonding FRP sheets to the tension-side surface of concrete for reinforcing the existing RC slabs and beams. In the past, externally bonded systems have shown their effectiveness in strengthening RC structures [27]. The use of bonded steel plates and bars for the strengthening and rehabilitation of RC structures has been popular for years [45,46]. Recently, several new techniques have used the light weight, high strength, corrosion resistant FRP laminates for repairing and retrofitting applications [47–49].

(a) EB technique (b) NSM technique

Figure 2.6 Strengthening techniques [27].

The use of EB FRP laminates has been one of the most attractive methods for strengthening RC structures and a large number of research and practical projects have been undertaken [45,50]. Adhesively bonding FRP CFRP plates to the surfaces of RC structures is now a well-established form of retrofitting with advanced design rules and mathematical models that quantify the debonding mechanisms. However, externally bonded plates tend to debond at low strains which limit the effectiveness of this retrofitting technique [51].

The performance of the FRP-to-concrete interface in providing an effective stress transfer is an important issue. Indeed, a number of failure modes in FRP strengthened RC members are directly caused by interfacial debonding between the FRP and the concrete. One of the failure modes, referred to as intermediate crack induced debonding (IC debonding), involves debonding which initiates at a major crack and propagates along the FRP-concrete interface. The research on IC debonding of EB FRP plates has reached the stage where fundamental governing mathematical models have been established and at which the major parameters governing IC debonding have been identified and quantified [6,52–56]. Also increasing the shear capacity of RC beams by adhesively bonding FRP to the sides of the beam, where the fibers are in the transverse or vertical direction is now a convenient, inexpensive and well-known procedure [57–59].

2.3.2 Near surface mounted strengthening technique

The NSM FRP has become an attractive method for strengthening RC members and masonry increasing their flexural and shear strength. In this technique, the FRP reinforcement is bonded into grooves cut into the concrete cover. The NSM FRP technique has been used in many applications and it presents several advantages over the EB FRP technique in strengthening concrete structures and masonry walls [14,15,60–62].

The most important advantages are that the application of NSM reinforcement does not require any surface preparation work except grooving; once the NSM reinforcement is protected by the concrete cover, it is then suitable to strengthen the negative moment regions of beams and slabs; a significant decrease of harm resulting from fire, mechanical damages and other effects; NSM reinforcement is less prone to debonding from the concrete substrate, and furthermore, the aesthetics of a strengthened structure with NSM reinforcement is virtually unchanged [14,15].

Although the bond performance is greatly improved as compared with the EB system, it is still the key factor in the design of NSM FRP strengthened elements. There are two interfaces in this technique, the bar-epoxy and the concrete-epoxy, in which the bond is affected by factors which include FRP properties, FRP surface treatment, bar size, groove surface, groove geometry, adhesive, test setup and concrete properties [15]. Now, this technology is included in some of the existing codes and guidelines [63–65].

2.3.2.1 Installation of NSM FRP reinforcement

Details of the procedure of installation of NSM FRP laminates and bars to concrete can be found elsewhere [15,34,66–68]. Two main methods can be found in the literature to form the grooves. The application of NSM laminates in concrete using the first method was discussed in detail by Barros and Fortes [69] as follows:

1- Slits were cut in the concrete cover on the tension face of the beam using a diamond cutter.
2- The compressed air was used to clean the slits.
3- The CFRP laminates were cleaned by acetone.
4- The slits were filled with the epoxy adhesive.
5- The epoxy adhesive was applied on the faces of the CFRP laminates.
6- The CFRP laminates were introduced into the slits and the excess epoxy adhesive was removed.

The second method is an easy method to make grooves [66] for experimental tests. Before concrete casting, plastic strips with the dimensions of the needed grooves are installed at the bottom of the wooden mold in the positions needed. After concrete curing, the plastic strips were removed and the grooves are left at the bottom surface of the beam. The NSM bars or strips are applied as discussed before [69]. When applying pre-stressing FRP reinforcement as NSM, the NSM FRP strips or bars are pre-stressed prior to bonding [70].

2.4 Bond between NSM FRP and concrete

The bond between FRP composites and concrete is very important for the performance of the NSM FRP strengthening system. An adequate bond, using a suitable adhesive material, means that the applied load transfers well from concrete to FRP composites and thus the FRPs is effective in increasing the strength of repaired RC members [4]. The common tests for the bond between NSM FRP and concrete are the pull-out test using direct single-face shear [71], the pull-out test using direct double-face shear [72] and the beam pull-out test (Figure 2.7) [73].

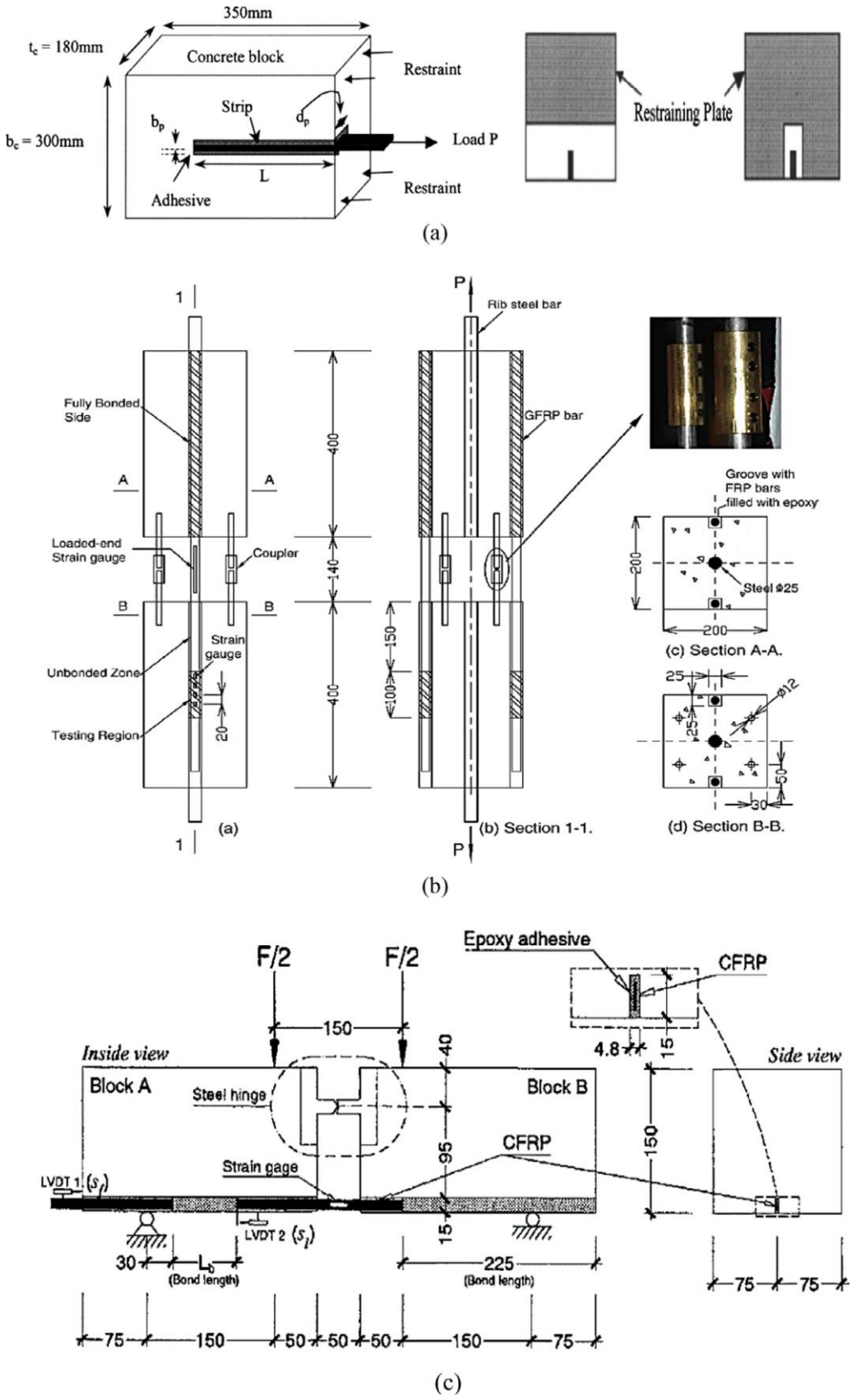

Figure 2.7 Typical test methods; (a) Pull-out direct single-face shear test [71], (b) Pull-out direct double-face shear test [72], (c) Beam pull-out test [73].

Beam pull-out test presents more difficulties, such as the bigger size of the specimen, and the difficulty to monitor crack beginning and progress throughout the test. The double-face shear testing controls the disadvantages of beam testing. Nevertheless, any variation in the FRP positions is able to cause flexural effects, leading to faults in the results. Therefore, single-face shear testing can control this problem by using fully-restraining support to avoid eccentric loading throughout the test [4].

2.4.1 Failure modes of the bond between NSM FRP-concrete

Different failure types have been reported in the literature about the bond between NSM FRP-adhesive-concrete, as follows [4]:

2.4.1.1 Debonding of FRP from concrete

This type of failure is due to high applied shear stresses, the crack propagates in the concrete next to the NSM FRP. This type of failure was observed in specimens with weak concrete or with high tensile strength adhesive [15,17,44,71,74–76], as shown in Figure 2.8a.

Figure 2.8 Failure modes of NSM FRP pull-out specimens; (a) Debonding of FRP from concrete [71], (b) Rupture of FRP [17], (c) Pull-out of FRP [44], (d) Splitting of adhesive [15].

2.4.1.2 Rupture of FRP

This type of failure happens as a result of efficient confinement, which was observed in NSM specimens with adequate bonded lengths [17,71,76], as shown in Figure 2.8b.

2.4.1.3 Pull-out of FRP

This type of failure occurs as a consequence of the weak bond between the adhesive and the concrete or the adhesive and the NSM FRP, at the adhesive-concrete substrate

or at the NSM FRP adhesive interfaces. This type of failure was noticed in NSM FRP specimens with inadequate bonded lengths or with low tensile strength adhesive [15,17,37,38,44,71,73–80], as shown in Figure 2.8c.

2.4.1.4 Splitting of adhesive

This type of failure happens on account of the small NSM groove depth, which led to the local splitting of the adhesive cover without cracking in the concrete substrate [15,44,77,80], as shown in Figure 2.8d.

2.4.2 Parameters affecting the bond property

Many factors influence the bond performance between the NSM system elements (FRP, adhesive and concrete substrate), as indicated next [4].

2.4.2.1 FRP dimensions

Increasing the width of the FRP strip can increase the NSM strengthening efficiency (ultimate load supported through the joint) as a result of effective confinement coming from embracing concrete. Increasing the thickness of the FRP strip can also increase NSM strengthening efficiency (ultimate load supported through the joint) because of the increased cross-section area of the FRP strip. Therefore, FRP strips that have big aspect-ratios (FRP strip width/FRP strip thickness) are extra effective in increasing NSM strengthening efficiency [71].

2.4.2.2 Concrete strength

It has been observed that the NSM FRP strengthening efficiency (ultimate load carried by the joint) increases as the concrete strength increases because the failure load is related to the concrete tensile strength [71]. Moreover, it has been reported that the use of low concrete strength caused most NSM FRP specimens to fail at the concrete-adhesive interface at low ultimate pull-out load [17].

2.4.2.3 Bonded length

The strengthening efficiency using NSM FRP system rises when using larger FRP bonded length, and it does not increase greatly after the critical bond length [38,44,71,74,77,78].

2.4.2.4 Adhesive material type

The performance of NSM specimens which used cement paste to bond the FRP to the concrete substrate is not as satisfactory as that of the counterpart NSM specimens which used epoxy as the adhesive. This is probably due to the low mechanical strength of cement adhesive [44,76,79].

2.4.2.5 Groove sizes

The behavior of the bond strength is related to the failure mode. Using a large groove size can increase the bond strength if the failure at the NSM FRP-epoxy interface is the controlling failure mode, because the bigger groove size delays failure [44,78]. Using large groove size can decrease the bond strength if the failure takes place at the interface between epoxy-concrete, because of the non-uniform stress distribution along the groove's perimeter [44,78]. For NSM specimens that use cement paste as adhesive, bigger groove sizes reduce the ultimate load capacity compared to smaller groove sizes, because of the increase of the shrinkage in the cement adhesive [44,76].

2.5 Flexural behavior of NSM FRP strengthened RC members

When the NSM is used for flexural strengthening, bars (circular and square cross-section) or rectangular strips are the most common FRP reinforcement types, as shown in Figure 2.9 [81]. Based on published research in the field of flexural strengthening with NSM FRP bars/strips, the most interesting observations are described and discussed in the following paragraphs [81].

De Lorenzis et al. [82] conducted one of the first tests on RC T-section beams strengthened with CFRP and GFRP bars. Test results indicated increase in the ultimate load of the strengthened specimens in comparison with the reference ones. Also, they showed that the efficiency of the NSM technique depends on the bond length of the NSM reinforcement.

Täljsten et al. [61] tested rectangular beams in four point bending test configuration. Two different dimensions of square grooves with 10 mm for cement grout and 15 mm for epoxy grout were used. Rupture of the rods occurred in the beam with the epoxy adhesive while FRP-adhesive slipping occurred in the beam with the cement grout.

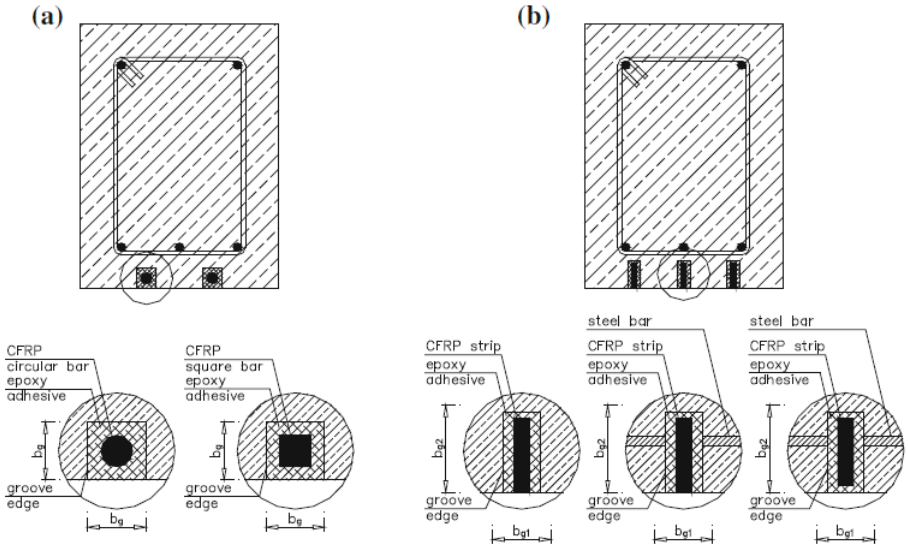

Figure 2.9 Flexural strengthening of RC members with: NSM (a) bars and (b) strips [81].

Hassan and Rizkalla [83] carried out bond tests on nine T-section RC beams strengthened with NSM CFRP strips with variable embedment lengths. The maximum strain of the CFRP bars ranged from 0.7 to 0.8 % for embedment lengths below 800 mm. Results showed an increase in the CFRP strain during its debonding, with the increase in the embedment length. Failure of the beams with ribbed NSM FRP round bars occurred by splitting of the adhesive for CFRP bond length below 800 mm. On the other hand, in the case of beams strengthened with NSM strips, rupture of the strips occurred when the embedment length was larger than 850 mm.

El-Hacha and Rizkalla [34] tested T-section beams strengthened with CFRP strips or bars and thermoplastic GFRP strips in three point bending test. The use of NSM FRP reinforcement enhanced the flexural stiffness and significantly increased the ultimate load-carrying capacity of strengthened specimens. FRP-adhesive splitting was the dominant failure mode for the beams strengthened with NSM CFRP bars as a result of the high tensile stresses at that interface.

Barros and Fortes [69] and Barros et al. [16] investigated RC beams strengthened in flexure with variable number of NSM CFRP strips and different steel reinforcement ratios. Test results indicated an almost double increase in the load carrying capacity. Significant increases in the load at steel yielding and concrete cracking points for the strengthened beams, proved the higher efficiency of the NSM technique in comparison with EBR one. Teng et al. [37] investigated the influence of the embedment length of the strip. Test results of the beams strengthened with the shortest embedment length

of 500 mm confirmed no effect of the strengthening on the ultimate load and on the beam's stiffness. The beams with medium embedment length of the strip, ranging from 1200 to 1800 mm, indicated increases in the load bearing capacity. Those beams failed by concrete cover separation starting from the cut-off region towards the maximum moment region. Finally, the longest embedment length showed the propagation of debonding from the maximum moment region towards the cut-off section.

The results of 12 T-section RC beams tested by Castro et al. [84] indicated failure due to intermediate crack debonding in the beams strengthened with CFRP strips and GFRP bars. Beams strengthened with CFRP bars failed by bar-adhesive slipping. Novidis and Pantazopoulou [85] confirmed very promising results of the NSM technique in comparison to the EBR. The results indicated that the depth at which the FRP is bonded into the longitudinal grooves influences the strengthening gain. Kotynia [86] tested three series of RC beams strengthened with NSM CFRP strips. The influence of the following parameters on the strengthening efficacy was investigated: CFRP depth, concrete cover thickness, longitudinal tensile steel, CFRP percentages, and concrete strength. Cutting of the steel stirrups in the tensile zone of the beam during the application of strips did not influence the ultimate load capacity.

Based on 12 specimens, Kalayci [87] investigated the influence of the groove size on the strengthening gain. The beams where tested with one type of strip/bar bonded into three different groove sizes. The ultimate loads reached for undersized groove specimens strengthened with CFRP strips was similar to the loads in the control specimens, even though the mid-span deflections were lower. Undersized and control groove beams had identical modes of failure: concrete and adhesive splitting. However, in the oversized specimens only concrete splitting occurred. Beams strengthened with CFRP bars reached similar deflections and ultimate loads in the control and undersized grooves specimens but, in the undersized specimens, adhesive splitting failure was observed. One of the oversized specimens failed by adhesive splitting while the other one by concrete splitting. Tests showed that smaller grooves led to adhesive splitting failures and bigger ones led to concrete splitting failures.

Sharaky et al. [88] studied experimentally and numerically the behavior of bottom and side NSM strengthened RC beams using GFRP bars with and without end anchorage made by bent 150 mm from the two ends of the NSM bars by 45˚ or 90˚. They found that the load carrying capacity for the strengthened RC beams with bottom NSM bars

was higher than side NSM strengthened ones due to the internal arm effect. The highest ratio of improvement in the load carrying capacity of strengthened beams compared with the control beam was 201% for strengthened beam with bottom NSM bars having end anchorage inclined by 45˚while the lowest ratio was 142% for the same strengthened beam with side NSM. Sharaky et al. [89] studied the effectiveness of axial stiffness and of the type of confinement of NSM FRP reinforcement on the strengthened beam bearing capacities and failure modes. They found that the yield load ratio of the strengthened beams (with respect to the control beams) was proportional to the axial stiffness ratio of NSM FRP reinforcement. The failure of the strengthened beams became concrete cover separation when the axial stiffness ratio reached a critical value, and subsequently the ultimate load of strengthened beams was not affected by increasing axial stiffness ratio beyond this value. This critical value of stiffness ratio was experimentally found to be at about 1.25. The confinement significantly enhanced the load carrying capacity of the RC beams with small increase in their steel reinforcement yielding load. The ultimate load of the strengthened beams without concrete cover confinement ranged between 150% and 170% of the ultimate load of the control beam.

To improve the performance in front of concrete cover separation and enhance bond strength, they [89] investigated the use of mechanical interlocking with shear connectors (concrete cover confinement) or transverse wrapping. The load carrying capacity was increased by up to 23.3% for strengthened beams and by 33% for the ultimate load of conventional strengthened beams. The effect of interaction between FRP strips and internal reinforcement on the flexural behavior of NSM strengthened RC beams was studied by Sharaky et al. [90]. They investigated the position, arrangement and area of glass fiber reinforced polymer (GFRP) strips using six strengthened beams in addition to one control beam. They found that the installed NSM GFRP side by side has a lower interfacial stress than those installed separated. This improvement is more obvious in the case of NSM strips installed near the internal reinforcement. Furthermore, the installed NSM strips in deep groove experienced higher load carrying capacity than those installed in shallow groove for both patterns. This might be due to delaying or preventing the peeling/debonding failure. The ultimate load of the beam upgraded with one NSM strip adjacent to the stirrups (in

deeper groove) is about 1.5 times that of one NSM strip installed near the bottom surface of the beam. This ratio decreased with increasing the area of NSM GFRP strips. All the tests mentioned by Sena-Cruz et al. [81] and Al-Saadi et al. [4] showed a significant effect of the FRP and steel reinforcement ratios likewise CFRP elasticity modulus on the ultimate loads and the CFRP strain utilization. The increase in the CFRP stiffness led to an ultimate load increase. However, it causes a decrease in the CFRP debonding strain.

2.5.1 Modes of failure

The following failure modes appeared in the experimental tests of the RC members strengthened in flexure with NSM FRP reinforcement [81].

2.5.1.1 Interfacial debonding

Interfacial debonding or adhesive cover splitting at the FRP-adhesive interface near the anchorage zone observed in the RC members NSM strengthened in flexure referred to similar failure modes observed in the bond tests as shown in Figure 2.10.

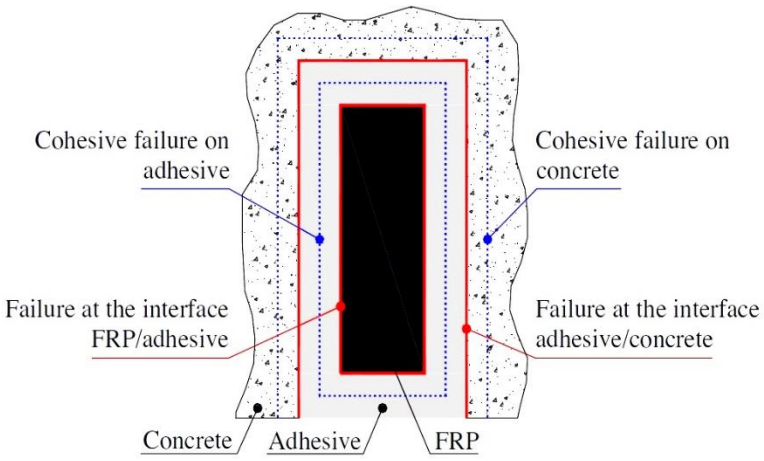

Figure 2.10 Interfacial debonding [91].

2.5.1.2 Concrete cover separation

Concrete cover separation is more common for RC members strengthened with lower distances between the several grooves of the strengthening system since this can led to an undesirable group effect. This is also more frequent for decreasing tensile strengths of the concrete cover. In many tests, bond cracks inclined at approximately 45° to the beam axis formed on the soffit of the beam. Upon reaching the edges of the beam's soffit, these cracks may propagate upwards on the beam sides maintaining a

45° inclination within the cover thickness. Then, they can propagate horizontally at the level of the steel tension bars [16,46,69,82,86,92].

Bar/strip end concrete cover separation is typical for the extremities of NSM FRP reinforcement at a significant distance from the supports (Figure 2.11). This failure starts from the cut-off section and propagates to the mid span of the RC member [16,37,93,94].

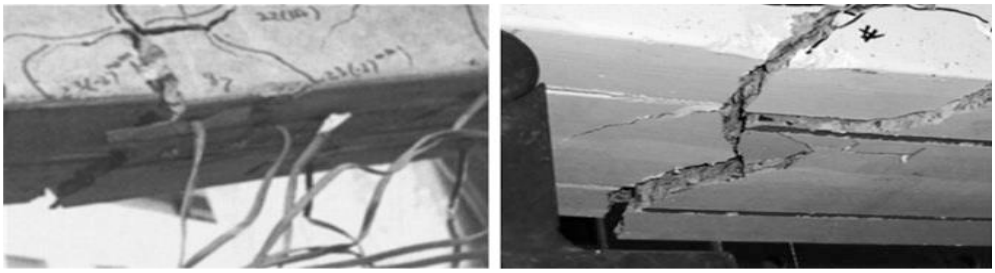

Figure 2.11 Failure by strip end cover separation [37,94].

Bond cracks, within or close to the maximum moment region, together with pre-existing flexural and/or flexural-shear cracks may isolate triangular or trapezoidal concrete wedges. From those, one or more will eventually split off [16,94].

Flexural crack-induced cover separation is similar to the intermediate crack debonding in reinforced concrete members externally bonded with FRP materials. Concrete cover separation is followed by flexural concrete cracking propagating along the NSM reinforcement, involving one of the shear spans and the maximum bending moment region (Figure 2.12) [16,69,82,86,92,94].

Figure 2.12 Failure by intermediate crack debonding with adjacent cover concrete [86].

Flexural-shear crack-induced cover separation is similar to the EBR technique, when diagonal shear crack intersects the FRP, debonding initiates due to shear and normal interfacial stresses on the side of the crack and propagates towards the FRP

reinforcement end. The failure generates in the concrete adjacent to the adhesive-concrete interface and promotes the concrete cover separation (Figure 2.13a) [94]. When using NSM with high depth strips, a longitudinal fracture along the strip can be formed due to the relatively high moment of inertia, which leads to the fracture along the FRP strip (Figure 2.13b) [94].

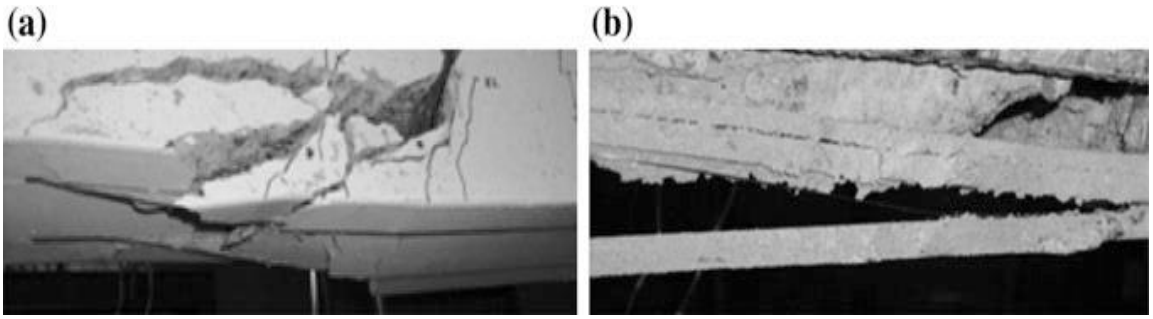

Figure 2.13 Failure by concrete cover separation: (a) Followed by flexural shear failure crack propagation, (b) Fracture along the NSM strip [94].

Beam edge cover separation occurred when the FRP NSM bar is located near the beam's edge, and detachment of the concrete cover appears along this edge (Figure 2.14).

Figure 2.14 Failure by the beam edge concrete cover separation [15].

2.5.1.3 Concrete crushing and FRP rupture

In addition to the aforementioned modes of failure, concrete crushing and FRP rupture may also occur in RC beams strengthened by NSM reinforcement (Figure 2.15). The concrete crushing failure occurs when the concrete reaches its crushing strain before the FRP NSM reinforcement fails. The FRP rupture takes place when concrete crushing and the debonding failure are prevented. The existing researches indicate that FRP rupture is more likely for the NSM strips than for NSM bars [27].

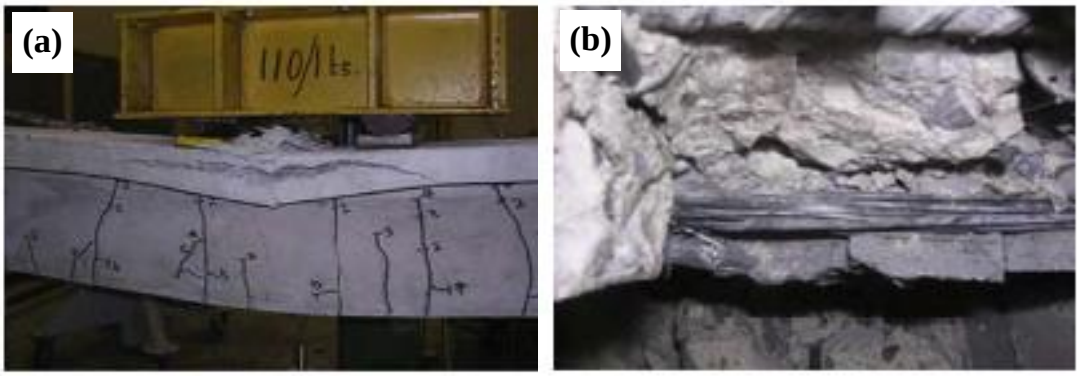

Figure 2.15 Failure modes observed in strengthened RC beams with NSM reinforcement; (a) Concrete crushing, (b) FRP rupture [27].

2.6 Creep of materials used in the NSM system

Creep is a time dependent deformation and can be defined as the increase of the strain with time due to constant applied stress and temperature. The creep rate depends on material properties, temperature, applied load and time. The strain versus time relation at constant stress and temperature is illustrated in Figure 2.16 and it can be divided into three stages: primary creep in which the creep rate decreases, secondary creep in which the creep rate is almost constant and tertiary creep where the creep rate increases till creep rupture [95].

The understanding of the time-dependent behavior of the materials involved in the NSM FRP system (FRPs, concrete and adhesive) becomes essential, because the creep of these materials may cause a continuous variation and time-dependent deformations in the strengthened element [33].

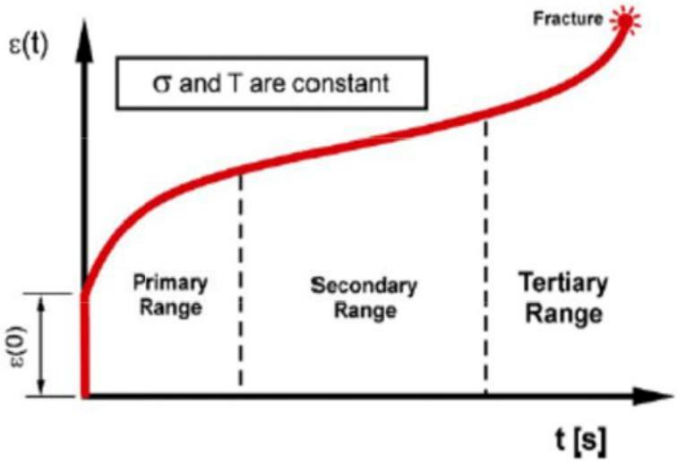

Figure 2.16 Stages of creep [96].

2.6.1 Creep of concrete

When concrete is subjected to a sustained stress, creep strain develops gradually with time as shown in Figure 2.17. Creep increases with time at a decreasing rate. In the period immediately after initial loading, creep develops rapidly, but the rate of increase slows appreciably with time. Creep is generally thought to approach a limiting value as the time after first loading approaches infinity. About 50 percent of the final creep develops in the first 2–3 months and about 90 percent after 2–3 years. After several years under load, the rate of change of creep with time is very small [97].

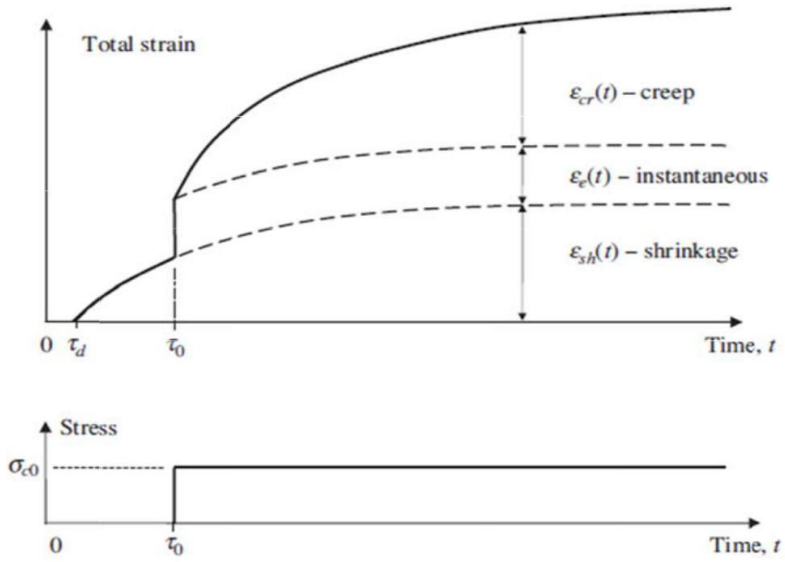

Figure 2.17 Concrete strain components under sustained load [97].

After removing the sustained load, a large amount of creep strain is not recoverable, the amount of irrecoverable strain/deformation known as residual strain/deformation [98]. Figure 2.18 illustrates creep strain, elastic recovery, creep recovery, and irrecoverable creep.

Major factors affecting the rate and ultimate values of creep and shrinkage of concrete include compressive strength, stress level at which the concrete is subjected to, environmental conditions during curing and during the life of the structure, age at loading, and mix proportions. For concrete stresses below a value around 40 % of its compressive strength, creep can be considered linear (i.e. it is proportional to the applied stresses) [99,100].

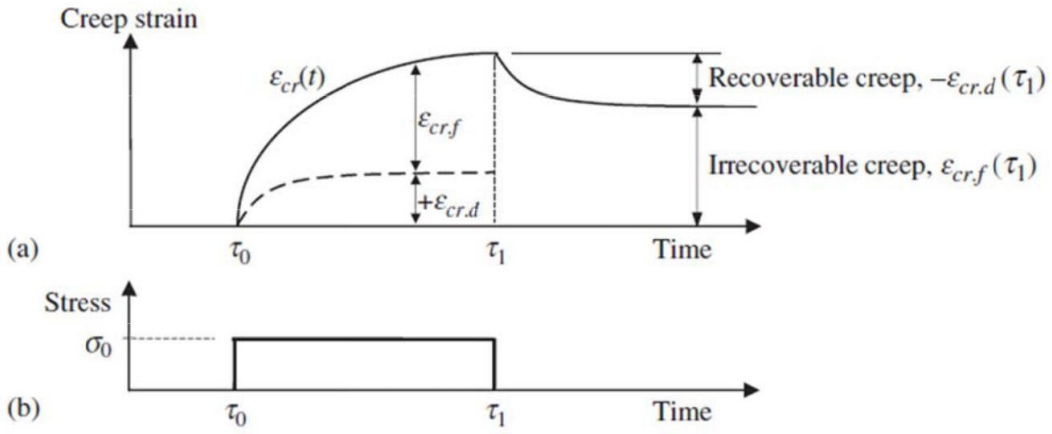

Figure 2.18 Recoverable and irrecoverable creep components [97].

Numbers of theoretical models were developed to predict the time-dependent behavior of concrete [101–103]. Many codes and guidelines are available to calculate the creep strain in concrete such as CEB-FIP Model Code [99], ACI Committee 318 [104] and ACI Committee-209R-92 [105].

2.6.2 Creep of FRP

FRP materials subjected to constant load overtime can suddenly fail after a time period referred to as the endurance time. This type of failure is known as creep-rupture [106]. Creep rupture tests have been carried out using FRP bars of Carbon (CFRP), Glass (GFRP) and Aramid (AFRP). A linear relationship of creep rupture strength with time was obtained. And it was clear that glass fibers are the most susceptible to the creep rupture, while carbon fibers are the least [107].

The creep behavior of a carbon fiber/epoxy matrix composite was studied by Goertzen and Kessler [108]. CFRP Specimens were loaded up to 77% ultimate tensile strength (UTS) and it was observed that, the carbon fiber composites are resistant to creep rupture under ambient conditions as no creep rupture failures were observed.

A simple model based on a linear viscoelastic approach was suggested to predict FRP strain under sustained load [109] as the following equation:

$$\varepsilon = \varepsilon_0 + \varepsilon_t t^n \tag{2.1}$$

where ε is the total strain, ε_0 is the stress dependent and time independent elastic strain, ε_t is the stress dependent and time dependent elastic strain, t is the time after loading in hours and n is the material constant.

Creep effect on FRP composites can be predicted using an effective modulus of elasticity following the same approach stated for creep of concrete as the following equation:

$$E_f(t) = \frac{E_f}{1+\varphi_f(t)} \quad (2.2)$$

where $E_f(t)$ is the FRP modulus of elasticity at time t after loading, E_f is the initial FRP modulus of elasticity and $\varphi_f(t)$ is the creep coefficient which can be determined through the FRP strains as follow:

$$\varphi_f(t) = \frac{\varepsilon_f(t)-\varepsilon_f(t_0)}{\varepsilon_f(t_0)} \quad (2.3)$$

where $\varepsilon_f(t)$ is the total strain of FRP at time t after loading, $\varepsilon_f(t_0)$ is the instantaneous strain of FRP at loading time.

An alternative equation suggested by Holmes and Just [110] to calculate the FRP creep coefficient is:

$$\varphi_f(t) = \left(\frac{t}{t_0}\right)^m - 1 \quad (2.4)$$

where t is the time in hours after application of loading, t_0 = 1 hour and m is the slope of the best-fit line relating log $\varepsilon_f(t)$ and log(t/t_0)

2.6.3 Creep of adhesive

A structural adhesive can be defined as a load-bearing material with high modulus and strength that can transmit stress without loss of structural integrity. Some advantages of epoxy-based structural adhesives are the equal distribution of stresses over a large area while minimizing stress concentrations, joining dissimilar materials, and reducing the overall weight and manufacturing costs. However, epoxy resins, being viscoelastic in nature, exhibit unique time-dependent behavior. This leads to a great concern in assessing their long-term load-bearing performance [111].

The long term creep of epoxy was investigated through an experimental program, testing resin specimens under three different levels of tensile stress up to 5.7 years showing that epoxy resin exhibits considerable creep and the total strains exceed the instantaneous ones by 4.3 to 4.7 times as shown in Figure 2.19 [112].

At constant high stress level (80 % of the ultimate strength), the behavior of structural adhesives changes significantly and failure is reached very quickly [113].

The creep behavior of epoxy adhesives can be modeled using rheological models and can be described by mean of Hookean springs and Newtonian dashpots [114]. Some analytical models have been suggested to predict the creep behavior of adhesives based on Burger's model of viscoelastic materials, shown in Figure 2.20. Therefore, the strain at any time t, $\varepsilon_{Creep}(t)$, can be computed using equation 2.5.

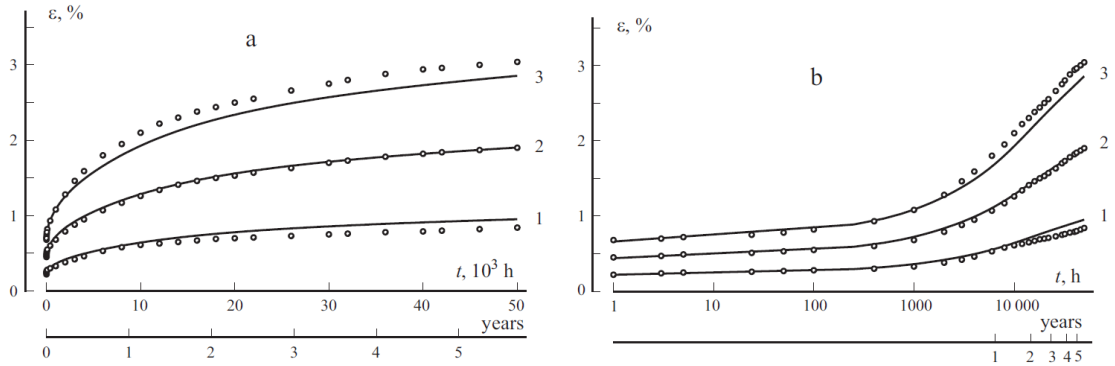

Figure 2.19 Creep strain with time at different sustained stress levels [112].

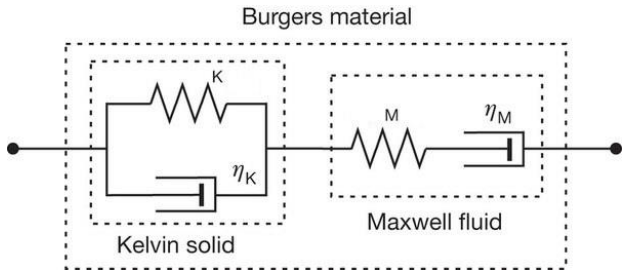

Figure 2.20 Burger's model of viscoelastic materials [114].

$$\varepsilon_{Creep}(t) = \frac{\sigma}{E_M} + \frac{\sigma}{\eta_M}t + \frac{\sigma}{E_K}\left(1 - exp\left(\frac{E_K}{\eta_K}t\right)\right) \tag{2.5}$$

where σ is the applied stress, E_M and η_M are the elastic modulus and coefficient of dynamic velocity of Maxwell's chain, E_K and η_K are the elastic modulus and coefficient of dynamic velocity of Kelvin's chain.

Feng, et al. [111] proposed a model to predict the tensile creep strain of adhesive as follows:

$$\varepsilon(t,T) = \frac{\sigma_0}{E_0} + \sigma_0\left(\frac{1}{E_e} - \frac{1}{E_0}\right)\left(1 - e^{-(t/t^*)^{1-n}}\right) \tag{2.6}$$

where σ_0 is the applied stress, E_0 is the initial young modulus, t^* is the retardation time, which corresponds to the time instant at which 63% of the Kelvin's steady-state

strain is attained, n is a factor to take moisture absorption into account and E_e is the equilibrium modulus, which can be calculated by the following equation:

$$E_e = 2G_f(1-\nu) \tag{2.7}$$

where G_f is the rubbery plateu shear modulus and ν is the Poisson's ratio.

Another model was proposed by Majda and Skrodzewicz [96] in which coefficients of dynamic viscosity, η_0 and η_1, and the elastic moduli of the relaxation response, E_1 and E_2, are defined as a function of the applied stress, σ.

$$\varepsilon(t) = \sigma\left[\frac{1}{E_1} + \frac{t}{\eta_1} + \frac{1}{E_2}\left(1 - exp\left(\frac{-E_2}{\eta_2}t\right)\right)\right] \tag{2.8}$$

A modification to the model proposed by Feng, et al. [111] was suggested by Costa and Barros [115] in order to improve the prediction of the experimental strains, for that a new parameter *n* was introduced as follows:

$$\varepsilon_{Creep}(t) = \frac{\sigma}{E_M} + \frac{\sigma}{\eta_M}t + \frac{\sigma}{E_K}\left(1 - exp\left(\frac{E_K}{\eta_K}t\right)^{1-n}\right) \tag{2.9}$$

2.7 Effect of sustained loading on bond between NSM FRP-concrete

Although many studies were carried out on the short-term bond behavior of NSM FRP, so far little attention has been paid to the time-dependent bond-slip response of RC members strengthened with NSM FRP under environmental conditions and sustained loading, thus resulting in a general lack of research into this topic. An overview of some studies that investigated the long-term behavior of NSM FRP reinforcement system is carried out here.

Borchert and Zilch [116] carried out an experimental program, studying the effect of adhesive properties on the long-term bond behavior of concrete blocks strengthened with NSM CFRP strips when subjected to different levels of prestressing. The main test parameters were the temperature (20˚C to 50˚C), the curing time (1 to 28 days) and the applied prestressing force (40% to 80% of the short-term bond capacity). The used bonded length was 100 mm. Results obtained showed that increasing the curing period reduced the creep effects, and increasing the temperature near the T_g significantly affected the system performance, causing sudden losses in the CFRP

strains. In the same study, an analytical procedure to model the time-dependent bond behavior of NSM FRP strips was introduced. The proposed model assumed that the bond of NSM system is related to the adhesive bond-slip behavior. The model was based on a non-linear bond-slip law, similar to that used for bond of deformed steel bars in concrete. Although the proposed model showed good agreement with the experimental results, some limitations were observed. For example, the coefficients were valid only for the adhesive used and their applicability shall be checked for different types of adhesives.

Silva et al. [117] performed an experimental program to study the long-term bond of concrete elements strengthened with NSM CFRP strips through beam tests. Each specimen was composed of two equal size concrete blocks, each block having dimensions of 150 mm x 200 mm in cross-section and 385 mm length. The two blocks were connected through a steel hinge at the top and the CFRP reinforcement was installed at the bottom. In each block, five stirrups of 6mm diameter were distributed along the length to avoid shear failure. Additional longitudinal reinforcement, 2ϕ8, was provided at the bottom and the top of each block. The CFRP strips used were 1.4 mm thickness and 10 mm width, and the bonded length and anchorage length in the reaction block were 60 mm and 335 mm, respectively. A sustained load of approximately 7 kN was applied through two steps (1.7 kN and 5.3 kN for the first and the second steps, respectively). Specimens were divided into five groups. First and second group were left unloaded and loaded, respectively, in laboratory conditions. The other three groups were loaded and subjected to the following conditions: immersion in a water tank at 20˚C with 0% of chlorides; immersion in a water tank at 20˚C with 3.5% of chlorides; and exposure to wet/dry cycles with water at 20˚C and 3.5% of chlorides. Results showed that the creep effect was found to be practically negligible and the loaded end slip was mainly controlled by the laboratory temperature. Besides, similar behaviors were observed in the case of specimens immersed in pure water at 20˚C and those subjected to wet/dry cycles with water with 20˚C and 3.5% of chlorides.

Derias et al. [118] studied the durability of nine RC beams strengthened with NSM system using GFRP strips and two types of CFRP strips. Sustained load equal to 40% of the ultimate load carrying capacity was applied. Some beams were subjected to high temperature and some other were left in room conditions. Results showed

deterioration in the epoxy-concrete interface and changes in failure modes due to the extreme environmental conditions.

Emara et al. [119] studied experimentally the bond of NSM CFRP laminates in concrete using single shear pull-out tests. Short-term and long-term tests in which different levels of sustained loading were carried out. The parameters of the study were the sustained loading level (25% and 50% of the failure load), the groove width (5 and 10 mm) and the bonded length, L_b, (60, 90 and 120 mm). The slip evolution with time under the different loading and environmental conditions was monitored during the test period of 1000 hours. They found that specimens with bonded length equal to 90 and 120 mm showed similar behaviors within the same test condition. For all bonded lengths used, increasing the sustained loading level from 25% to 50% increased the total slip, by almost the double, at any time along the testing period. When the groove width increased from 5 to 10 mm, the total slip values reduced for all bonded lengths. The average reduction was 0.82, 0.91 and 0.93 for specimen with L_b equal to 60, 90 and 120 mm, respectively. The ratio between the total slip at 1000 h of sustained loading to the instantaneous slip at the time of application of the sustained load (t = 0) was almost similar for all tested specimens. The ratios obtained were 1.77, 1.77 and 1.88 for specimens subjected to sustained loading equal to 25% with L_b equal to 60, 90 and 120 mm, respectively, and 1.75, 1.76 and 1.75 in case of specimens subjected to sustained loading equal to 50% with L_b equal to 60, 90 and 120 mm, respectively. The authors developed a simplified analytical methodology, based on a bi-linear interface model, using the effective modulus method achieving a good agreement between analytical and experimental results.

Thirty-three single shear pull-out specimens were subjected to monotonic and sustained loading by Emara et al. [120]. Nine specimens were tested under a direct pull-out shear test to obtain their load capacity. These specimens were divided into three groups, three specimens each, with different three values of L_b of 60, 90 and 120mm. For the long-term pull-out tests, twenty-four specimens were tested under sustained loading conditions for 1000 hours. These specimens were organized in four test series in which three bonded lengths, equal to 60, 90 and 120 mm, were used, and two levels of sustained loading, equal to 25% and 50% of the short-term load capacity, were applied. In addition, for each test series, different levels of temperature (20°C and 40°C) and relative humidity (55% and 90%) were applied. The authors found that

at 20 °C, increasing the humidity had no significant effect on the slip time behavior when a sustained loading level equal to 25% was applied. On the other hand, an increase of the total slip between 1.23 and 1.28 was observed when increasing the loading level to 50% within the same test conditions. The effect of increasing humidity was more evident in the case of the specimens tested at 40°C than in those tested at 20°C.

2.8 Long-term behavior of FRP strengthened RC members

In the case of reinforced concrete, the reinforcement bars will inhibit the shrinkage in concrete volume and therefore cause curvature to occur. Major factors affecting the rate and ultimate values of creep and shrinkage of concrete include compressive strength, stress level at which the concrete is subjected to, environmental conditions during curing and during the life of the structure, age at loading, and mix proportions [121].

Several approaches are available to calculate the long-term deflection of RC beams due to sustained loading. Among them, the approach of ACI Committee 318 [104], and methods proposed by Ghali et al. [122], and Gilbert [102] are noteworthy. The ACI approach [104] suggests a multiplier to account for the time-dependent deflection due to creep and shrinkage, which is simple and convenient for use. The other two approaches calculate creep and shrinkage deflections separately, by considering strain compatibility and force equilibrium across sections, and are based on age-adjusted effective modulus.

Because of the scarceness of the long-term studies on NSM strengthening technique, it is important to review the long-term studies on the externally bonded strengthening technique, which is the closest technique, to understand the time dependent flexural behavior of FRP strengthened RC members under sustained loading.

2.8.1 EB FRP strengthened RC members under sustained loading

Based on the existing works on RC beams strengthened in flexure with EB FRP reinforcement under sustained loading [23–26,121,123–142], the most interesting observations are described and discussed in the following paragraphs.

Plevris and Triantafillou [138] aimed at developing a fundamental understanding of the time-dependent (creep and shrinkage) behavior of reinforced-concrete beams strengthened with FRP laminates. They proposed an analytical procedure for the deformation of cross sections based on the age-adjusted effective-modulus method (AEMM) for concrete. Then the authors carried out a parametric study assessing the effect of the type and the area fraction of composite material and of the area fraction of steel reinforcement on the long-term response of strengthened elements. The authors carried out an experimental program that consisted of three RC beams (one control beam, one strengthened with 0.82 mm CFRP thickness and one strengthened with 1.42 mm CFRP thickness). All beams were tested under sustained loading using air cylinder and precision regulator at middle span. The loads were applied after 49 days from casting for 250 days. Finally, they used the analytical model to predict the deflections of their RC beams integrating the curvature of cracked sections, ignoring the un-cracked sections. The authors concluded that increasing the area of FRP in general tends to restrain the reduction of stress in the concrete compressive zone.

Tan and Saha [121] studied the long-term deflection characteristics of externally FRP-bonded beams under sustained loads. Nine reinforced concrete beams (100x125 mm in cross section and 2000 mm in total length), six of which were externally bonded with GFRP composite laminates, were subjected to sustained loads for 2 years. The test parameters were the ratio of FRP to the RC section and sustained load level. The long-term deflections of the beams were reduced 23 and 33% with FRP ratios of 0.64 and 1.92%, respectively. The total beam deflections were accurately predicted by the adjusted effective modulus method, and overestimated by about 20% by the effective modulus method.

Al Chami et al. [142] investigated the creep behavior of experiments on the time-dependent behavior of carbon FRP-strengthened concrete beams. Twenty-six RC beams with and without bonded CFRP laminates and with different reinforcement ratios were used to evaluate the contribution of the external reinforcement on the creep resistance of the beams. High levels of sustained load were used in order to determine the maximum sustained load that can be applied without any risk of creep failure. The applied sustained loads varied from 59% to 78% of the ultimate static capacities of the un-strengthened beams. For most of the long-term tests, the applied sustained loads were higher than the service loads. This was done to account for the

fact that strengthening is typically required when a structure is expected to carry increased service loads. The results confirm that FRP strengthening is effective for increasing the ultimate capacities of the beams; however, there is virtually no improvement in performance with regard to the long-term deflections.

El-Sayed et al. [134] investigated the long-term deflection and cracking characteristics of wide shallow RC beams strengthened with carbon FRP (CFRP) plates. Five full scale wide shallow beams were constructed: two beams were tested under static loading and three beams were tested under sustained load for a period of 600 days. Three of the beams were strengthened with CFRP plates bonded to the soffit of the beams and two beams were un-strengthened serving as control. The long-term beam deflection was compared with the predictions of the effective modulus approach considering two different concrete creep models. The authors concluded that the beams strengthened with CFRP plates showed significant improvement in the short-term deflection and crack width compared to the un-strengthened beam. The strengthened beams, however, did not show that much improvement in the long-term behavior. The effective modulus approach was found to reasonably predict the additional long-term deflection of the beams depending on the incorporated concrete creep model. Further, an analytical procedure for predicting the long-term crack width of the beams was presented.

The long-term deflection behavior of two RC beams with similar dimensions and material properties was monitored by Reda Taha et al. [26]. One beam was externally strengthened with FRP strips, whereas the other was used as a control specimen. Both beams have been subjected to sustained loading for over 6.5 years. The authors aimed to assess the significance of creep in the epoxy adhesive and whether such creep might allow the FRP strips to unload over time. Slip movements at the ends of the FRP strips were also monitored. The experimental deflections were compared to deflection predictions using ACI Committee-209R-92 [105] and CEP-FIP Model Code 90 [143]. The authors used two analytical approaches: step-by-step time analysis and finite element (FE) modeling. They concluded that both techniques demonstrate that creep of the adhesive layer can account for the differences observed between the predicted and actual behaviors of the beams.

A theoretical study of the time-dependent behavior of FRP strengthened RC cracked sections subjected to sustained loading was performed by Marí et al. [132]. Based on

it, a simplified method for the calculation of long-term deflections has been proposed and verified with available experimental results. Their method has been used to study the influence of the FRP ratio on the short and long-term deflections on RC beams. They concluded that the observed reduction of long-term deflections is mainly due to the reduction of short-term deflections due to the increment of stiffness caused by FRP laminates, and that the constraint produced by the FRP laminates to the long-term increment of curvature is small. Furthermore, the effectiveness of the FRP in reducing long-term deflections depends on the tensile and compressive reinforcement ratios and on whether the FRP laminates are bonded before or after the instantaneous deflection has taken place.

Oller and Marí [131] studied the effect of concrete creep on the interfacial shear stresses and consequently on the debonding failure load. They provided a simplified formulation for the instantaneous and time-dependent bond stresses under sustained load. Its reliability is analyzed through the results obtained by a non-linear time-dependent analysis model.

Benyoucef et al. [140] investigated the time-dependent behavior of RC beams bonded with thin composite plate theoretically by including the effect of the adherent shear deformations. The considered time effects came from shrinkage and creep deformations of the concrete. The influence of creep and shrinkage effect relative to the time of the casting and the time of the loading of the beams was taken into account. Numerical results were presented to illustrate the significance of time-dependent of adhesive stresses. The study showed that the interfacial stresses take a peak value during the first months and begin to decrease until they become almost constant after a very long time. In addition, the interfacial shear stress is affected considerably by the relative humidity, contrarily to the interfacial normal stress which is slightly affected. Also, Tounsi and Benyoucef [141] and Fahsi et al. [127] have presented interfacial stresses model to study the adherent deformations.

The time-dependent flexural cracking behavior of RC beams strengthened with externally bonded composite materials was investigated with a focus on the creep effects by Hamed and Bradford [25]. A theoretical model was developed, which accounts for the creep of the different materials involved, and which also accounts for the time-dependent cracking and the tension-stiffening phenomenon. The deformability of the adhesive layer in shear and through its thickness, as well as its

ability to transfer shear and vertical normal stresses, was considered in the model. The capabilities of the model were demonstrated through numerical examples including a comparison with test results available in the literature. The authors concluded that the creep causes a significant redistribution of internal forces and the interfacial stresses at the adhesive interfaces with time, which should be carefully considered in the design of FRP strengthened members.

Hamed and co-workers [24,25,133] concluded that the creep of the adhesive layer leads to a reduction in the interfacial adhesive edge stresses with negligible effect upon the deformations and axial forces. This release in the stresses highly depends upon the viscoelastic characteristics of the adhesive. Thus, in some cases, viscoelastic adhesives may have a favorable effect on the behavior of strengthened beams.

Long-term behavior, deformation recovery, and residual strength of FRP-plated beams were evaluated by Hong and Park [135]. Three concrete beams were fabricated: one control, one CFRP-plated, and one GFRP plated. All beams sustained constant loads for 550 days and were then unloaded for 60 subsequent days to evaluate the deformation recovery performances. During this period, the strains of the FRP plates and internal reinforcing steels, cracks, and deflections were recorded for comparison. The authors predicted the long-term strains and deflections of the FRP-plated beams using previous analytical methods. The validity and accuracy of the methods were obtained by comparing the analytical and experimental results.

Jiang et al. [136] studied the influence of preload and FRP stress-lagging on the time dependent behaviors of strengthened concrete beams. Three concrete beams were fabricated: one beam (B1) strengthened directly without any preload; one beam (B2) preloaded, fully unloaded and then strengthened; one beam (B3) preloaded by the same value of force as B2, but strengthened with the preload remaining. Sustained loads were applied to test beams and their deformations and cracking patterns were recorded for comparison. They found that beam B1 presented the largest long-term deformation with the most evident crack propagation in load sustained period, followed by beam B2 and beam B3. Therefore, they concluded that the state of cracks opening influences the long-term deformations. The preloads before strengthening may cause more adequate cracks opening when load sustaining begins. Such mature development of cracks at immediate loading makes the existing cracks are unlikely to further propagate in load sustained period. Hence, the effect that section stiffness is

reduced by further propagation of existing cracks and newly developed cracks is weakened. As a result, the long-term deflections can be better controlled and present less increment. This may imply that proper opening and propagation of cracks have positive effects to control the long-term deformations.

Bouziadi et al. [137] carried out a nonlinear numerical analysis to predict the creep response of RC beams externally strengthened using CFRP and GFRP laminates. The Burger's rheological model was used to evaluate the flexural creep response (compressive and tensile creep) and then to validate the findings with experimental results. They found that the Burger's model effectively predicts the creep of CFRP-bonded RC. Furthermore, parametric studies were performed to investigate the effects of: three fiber orientations of CFRP composites (0°, 45° and 90°), the CFRP thickness, and the type of FRP (CFRP and GFRP). According to the numerical results, they found that the major reduction in creep strain was obtained with the 45° orientation of CFRP. An increase in CFRP-thickness significantly lowered the creep strain. Moreover, the CFRP laminates proved to be more effective than GFRP in improving the creep response.

2.8.2 NSM FRP strengthened RC members under sustained loading

In comparison with other methodologies, a general lack of studies on the time dependent flexural behavior of NSM FRP strengthened RC members under sustained loading is observed in the analysis of the existing literature.

The first 133 days results of simply supported eight NSM strengthened RC slabs with CFRP strips have been presented by Sena-Cruz et al. [144]. The authors tested these slabs under four point bending sustained loading in different environmental conditions. The creep load applied to each slab was defined as 33% of the ultimate load of the reference slab monotonically tested up to failure. The average creep deformation for all the eight studied slabs was about 20% of the total deflection. The crack widths were also monitored.

Various sustained load levels were applied to NSM strengthened RC beams with CFRP strips for 4000 hours (≈167 days) by Kim and Khan [145] and their performance was examined with a focus on residual capacity and failure characteristics. The sustained load significantly influences the residual load-carrying capacity of the long-term beams, while its effect is not critical on residual stiffness. The authors concluded that,

the failure mode of the strengthened beams is controlled by the number of NSM CFRP strips and the degree of sustained load. The long-term load accelerates stress concentrations near the CFRP termination, and the accumulated damage propagates along the CFRP-concrete interface.

To summarize, too little attention has been paid to the time dependent flexural behavior of NSM FRP strengthened RC members under sustained loading, which can be affected by several governing parameters. This puts in evidence the general lack of research into this topic and the huge need of data and knowledge about it.

The main objective of the present work is to study the long-term and residual flexural behavior of NSM FRP strengthened RC beams.

CHAPTER 3 EXPERIMENTAL PROGRAM

3.1 Introduction

The literature review chapter reflected the scarceness of existing works dealing with the sustained loading effects on the RC members strengthened with NSM FRP reinforcement, wherefore an experimental program was designed to investigate the flexural behavior of RC members strengthened with NSM FRP reinforcement under long-term sustained loading. Parameters in this program were chosen depending on the collected data from previous literature work. The selected parameters were CFRP area (stiffness), tension steel reinforcement ratio (stiffness), concrete type, sustained load level, ratio between compression and tension steel ratio and loading history. Details of the experimental program conducted in this research are presented in this chapter. First, the test matrix of the specimens is provided followed by a fabrication description of the beams' specimens involving the RC beams preparation and the application of NSM strengthening technique. The instrumentation and test setup of short and long-term tests are after described. At the end, details of the materials characterization procedure, results and discussions are illustrated.

3.2 Test Matrix

The test matrix of this work involved 28 RC beams divided into two series, A and B, with two concrete batches of different compressive strength. In each series, some of the beams were strengthened with CFRP strips using the NSM strengthening technique and the others were un-strengthened. Series A was divided into two groups, A1 and A2, while series B was divided into three groups, B1, B2, and B3. The beams of the first group in each series, A1 and B1, were tested at the age of 55 days to determine the short-term flexural behavior of un-strengthened and strengthened beams. Other groups, A2, B2, and B3, were subjected to long term test with different sequences as shown in Table 3.1. Each sequence contained some of the three stages indicated in the table. The 1st stage is a short term test for two loading/unloading cycles up to service design load P_D, with a minimum load of 2 kN which enough to ensure that the beams are cracked under the service conditions, before sustained loading. The 2nd stage is the application of sustained loading with a sustained load P_s, designed to obtain

instantaneous maximum concrete compressive stress at the top of mid-span section, σ_{co}, lower than 0.4 times the concrete compressive strength, f_c, to keep the linear creep behavior of concrete according to CEB-FIP Model Code 2010 [99]. The 3rd stage is a short-term test under monotonic loading up to failure, after removing the sustained loads to study the effect of the sustained loading on the residual flexural behavior.

Table 3.1 Details of loading sequences.

Sequence	1st stage Two loading/unloading cycles between P_D and 2 kN	2nd stage Sustained loading	3rd stage Monotonic Loading up to failure
I	At 60 days age	At $\sigma_{co} = 0.34f_c$ From 75 to 345 days age	At 365 days age
I`	At 50 days age	At $\sigma_{co}(un) = 0.4f_c$ From 56 to 345 days age	
II		At $\sigma_{co}(un) = 0.4f_c$ From 56 to 345 days age	At 365 days age
II`		At $\sigma_{co}(un) = 0.3f_c$ From 56 to 345 days age	At 365 days age
II"	At 28 days age*	At $\sigma_{co}(un) = 0.3f_c$ From 56 to 345 days age	At 365 days age
III		Without loading	At 365 days age
III`	At 28 days age*	Without loading	At 365 days age

* Before applying of NSM strengthening.
P_D: Service design load, f_c: Concrete compressive strength, σ_{co}: Concrete compression stress at top of mid-span section in beam, $\sigma_{co}(un)$: Concrete compression stress at top of mid-span section in un-strengthened beam.

The selected dimensions of all beams were the same: depth = 180 mm, width = 140 mm, total length = 2400 mm with supported length = 2100 mm, depth of tension steel = 146 mm, depth of compression steel = 26 mm. For the strengthened beams: depth of CFRP = 172 mm, bonded length of CFRP strips = 1800 mm. All beams were designed according to Eurocode 2 [100] and fib Bulletin 14 [12]. All beams had the same shear reinforcement, stirrups of 1ϕ6 mm@100 mm, which was designed to avoid shear failure. The details of the specimens' matrix for each series are described in the following sections. The strengthening materials are S&P CFRP strips and S&P 220 epoxy resin. The configuration and dimensions of grooves followed recommendations from fib Bulletin 14 [12], ACI Committee 440 [63] and the supplier instructions of strengthening materials [146]. According to fib Bulletin 14 [12], the clear edge distance ≥ 2 strip width, clear groove spacing ≥ 4 strip width. According to ACI Committee 440 [63], the groove width ≥ strip thickness + 3 mm, groove depth ≥ 1.5 strip depth.

The identification of the beams is as follows: the 1st letter indicates the series of beams (A = 1st series, B = 2nd series); the 2nd letter indicates the strengthening condition (R = un-strengthened, S = strengthened with single CFRP area, D = strengthened with Double CFRP areas, T = strengthened with triple CFRP areas) ;the following digit indicates the interior reinforcement details and curing period (1 = 2ϕ6 in compression, 2ϕ10 in tension and curing period of 12 days, 2 = 2ϕ10 in compression, 2ϕ16 in tension and curing period of 12 days, 3 = 2ϕ6 in compression, 2ϕ10 in tension and curing period of 28 days, 4 = 0 in compression, 2ϕ10 in tension and curing period of 28 days); the last letters indicate the loading condition (I, I`, II, II`, II", III and III` = long term test sequence according to Table 3.1; sh = short term loading; sh` = short term loading of beam strengthened after two loading/unloading cycles).

3.2.1 Series A

Series A divided into two similar groups, A1 and A2, of 5 beams each with target concrete strength of 25 MPa. The selected parameters to be studied in the first series of beams were CFRP area reflecting the effect of the CFRP stiffness and the ratio of tension steel reinforcement reflecting the effect of the tension reinforcement stiffness. Table 3.2 shows the test matrix of series A beams involving the tension steel reinforcement area, A_s, the compression steel reinforcement area, $A_{s'}$, the CFRP area, A_f, curing time and identification, ID, of beams in each group. The reinforcement and strengthening details of Series A are shown in Figure 3.1.

Table 3.2 Test matrix of series A beams.

Group of beams	$A_{s'}$, mm²	A_s, mm²	A_f, mm²	Curing time, days	ID of beams	
					Group A1	Group A2
AR1	2ϕ6 = 56.6	2ϕ10 = 157.1	0	12	AR1sh	AR1I
AS1	2ϕ6 = 56.6	2ϕ10 = 157.1	2 strips (1.4*10) = 28		AS1sh	AS1I
AD1	2ϕ6 = 56.6	2ϕ10 = 157.1	2 strips (2.8*10) = 56		AD1sh	AD1I
AR2	2ϕ10 = 157.1	2ϕ16 = 402.1	0		AR2sh	AR2I
AS2	2ϕ10 = 157.1	2ϕ16 = 402.1	2 strips (1.4*10) = 28		AS2sh	AS2I

Group A1 beams were prepared for short term tests under monotonic loading up to failure to investigate the flexural short term behavior. Group A2 beams were prepared for long term test under sustained loading to investigate the time dependent flexural behavior due to creep and shrinkage of constitutive materials. All beams of group A2

followed the loading sequence I described in Table 3.1. The applied sustained load was at σ_{co} equal 0.34*fc*.

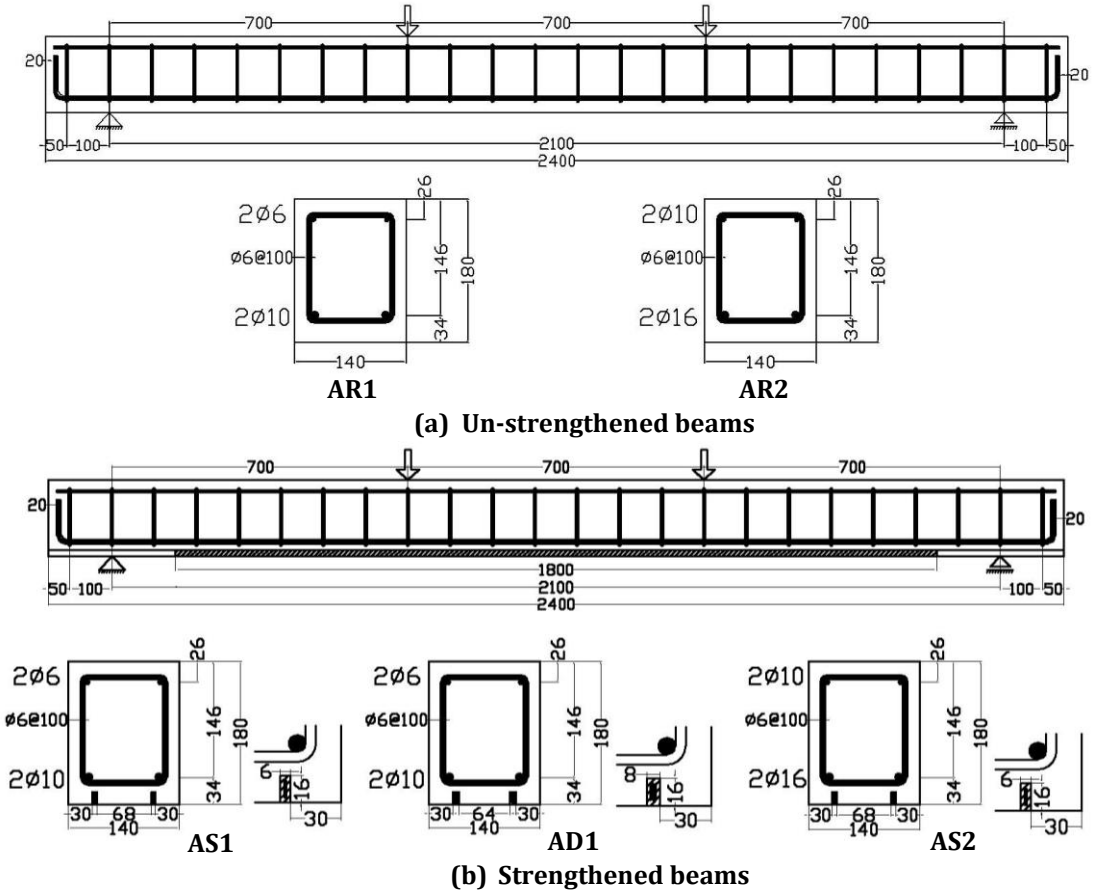

Figure 3.1 Reinforcement and strengthening details of series A beams.

Each group of beams included two reference RC beams with different tension steel reinforcement ratio (Area of steel/ (width of RC section ˣ depth of tension steel)). Beam AR1 had 0.77% tension steel ratio (2ϕ10 mm) and 0.28% compression steel ratio (2ϕ6 mm) and beam AR2 had 1.97% tension steel ratio (2ϕ16 mm) and 0.77% compression steel ratio (2ϕ10 mm), and included three NSM strengthened beams with CFRP strips. Two of strengthened beams had the same steel reinforcement of beam AR1, beam AS1 with two CFRP strips of 1.4 mm thickness and 10 mm width in two grooves of 16 mm depth and 6 mm width, and beam AD1 with two grooves with groove of 16 mm depth and 8 mm width and double CFRP area of beam AS1 with two bonded CFRP strips of the same dimensions in each groove. The third strengthened beam AS2 had the same steel reinforcement of beam AR2 and two CFRP strips of 1.4 mm thickness and 10 mm width in two grooves of 16 mm depth and 6 mm width. The edge distance of the grooves for all strengthened beams was 30 mm as shown in Figure 3.1.

The ratio between compression and tension steel was 0.36, the same for all beams, to eliminate its effect on long term behavior.

3.2.2 Series B

Series B was composed of eighteen beams with target concrete strength of 40 MPa. This series was divided into three groups notated as B1, B2 and B3 and presented in Table 3.3. The selected parameters to be studied in the second series of beams were concrete type, the ratio between compression and tension steel, level of sustained load, CFRP area reflecting the effect of the CFRP stiffness, loading sequence, ageing, the curing time of concrete and the previous shrinkage of concrete.

Table 3.3 shows the test matrix of series B beams indicating the tension steel reinforcement area, A_s, the compression steel reinforcement area, $A_{s'}$, the CFRP area, A_f, curing time and ID of beams in each group.

Table 3.3 Test matrix of series B beams.

Group of beams	$A_{s'}$, mm²	A_s, mm²	A_f, mm²	Curing time, days	ID of beams		
					Group B1	Group B2	Group B3
BR1	2ϕ6 = 56.6	2ϕ10 = 157.1	0	12		BR1I`	
BS1	2ϕ6 = 56.6	2ϕ10 = 157.1	2 strips (1.4*10) = 28			BS1I`	
BR3	2ϕ6 = 56.6	2ϕ10 = 157.1	0	28		BR3II	
					BR3sh	BR3II`	BR3III
BS3	2ϕ6 = 56.6	2ϕ10 = 157.1	2 strips (1.4*10) = 28	28		BS3II	
					BS3sh	BS3II`	BS3III
					BS3sh`	BS3II"	BS3III`
BT3	2ϕ6 = 56.6	2ϕ10 = 157.1	3 strips (2.8*10) = 84	28	BT3sh	BT3II`	BT3III
BR4	0	2ϕ10 = 157.1	0	28		BR4II`	
BS4	0	2ϕ10 = 157.1	2 strips (1.4*10) = 28	28		BS4II`	

The reinforcement and strengthening details of the second series are shown in Figure 3.2. All series B beams had 0.77% tension steel reinforcement ratio (2ϕ10 mm) and 0.28% compression steel reinforcement ratio (2ϕ6 mm) with ratio equal 0.36 of tension steel except beams BR4 and BS4 that did not have compression steel. All strengthened beams had two CFRP strips of 1.4 mm thickness and 10 mm width with groove dimensions of 16 mm depth and 6 mm width, and edge distance of 30 mm, except BT3 beams that had A_f equal to three times that of the other strengthened beams, to study the effect of CFRP area, and three CFRP strips of 2.8 mm thickness and 10 mm width with the same groove dimensions, and edge distance of 21 mm and inner distance between two grooves of 40 mm (Figure 3.2).

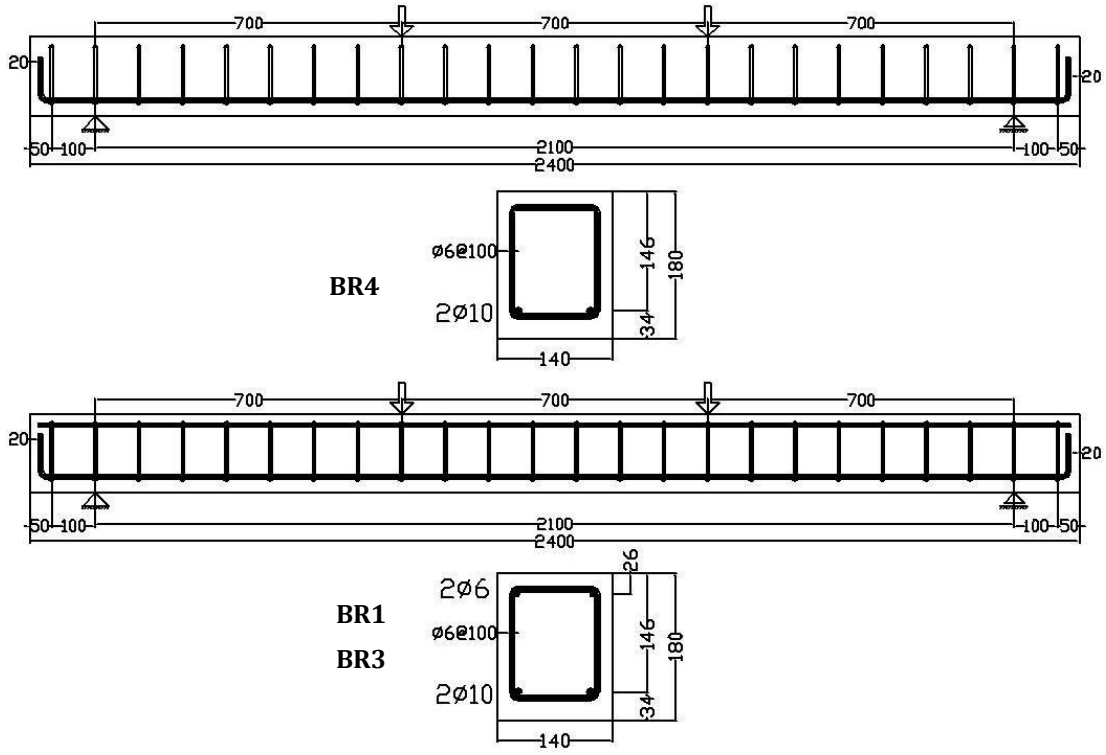

(a) Un-strengthened beams

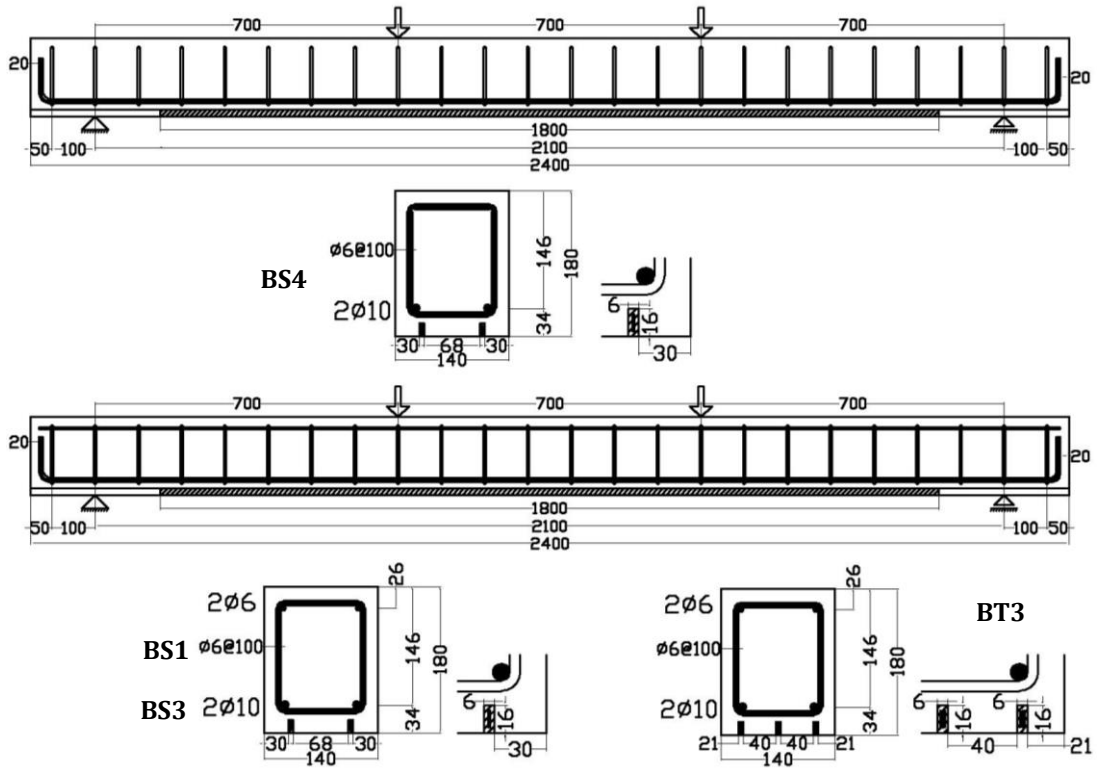

(b) Strengthened beams

Figure 3.2 Reinforcement and strengthening details of series B beams.

Beams BR1I` and BS1I` had a curing time of 12 days like series A beams to study the effect of the concrete type at similar conditions. The rest of series B beams had a curing period of 28 days.

Group B1 consisted of four beams, BR3sh, BS3sh, BS3sh` and BT3sh, prepared for short term tests under monotonic loading up to failure to investigate the flexural short term behavior.

Group B2 consisted of ten beams prepared for long term test under sustained loading to investigate the time dependent flexural behavior due to creep and shrinkage of constitutive materials. The sustained loads of the strengthened beams were taken equal to the sustained loads of their un-strengthened counterparts. The load level for all beams was chosen to obtain σ_{co} in the un-strengthened beams equal to $0.3f_c$, except for the beams of high level of loading that was taken equal to $0.4f_c$. The loading sequences of beams were sequence I` for beams BR1I` and BS1I`, sequence II for beams BR3II and BS3II, sequence II` for beams BR3II`, BS3II`, BT3II`, BR4II` and BS4II` and sequence II" for beam BS3II".

Group B3 consisted of four beams prepared to be kept without loading during the sustained loading of group B2 and to be tested under monotonic loading up to failure at the of the sustained loading period, to investigate the effect of the aging on the flexural short term behavior. The loading sequences were sequences III for beams BR3III, BS3III and BT3III and sequences III` for beam BS3III`. The details of the loading sequences are described in Table 3.1.

3.3 Fabrication of Beam Specimens

The fabrication of the beams consisted of two main stages. The first stage was a preparation of RC beams which included reinforcement, casting and curing. The second stage was the application of near surface mounted technique for the strengthened beams which included grooves, CFRP reinforcement and resin application and curing. The details of these stages are illustrated in the following sections.

3.3.1 RC beams preparation

3.3.1.1 Reinforcement cages

The reinforcement cages were prepared separately with the designed tension, compression and shear reinforcement as shown in Figure 3.3.

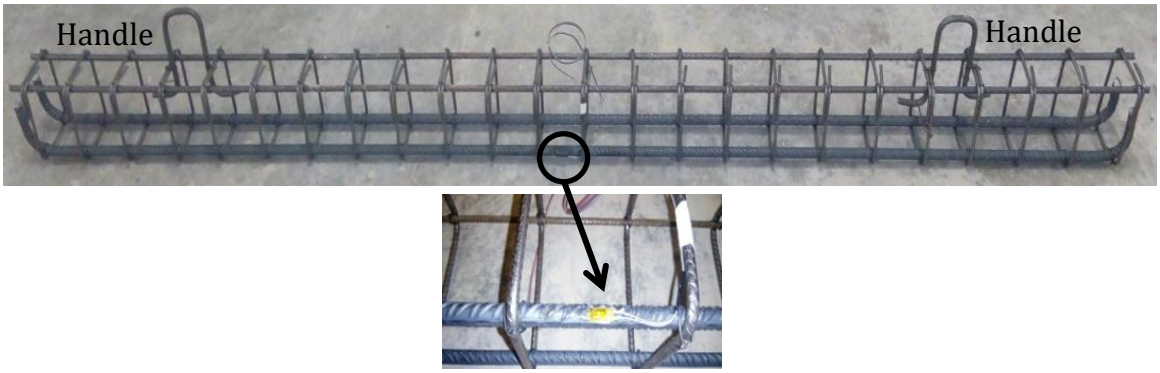

Figure 3.3 Steel reinforcement cage and instrumentation of tension steel strain gage.

All reinforcement elements were arranged carefully in each cage to achieve the designed dimensions. Two steel handles of 10 mm diameter were used to facilitate the handing of the beams, one handle at distance of 400 mm from each end of the beam. The mid-span strain gage of the tension steel for each cage was installed at one of the tension reinforcement bars and protected from humidity and alkalinity of concrete.

3.3.1.2 Molds preparation

The molds were prepared to accommodate the reinforcement cages, which were carefully placed inside the molds. Plastic spacers were used to allocate the reinforcement cage at the correct bottom and side distance from the molds as shown in Figure 3.4. Figure 3.5 shows the arrangement of the molds involving the reinforcement cages ready for casting. Steel cylinders with dimensions of 150 mm diameter and 300 mm height were prepared to cast the concrete cylinder for short term characterization as shown in Figure 3.6.

Figure 3.7 shows molds of concrete specimens for creep and shrinkage and its instrumentation. Cartoon cylinders with inside plastic cover of 150 mm inner diameter were used to manufacture the molds for the characterization specimens of concrete creep and shrinkage with height of 300 mm for shrinkage cylinders and 450 mm for creep cylinders. Wood molds of 180 mm depth, 140 mm width and 1000 mm length

were prepared to cast plain concrete prisms with the section of RC beams for shrinkage measuring.

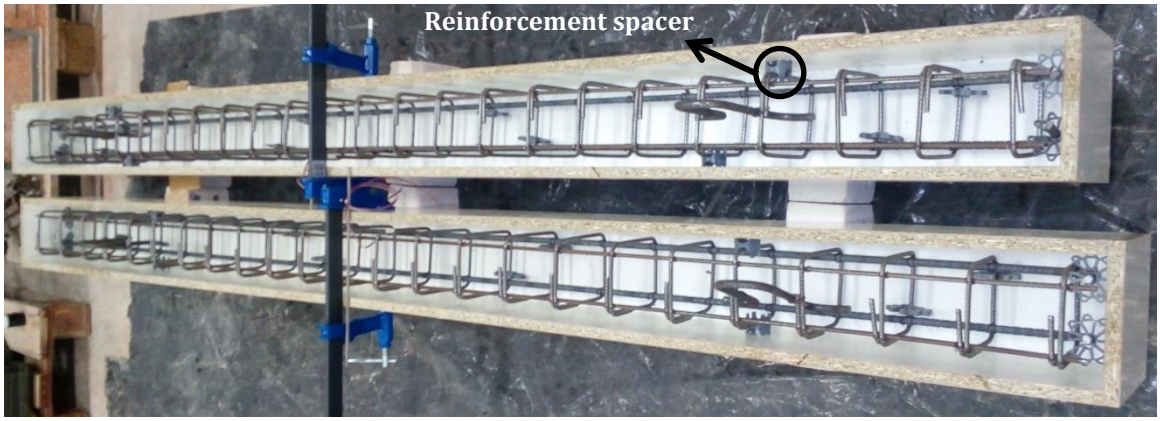

Figure 3.4 Installation of the steel reinforcement cages to the molds.

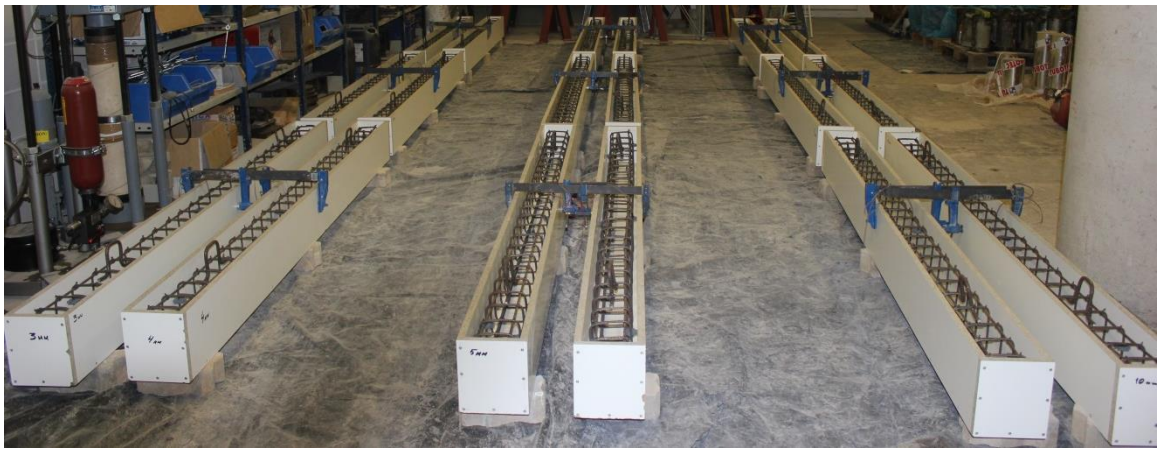

Figure 3.5 Arrangement of beams before casting.

Figure 3.6 Molds of concrete specimens for short term characterization.

Figure 3.7 Molds of concrete specimens for creep and shrinkage and their instrumentation.

3.3.1.1 Concrete casting and curing

The beams of each series were cast in the same batch together with several cylinders to determine the concrete mechanical properties. During the casting, the concrete was vibrated using mechanical vibrators. Just after casting, the top concrete surface was levelled. Figure 3.8 shows some of the specimens after casting and levelling. Beams and cylinders were demolded five days after casting.

Figure 3.8 Specimens after casting and levelling.

Figure 3.9 shows some of the specimens after demolding. All specimens were covered with plastic sheets after casting then with wet cotton and plastic sheets after demolding until the end of the curing period for each series. The curing period for series A was 12 days, while series B had two periods of curing, 12 days for two beams with their characterization specimens (short term cylinders, creep cylinders, shrinkage cylinders and shrinkage prism) and 28 days for the rest beams of the series with their characterization specimens. All beams and cylinders were kept in the same environmental conditions until testing.

Figure 3.9 Specimens after demolding.

3.3.2 NSM Strengthening

3.3.2.1 Formation of grooves

The grooves were formed in the concrete cover on the tension face using a saw cut electric machine with steel guide system as shown in Figure 3.10. Two grooves for each strengthened beam in series A were cut with 16 mm depth and two different widths, 6 mm for the groove of one strip 1.4 mm×10 mm and 8 mm for the groove with two bonded strips 1.4 mm ×10 mm with 30 mm edge distance. All grooves of the series B were cut with 16 mm depth and 6 mm width. The beams with two grooves had edge distance of 30 mm. The edge distance was 21 mm and the clear distance between two

grooves was 40 mm for the beams with three grooves which were strengthened with three strips of 2.8 mm×10mm.

Figure 3.10 Formation of grooves.

3.3.2.2 Installation of CFRP strips in the grooves

The CFRP strips were installed after at least ten days from the end of concrete curing to avoid the possible effect of humidity on the adhesive epoxy behavior. Compressed air was used to clean the grooves at the age of strengthening and the rest of the concrete surface was covered by plastic tapes as shown in Figure 3.11.

Figure 3.11 Installation of CFRP strips in the grooves.

The CFRP laminates were cut with lengths of 1800 mm plus 30 mm for each end to measure the end slip and cleaned by acetone. One of CFRP strips in each strengthened beam was instrumented using four strain gages along half of its length. The two components epoxy adhesive was mixed and the grooves were filled with it. The epoxy adhesive was applied on the faces of the CFRP laminates along the selected bonded

length 1800 mm and the CFRP laminates were centered longitudinally and transversally and introduced into the grooves achieving the designed depth of the strips. The strengthened faces were levelled, and the excess of epoxy adhesive was removed. The plastic tapes were removed after levelling of the adhesive as shown in Figure 3.11 and the beams were kept in the same environmental conditions at least ten days before any test to cure the epoxy. The strengthening was applied 10 days after the end of concrete curing to avoid the possible effect of concrete surface humidity on the resin.

3.4 Instrumentation and Test Setup

The instrumentation of the beams under short term and long-term tests is shown in Figure 3.12. All beams were simply supported over a span of 2100 mm and tested under four-point bending at third point. A preformed crack of 16 mm depth was cut using a saw cut electric machine at mid span section along the beam width for all beams to ensure the cracking of this section and measure the crack width. For the strengthened beams, this preformed crack was cut before strengthening.

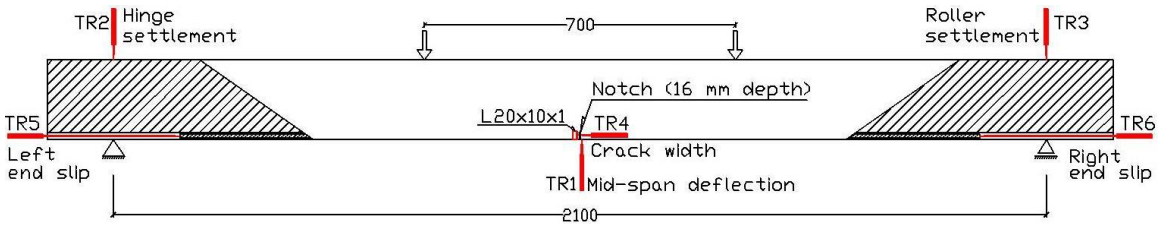

(a) Displacement transducers.

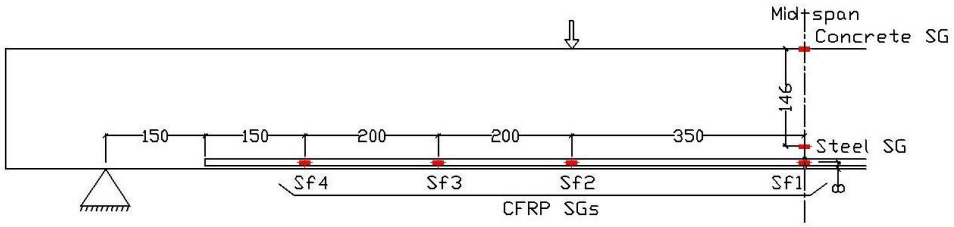

(b) Strain gages.

Figure 3.12 Schematic diagram of displacement transducers and strain gages instrumentation.

3.4.1 Monitoring of displacement and strains

The distribution of displacement transducers is shown in Figure 3.12a. The instrumented transducers for all beams were as follow: one transducer (TR1) to measure the mid span deflection, two transducers (TR2 and TR3) to measure the

supports' settlements and one transducer (TR4) to measure the crack width. An aluminum angle (L20×10×1) was glued beside the preformed crack against TR4 to measure the crack width. Two transducers (TR5 and TR6) were used for the strengthened beams to measure the end slip of the CFRP strip.

The distribution of the strain gages is shown in Figure 3.12b. Two strain gages were used at the mid-span section for all beams, one to measure the concrete strain at the top (Concrete SG) and another gage to measure the tension steel strain (Steel SG). Four more strain gages were used to measure the longitudinal strains in the CFRP strip, one at mid span (Sf1), one at loading point (Sf2) and the other two placed at every 200 mm from loading point (Sf3 and Sf4).

3.4.2 Loads application

A servo-controlled hydraulic jack with a capacity of 300 kN with a steel spreader beam to transmit the load to two rollers located at 700 mm from the beam supports, was used for all short term flexural tests as shown in Figure 3.13.

Figure 3.13 Setup and instrumentations of short-term test.

The loads were applied in displacement control mode at a displacement rate of 0.6 mm/min. The sustained loads were applied using designed steel frames and attaching two lots of concrete blocks 700 mm apart and at 700 mm distance from each beam support, each

concrete block weights almost 30 kg, as shown Figure 3.14. The sustained loads were applied slowly with hydraulic cranes to achieve the static loading rate.

Figure 3.14 Setup and instrumentation of sustained loading test.

The applied service design loads, P_D, and the applied sustained loads, P_s, were calculated using Eurocode 2004 [100] and fib bulletin 14 [12] and their values are listed in Table 3.4. The target values of the instantaneous concrete stress, σ_{co}, at the top of mid-span section of each beam are also listed in Table 3.4.

3.5 Materials Characterization

The short-term mechanical properties of concrete, steel bars, CFRP strips and adhesive material were obtained using standardized methods. The mechanical properties under sustained loading of concrete, CFRP strips and adhesive material were also experimentally determined using standardized methods. The residual mechanical properties of concrete and adhesive material after the sustained loading were experimentally determined, as well. These tests and a discussion of the results are presented in this chapter.

Table 3.4 Applied loads for beams of group A2 and group B2.

	Beam ID	P_D, kN	P_s, kN	σ_{co}, MPa
Group A2 from series A	AR1I	19.87	12.40	11.25 (0.340f_c)
	AS1I	31.17	13.62	11.25 (0.340f_c)
	AD1I	37.67	14.71	11.25 (0.340f_c)
	AR2I	45.15	18.16	11.25 (0.340f_c)
	AS2I	51.58	18.74	11.25 (0.340f_c)
Group B2 from series B	BR1I'	20.31	14.19	12.83 (0.300f_c)
	BS1I'	35.25	14.19	11.72 (0.274f_c)
	BR3II	0	18.93	17.11 (0.400f_c)
	BR3II'	0	14.19	12.83 (0.300f_c)
	BS3II	0	18.93	15.61 (0.365f_c)
	BS3II'	0	14.19	11.72 (0.274f_c)
	BS3II"	20.31*	14.19	11.72 (0.274f_c)
	BT3II'	0	14.19	10.24 (0.240f_c)
	BR4II'	0	13.87	12.83 (0.300f_c)
	BS4II'	0	13.87	11.74 (0.275f_c)

* This beam was subjected to this load at the end of curing time, 28 days concrete age, before applying of NSM strengthening.
P_D: The applied service design load, P_s: the applied sustained load, σ_{co}: The target values of the instantaneous concrete stress.

3.5.1 Concrete

Two different concrete grades were used, one for each series of beams with target characteristic compressive strength, f_{ck} of 25 MPa for the first series and 40 MPa for the second series. All concrete mixtures were obtained from a local ready-mix company. The characterization specimens were prepared according to the selected standard method for each characterization test and kept in the same exposure conditions of temperature and humidity until testing for each series of beams. The details and results of each test and its discussion are presented in the next sections.

3.5.1.1 Short term

Two groups of concrete cylindrical specimens (Ø = 150 mm, L = 300 mm) were cast from the same batch of each series to determine the short-term mechanical properties and residual mechanical properties after the sustained loading. From these cylinders, the compressive strength f_c, compressive modulus of elasticity E_c and tensile strength f_{ct} were tested. The tests were carried out at the laboratory of structures of the University of Girona. The equipment used to perform these tests was a universal SERVOSIS MUE-60 model with a capacity of 600 kN.

The compressive strength f_c was determined from cylindrical specimens. The compressive strength was determined according to UNE-EN 12390-3 Standard [147], testing the specimens at the same temperature and humidity conditions as the beam specimens.

The modulus of elasticity of concrete E_c is one of the main parameters affecting the flexural behavior of RC beams since it is directly related to the stiffness. With the purpose of accurately determining E_c, each of the tested cylindrical specimens was instrumented with three strain gauges located at 120°. The test was carried out following ASTM C 469-87 Standard [148]. The procedure consists of performing three cycles of compressive loading up to a value of 40% of the compressive strength. The modulus of elasticity is evaluated as the mean value of the last two cycles of loading, using the following expression:

$$E_c = \frac{\sigma_2 - \sigma_1}{\varepsilon_2 - \varepsilon_1} \tag{3.1}$$

where ε_1 has a value of 50x10^{-6}, ε_2 is the corresponding strain to 40% of the concrete strength, and σ_1 and σ_2 are the stresses corresponding to the previous strains.

The tensile strength f_{ct} is the concrete mechanical property that presents the largest scatter of values. It is influenced by the superficial shape and structure of aggregates and can be substantially reduced by environmental effects [99,149]. Different definitions for the tensile strength can be distinguished: the axial tensile strength (the tensile strength of a specimen subjected to an axial stress), the flexural tensile strength (that of a specimen subjected to a flexural stress) or the splitting tensile strength (derived from the well-known Brazilian test).

In this work, the concrete tensile strength was determined by splitting tensile tests on cylindrical specimens. The splitting tensile strength $f_{ct,sp}$ was tested according to UNE-EN 12390-6 Standard [150], at the same temperature and humidity conditions that the beam specimens were tested. Its value was transformed to the tensile strength f_{ct} following Model Code 2010 [99] formulation:

$$f_{ct} = \alpha_{sp} \cdot f_{ct,sp} \tag{3.2}$$

where $\alpha_{sp} = 1$.

For series A, eighteen concrete cylindrical specimens (150x300 mm) were cast from the same concrete batch of the series. These cylinders were divided into two groups

with nine cylinders for each to determine the mechanical properties before and after the sustained loading of beams.

For series B, thirty-six concrete cylindrical specimens (150x300 mm) were cast from the same batch of the series, eighteen for each curing period of 12 days and 28 days. For each curing period, nine cylinders were tested before the sustained loading of beams and nine cylinders were tested after the sustained loading of beams.

The concrete characterization tests were carried out at the age of 48 days before the sustained loading of beams and 365 days after the sustained loading of beams. The mean values of the concrete mechanical properties deduced from the cylindrical specimens before and after the sustained loading are listed in Table 3.5.

Table 3.5 Mean values of the concrete properties.

Property	Before the sustained loading			After the sustained loading		
	Series A	Series B 12 days curing	Series B 28 days curing	Series A	Series B 12 days curing	Series B 28 days curing
f_c, MPa	33.00	37.85	42.77	36.00	37.44	36.83
E_c, GPa	30.00	28.81	29.12	31.00	24.04	24.47
f_{ct}, MPa	2.91	2.55	3.25	2.44	2.54	2.44

3.5.1.2 Creep and shrinkage

In order to determine the creep coefficient of concrete according to ASTM C512-02 [151], for each mixture and each curing period, two concrete cylinders ($Ø$ = 150 mm, L = 450 mm) with embedded strain gauges were stacked in a loading frame with a constant pressure lower than 40% of the concrete compressive strength as shown in Figure 3.15.

The cylinders were loaded at the same time as the beams. One additional concrete cylinder (Ø = 150 mm, L = 300 mm) was left unloaded and was also instrumented to determine free shrinkage strain. A concrete prism of the same concrete beam section (140 mm*180 mm) and length of 1 m was left unloaded and was also instrumented to determine free shrinkage strain and to know the section shape effect on shrinkage. The molds of concrete specimens for creep and shrinkage and its instrumentation with the embedded strain gage are shown in Figure 3.7. The specimens of creep and shrinkage after demolding are shown in Figure 3.9.

Figure 3.15 Creep load application on the concrete creep cylinders.

The strains of shrinkage concrete cylinders and beam prisms were registered from the end of curing for each mixture to know the previous shrinkage strains before the application of loads. The concrete creep coefficient is evaluated using the following expressions,

$$\varphi(t,t_o) = \frac{\varepsilon_c(t,t_o)-\varepsilon_{cs}(t,t_o)-\varepsilon_{ci}(t_o)}{\varepsilon_{ci}(t_o)} \quad (3.3)$$

where t is the loading time, t_o is the concrete age at the start of loading, $\varphi(t,t_o)$ is the creep coefficient, $\varepsilon_c(t,t_o)$ is the total concrete strain, $\varepsilon_{cs}(t,t_o)$ is the concrete shrinkage strain and $\varepsilon_{ci}(t_o)$ is the instantaneous concrete strain. The temperature and relative humidity were registered from the cast day up to the end of all tests.

Figure 3.16a shows the previous shrinkage strain of concrete cylinder and prism, with curing period of 12 days, before the creep loading for series A. Figure 3.16b shows the registered temperature and relative humidity during this period.

The creep cylinders of series A were loaded at concrete age, t_o of 75 days with constant pressure of 9 MPa for loading time, t of 270 days. The average registered instantaneous concrete strain of the first series is 300 με. Figure 3.17a shows the concrete creep coefficient with time of two specimens and the average value for series A. Figure 3.17b shows the concrete shrinkage strain of concrete cylinder and prism during the creep loading. Figure 3.17c shows the registered temperature and relative humidity along the test.

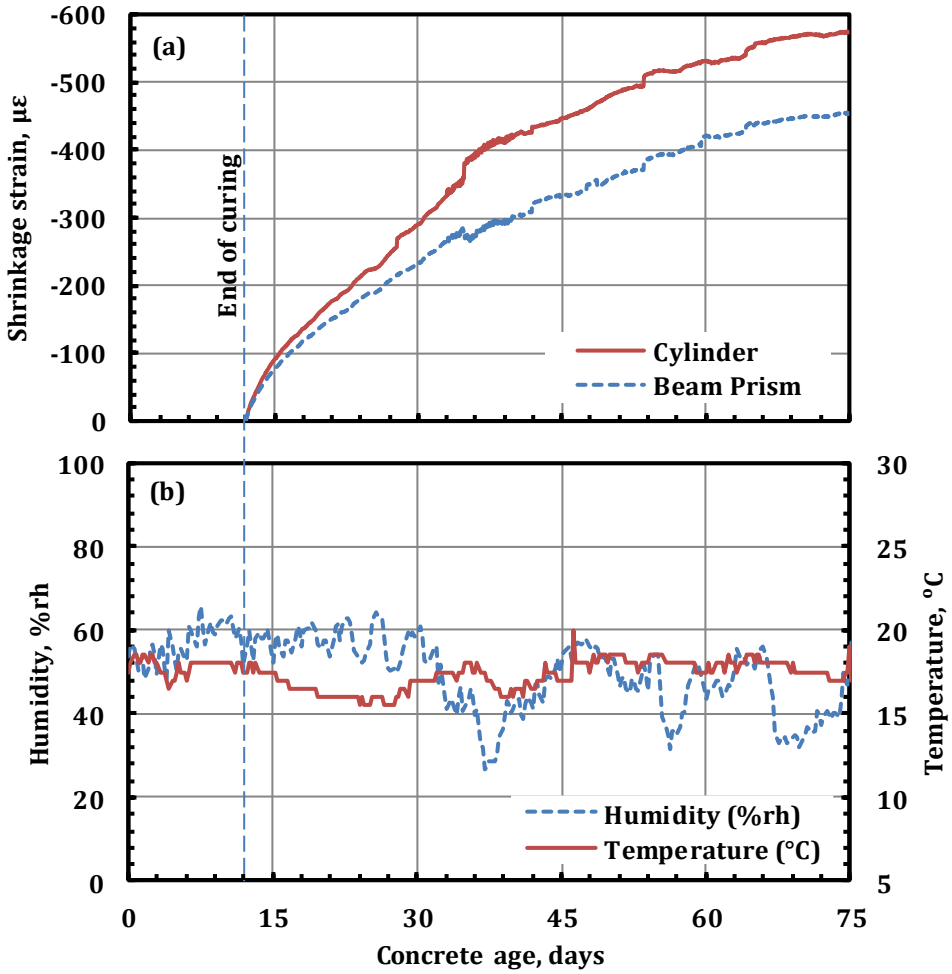

Figure 3.16 (a) Concrete shrinkage strain, and (b) Registered temperature and relative humidity, before loading for series A.

The creep cylinders of series B were loaded at concrete age, t_o of 56 days with constant pressure of 11 MPa for loading time, t of 290 days. The average registered instantaneous concrete strains of the second series are 439 με for the cylinders with 12 curing days and 433 με for the cylinders with 28 curing days.

Figure 3.18a shows the previous shrinkage strain of concrete cylinders and prisms, with curing period of 12 days (12d) and 28 days (28d), before the creep loading for series B. Figure 3.18b shows the registered temperature and relative humidity during this period.

Figure 3.19a shows the average values of concrete creep coefficient with time for series B with curing time of 12 days (12d) and 28 days (28d). Figure 3.19b shows the shrinkage strain of the concrete cylinders and prisms, with curing period of 12 days (12d) and 28 days (28d), during the creep loading of series B. Figure 3.19c shows the registered temperature and relative humidity along the test.

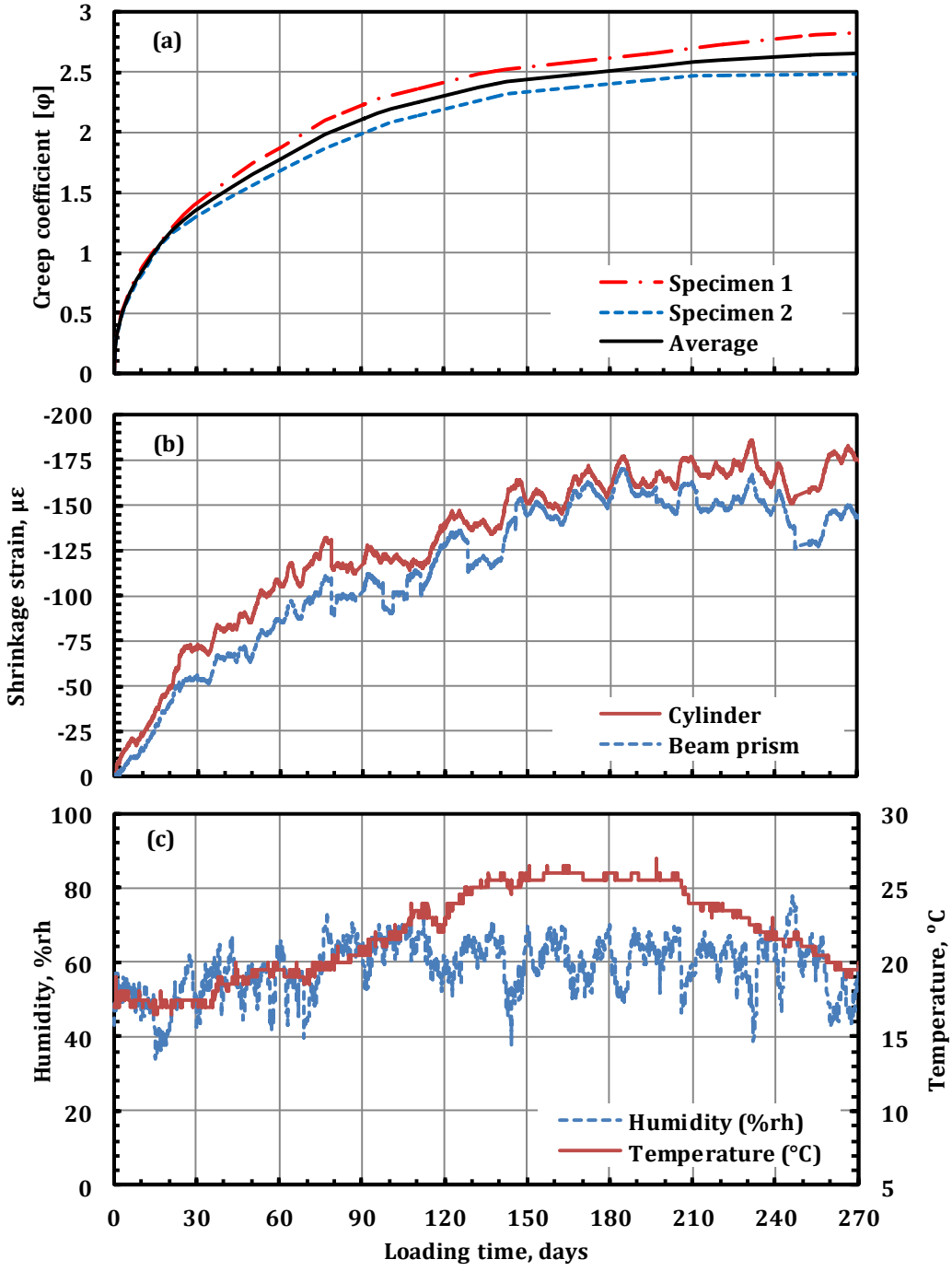

Figure 3.17 (a) Concrete creep coefficient, (b) Concrete shrinkage strain, and (c) Registered temperature and relative humidity, during the creep test time for series A.

3.5.2 Steel reinforcement

Tensile tests were carried out on specimens of steel bars according to the standard specifications UNE-EN ISO 15630-1 [152] to determine their yield strength, f_{ys}, ultimate strength, f_{us}, and elastic modulus, E_s. The mean values of obtained properties are summarized in Table 3.6.

Table 3.6 Mean values of steel tensile properties.

Bar Diameter, mm	E_s, GPa	f_{ys}, MPa)	f_{us}, MPa
6	205	515	620
10	205	515	620
16	205	515	620

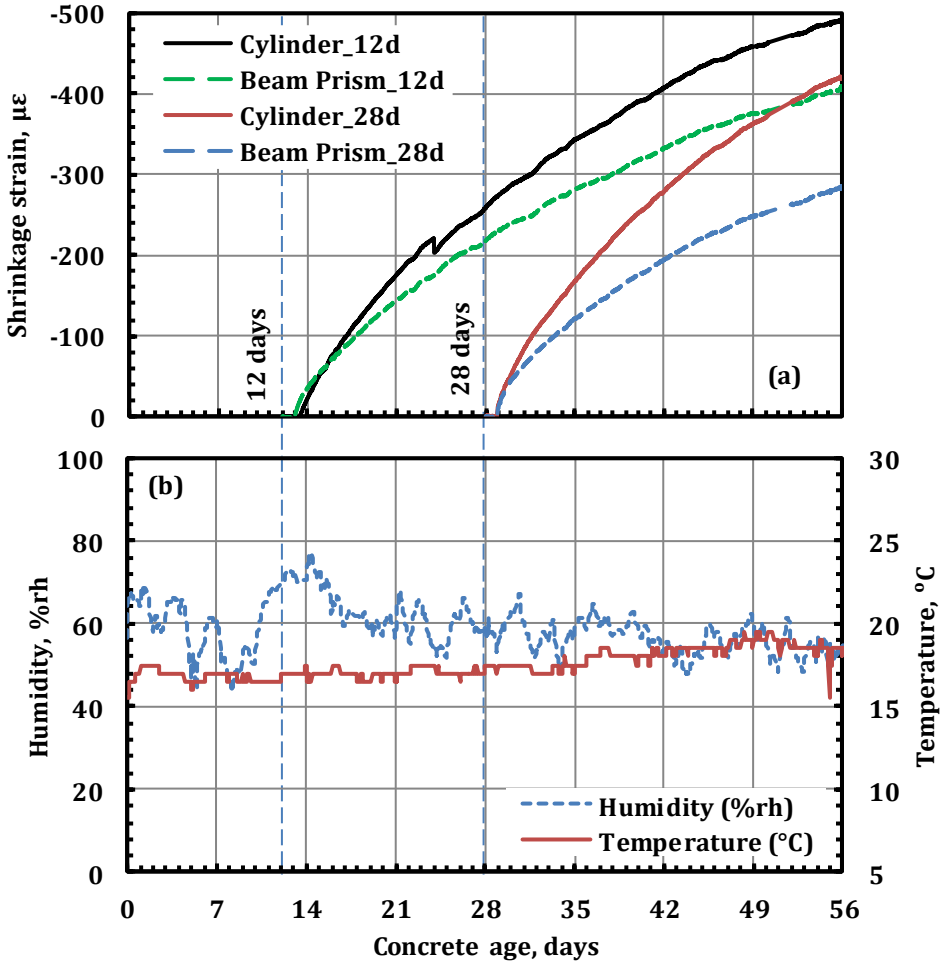

Figure 3.18 (a) Concrete shrinkage strain, and (b) Registered temperature and relative humidity, before loading for series B.

3.5.3 CFRP reinforcement

Two thicknesses of S&P CFRP strips, 1.4 mm (Type 1) and 2.8 mm (type 2), with the same width of 10 mm were used as strengthening reinforcement. For the characterization of the used CFRP strips, specimens were prepared according to the selected standard method for each characterization test. The details and results of each test and its discussion are presented next.

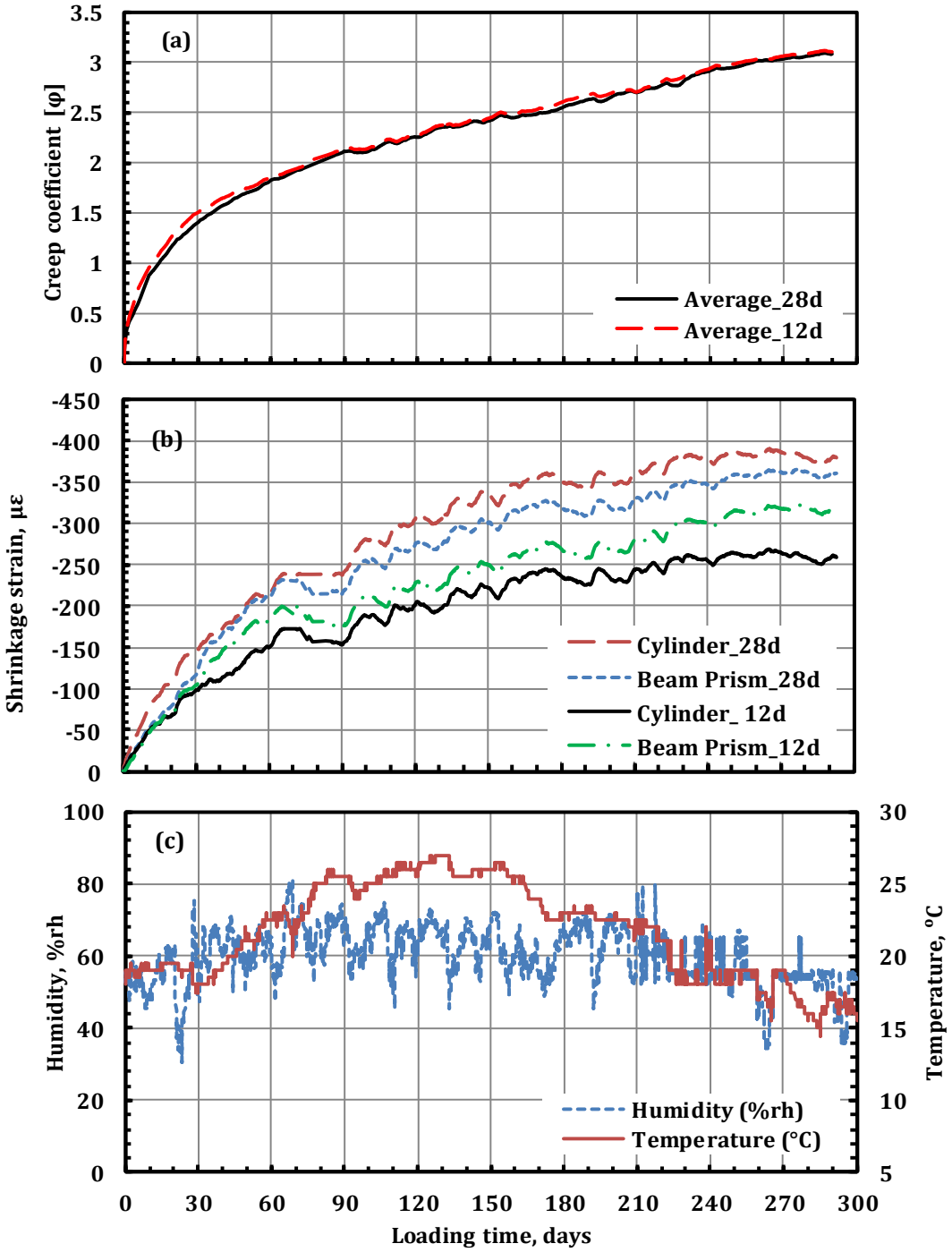

Figure 3.19 (a) Concrete creep coefficient, (b) Concrete shrinkage strain, and (c) Registered temperature and relative humidity, during the creep test time for series B.

3.5.3.1 Short term tensile of CFRP strips

The short term mechanical properties of the CFRP strips under tensile loading were tested following ASTM D7565/D7565M [153] standard. Five specimens were tested for each thickness with gage length of 100 mm. Two longitudinal stain gages were installed on each specimen.

Plastic tapes were glued to the ends of each specimen with the proper adhesive to avoid the friction effects of machine grips as shown in Figure 3.20a. The tensile tests were performed in a universal testing machine with displacement control at a loading rate of 2 mm/min. The typical mode of failure is shown in Figure 3.20b. The calculated mechanical tensile properties are the ultimate tensile strength, $f_{f,u}$ in MPa, the modulus of elasticity, E_f in GPa and the ultimate tensile strain, $\varepsilon_{f,u}$ in με. The mean values of the tensile mechanical properties for the two types are listed in Table 3.7.

(a) CFRP specimen end **(b) CFRP failure mode**

Figure 3.20 Tensile characterization of CFRP strips.

Table 3.7 Mean values of CFRP strips tensile properties.

Property	Type 1 (1.4 mm thickness)	Type 2 (2.8 mm thickness)
$f_{f,u}$, MPa	2434.54	2004.16
E_f, GPa	160.90	158.25
$\varepsilon_{f,u}$, με	1509.47	1267.34

3.5.3.2 Tensile creep of CFRP strips

In order to monitor the time dependent deformation of the CFRP strips under sustained loading, two specimens from the type 1 (1.4 mm thickness) with gage length of 1 m were subjected to constant tensile stress of 48.5% of its ultimate tensile strength for 360 days under the same environmental conditions as the tested RC

beams. Two longitudinal stain gages were installed on each specimen. A special cantilever arm device with steel weights and special grips was used. Figure 3.21 shows the total strains of two CFRP strips with time under tensile creep loading with instantaneous strain of 7270 με.

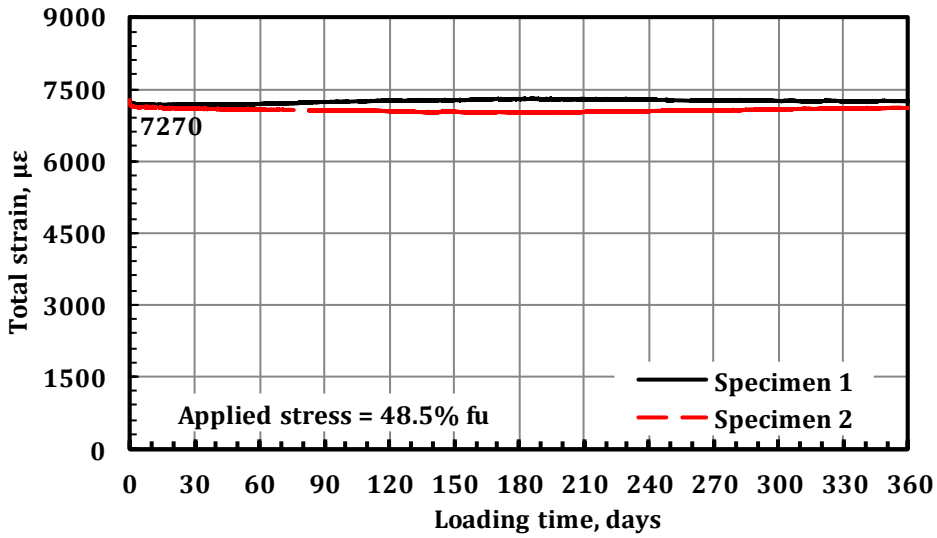

Figure 3.21 Total strain of CFRP strips under tensile creep loading.

3.5.4 Epoxy adhesive material

The S&P 220 resin, used to bond S&P CFRP strips, is the commercially produced solvent-free, thixotropic two component epoxy resin adhesive chosen in this study. According to the manufacturer datasheet [154], the package contained component A (a light grey-colored resin) and component B (a black colored hardener). Component A contains 5% to 10% Neopentyl glycol diglycidyl ether and 20% to 25% Bisphenol A, while component B has 1% to 2.5% Piperazine, 20% to 25% Triethylenetetramine, 3.6% Diazaoctanethylenediamin and 20% to 25% Poly (oxypropylene) diamine. Both components should be mixed slowly, in a proportion of 4A:1B (by weight), until a uniformly grey color (without any streaks) is obtained.

Twelve doge-bone shaped specimens of resin were fabricated in accordance with ISO 527-2 [155] at the same time of the strengthening of series B beams. The resin was casted in PTFE molds with base plates of aluminum and transparent plastic sheets to avoid the adhesion between the aluminum and the epoxy. The molds were painted with Vaseline cream to facilitate the demolding process. Each mold was covered with a transparent plastic sheet after filling the mold with resin and rolled with a heavy

smooth steel roller to get flat surface. After one day the specimens were demolded and kept for curing in the same environmental conditions of tested RC beams up to the test time. Figure 3.22 shows the resin specimen shape and its designed dimensions.

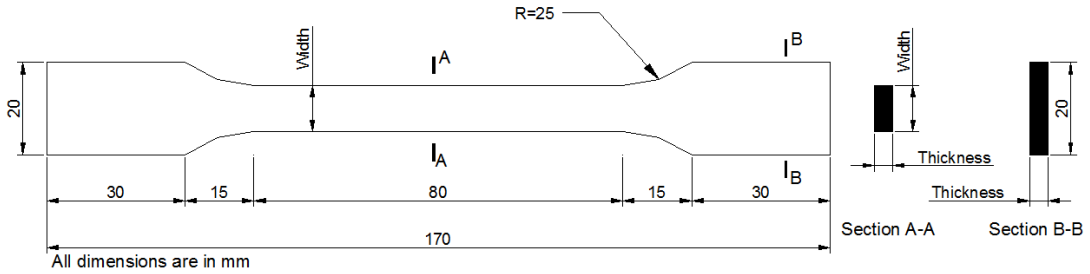

Figure 3.22 Resin specimen.

Figure 3.23 shows the resin casting molds and specimens after demolding. Eleven of the fabricated specimens were used in tensile short term and long-term characterization tests. Each specimen was instrumented with two longitudinal strain gauges glued onto the center of each face.

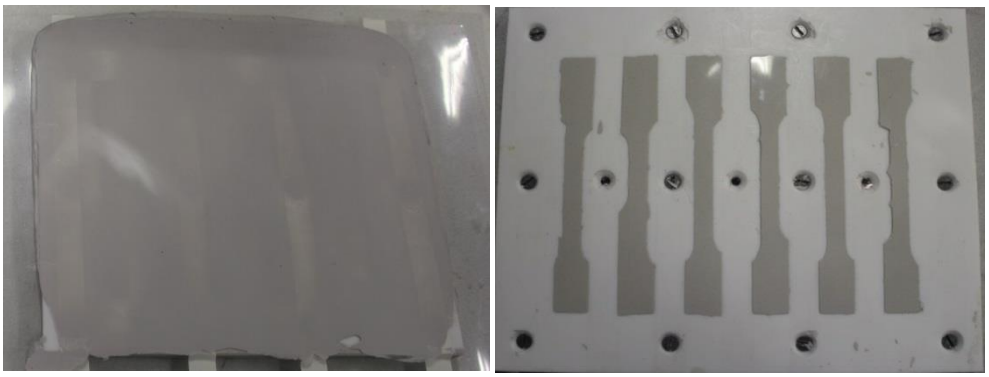

(a) Specimens casting **(b) Specimens demolding**

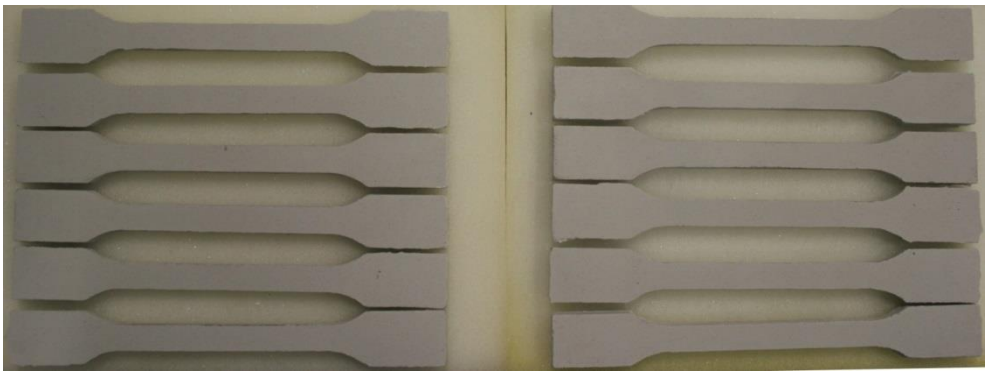

(c) Specimens after demolding

Figure 3.23 Fabrication of resin specimens.

The width and thickness of the tested specimens were measured at three different positions to determine their average cross section. The average cross section measured dimensions are presented in Table 3.8 with the purpose of each test. The details and results of each test and its discussions are presented next.

Table 3.8 Cross section dimensions of the resin specimens.

Characterization test	Specimen ID	*Thickness, mm*	*Width, mm*
Tensile before sustained loading	Specimen 1	5.17	10.50
	Specimen 2	5.28	10.08
	Specimen 2	5.05	10.28
Tensile after ageing	Aged_1	5.13	10.30
	Aged_2	5.13	10.17
Creep and tensile after sustained loading	20%_1	5.03	9.73
	20%_2	5.05	9.97
	40%_1	5.03	10.23
	40%_2	5.07	10.00
	60%_1*	5.20	9.95
	60%_2*	5.10	9.97

* These two specimens failed after 7.8 hours of sustained loading.

3.5.4.1 Short term tensile test of adhesive material

Short term tensile tests were carried out according to ISO 527-1 specifications [156] to determine the tensile strength, $f_{a,u}$ and modulus of elasticity, E_a of the adhesive and ultimate tensile strain, $\varepsilon_{a,u}$. Three specimens (specimen1, specimen 2, and specimen 3) were tested before the sustained loading at age of 14 days. After sustained loading of 290 days, the ageing and creep specimens were tested under monotonic tensile loading up to failure to know the effect of sustained loading and ageing effects on the residual tensile properties. The specimens, which were tested after sustained loading, were two aged (Aged_1 and Aged_2), two previously loaded by 20% of $f_{a,u}$ (20%_1 and 20%_2) and two previously loaded by 40% of $f_{a,u}$ (20%_1 and 20%_2). The tensile tests were performed in a universal testing machine with displacement control at a loading rate of 1 mm/min as shown in Figure 3.24a. Axial tensile extensometer of 25 mm gage length was instrumented beside the strain gages as shown in Figure 3.24b. The observed typical mode of failure is presented in Figure 3.24c.The load and longitudinal strains were registered during the test and tensile stress-strain curves were obtained.

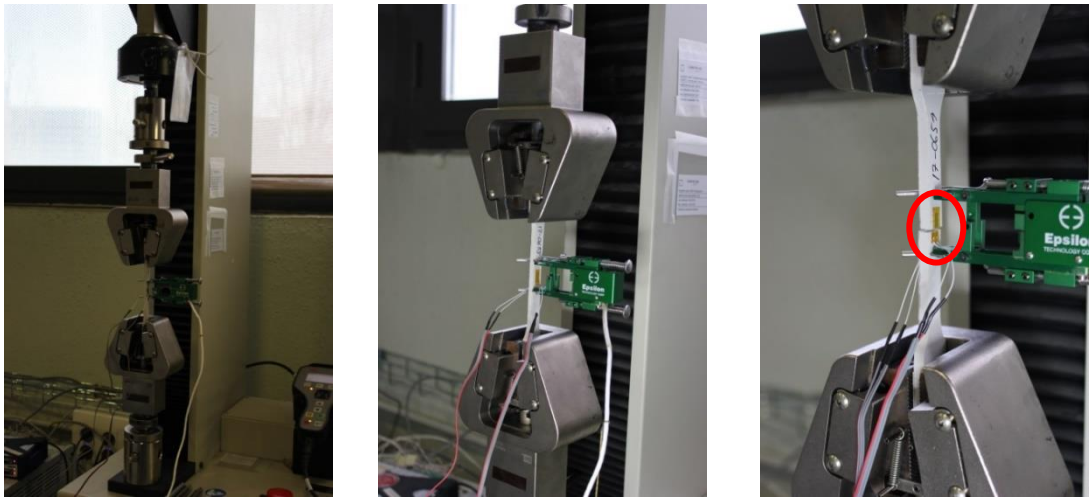

(a) Tensile machine (b) Test setup and instrumentation (c) Failure mode

Figure 3.24 Short term tensile test of S&P220 resin: Setup, instrumentations and failure mode.

The tensile stress in MPa versus tensile strain in με curves before and after sustained loading are presented in Figure 3.25 and Figure 3.26, respectively.

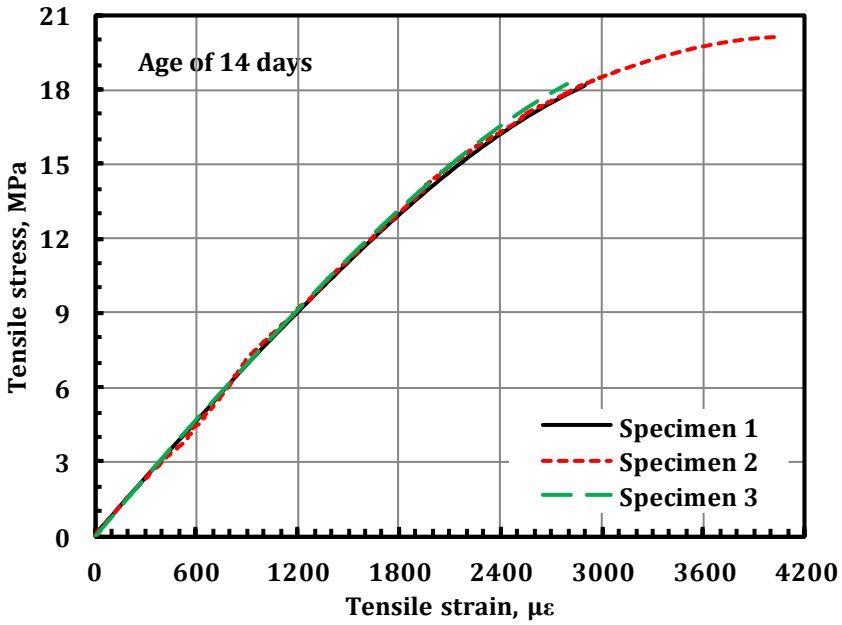

Figure 3.25 Stress – strain curves of S&P 220 resin specimens at 14 days age.

The mean values of adhesive tensile properties before and after sustained loading are listed in Table 3.9. The modulus of elasticity was calculated, according to ISO 527-1 [156], as the slope of the secant line in the stress-strain diagram between 0.05% and 0.25% strains. The resin specimens of 40% $f_{a,u}$ sustained load did not arrive at 0.25% strain. Therefore, the slope of the secant line in the stress-strain diagram between

0.05% and 0.15% strains was calculated and reported in Table 3.9 as $E_{a,\varepsilon=0.15\%}$ to know the change of resin stiffness.

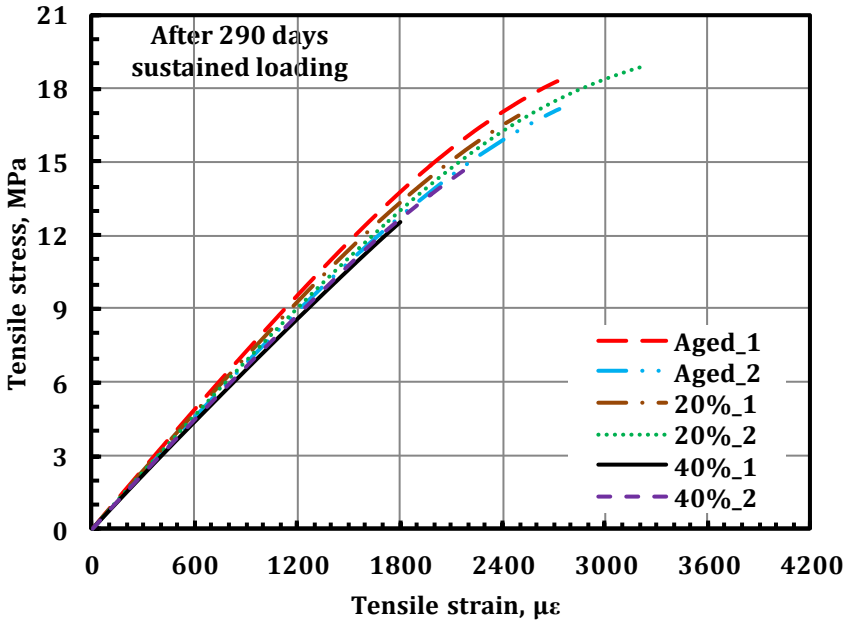

Figure 3.26 Residual stress – strain curves of S&P 220 resin specimens after 290 days sustained loading.

It can be seen that the ageing of resin, as the sustained loading with 20%$f_{a,u}$, reduced the ultimate tensile strength and strain while the stiffness did not have a noticeable change. This means that the free strain due to shrinkage, temperature and relative humidity, was more effective than creep of 20%$f_{a,u}$ sustained loading on the tensile properties of this resin. The decrease in the ultimate tensile strength and strain of 40%$f_{a,u}$ specimens was higher than the others and the stiffness had a noticeable decrease.

Table 3.9 Mean values of the adhesive tensile properties.

Property	Before the sustained loading	After the sustained loading		
		Aged	*20% $f_{a,u}$*	*40% $f_{a,u}$*
$f_{a,u}$ (MPa)	19.50	18.39	19.12	14.17
E_a (MPa)	6501	6463	6431	-----*
$E_{a,\varepsilon=0.15\%}$ (MPa)	7298	7352	7299	6972
$\varepsilon_{a,u}$(με)	3250	2727	3053	2017

* These specimens were failed at maximum strain below 0.25%.

3.5.4.2 Tensile creep of adhesive material

Six of the fabricated resin dog-bone shaped specimens were used for the tensile creep tests. Tests were carried out in the same environmental condition of temperature and humidity for RC beams of series B and at the same time of sustained loading and unloading of the beams. Loads were applied using gravity loading systems with a multiplication factor of 4 as shown in Figure 3.27a. Setup and instrumentation of this test are shown in Figure 3.27b. The sustained loads were applied at resin age of 14 days and removed after 290 days at resin age of 306 days.

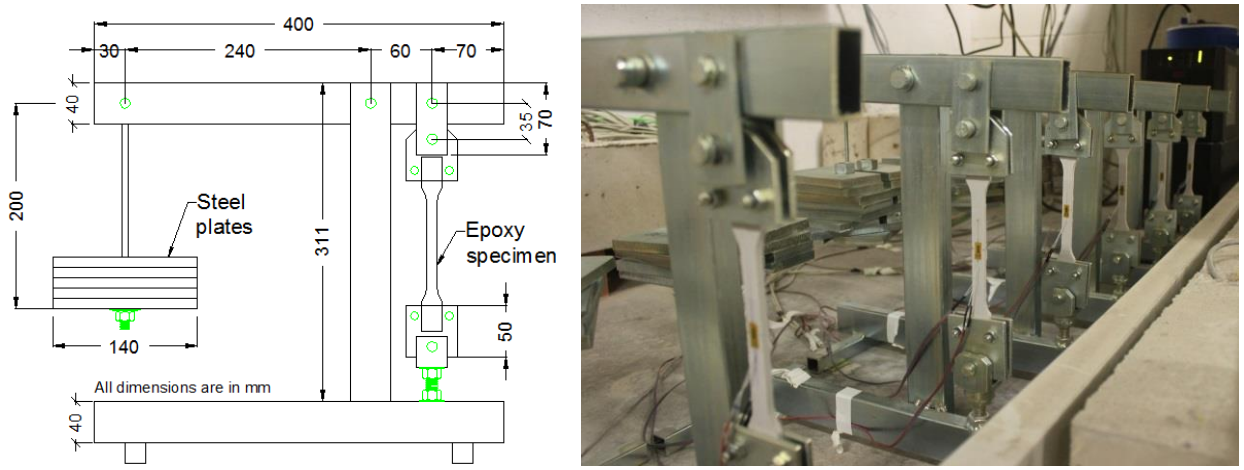

(a) Loading frame details **(b) Test setup and instrumentations**

Figure 3.27 Tensile creep test of resin: loading frame details and test setup and instrumentation.

The strain gauges were connected to an automatic acquisition system to register the longitudinal strain during the test period. The temperature and relative humidity were registered. Two resin specimens more were instrumented with longitudinal strain gages and left in the environmental conditions without loading for ageing and to register the free shrinkage.

The applied sustained load levels were 20%, 40% and 60% of the ultimate tensile strength, i.e. 3.9 MPa, 7.8 MPa and 11.7 MPa, respectively, which are similar to the applied load levels in the literature [96,115,157,158] and cover the linear part of the short-term stress-strain curve. The applied stress values and levels and the corresponding instantaneous strains are reported in Table 3.10. The tensile secant modulus of each specimen at instantaneous loading was calculated as ratio between the applied stress and its corresponding instantaneous strain and reported in Table 3.10 in MPa.

Table 3.10 Instantaneous values of the resin creep test.

Specimen ID	Applied stress, MPa ($\%f_{a,u}$)	Instantaneous strain, με	Secant modulus, MPa
20%_1	3.9 ($20\%f_{a,u}$)	530	7359
20%_2	3.9 ($20\%f_{a,u}$)	673	5795
40%_1	7.8 ($40\%f_{a,u}$)	1043	7478
40%_2	7.8 ($40\%f_{a,u}$)	1001	7792
60%_1*	11.7 ($60\%f_{a,u}$)	1648	7100
60%_2*	11.7 ($60\%f_{a,u}$)	1577	7419

* These specimens failed after a very short time (7.8 hours) from application of sustained loading.

The creep coefficient of each resin specimen is evaluated using the following expressions,

$$\boldsymbol{\varphi_r(t)} = \frac{\boldsymbol{\varepsilon_r(t) - \varepsilon_{free}(t) - \varepsilon_{r,i}}}{\boldsymbol{\varepsilon_{r,i}}} \quad (3.4)$$

where t = loading time, $\varphi_r(t)$ = creep coefficient of resin, $\varepsilon_r(t)$ = total strain of resin, $\varepsilon_{free}(t)$ = average free strain of the aged resin specimens and $\varepsilon_{r,i}$ = instantaneous strain of resin.

The total strains with time under the creep loading and after removing the creep load for the resin specimens of 20% and 40% stress level are presented in Figure 3.28a. The values of the instantaneous strains, $\varepsilon_{r,i}$ and strain after removing creep pressure, $\varepsilon_{r,a}$ are presented also on the same figure. Figure 3.28b shows the free strain of the aged resin specimens and its average values due to shrinkage, temperature and humidity along the creep test time.

The resin creep coefficients with time of the resin specimens of 20% and 40% stress level are presented in Figure 3.29a. The curves of 60% stress level are not presented in these figures because its specimens failed after a very short time (7.8 hours) from application of sustained loading with creep coefficients of 0.22 and 0.21 for 60%_1 and 60%_2 specimens, respectively. Figure 3.29b shows the registered temperature and relative humidity along the test.

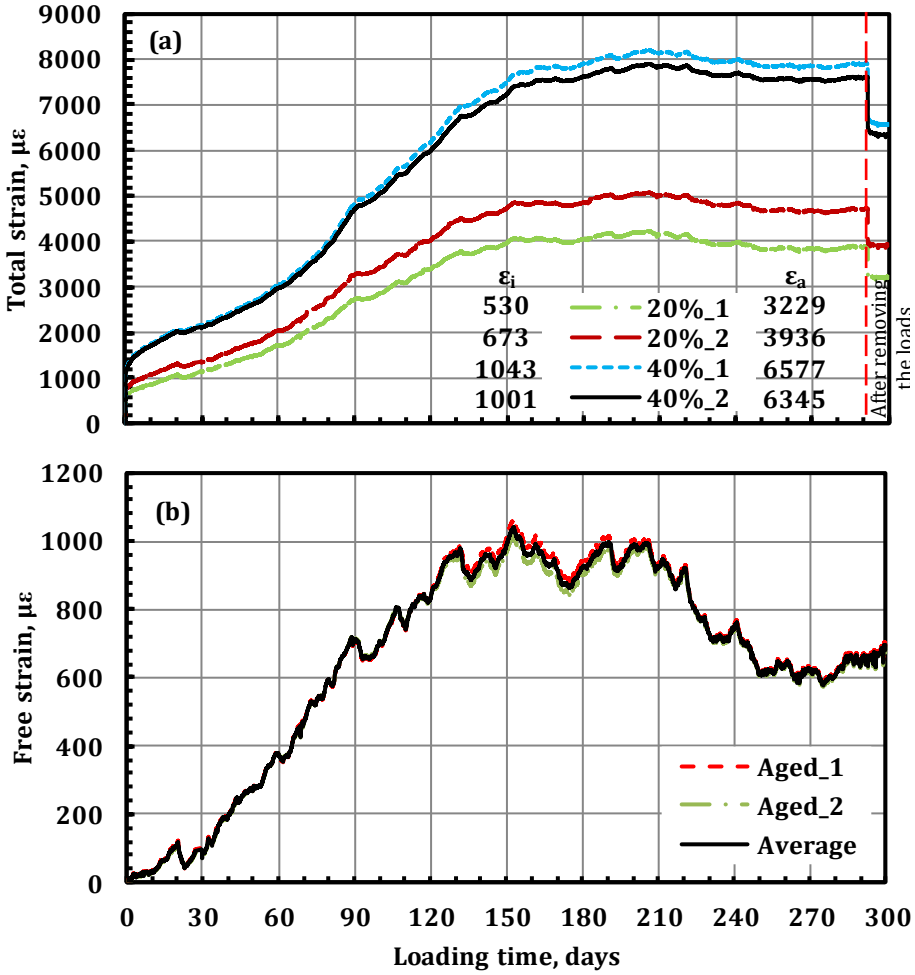

Figure 3.28 (a) Total tensile strain, and (b) Free strain, during the tensile creep test of resin.

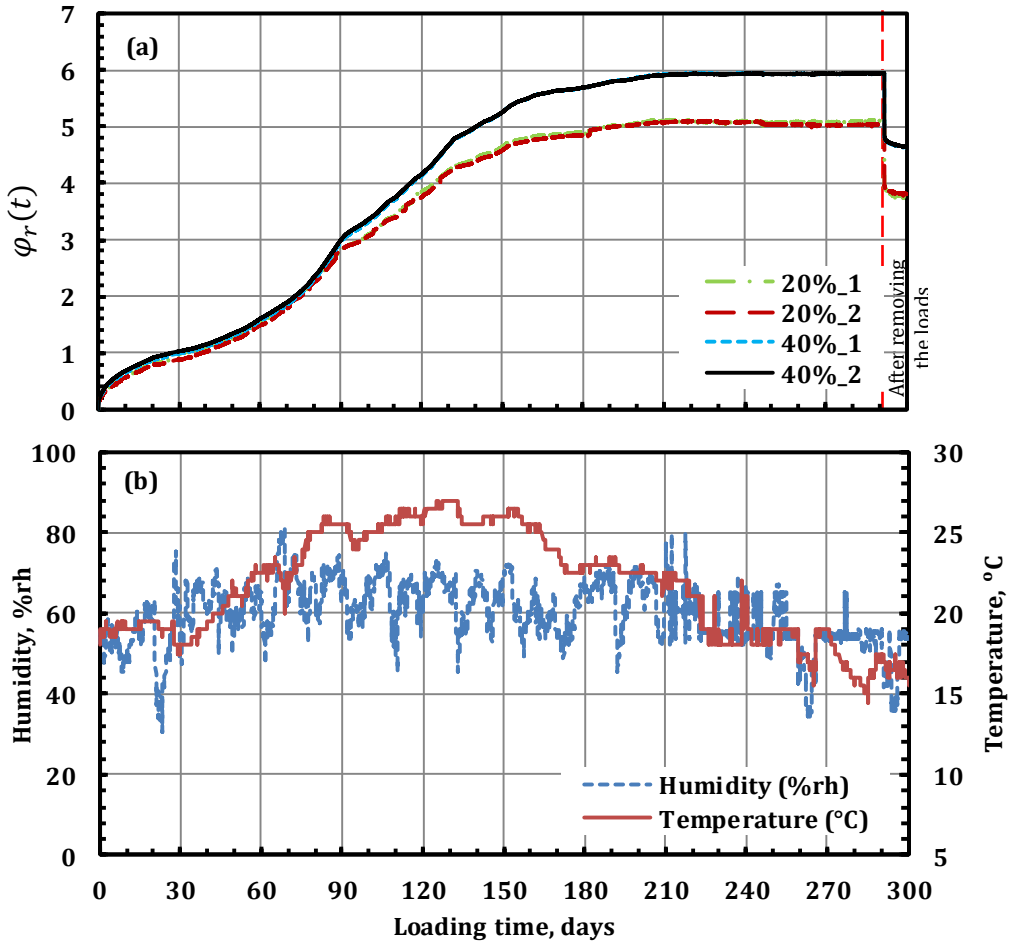

Figure 3.29 (a) Resin creep coefficient, and (b) Registered temperature and relative humidity, during the tensile creep test of resin.

CHAPTER 4 RESULTS AND DISCUSSION

4.1 Introduction

The significant experimental results of short-term flexural tests and sustained loading of all beams are presented and discussed in this chapter in detail.

4.2 Short Term Flexural Behavior

This section presents the experimental results and analysis of the short-term tests carried out on the beams of group A1 from series A and group B1 from series B. The tested parameters and the full details of these beams were described in CHAPTER 3. These beams were tested under flexural four points loading up to failure to investigate the short-term behavior. These beams involved un-strengthened beams and NSM strengthened RC beams with CFRP strips. The studied beams included different CFRP areas, tensile reinforcement ratios, concrete types and strengthening sequences. The presented experimental results are discussed in terms of load-deflection response, mode of failure, deformability and ductility indices, cracking behavior with load, strains variation of constitutive materials (steel, concrete and CFRP strips) and slip of CFRP strips with load of strengthened beams. The results of each series are presented and discussed in the following.

4.2.1 Un-strengthened beams

Three reference un-strengthened beams were investigated; two beams, AR1sh and AR2sh, from group A1 with concrete strength of 33 MPa and one beam, BR3sh, from group B1 with concrete strength of 42.77 MPa. The beams had different reinforcement ratios; tension steel ratio, ρ = 0.77% and compression steel ratio, ρ' = 0.28% in beams AR1sh and BR3sh and ρ = 1.97% and ρ' = 0.77% in beam AR2sh.

4.2.1.1 Load-deflection responses and failure modes

The load-deflection curves of the un-strengthened beams tested in groups A1 and B1 are presented in Figure 4.1. These curves show the applied load, P, in kN on the vertical axis as a function of the mid-span deflection, δ, in mm on the horizontal axis. The three

un-strengthened beams show three stages defined at their ends by cracking, yielding and failure points, respectively.

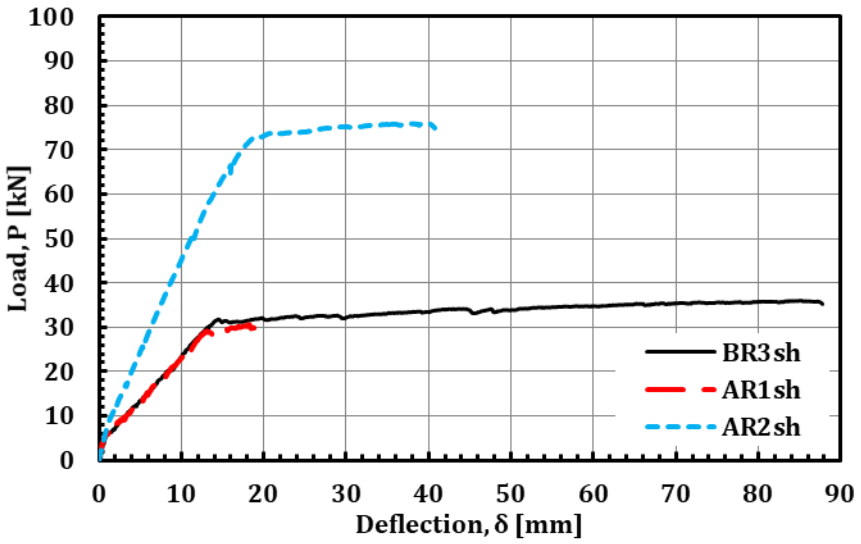

Figure 4.1 Load-deflection curves of the un-strengthened beams.

There is no significant effect of concrete strength on the flexural behavior of under-reinforced RC beams. All beams failed with the same failure mode of concrete crushing at the top the beam's mid-span, after steel yielding, as shown in Figure 4.2a and b, respectively. Therefore, it can be concluded that the increase in the concrete strength did not achieve a noticeable effect on the flexural behavior of the un-strengthened RC beams.

(a) Beam BR3sh **(b) Beam AR2sh**

Figure 4.2 Failure modes of the un-strengthened beams.

The summary of the loads and deflections at the main points of each beam and its failure mode are reported in Table 4.1. This table presents the values of cracking load, P_{cr} in kN, cracking deflection, δ_{cr} in mm, yield load, P_y in kN, yield deflection, δ_y in mm, ultimate load, P_u in kN, and the deflection at the ultimate load, δ_u in mm. The ratio between the stage load and its corresponding deflection is also listed in this table for

each beam at cracking point, $(P/\delta)_{cr}$, yield point, $(P/\delta)_y$ and failure point, $(P/\delta)_u$ in kN/mm. These values reflect the change of the effective stiffness of beams in each stage. The failure modes of the studied beams are listed in the last column.

Table 4.1 Summary of load-deflection results for the tested beams.

	Beam ID	P_{cr} [kN]	δ_{cr} [mm]	$(P/\delta)_{cr}$ [kN/mm]	P_y [kN]	δ_y [mm]	$(P/\delta)_y$ [kN/mm]	P_u [kN]	δ_u [mm]	$(P/\delta)_u$ [kN/mm]	Failure Mode
Group A1	AR1sh	5.43	0.55	9.87	29.04	12.92	2.25	---[a]	--- [a]	--- [a]	--- [a]
	AS1sh	5.67	0.56	10.13	38.26	15.56	2.46	58.52	54.30	1.08	FR+ICs
	AD1sh	6.50	0.62	10.48	44.76	15.28	2.93	73.09	47.44	1.54	ECs
	AR2sh	4.35	0.41	10.61	72.55	19.70	3.68	76.08	39.90	1.91	CC
	AS2sh	4.65	0.41	11.34	81.80	21.36	3.83	98.35	50.70	1.94	CC+ICs
Group B1	BR3sh	5.80	0.70	8.29	31.90	14.50	2.20	36.08	85.10	0.42	CC
	BS3sh	7.10	0.78	9.10	42.50	15.20	2.80	65.98	55.80	1.18	FR+ICs
	BT3sh	8.70	0.92	9.46	57.00	16.30	3.50	82.65	33.53	2.47	ECs
	BS3sh'	--- [b]	--- [b]	--- [b]	42.00	13.60	3.09	64.04	52.61	1.22	ICs

[a] The test of this beam test was stopped after yielding and before failure.

[b] This beam doesn't have cracking point because it was loaded up to service load before strengthening.

FR: Rupture of CFRP strip, ECs: Cover concrete separation at CFRP strip end, CC: Concrete crushing, ICs: Intermediate flexural crack induced concrete cover separation.

Beam AR2sh, which has larger reinforcement ratio, shows a bit higher cracking stiffness than beam AR1sh, which in turn shows larger cracking load and deflection as reported in Table 4.1. The load, deflection and effective stiffness at yield point increased by increasing the reinforcement ratio as shown Figure 4.1. As reported in Table 4.1, P_y, δ_y and $(P/\delta)_y$ increased due to the increase in RC section stiffness by increasing the reinforcement area. Due to the same reason, the load carrying capacity and the effective beam stiffness in third stage increased by increasing the reinforcement ratio, while the ultimate deflection decreased as shown Figure 4.1.

4.2.1.2 Variation of strains with load

The concrete strain at the top of RC section, ε_c, and tension steel strain, ε_s, at the mid-span of the three un-strengthened beams were plotted on horizontal axis in $\mu\varepsilon$ versus load, P in kN in Figure 4.3 for the un-strengthened beams. The concrete strains are presented in the left side with negative values and the steel strains are presented in

the right side with positive values. All steel strain gages were failed before the failure of the beams. Therefore, only the first 6000 $\mu\varepsilon$ of steel strain are presented.

As shown in Figure 4.3, the load-strain curves of beams AR1sh and BR3sh are very close, although these beams have different concrete strengths. This finding supports the previous conclusion regarding the effect of concrete strength on the flexural behavior of the un-strengthened under-reinforced RC beams.

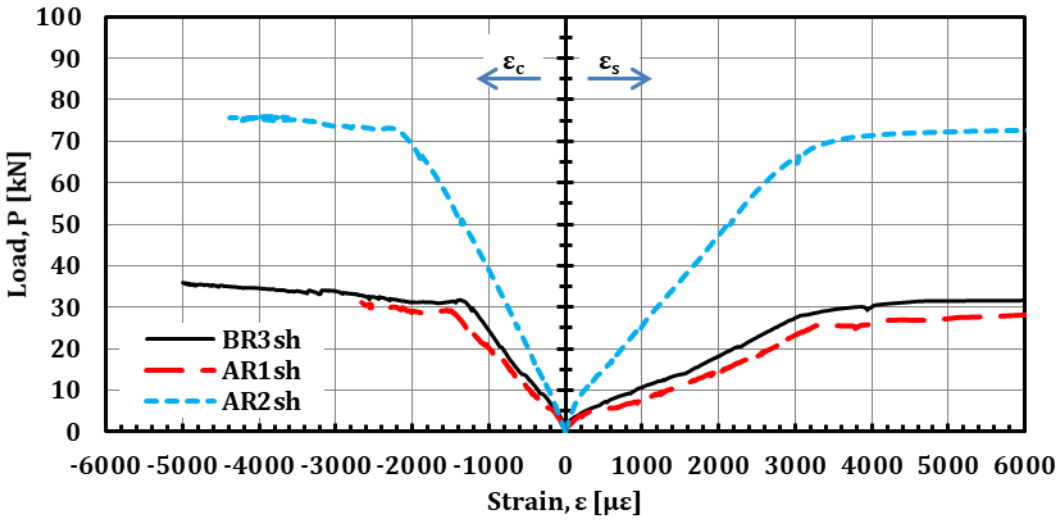

Figure 4.3 Concrete and tensile steel strains at mid-span section for the un-strengthened beams.

Beam AR2sh with higher steel reinforcement ratio showed higher loads at the same strain compared to the beams with lower steel reinforcement ratio. However, it showed higher concrete strain at yield. This might be due to the higher stiffness of beam AR2sh delaying the steel yielding and allowing the concrete produces more strain at the top of the beam.

4.2.1.3 Load-cracking responses

The crack width, ω was measured in mm at a notch preformed at mid-span section for the three un-strengthened beams and plotted on the horizontal axis versus load, P in kN, on the vertical axis in Figure 4.4.

The crack patterns were detected by visual inspection and drawn using permanent colored makers at different loads. The crack patterns along the middle third of each beam, which has constant moment, are presented in Figure 4.5 at constant load of 25.4 kN, below the lowest yield point of beams.

The values of measured crack widths for the beams in groups A1 and B1 at yield load, ω_y, and at ultimate load, ω_u, are summarized in Table 4.2. Moreover, the crack spacing, s, at the constant load for each beam were measured in mm and listed in Table 4.2 as minimum crack spacing, s_{min}, maximum crack spacing, s_{max}, mean crack spacing, s_{mean} and its standard deviation, s_{SD}. Also, the crack width at the constant load, ω_c, for each beam is presented in Table 4.2.

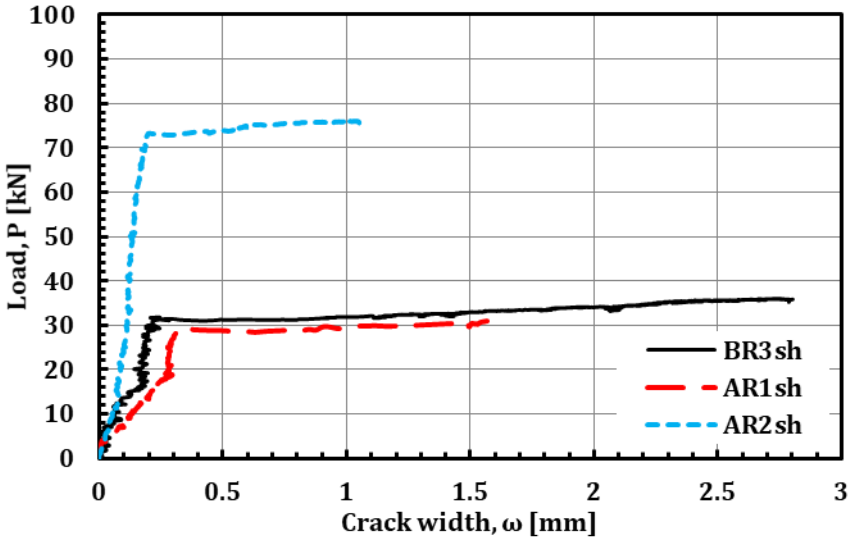

Figure 4.4 Load-crack width curves of the un-strengthened beams.

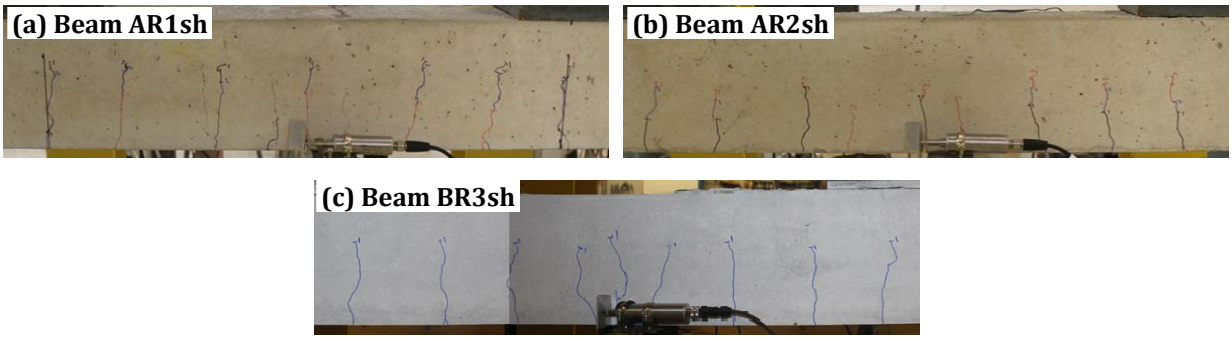

Figure 4.5 Crack patterns along the middle third of the un-strengthened beams at load of 25.40 kN.

Beam AR2sh with high tension steel ratio of 1.97% presented lower crack widths compared to beams AR1sh and BR3sh with low tension steel ratio of 0.77% (see Figure 4.4). At the same load of 25.4 kN as reported in Table 4.2, ω_c decreased from 0.262 mm and 0.185 mm in beams AR1sh and BR3sh to 0.096 mm in beam AR2sh with percentages of 63% and 48%, respectively. This is because the high reinforcement ratios decreased the tension steel strains.

Even the higher yield and ultimate loads of the beam with high steel reinforcement ratio than beams with low steel reinforcement ratio, decreases in ω_y and ω_u by increasing the reinforcement ratio are also observed. As presented in Table 4.2, ω_y decreased from 0.309 mm and 0.228 mm in beams AR1shand BR3sh to 0.18 mm in beam AR2sh with percentages of 42% and 21%, respectively. ω_u decreased form 2.728 mm in beam BR3sh to 1.024 mm in beam AR2sh with percentage of 63%.

The crack patterns at constant load, P_c of 25.4 kN showed the same number of cracks (9 cracks) along the middle third for the beams, AR1sh and AR2sh, with different reinforcement ratios and the beam of higher concrete strength, BR3sh, as shown in Figure 4.5a, b and c, respectively. Moreover, the descriptive statistical values of *s* for these beams didn't show a big difference in the values of s_{min}, s_{max}, s_{mean} and s_{SD} as presented in Table 4.2. This reflects that despite the decrease in the crack width at the same applied load by increasing steel reinforcement or concrete strength, these parameters had a little influence on the crack pattern of the studied un-strengthened beams.

Table 4.2 Summary of the cracking results for the tested beams.

	Beam ID	ω_c [mm]	Crack spacing at P_c, s [mm]				P_y [kN]	ω_y [mm]	P_u [kN]	ω_u [mm]
			s_{min}	s_{max}	s_{mean}	s_{SD}				
Group A1	AR1sh	0.262	50	136	86.13	29.47	29.04	0.309	--- [a]	--- [a]
	AS1sh	0.167	50	111	87.25	22.12	38.26	0.260	58.52	1.046
	AD1sh	0.102	52	117	87,00	23.05	44.76	0.201	73.09	0.629
	AR2sh	0.096	48	117	88.13	22.80	72.55	0.180	76.08	1.024
	AS2sh	0.089	65	127	85.88	21.89	81.80	0.288	98.35	0.778
Group B1	BR3sh	0.185	28	120	87.50	32.11	31.90	0.228	36.08	2.728
	BS3sh	0.019[b]	41	123	86.57	29.27	42.50	0.130	65.98	0.510
	BT3sh	0.116	55	121	88.55	24.29	57.00	0.176	82.65	0.370
	BS3sh'	0.156	22	116	59.35	34.36	42.00	0.376	64.04	1.174

[a] The test of this beam test was stopped after yielding and before failure.
[b] The crack at the preformed notch in beam BS3sh started late, while two cracks around it started before.

4.2.2 Strengthened beams

Six strengthened beams were investigated; three beams, AS1sh, AD1sh and AS2sh, from group A1 with concrete strength of 33 MPa and three beams, BS3sh, BS3sh` and

BT3sh, from group B1 with concrete strength of 42.77 MPa. Different reinforcement ratios were used; tension steel ratio, ρ = 0.77% and compression steel ratio, ρ' = 0.28% in beams AS1sh, AD1sh, BS3sh, BS3sh` and BT3sh and $\rho$ = 1.97% and $\rho'$ = 0.77% in beam AS2sh. Different areas of CFRP were used: $A_f$ of 28 mm$^2$ as two CFRP strips of 1.4 mm thickness and 10 mm width in beams AS1sh, AS2sh, BS3sh and BS3sh`; A_f of 56 mm^2 as four CFRP strips of 1.4 mm thickness and 10 mm width in beam AD1sh; and A_f of 84 mm^2 as three CFRP strips of 2.8 mm thickness and 10 mm width in beam BT3sh. All beams were strengthened without any previous loading except beam BS3sh` that was strengthened after pre-cracking under short term loading up to service design load of un-strengthened beam for two loading cycles at the end of curing period of 28 days.

4.2.2.1 Failure modes and load-deflection responses

The modes of failure for the strengthened beams in group A1 are shown in Figure 4.6. Beam AS1sh had failure mode of CFRP rupture followed by intermediate concrete cover separation (ICs), see Figure 4.6a. Beam AD1sh had failure mode of concrete cover separation at the end of CFRP strip (ECs), see Figure 4.6b. This means that increasing the area of NSM strip converted the mode of failure from ICs (ductile failure) to ECs (brittle and catastrophic failure). Beam AS2sh had failure mode of concrete crushing at the top beam with intermediate concrete cover separation flexural crack at bottom of beam, Figure 4.6c. By comparing beam AS1sh and beam AS2sh, decrease the stiffness ratio of CFRP strip to main tensile reinforcement of the beam avoided the rupture of CFRP strip. The observed modes of failure are similar to the summarized failure modes in De Lorenzis and Teng [15] and Sena-Cruz et al. [81]. The modes of failure for the strengthened beams in group B1 are shown in Figure 4.7. Beam BS3sh failed by CFRP rupture followed by concrete cover separation (FR+ICs) as shown in Figure 4.7a. However, beam BS3sh` failed by intermediate flexural induced concrete cover separation (ICs) as shown in Figure 4.7b. This might be due to the larger number of cracks observed in beam BS3sh` reducing the crack spacing along the constant moment part leading to higher shear stresses causing interface failure between concrete and epoxy before occurrence of CFRP rupture. Beam BT3sh had failure mode of concrete cover separation at the end of CFRP strip (ECs), see Figure

4.7c. This finding supports the previous observation which is "increasing the area of NSM strip converted the mode of failure from ductile failure, ICs, to brittle failure, ECs".

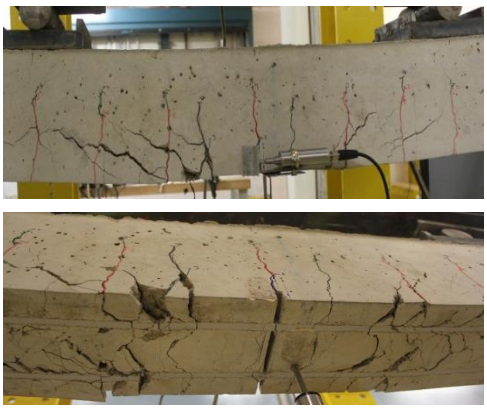

(a) AS1sh

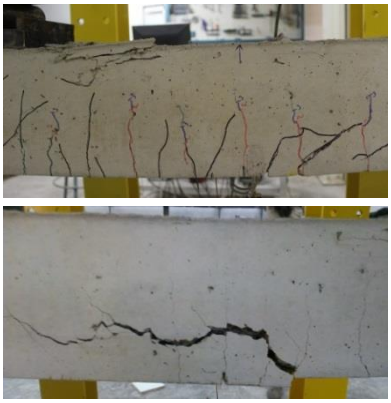

(c) AS2sh

(b) AD1sh

Figure 4.6 Failure modes of the strengthened beams in group A1.

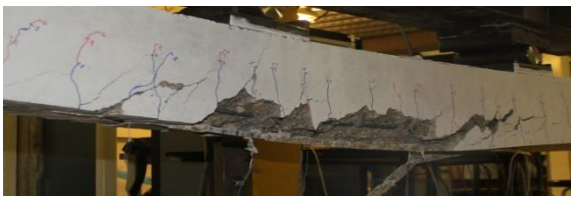

(a) BS3sh

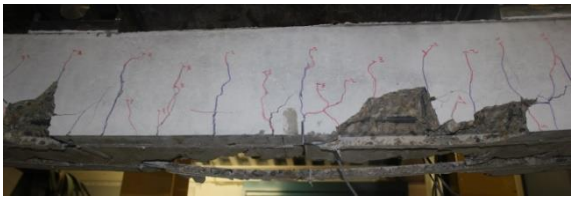

(b) BS3sh`

(C) BT3sh

Figure 4.7 Failure modes of the strengthened beams in group B1.

The load-deflection curves of strengthened beams tested in groups A1 and B1 are presented in Figure 4.8. The load-deflection curves of the un-strengthened beams are also plotted for comparison. All beams show three stages defined at their ends by cracking, yield and failure points, respectively.

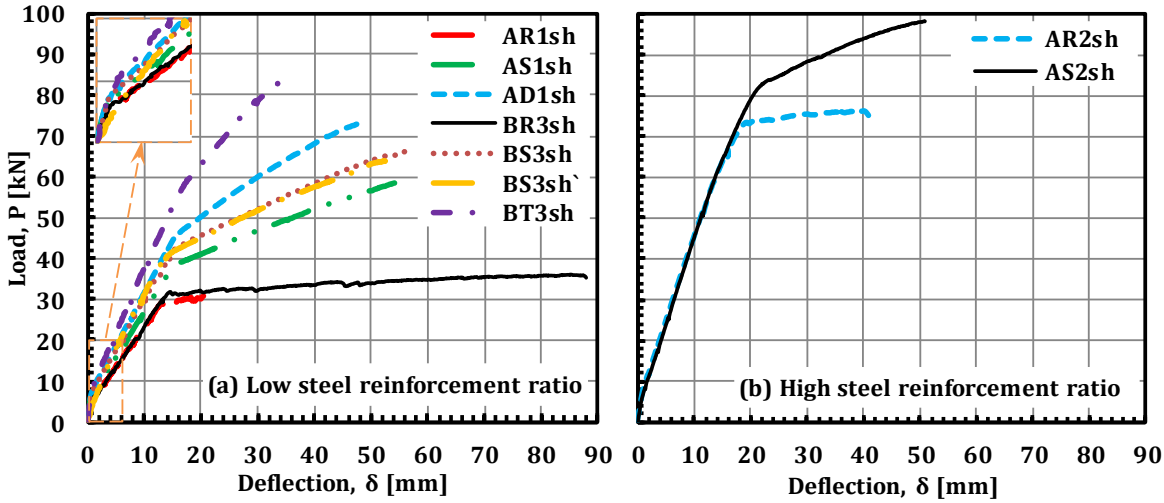

Figure 4.8 Load-deflection curves of the tested beams.

The summary of the loads and deflections at the main points of each load deflection curve and the modes of failure are reported in Table 4.1.

As shown in Figure 4.8a, the pre-cracked beam BS3sh` showed load-deflection response lower than that in the virgin beam BS3sh up to almost the pre-cracking load. After this load, it was observed that the behavior of the pre-cracked beam BS3sh` was identical to that of virgin beam BS3sh up to failure. This means that this matching happened when the generated cracks in the virgin beam reached to equal lengths as those of the virgin one at almost the pre-cracking load. A similar finding was reported for pre-cracked RC beams under mode I (tensile crack) by Sallam et al. [159] regarding beams with rectangular section and Yehia and Wahab [160] regarding T-flanged beams and reported by Abou El-Mal et al. [161] for pre-cracked RC beams under mode II (shear crack). This also can be seen in Table 4.1 from the small difference between the reported values of load and deflection at yield and failure points.

Unlike the unnoticeable effect of the concrete strength in the un-strengthened beams, the use of higher concrete strength in strengthened beams BS3sh and BS3sh` enhanced their flexural behavior compared to beam AS1sh of lower concrete strength as shown

in Figure 4.8a. This can be due to the additional function of the concrete cover in the strengthened beams as a transmission media for the resistance force in CFRP strips. Therefore, the increase of concrete cover strength increased the load transfer efficiency of NSM strengthened RC sections leading to higher stiffness of whole strengthened beam enhancing its flexural behavior. This observation is in agreement with finding obtained by Sallam et al. [159].

As presented in Table 4.1, by increasing the concrete strength P_{cr} and δ_{cr} increased from 5.67 kN and 0.56 mm in beam AS1sh to 7.10 kN and 0.78 mm in beam BS3sh with percentages of 25% and 39%, respectively. There may be two reasons for this difference. Firstly, it might be due to higher concrete tensile strength of beam BS3sh. Secondly, the higher values of concrete shrinkage strain in group A1 induced tensile stresses in concrete than those in group B1 that might significantly affected the cracking resistance [149,162,163].

By increasing the concrete strength, P_y increased from 38.26 kN in beam AS1sh to 42.50 kN and 42 kN with percentages of 11% and 10% in beams BS3sh and BS3sh`, respectively. The load carrying capacity also increased from 58.52 kN in beam AS1sh to 65.98 kN and 64.04 kN with percentages of 13% and 10% in beams BS3sh and BS3sh`, respectively.

Regarding the effect of CFRP strengthening area, the cracking load, deflection and stiffness increased by increasing area of CFRP as shown in Figure 4.8a. For group A1, Table 4.1 presents that P_{cr}, δ_{cr} and $(P/\delta)_{cr}$ slightly increased by NSM strengthening for beam AS1sh with A_f of 28 mm^2 with percentage of 4.42%, 1.82% and 2.63%, respectively. By doubling A_f in beam AD1sh to 56 mm^2, these values increased with percentage of 19.71%, 12.73% and 6.18%, respectively, compared to the reference beam AR1sh. For group B1, P_{cr}, δ_{cr} and $(P/\delta)_{cr}$ increased by NSM strengthening with A_f of 28 mm^2 in beam BS3sh with percentage of 22.41%, 11.43% and 9.77%, respectively. By increasing A_f three times in beam BT3sh to 84 mm^2, these values increased with percentage of 50%, 31.43% and 14.11%, respectively, compared to beamBR3sh. The increases in values of the cracking stage by increasing CFRP area were due to increasing the beam stiffness in the tensile side. The enhancement of the cracking stage

values by increasing CFRP area in group B1 due to its higher concrete cover strength was more noticeable than that in group A1.

The load, deflection and effective stiffness at yield point also increased by increasing area of CFRP strips as shown in Figure 4.8a. For group A1, Table 4.1 presents that P_y, δ_y and $(P/\delta)_y$ increased by NSM strengthening with A_f of 28 mm^2 in beam AS1sh with percentage of 31.75%, 20.43% and 9.33%, respectively. As A_f was doubled to 56 mm^2 in beam AD1sh, these values increased with percentage of 54.13%, 18.27% and 30.22%, respectively compared to beam AR1sh. For group B1, P_y, δ_y and $(P/\delta)_y$ increased by NSM strengthening with A_f of 28 mm^2 in beam BS3sh with percentages of 33.23%, 4.83% and 27.27%, respectively. As A_f increased three times to 84 mm^2 in BT3sh, these values increased with percentage of 78.68%, 12.41% and 59.09%, respectively compared to beam BR3sh. The results at yield point were enhanced by increasing CFRP area due to the gained stiffness in the tension side growing the neutral axis depth especially at the cracked sections. Therefore, the yield of the tensile steel reinforcement was delayed enhancing the yield point position on load deflection curve.

It can be seen also, from Figure 4.8a, a noticeable improving in the load carrying capacity and the effective beam stiffness in third stage by increasing CFRP area, while the ultimate deflection decreased. The registered values of group A1 at failure points in Table 4.1 show that, P_u and $(P/\delta)_u$ increased by NSM strengthening with A_f of 28 mm^2 in beam AS1sh with percentages of 62% and 157%, respectively, while δ_u decreased with percentage of 36%. As A_f was doubled to 56 mm^2 in beam AD1sh, P_u and $(P/\delta)_u$ increased with percentage of 103% and 267%, respectively, while δ_u decreased with percentage of 44% compared to beam BR3sh (which had flexural behavior close to beam AR1sh).

Beam AS1sh failed with CFRP rupture followed by concrete cover separation as shown in Figure 4.6a. The FRP rupture failure mode is one of the preferred failure modes according to available design criteria [12,63]. By increasing CFRP area in beam AD1sh the tensile resistance of strips increased delaying this mode of failure and increasing the load carrying capacity. While, the stress concentration at the end of CFRP strips was magnified causing concrete cover separation at the cut-off point of CFRP strips as shown in Figure 4.6b. Although this premature mode of failure happened at a value of

P_u higher than the value of AS1sh, it occurred at load and deflection lower than expected values in case of CFRP rupture.

For group B1, Table 4.1 presents that P_u and $(P/\delta)_u$ increased by NSM strengthening with A_f of 28 mm^2 in beam BS3sh with percentages of 83% and 181%, respectively, while δ_u decreased with percentage of 35%. The mode of failure changed from concrete crushing in the reference beam BR3sh to CFRP rupture followed by concrete cover separation in beam BS3sh as shown in Figure 4.7a, which is less ductile causing the decrease in ultimate deflection.

As A_f increased three times to 84 mm^2 in BT3sh, P_u and $(P/\delta)_u$ increased with percentages of 129% and 488%, respectively, while δ_u decreased with percentage of 60.60% compared to beam BR3sh. As discussed before in group A1, by increasing CFRP area in beam BT3sh tensile resistance of strips increased delaying the failure mode of CFRP rupture and increasing the load carrying capacity. While, the stress concentration at the end of CFRP strips was magnified causing concrete cover separation at the cut-off point of CFRP strips as shown in Figure 4.7c. Although this premature mode of failure happened at a value of P_u higher than the value of BS3sh, it occurred at load and deflection lower than expected values in case of CFRP rupture.

Although, beam BT3sh had one and half times of A_f used in beam AD1sh, the enhancement ratio of P_u in beam BT3sh to P_u in beamAD1sh was almost the same ratio of P_u in beam BS3sh to P_u in beam AS1sh, which had the same A_f. This is because the concrete cover strength was unable to resist the stress concentration at the end of CFRP strips due to the failure mode of concrete cover separation at the cut-off point of CFRP strip as long. This was unlike capability of the concrete cover strength to increase load carrying capacities of the strengthened beams in other failure modes.

Regarding the effect of steel reinforcement ratio, beam AS2sh with higher steel ratio and NSM strengthened using 28 mm^2 of CFRP showed enhanced flexural behavior compared to un-strengthened beam AR2sh as shown in Figure 4.8b. As presented in Table 4.1, P_{cr} and $(P/\delta)_{cr}$ increased with percentages of 6.90% and 6.88%. P_y, δ_y and $(P/\delta)_y$ increased with percentages of 12.75%, 8.43% and 4.08%, respectively. However, these percentages between beams of lower steel ratio, AS1sh and AR1sh, were 31.75%, 20.43% and 9.33%, respectively. The ratio between strengthening

CFRP stiffness to tension steel stiffness in beam AS2sh was lower than that in beam AS1sh. Therefore, the percentage of gained stiffness, which moves the neutral axis toward the tension side, was lower in beams with ρ of 1.97% than those with ρ of 0.77% reducing the enhancement of the yield point position on load deflection curve in the beams with ρ of 1.97%.

As shown in Figure 4.8b, the load carrying capacity, ultimate deflection and the effective beam stiffness in third stage were improved by NSM strengthening with CFRP area of 28 mm^2. As reported in Table 4.1, P_u, δ_u and $(P/\delta)_u$ of beam AS2sh increased with percentage of 29.27%, 27.07% and 1.57%, respectively, compared to beam AR2sh. Beam AS2sh failed with concrete crushing, which was the same failure mode of un-strengthened beam AR2sh, gathered with intermediate crack concrete cover separation as shown in Figure 4.6c. This means that the failing with the same failure mode of the un-strengthened (concrete crushing) made the ultimate deflection increased like ultimate load and effective stiffness in beams with higher steel reinforcement ratio.

4.2.2.2 Deformability and Ductility

The NSM CFRP strengthened RC beams should be designed for sufficient strength and ductility to satisfy the ultimate limit states and to avoid catastrophic brittle failure. The ductility concept is related to the safety of the structure to provide an opportunity for the deflections to be observed if the loads become too large. Consequently, proper corrective actions can be achieved before failure. Ductility is the ability of a member to undergo deformation after its initial yielding without any significant reduction in yield strength while deformability is the member capability to deform before failure [164]. Conventional ductility indices use displacement, curvature or rotation at yielding and ultimate stages as basis for the computations. In this case, the load-deflection response is almost an elastic-plastic curve where there is a negligible difference between the yield and ultimate loads.

From a design point of view, the ductility index of a concrete beam reinforced with steel bars (conventional RC beam) provides a measure of the energy absorption capability [165,166]. Since the RC beams strengthened with FRP materials acquire a significant difference between the yield and ultimate loads in the load-deflection response, the conventional ductility indices are not an appropriate measure of the

energy absorption capacity. Therefore, the use of the concept of deformability as a measure of the energy absorption is more appropriate than the concept of conventional ductility which is a measure of deflection capability.

Displacement ductility index, μ_D and deformability factor, μ_E were used to describe ductility deformability of the studied beams for investigation the effect of NSM CFRP strengthening on the flexural ductility of beams.

Displacement ductility index, μ_D is defined as the ratio of the ultimate deflection, δ_u to the yield deflection, δ_y measured at mid-span section as represented in equation 4.1.

$$\mu_D = \frac{\delta_u}{\delta_y} \tag{4.1}$$

Deformability factor, μ_E is defined as the ratio of the energy absorption at ultimate load to the energy absorption at service or a limiting curvature or yielding, as presented in equation 4.2 [63]. The energy absorption is the area under load-deflection curve.

$$\mu_E = \frac{E_u}{E_y} \tag{4.2}$$

where E_u is the area under load-deflection curve up to ultimate load and E_y is the area under load-deflection curve up to yield point.

The values of μ_E indices and μ_D factors of the beams in groups A1 and B1 were calculated and reported in Table 4.3. Also, the values of the energies absorption, E_u and E_y were calculated in kN.mm and reported in Table 4.3 in addition to the values of δ_y and δ_u in mm.

It can be seen from Table 4.3 that the increasing of CFRP area reduced ductility of the NSM strengthened beams according to μ_D indices and μ_E factors. For group A1, μ_D decreased from 3.49 for beam AS1sh, with A_f of 28 mm^2, to 3.10 in beam AD1sh, with A_f of 56 mm^2, with decreasing percentage of 11.18% and μ_E decreased from 6.60 for AS1sh to 6.11 in AD1sh decreasing percentage of 7.43%. This might be due to the change of failure mode from FRP rupture in beam AS1sh, which is one of the recommended failure modes after steel yielding [12,63], to concrete cover separation at strip end in beam AD1sh, which is a catastrophic brittle failure.

Table 4.3 Ductility indices and deformability factors for the tested beams.

	Beam ID	Ductility			Deformability		
		δ_y [mm]	δ_u [mm]	$\mu_D=\delta_u/\delta_y$	E_y [kN.mm]	E_u [kN.mm]	$\mu_E=E_u/E_y$
Group A1	AR1sh	12.92	--- [a]	--- [a]	207	--- [a]	--- [a]
	AS1sh	15.56	54.30	3.49	339	2238	6.60
	AD1sh	15.28	47.44	3.10	382	2335	6.11
	AR2sh	19.70	39.90	2.03	763	2353	3.08
	AS2sh	21.36	50.70	2.37	979	3675	3.75
Group B1	BR3sh	14.50	85.10	5.87	262	2665	10.18
	BS3sh	15.20	55.80	3.67	369	2597	7.04
	BT3sh	16.30	33.53	2.06	522	1723	3.30
	BS3sh'	13.60	52.61	3.87	328	2374	7.25

[a] The test of this beam test was stopped after yielding and before failure.

For group B1, μ_D decreased from 5.87 in reference beam BR3sh to 3.67 by NSM strengthening with A_f of 28 mm^2 in beam BS3sh and to 2.06 by NSM strengthening with A_f of 84 mm^2 in beam BT3sh with percentages of 37.48% and 64.91%, respectively, compared to the reference beam BR3sh. And μ_E decreased from 10.18 in reference beam BR3sh to 7.04 in beam BS3sh and to 3.30 in beam BT3sh with percentages of 30.85% and 67.58%, respectively, compared to the reference beam BR3sh. The key point of this decrease in ductility is the change of failure mode from concrete crushing in reference beam BR3sh to FRP rupture in beam BS3sh then to concrete cover separation at strip end in beam BT3sh.

The decreasing percentages of μ_D and μ_E in beam BT3sh, with A_f of 84 mm^2, compared to beam BS3sh, with A_f of 28 mm^2, were 43.87% and 53.13%, respectively. These percentages are larger than the decreasing percentages by increasing A_f from 28 mm^2 to 56 mm^2 in group A1, although, the failure mode in both cases changed to concrete cover separation at strip end, ECs. This is due to occurrence of this mode more rapid by increasing strengthening reinforcement reducing the ultimate deflection, energy absorption and consequently the beam ductility.

NSM strengthening of RC beam AS2sh of higher steel reinforcement ratio with CFRP area of 28 mm^2 improved the ductility compared to un-strengthened beam AR2sh as reported in Table 4.3. On the opposite NSM strengthening of RC beam BS3sh of lower steel reinforcement ratio with the same CFRP area reduced the ductility compared to

un-strengthened beam BR3sh. The values of μ_D and μ_E increased from 2.03 and 3.08 in reference beam AR2sh to 2.37 and 3.75 in strengthened beam AS2sh with percentages of 16.75% and 21.75%, respectively. However, μ_D and μ_E decreased from 5.87 and 10.18 in reference beam BR3sh to 3.67 and 7.04 in strengthened beam BS3sh with percentages of 37.48% and 30.85%, respectively. This may be attributed to both of un-strengthened and strengthened beams with ρ of 1.97%, AR2sh and AS2sh, failed with the same mode of concrete crushing, while the failure mode changed from concrete crunching in beam BR3sh to FRP rupture in beam BS3sh.

The pre-cracking of RC beam up to service design load before NSM strengthening with CFRP strips marginally affected the ductility compared to the strengthened RC beam without any previous loading as reported in Table 4.3. The values of μ_D and μ_E slightly increased from 3.67 and 7.04 in beam BS3sh to 3.87 and 7.25 in beam BS3sh` with percentages of 5.45% and 2.84%, respectively. However, $\delta_u$ and $E_u$ slightly decreased from 55.80 mm and 2597 kN.mm in beam BS3sh to 52.6 1mm and 2374 kN.mm in beam BS3sh` with percentages of 5.72% and 8.59%, respectively. This supports the finding that the flexural behavior of the pre-cracked beam is identical to that of the virgin beam after the pre-cracking load.

The reported values in Table 4.3 reflected that the using of different concrete type marginally affected the ductility of strengthened beam BS3sh compared to the strengthened beam AS1sh, which had same construction details and failure mode, but the concrete compressive strength of beam BS3sh was higher than it in beam AS1sh. The values of μ_D and μ_E slightly increased from 3.49 and 6.60 in beam AS1sh to 3.67 and 7.04 in beam BS3sh with percentages of 5.16% and 6.67%, respectively.

4.2.2.3 Load-cracking responses

The crack width, ω, was measured in mm at notch preformed at mid-span section for the strengthened beams and plotted on the horizontal axis versus load, P in kN on the vertical axis in Figure 4.9 for groups A1 and B1. Moreover, the load-crack width curves of the un-strengthened beams were plotted in same figure for comparison.

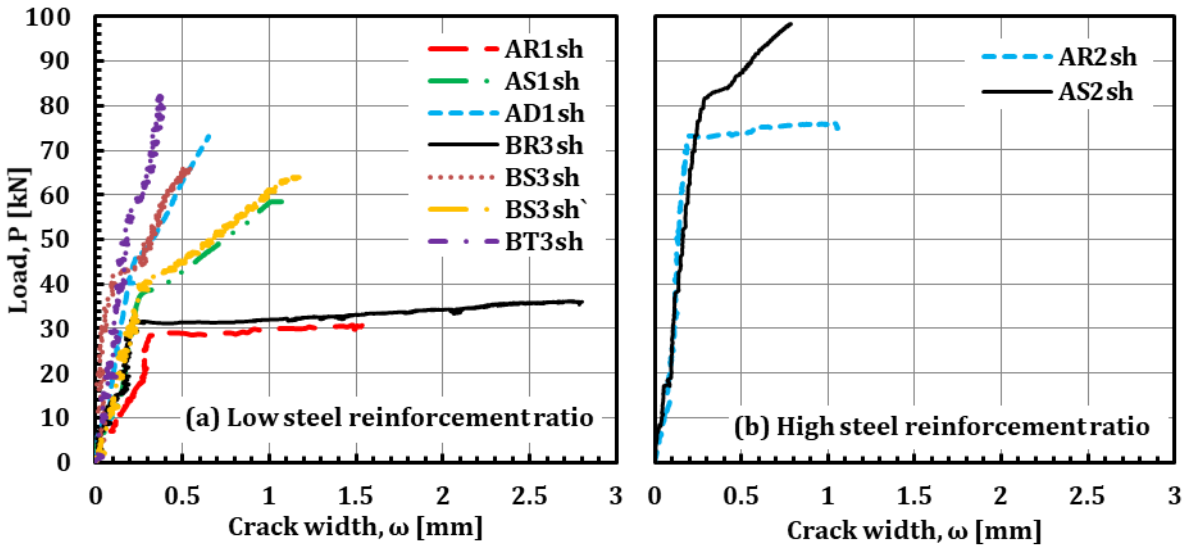

Figure 4.9 Load-crack width curves for the tested beams.

The crack patterns were detected by visual inspection and drawn using permanent colored makers at different loads. The crack patterns at the middle third, which has constant moment, of each strengthened beam were captured at constant load, P_c, of 25.4 kN and presented in Figure 4.10.

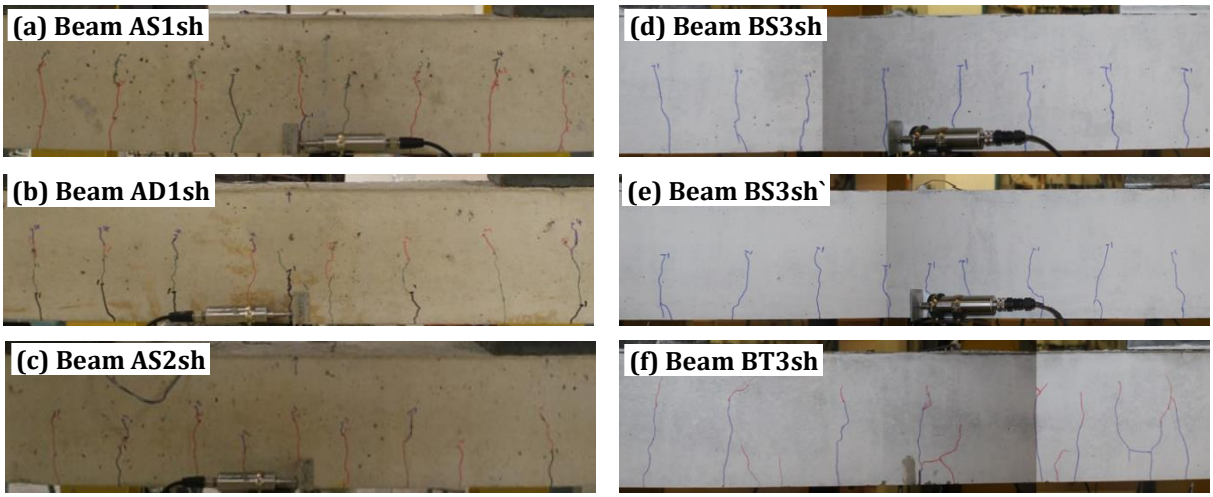

Figure 4.10 Crack patterns along the middle third of the strengthened beams at load of 25.40 kN.

The values of ω_y, ω_u, ω_c and the descriptive statistical values of s as s_{min}, s_{max}, s_{mean} and s_{SD} are summarized in Table 4.2. The crack at the preformed notch in beam BS3sh from group B1 started after applied load around 25 kN as shown from its P-ω curve plotted in Figure 4.9a, while two cracks started earlier around it as shown in Figure 4.10d.

Therefore, the pre-cracked beam BS3sh` was used for the crack widths comparison instead of beam BS3sh because of their identical behavior after the pre-cracking load. The NSM strengthening of RC beams with different CFRP areas reduced the crack width by increasing CFRP area as shown in Figure 4.9a. The reported values of crack widths in Table 4.2 at different loads, P_c, P_y and P_u show this decrease in group A1 and B1. Compared to the un-strengthened beam AR1sh in group A1, ω_c and ω_y were reduced with percentages of 36.26% and 15.86%, respectively in beam AS1sh, strengthened with 28 mm^2 of CFRP, and 61.07% and 34.95%, respectively in beam AD1sh, strengthened with 56 mm^2 of CFRP. ω_u was reduced from 1.046 mm in beam AS1sh to 0.629 mm in beam AD1sh with percentage of 39.87%.

Compared to the un-strengthened beam BR3sh in group B1, ω_c, ω_y and ω_u were reduced with percentages of 37%, 23% and 87%, respectively, in beam BT3sh, strengthened with 84 mm^2 of CFRP. However, in beam BS3sh`, strengthened with 28 mm^2 of CFRP, ω_y increased with percentage of 65%, while ω_c and ω_u were reduced with percentages of 16% and 57%, respectively.

The crack patterns at P_c of 25.4 kN showed the same number of cracks (9 cracks) along the middle third for the beams with different CFRP areas in group A1 as presented in Figure 4.10a and b. It can be seen from the descriptive statistical values of crack spacing, s, listed in Table 4.2 that s_{min} values of these beams were almost the same and equal 50 mm in beams AR1sh and AS1sh and 52 mm in beam AD1sh, which is almost the spacing between the mid-span preformed notch and position of the nearest stirrup. s_{max} decreased from 136 mm in beam AR1sh to 111 mm in beam AS1sh and 117 mm in beam AD1sh. s_{mean} marginally changed from 86.13 mm with s_{SD} of 29.47 mm in beam AR1shto 87.25 mm with s_{SD} of 22.12 mm in beam AS1sh and 87 mm with s_{SD} of 23.05 mm in beam AD1sh.

The same observation was found in group B1 as presented in Figure 4.10d and f. It can be seen from the descriptive statistical values of s listed in Table 4.2 that, s_{min} of these beams increased from 28 mm in beam BR3sh to 41 mm in beam BS3sh and 55 mm in beam BT3sh. s_{max} marginally increased from 120 mm in beam BR3sh to 123 mm in beam BS3sh and 121 mm in beam BT3sh. s_{mean} marginally changed from 87.5 mm with

s_{SD} of 32.11 mm in beam BR3sh to 86.57 mm with s_{SD} of 29.27 mm in beam BS3sh and 88.55 mm with s_{SD} of 24.29 mm in beam BT3sh.

The strengthened beam of higher reinforcement ratio AS2sh presented lower crack widths compared to the strengthened beam of lower reinforcement ratio AS1sh as shown in Figure 4.9a and b. At the same load of 25.4 kN as reported in Table 4.2, ω_c decreased from 0.167 mm in beam AS1shto 0.089 mm in beam AS2sh with percentage of 47%. This is due to decreasing of the tension steel strains by increasing reinforcement ratio. Comparing the decreasing ratios of ω_c by NSM strengthening with same A_f of 28 mm^2, reflected an effect in beams with ρ of 1.97% lower than those of 0.77%. These decreasing ratios were 36% and 7% for beams with ρ of 0.77% and 1.97%, respectively. This might be due to the lower ratio between the added CFRP stiffness and tension steel stiffness in beam AS2sh compared to beam AS1sh.
Also, the crack width at the ultimate load, ω_u decreased from 1.046 mm in beam AS1sh to 0.778 mm in beam AS2sh with percentage of 26%. While, ω_y increased from 0.26 mm in beam AS1sh to 0.288 mm in beam AS2sh with percentage of 11%. This might be due to higher yield load of beam AS2sh, which equals 2.14P_y of beam AS1sh, increasing crack width at yield point.
The descriptive statistical values of s listed in Table 4.2 shows that, s_{min} and s_{max} of AR2sh and AS2sh beams increased from 48 mm and 117 mm in beam AR2sh to 65 mm and 127 mm in beam AS2sh, respectively. However, s_{mean} slightly decreased from 88.13 mm with s_{SD} of 22.80 mm in beam AR2sh to 85.88 mm with S_{SD} of 21.89 mm in beam AS2sh.

The crack pattern along the middle third of pre-cracked beam BS3sh` at P_c, shown in Figure 4.10e, represented more cracks (13 cracks) compared with un-strengthened beam BR3sh (9 cracks), shown in Figure 4.5c, and strengthened smooth beam BS3sh (9 cracks), shown in Figure 4.10d. Also, the descriptive statistical values of s listed in Table 4.2 represent decreases in s_{min}, s_{max} and s_{mean} from 41 mm, 123 mm and 86.57 mm in un-pre-cracked beam BS3sh to 22 mm, 116 mm and 59.35 mm in pre-cracked beam BS3sh` with percentages of 70%, 6% and 40%, respectively. This reflected that,

the previous loading of RC beam before strengthening made more concrete in tension out of work.

4.2.2.4 Load- end slip of CFRP strip responses

The end slips of CFRP strip at its two ends, *S1* and *S2*, were measured and plotted on the horizontal axis in mm versus load, *P* in kN in Figure 4.11 for NSM strengthened beams in groups A1 and B1.

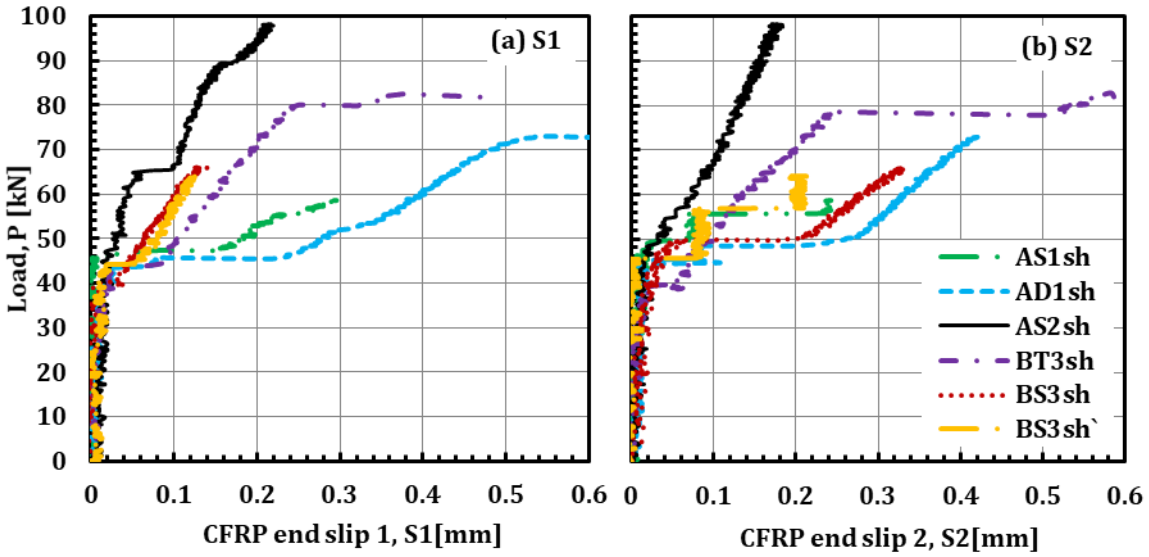

Figure 4.11 Load-CFRP end slip curves of the strengthened beams.

The values of end slips at yield loads, $S1_y$ and $S2_y$, and ultimate loads, $S1_u$ and $S2_u$, are summarized in Table 4.4.

Table 4.4 Summary of the CFRP end slip results for the strengthened beams.

	Beam ID	P_y [kN]	$S1_y$ [mm]	$S2_y$ [mm]	P_u [kN]	$S1_u$ [mm]	$S2_u$ [mm]
Group A1	AS1sh	38.26	0.00	0.00	58.52	0.30	0.25
	AD1sh	44.76	0.08	0.08	73.09	0.60	0.43
	AS2sh	81.80	0.13	0.13	98.35	0.22	0.18
Group B1	BS3sh	42.50	0.03	0.03	65.98	0.12	0.33
	BT3sh	57.00	0.13	0.12	82.65	0.38	0.58
	BS3sh`	42.00	0.01	0.00	64.04	0.13	0.20

The increasing of CFRP area in NSM strengthening of RC beams magnify the slips of CFRP strip at its both ends as shown in Figure 4.11 for strengthened beams in groups A1 and B1. As reported in Table 4.4 for group A1, the values of $S1_y$ and $S2_y$ increased

from nothing in beam AS1sh, with A_f of 28 mm^2, to 0.08 mm in beam AD1sh, with A_f of 56 mm^2. The values of $S1_u$ and $S2_u$ increased from 0.3 mm and 0.25 mm in beam AS1sh to 0.6 mm and 0.43 mm in beam AD1sh with percentages of 100% and 72%, respectively.

For group B1, the values of $S1_y$ and $S2_y$ increased from 0.03 mm in BS3sh, with A_f of 28 mm^2, to 0.13 mm and 0.12 mm with percentages of 333% and 300%, respectively, in beam BT3sh, with A_f of 84 mm^2. The values of $S1_u$ and $S2_u$ increased from 0.12 mm and 0.33 mm in beam BS3sh to 0.38 mm and 0.58 mm in beam BT3sh with percentages of 217% and 75.76%, respectively. The lower ratio between the perimeter and area of the thicker strips might attribute the previous observation.

The end slip at ultimate load of the strengthened beams with lager A_f, AD1sh and BT3sh, magnified the shear stresses causing the premature failure at the strip end with concrete cover separation, ECs. This happened in both of beams at almost similar values of ultimate end slip equal 0.60 mm in beam AD1sh and 0.58 mm in beam BT3sh and with improvement percentage in the load carrying capacity beam of AD1sh compared to AS1sh and beam BT3sh compared to beam BS3sh equal 25% and 26%, respectively. Although, A_f ratio in AD1sh was double that in AS1sh and A_f ratio in BT3sh was three times that in BS3sh, the load carrying capacity of BT3sh did not much improve. This means that, after change in failure mode from FR to ECs by increasing A_f, there is a limit of additional A_f after it the load carrying capacity will be unable to increase or it possibly decrease.

The strengthened beam of higher steel reinforcement ratio, AS2sh, produced larger end slip prior yielding than the strengthened beam of lower steel reinforcement ratio, AS1sh, which in turn produced larger values after yielding up to failure as shown in Figure 4.11 for both ends of CFRP strip. As reported in Table 4.4, the values of $S1_y$ and $S2_y$ were zero in beam AS1sh, while their values were 0.13 mm at both ends of CFRP strip in beam AS2sh. This might be due to higher yield load of beam S2A, which equals 2.14P_y of beam AS1sh. The values of $S1_u$ and $S2_u$ were 0.3 mm and 0.25 mm in beam AS1sh, while their values were 0.22 mm and 0.18 mm in beam AS2sh, respectively. This might be because the difference in stiffness at cut off point of CFRP strip between

strengthened and un-strengthened RC section, was lower in beam AS2sh than it in beam AS1sh reducing the end slip at failure load in beam AS2sh.

The strengthened beam after preloading up to service load, BS3sh`, produced almost similar end slip compared to the strengthened beam without preloading, BS3sh at one its strip ends, *S1*, as shown in Figure 4.11a. This supports the previous finding from the load-deflection responses that the pre-cracked NSM strengthened beam has identical behavior to the virgin NSM strengthened beam after pre-cracking load.

Beam BS3sh` had a lower end slip at the other end, *S2* as shown in Figure 4.11b. Table 4.4 shows that, $S2_y$ of beam BS3sh` was zero while it was 0.03 in beam BS3sh and $S2_u$ decreased from 0.33 mm to 0.2 mm with percentage of 40%. This might be due to occurrence of failure at lower load with different mode of intermediate flexural crack induced concrete cover separation, ICs.

4.2.2.5 Variation of strains with load

The concrete strains at the top of RC section, ε_c, and tension steel strain, ε_s, at the mid-span of the six strengthened beams were recorded and plotted on horizontal axis in $\mu\varepsilon$ versus load, *P*, in kN as shown in Figure 4.12 for groups A1 and B1. Moreover, ε_c and ε_s versus *P* curves of the un-strengthened beams were plotted on the same figure for comparison. The concrete strains are presented in the left side with negative values and the steel strains are presented in the right side with positive values. All steel strain gages were failed before the failure of the beams. Therefore, only the first 6000 $\mu\varepsilon$ of steel strain are presented. Also, the steel strain gage of beam BS3sh` from group B1 was failed before loading. Therefore, the results of its steel stains are not presented.

The summary of concrete strains, ε_c and tension steel strains, ε_s at mid-span section at cracking, yield and ultimate loads for each beam are listed in $\mu\varepsilon$ in Table 4.5. Strain notations are tailed by $_{cr}$, $_y$, and $_u$ for cracking, yield and ultimate points, respectively. Because of load change at main points by strengthening, the values of strains divided by its corresponding load to illustrate the effect in numbers.

As shown in Figure 4.12a, the beams strengthened with A_f of 28 mm^2, AS1sh and BS3sh produced lower ε_c at the same loads compared to reference beams AR1sh and BR3sh, respectively. By increasing A_f to 56 mm^2 in beam AD1sh, ε_c was reduced at the same loads compared to beam AS1sh but with difference lower than beam AS1sh compared

to beam AR1sh. Also, increasing A_f to 84 mm² in beam BT3sh reduced ε_c at the same loads compared to beam BS3sh with difference lower than beam BS3sh compared to beam BR3sh, but better than group A1.

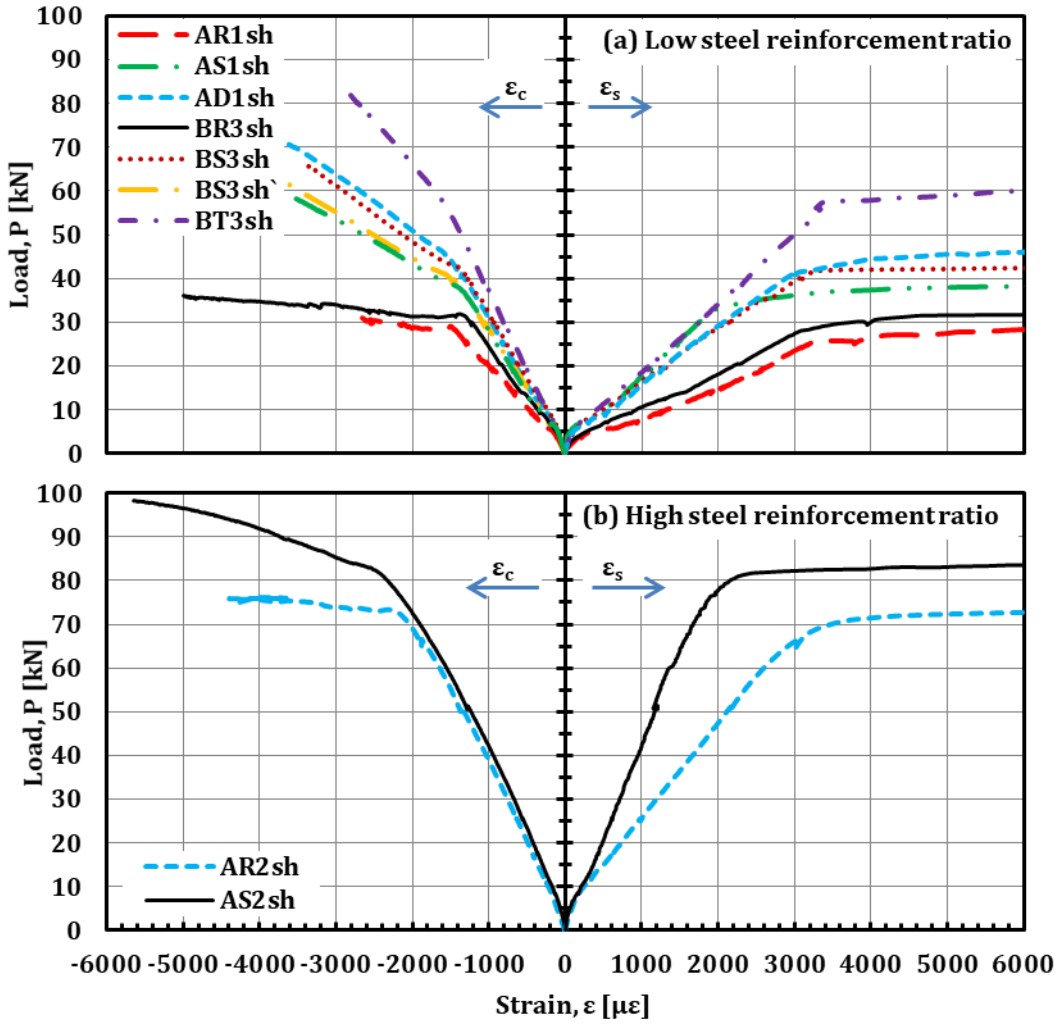

Figure 4.12 Strains of concrete and tensile steel at mid-span section for the tested beams.

The concrete strain at failure of beam AD1sh was higher than it in beam AS1sh, which means that the increasing of A_f would change the failure mode from CFRP rupture to concrete crushing, if the premature failures did not occur. The tension steel strains decreased by increasing A_f with difference between beam BT3sh and beam BS3sh almost equal the difference between beam BS3sh and beam BR3sh at yield point as shown in Figure 4.12a. As presented in Table 4.5, $\frac{\varepsilon_{s,y}}{P_y}$ changed from 243 in reference beam BR3sh to 152 in beams BS3sh and 59 in beam BT3sh with stepped decreases of 91 and 93, respectively.

Table 4.5 Concrete and tension steel strains for the tested beams.

	Beam ID	P_{cr} [kN]	$\varepsilon_{c,cr}$ [με]	$\frac{\varepsilon_{c,cr}}{P_{cr}}$	$\varepsilon_{s,cr}$ [με]	$\frac{\varepsilon_{s,cr}}{P_{cr}}$	P_y [kN]	$\varepsilon_{c,y}$ [με]	$\frac{\varepsilon_{c,y}}{P_y}$	$\varepsilon_{s,y}$ [με]	$\frac{\varepsilon_{s,y}}{P_y}$	P_u [kN]	$\varepsilon_{c,u}$ [με]	$\frac{\varepsilon_{c,u}}{P_u}$
Group A1	AR1sh	5.43	184	34	459	85	29.04	1493	51	7750	267	-- [a]	-- [a]	-- [a]
	AS1sh	5.67	113	20	102	18	38.26	1421	37	6400	167	58.52	3558	61
	AD1sh	6.50	127	20	210	32	44.76	1520	34	4000	89	73.09	3878	53
	AR2sh	4.35	90	21	77	18	72.55	2180	30	5405	75	76.08	4079	54
	AS2sh	4.65	60	13	50	11	81.80	2445	30	2620	32	98.35	5650	57
Group B1	BR3sh	5.80	156	27	378	65	31.90	1383	43	7753	243	36.08	4999	139
	BS3sh	7.10	127	18	216	30	42.50	1394	33	6452	152	65.98	3401	52
	BT3sh	8.70	180	21	300	34	57.00	1574	28	3343	59	82.65	2851	34
	BS3sh'	-- [b]	-- [b]	-- [b]	-- [c]	-- [c]	42.00	1697	40	-- [c]	-- [c]	64.04	3893	61

[a] The test of this beam test was stopped after yielding and before failure.
[b] This beam doesn't have cracking point because it was loaded up to service load before strengthening.
[c] The strain gage were failed.

The tension steel strains of beam AS2sh with higher steel reinforcement ratio were reduced by NSM strengthening compared to reference beam AR2sh as shown in Figure 4.12b. The decrease in strains by strengthening was lower than it in beam AS1sh with lower steel reinforcement ratio compared to reference beam AR1sh as shown in Figure 4.12a. The concrete strain in beam AS2sh had a slight decrease by NSM strengthening up to yield point as shown in Figure 4.12b. Then, it produced higher strains up to failure with value of 5650 $\mu\varepsilon$ obtaining the failure mode of the un-strengthened beam AR2sh, which failed by concrete crushing at ε_c of 4079 $\mu\varepsilon$ as reported in Table 4.5. This means that reason of this high increase in ε_c at failure load was scattering of concrete failure strain not the NSM strengthening.

Beam BS3sh`, which was strengthened after loading, showed higher concrete strains than beam BS3sh, strengthened without previous loading, as shown in Figure 4.12a. This can be seen in Table 4.5 at yield and failure points. $\frac{\varepsilon_{c,y}}{P_y}$ and $\frac{\varepsilon_{c,u}}{P_u}$ increased from 33 and 52 in beam BS3sh to 40 and 61 in beam BS3sh`, respectively.

The CFRP strain at mid-span section, ε_{f1}, was plotted on horizontal axis in $\mu\varepsilon$ versus load, P, in kN as shown in Figure 4.13. The CFRP strain gage at mid-span of beam AS1sh from group A1 was failed before loading. Therefore, its results are not presented.

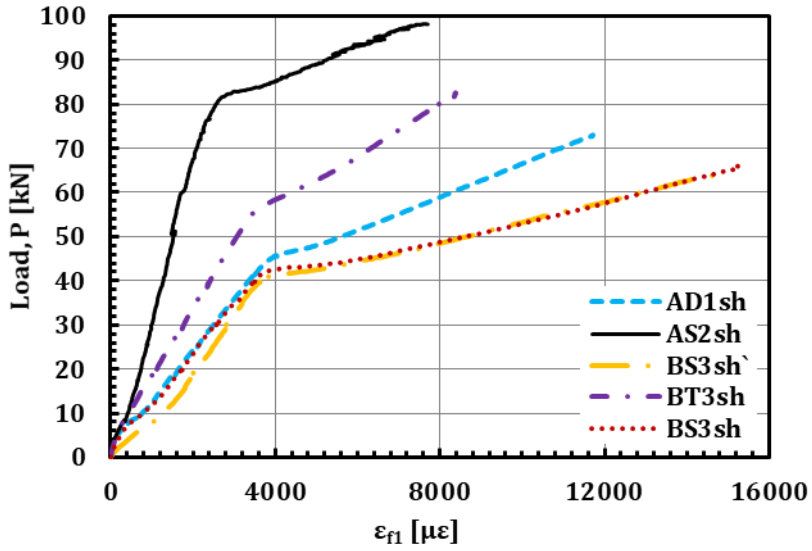

Figure 4.13 CFRP strains at mid-span section for the strengthened beams.

The CFRP strains at mid-span section at loads of cracking, $\varepsilon_{f1,cr}$, yield, $\varepsilon_{f1,y}$, and failure, $\varepsilon_{f1,u}$, for strengthened beams are summarized in $\mu\varepsilon$ in Table 4.6.

Table 4.6 CFRP strain results at mid-span section for the strengthened beams.

	Beam ID	P_{cr} [kN]	$\varepsilon_{f1,cr}$ [με]	P_y [kN]	$\varepsilon_{f1,y}$ [με]	P_u [kN]	$\varepsilon_{f1,u}$ [με]
Group A1	AS1sh	5.67	-- [c]	38.26	-- [c]	58.52	-- [c]
	AD1sh	6.50	283	44.76	3800	73.09	11708
	AS2sh	4.65	120	81.80	2765	98.35	7713
Group B1	BS3sh	7.10	385	42.50	4038	65.98	15235
	BT3sh	8.70	340	57.00	3720	82.65	8391
	BS3sh`	-- [b]	-- [b]	42.00	4605	64.04	13470

[b] This beam doesn't have cracking point because it was loaded up to service load before strengthening.
[c] The strain gage was failed.

The longitudinal strain distributions along half of the bond length of the CFRP strip were recorded using four strain gauges (Sf1 at mid-span, Sf2 at loading point, Sf3 and Sf4 at 350 mm and 150 mm from strip end, respectively) and plotted at several different loads in Figure 4.14 and Figure 4.15 for group A1 and group B1, respectively. The horizontal axes of these figures present the half length of CFRP strip from start at zero to mid-span at 900 mm. The crack patterns marked on the half of strengthened part at a load near to yielding are presented along its corresponding length on these figures with the positions of strain gages as vertical dash lines for each strengthened beam. The plotted strains were at cracking, yield and ultimate loads besides two

constant loads for each group. The constant loads were P1=25.4 kN and P2=40 kN for group A1 and P1=20.31 kN and P2=40 kN for group B1. Two of CFRP strain gages, Sf1 and Sf3 in beam AS1sh and Sf2 and Sf3 in beam AD1sh were failed. So, the strain distributions of these beams are not completed in Figure 4.14 for group A1. The strain values recorded by all the strain gauges increased with load.

Strain along CFRP strip in the middle third of beam AS2sh, as shown in Figure 4.14c, was higher than it along the rest of strip length. But it was 7713 $\mu\varepsilon$ as shown in Figure 4.13 and as reported in Table 4.6 (around 50% of the failure strain of CFRP), which couldn't cut the strip. While the narrower crack spacing, due to more cracks at the failure load, induced high shear stresses between middle third cracks leading to intermediate concrete cover separation at the same time of the concrete crushing of beam.

As shown in Figure 4.15 for group B1, the CFRP strain in beam BT3sh, which had A_f of 84 mm^2, was lower than it beam BS3sh, which had A_f of 28 mm^2, along all plotted strain profiles, although, beam BT3sh had higher cracking, yield, ultimate loads compared to beam BS3sh. This effect was clearer at mid-span section as shown in Figure 4.13.

The strains along CFRP in beam BS3sh`, shown in Figure 4.15c, showed values and profiles about them in beam BS3sh, shown in Figure 4.15a, up to yield load. While, beam BS3sh`showed lower strain values and different profile at failure load, where, the CFRP strains at 150 mm and 350 mm from strip end were very low compared to their values in beam BS3sh. Their values were 10200 $\mu\varepsilon$ and 12300 $\mu\varepsilon$ in beam BS3sh and 3100 $\mu\varepsilon$ and 10100 $\mu\varepsilon$ in beam BS3sh`, respectively. This reflects lower shear stresses at strip end of beam BS3sh`, which reduced the probability of the premature failure ECs more than it in beam BS3sh. On other hand, the loading of beam BS3sh` previous to NSM strengthening caused large number of cracks in the middle third compared to beam BS3sh leading to higher shear stresses causing another premature failure of ICs at maximum CFRP strain of 13470 $\mu\varepsilon$ on opposition of CFRP rupture at 15235 $\mu\varepsilon$ in beam BS3sh as reported in Table 4.6.

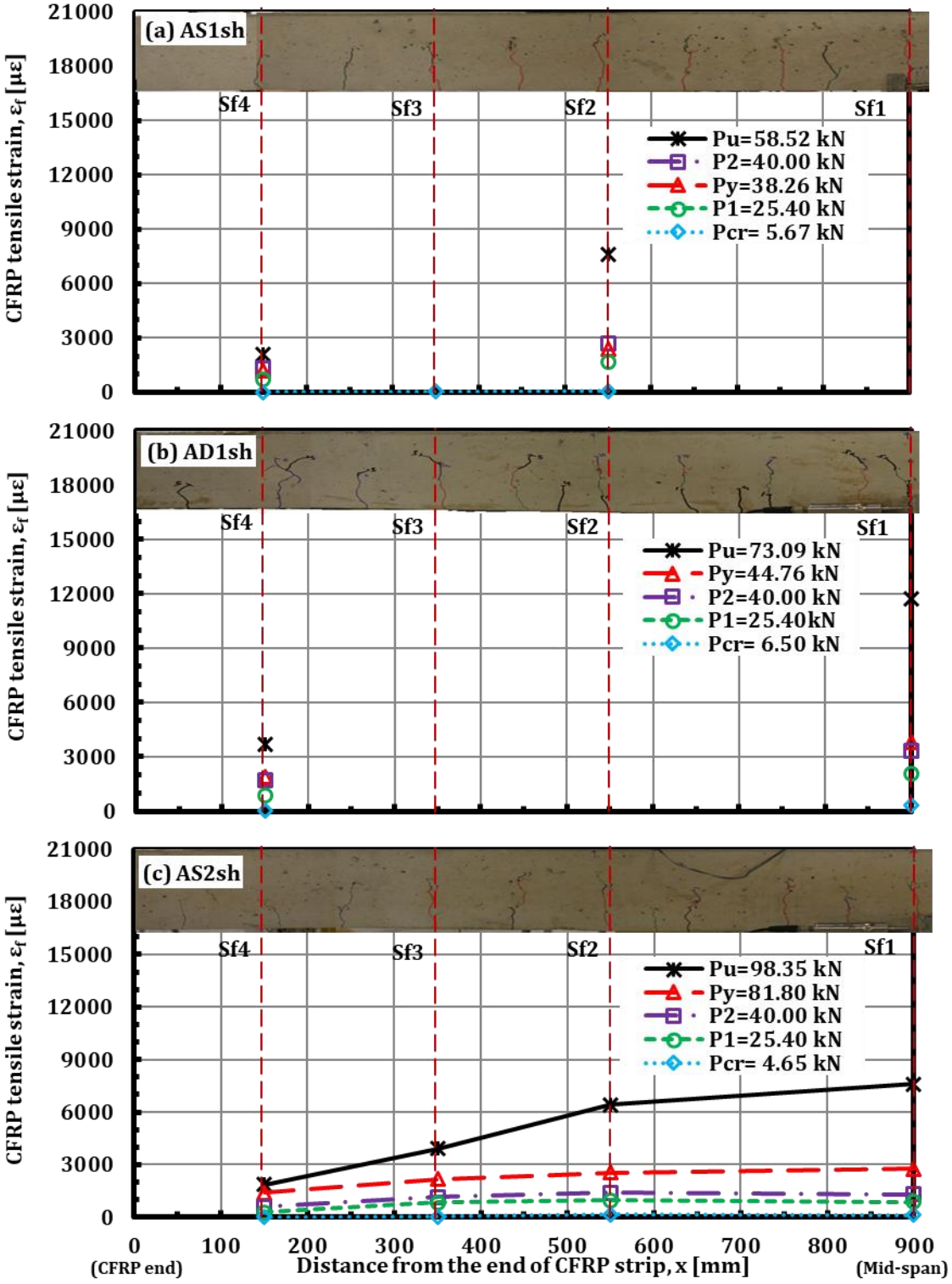

Figure 4.14 Longitudinal strain distribution along CFRP strip for strengthened beams in group A1.

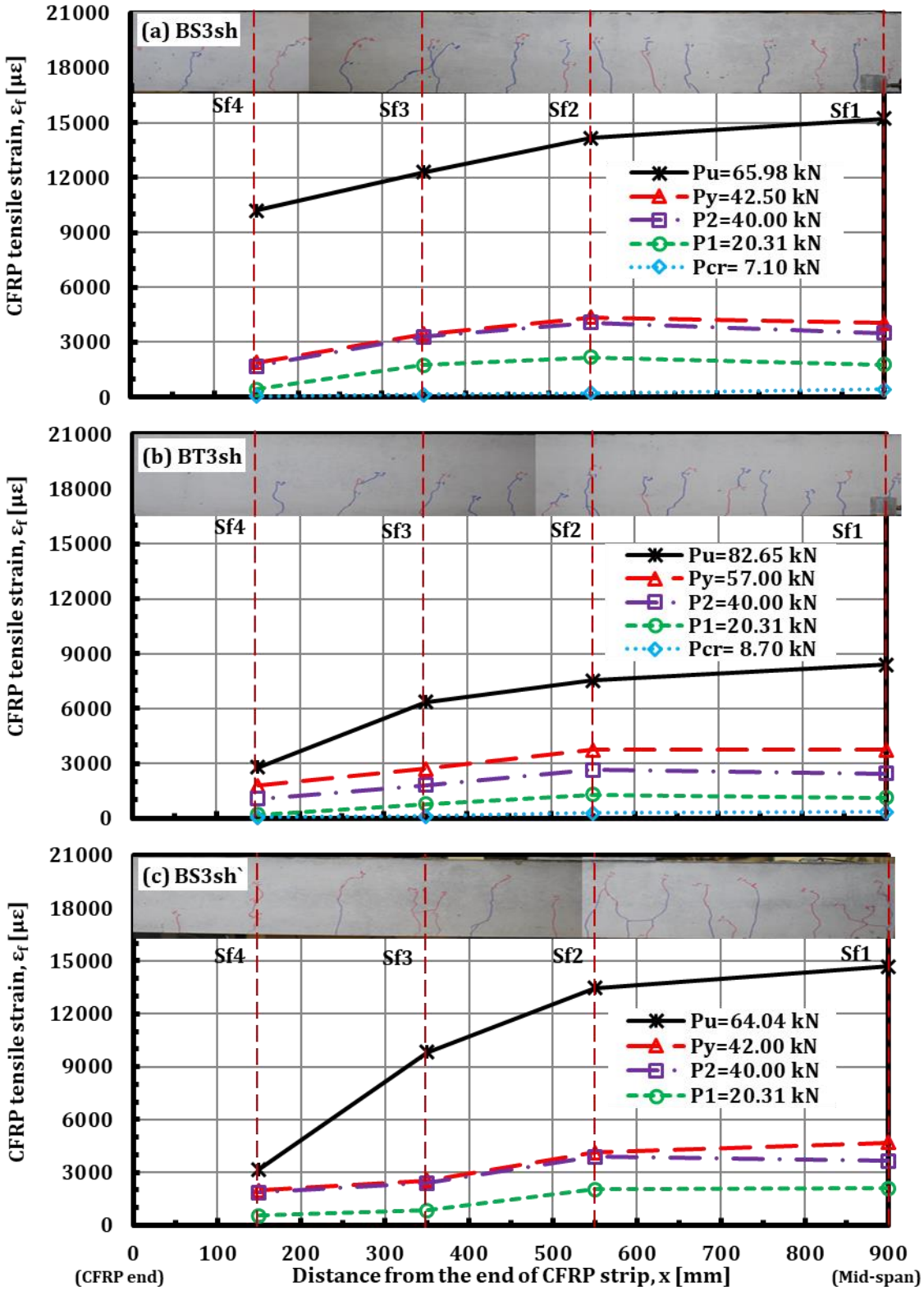

Figure 4.15 Longitudinal strain distribution along CFRP strip for strengthened beams in group B1.

4.3 Time Dependent Flexural Behavior under Sustained Loading

This section presents the experimental results and analysis for the sustained loading tests carried out on the beams of group A2 from series A and group B2 from series B. The tested parameters and the full details of these beams were described in Table 3.1 in CHAPTER 3. The presented experimental results are discussed in terms of loads, deflections, cracking, strains variation of constitutive materials (steel, concrete and CFRP strips) and slip of CFRP strips for strengthened beams. The results of each studied parameter are presented and discussed in the following.

4.3.1 Flexural behavior under two loading/unloading cycles

The results of the beams subjected to two loading/unloading cyclic are presented and discussed here. Group A involved three beams with ρ of 0.77% (un-strengthened beam AR1I and two strengthened beams; AS1I with A_f of 28 mm^2 and beam AD1I with A_f of 56 mm^2) and two beams with ρ of 1.97% (un-strengthened beam AR2I and strengthened beam AS2I). The two beams of group B2 had ρ of 0.77% and were un-strengthened beam BR1I` and strengthened beam BS1I` with A_f of 28 mm^2.

4.3.1.1 Load-deflection responses

The load-deflection curves of the tested beams under two loading/unloading cyclic are presented in Figure 4.16. This figure shows the relation between the applied load, P, in kN on the vertical axis and the deflection at mid-span section of each beam in mm on the horizontal axis.

All beams showed the initial linearity up to cracking with higher cracking loads for the strengthened beams than for the un-strengthened beams, due to the increase in un-cracked element stiffness by NSM strengthening. By increasing the load, the slope had a progressive decrease up to the service design load, P_D. During the two cycles, the slope had a significant change compared to that of the un-cracked stage. Moreover, all beams kept some permanent deflection, $\delta_{r,o}$, after the 2nd unloading cycle.

Table 4.7 includes the maximum load of two cycles, i.e. service design load (P_D), and its corresponding deflection (δ_D), the sustained load (P_s), and the ratio between the applied moment and cracking moment at service design loads, $M_D/M_{cr,}$ and at sustained loads, M_s/M_{cr}. The sustained load will be applied after the application of loading/unloading cycles.

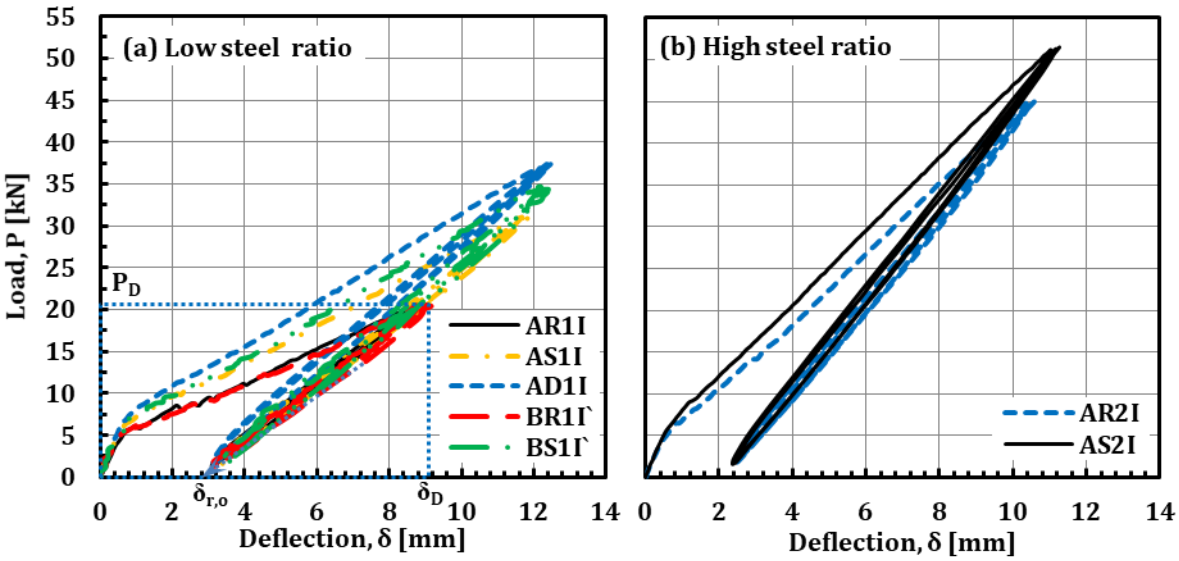

Figure 4.16 Load-deflection curves of the beams subjected to two loading/unloading cycles.

Table 4.7 Load-deflection results for the tested beams under two loading/unloading cycles.

	Beam ID	P_D [kN]	M_D/M_{cr}	δ_D [mm]	$\delta_{r,o}$ [mm]	P_s [kN]	M_s/M_{cr}
Group A2	AR1I	19.87	3.66	8.50	2.70	12.40	2.28
	AS1I	31.17	5.50	11.75	3.00	13.62	2.40
	AD1I	37.67	5.80	12.50	2.80	14.71	2.26
	AR2I	45.15	10.38	10.45	2.10	18.16	4.18
	AS2I	51.58	11.09	11.11	2.12	18.74	4.03
Group B2	BR1I`	20.31	3.98	8.75	3.02	14.19	2.78
	BS1I`	34.62	5.09	12.13	3.14	14.19	2.07

The un-strengthened beams AR1I and BR1I` showed similar load-deflection responses as shown in Figure 4.16a. This similarity happened despite the increase in the concrete strength of beam BR1I` compared to beam AR1I. Therefore, it can be concluded that the increase in the concrete strength had no effect on the flexural behavior of the un-strengthened RC beams. However, the using of higher concrete strength in strengthened beams BS1I` slightly enhanced its flexural behavior compared to beam AS1I of lower concrete strength. As discussed before, this may be due to the additional function of the concrete cover in the strengthened beams as a transmission media for the resistance force in CFRP strips. Therefore, the increase of concrete cover strength increased the load transfer efficiency of NSM strengthened RC sections leading to higher stiffness of whole strengthened beam enhancing its flexural behavior.

As a result of increasing P_D in the strengthened beams, their cracking levels were very high compared with the un-strengthened beams as can be seen from the values of M_D/M_{cr} listed in Table 4.7. The increase in cracking level by NSM strengthening was lower in series B beams. For series A beams, M_D/M_{cr} increased from 3.66 in beam AR1I to 5.50 in beam AS1I with difference of 1.84. While for series B beams, it increased from 3.98 in beam BR1I` to 5.09 in beam BS1I` with difference of 1.11. This might lead to reduce the increase in $\delta_{r,o}$ of these beams by NSM strengthening from 0.3 mm in series A beams to 0.12 mm in series B beams.

The linearity limit ($\sigma_{co} \leq 0.4 f_c$) for concrete creep behavior used to calculate the sustained loads according to Eurocode 2 [100], gave a limited increase in M_s/M_{cr} compared with the significant increase in M_D/M_{cr}. Application of the same instantaneous concrete stress of $0.34 f_c$ for series A beams led to increase sustained load of strengthened beam AS1I resulting higher value of M_s/M_{cr} compared to un-strengthened beam AR1I. While, the application of the same sustained load for series B beams led to decrease the value of M_s/M_{cr} of the strengthened beam BS1I` compared to the un-strengthened beam R1B'.

The strengthened and un-strengthened beams of higher steel reinforcement ratio started cracking at loads lower than beams of lower steel reinforcement ratio as shown in Figure 4.16a and b, respectively. These beams were left for 50 days after curing, and before testing the concrete shrinkage strain was around 424 $\mu\varepsilon$ from concrete prism and 574 $\mu\varepsilon$ from cylinders. The previous shrinkage of concrete was restrained by the reinforcement inducing tensile stresses in concrete that might significantly affect the cracking resistance and short-term deformations of RC elements [149,162,163]. This effect increases by increasing reinforcement ratio explaining the decrease in cracking load.

The strengthened beams of higher steel reinforcement ratio showed higher stiffness compared to the un-strengthened ones during the initial loading part. In the beams with higher ρ, the increase in this stiffness by NSM strengthening was lower compared with the beams with lower ρ. This might be due to the smaller ratio between added stiffness of CFRP to the tension steel stiffness in beams with higher ρ comparing with this ratio in beams with lower ρ.

The stiffness during the two loading/unloading cycles was a bit higher in beam AS2I compared to beam AR2I, while it was almost similar in beam AS1I compared to beam AR1I.

As a result of increasing P_D in the beams with higher ρ, their cracking levels were very high compared with the beams with lower ρ as can be seen from the values of M_D/M_{cr} listed in Table 4.7. Moreover, the NSM strengthening in the beams with higher ρ did not highly increase the M_D/M_{cr} unlike in the beams with lower ρ by adding the same CFRP area. This led to remaining almost equal values of $\delta_{r,o}$ in the beams with higher ρ.

The linearity limit for concrete creep behavior used to calculate the sustained loads according to Eurocode 2 [100], gave a limited increase in M_s/M_{cr} compared with the significant increase in M_D/M_{cr} by increasing steel reinforcement ratio. The higher values of P_s of the beams with higher ρ, led to higher values of in M_s/M_{cr} compared with the beams with lower ρ but decreasing by NSM strengthening.

The stiffness of strengthened beams during the initial part of loading was higher as the CFRP area was higher as shown in Figure 4.16. The stiffness during the two loading/unloading cycles was higher in beam AD1I, while it was almost similar in beam AS1I compared to reference beam AR1I.

Although, the observed equality in stiffness difference between beams AR1I and AS1I and between beams AS1I and AD1I after cracking as shown in Figure 4.16a, the deflection at service design load, δ_D, increased from 8.5 mm in reference beam AR1I to 11.75 mm by NSM strengthening with A_f of 28 mm^2 in beam AS1I with percentage of 38% then, it increased to 12.5 mm with a lower additional percentage of 9% by doubling A_f in beam AD1I as reported in Table 4.7. This was due to the increase of P_D from 19.87 kN in reference beam AR1I to 31.17 kN in beam AS1I with a percentage of 57% then, it increased to 37.67 kN with a percentage of 90% in beam AD1I.

As a result of the significant increase in P_D by NSM strengthening, the cracking levels of strengthened beams became very high. With respect to the reference beam AR1I, M_D/M_{cr} increased with percentage of 50% and 59% in beams AS1I and AD1I, respectively. However, the cracking levels at the sustained load, P_s, were almost around the reference beam cracking level. This is due to the linearity limit for concrete

creep behavior used to calculate the sustained loads according to Eurocode 2 [100], which gave a limited increase in P_s compared with the significant increase in P_D.

The permanent deflection observed after unloading increased from 2.7 mm in beam AR1I to 3 mm in beam AS1I and decreased again to 2.8 mm in beam AD1I as presented in Table 4.7. This might be due the near cracking levels of strengthened beams and more reinforcing by higher CFRP area in beam AD1I recovering deflection more than it in beam AS1I.

4.3.1.2 Load-cracking responses

The crack width, ω was measured in mm at a notch preformed at mid-span section for each beam and plotted on the horizontal axis versus load, P in kN on the vertical axis in Figure 4.17 for group A2.

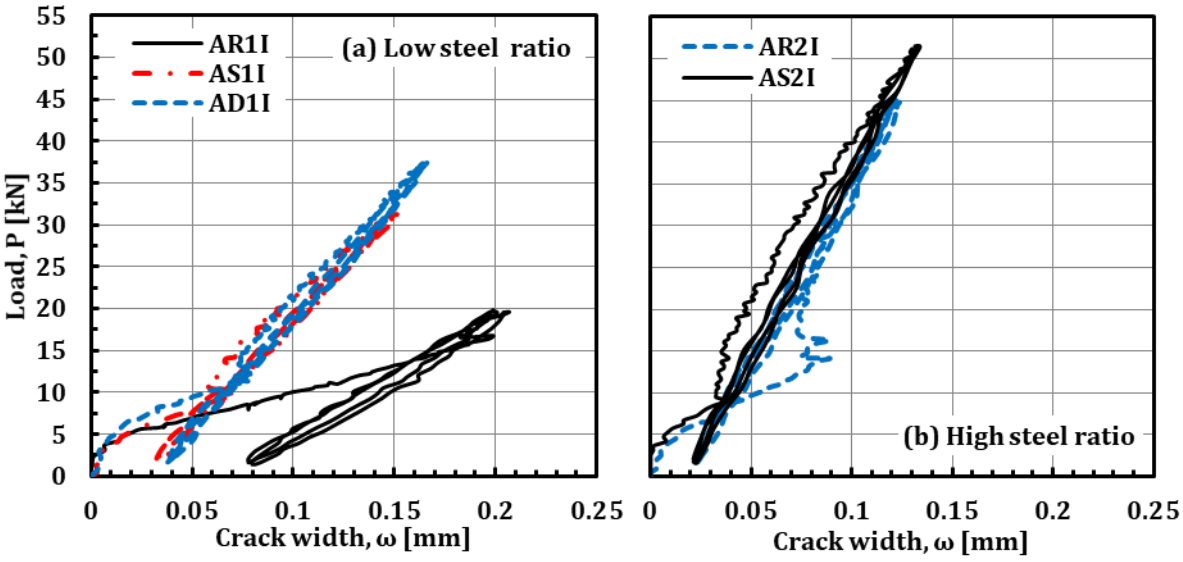

Figure 4.17 Load-crack width curves of the beams subjected to two loading/unloading cycles.

The crack patterns were detected by visual inspection and drawn using permanent colored makers at the end of the two loading/unloading cycles as shown in Figure 4.18 and Figure 4.19 for the un-strengthened and strengthened beams, respectively.

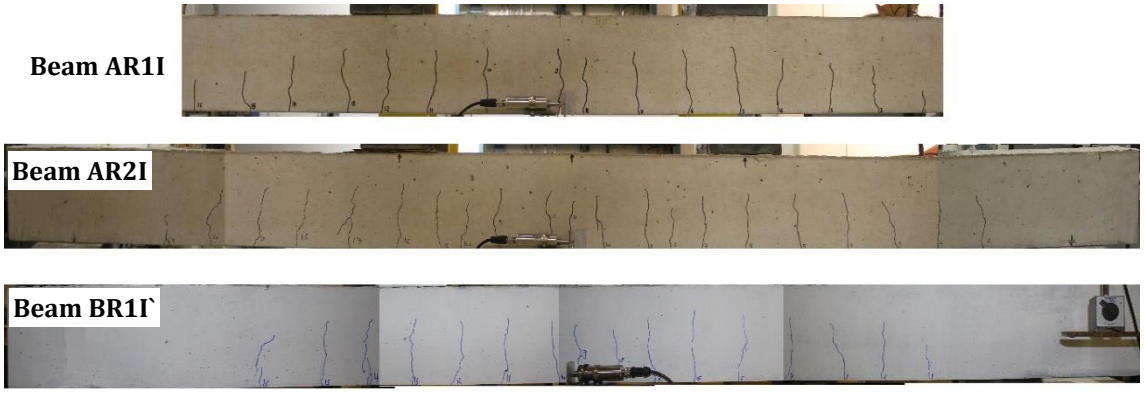

Figure 4.18 Crack patterns of the un-strengthened beams subjected to two loading/unloading cycles.

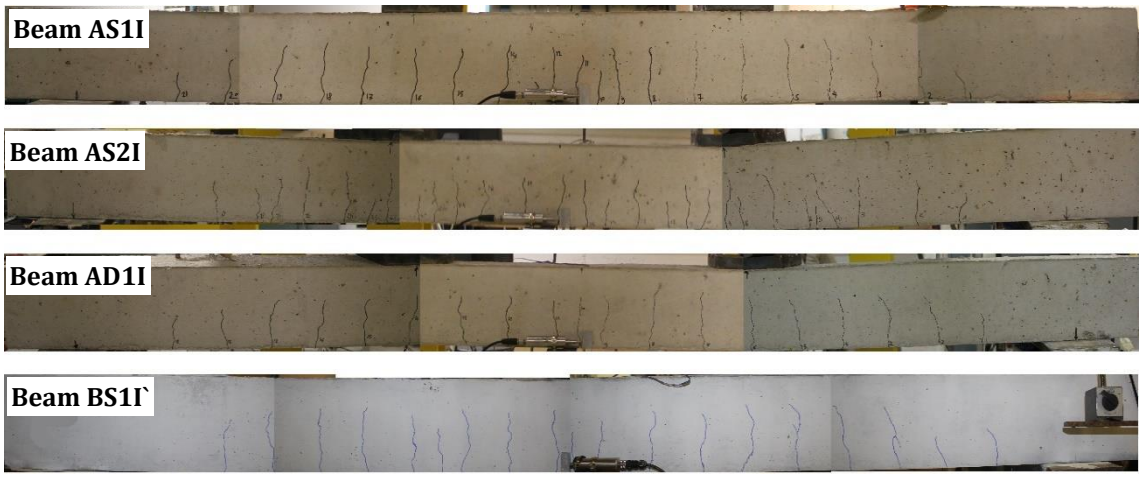

Figure 4.19 Crack patterns of the strengthened beams subjected to two loading/unloading cycles.

The values of the measured crack width for each beam at service design load, ω_D, and the permanent crack width, $\omega_{r,o}$, were summarized in Table 4.8. The crack spacing, s, along the middle third of each beam was measured in mm at the end of the two loading/unloading cycles and listed in Table 4.8 as minimum crack spacing, s_{min}, maximum crack spacing, s_{max}, mean crack spacing, s_{mean} and its standard deviation, s_{SD}. Also, the crack length, a, along the middle third of each beam was measured in mm at the end of the two loading/unloading cycles and listed in Table 4.8 as minimum crack length, a_{min}, maximum crack length, a_{max}, mean crack length, a_{mean} and its standard deviation, a_{SD}.

The un-strengthened beam BR1I` with higher concrete strength showed a bit higher crack width during loading compared to the un-strengthened beam AS1I with lower concrete strength. This can be noticed in Table 4.8 from the increase in the values of $\omega_D$ and $\omega_{r,o}$ in beam BR1I` compared to beam AS1I.

Table 4.8 Cracking results for the tested beams under two loading/unloading cycles.

	Beam ID	P_D [kN]	ω_D [mm]	$\omega_{r,o}$ [mm]	Cracks along the middle third of the beam							
					No. of cracks	Crack spacing, s [mm]				Crack length, a [mm]			
						s_{min}	s_{max}	s_{mean}	s_{SD}	a_{min}	a_{max}	a_{mean}	a_{SD}
Group A2	AR1I	19.87	0.20	0.07	8	45	145	105	30	102	125	117	7
	AS1I	31.17	0.15	0.03	11	35	103	70	26	47	122	102	24
	AD1I	37.67	0.17	0.04	9	46	116	87	26	106	131	118	8
	AR2I	45.15	0.12	0.02	11	34	104	70	26	83	122	105	12
	AS2I	51.58	0.13	0.02	14	27	92	53	18	60	115	93	20
Group B2	BR1I`	20.31	0.24	0.09	9	41	121	86	26	99	132	118	9
	BS1I`	34.62	0.15	0.03	10	39	111	77	29	80	128	111	16

On the strengthening effect, the strengthened beams of different concrete strengths showed almost the same load-crack width response as shown in Table 4.8, which shows the same values of ω_D and $\omega_{r,o}$ in beams AS1I and BS1I` with different concrete strengths. Using larger A_f of 56 mm^2 in beam AD1I did not affect a lot on the load-crack width response compared to beam AS1I with A_f of 28 mm^2 as shown in Figure 4.17a. The load-crack width curves of the beams with high steel reinforcement ratio, plotted in Figure 4.17b, show almost the same responses for un-strengthened beam AR2I and strengthened beam AS2I at their corresponding service design load. The similar values of ω_D and $\omega_{r,o}$ presented in Table 4.8 for the two beams support this finding.

As presented in Table 4.8, the number of cracks of the un-strengthened beam BR1I` of higher concrete strength was higher than it in the un-strengthened beam AR1I of lower concrete strength. However, the crack spacing and crack length in beam BR1I` were lower than them in beam AR1I. On the contrary, the number of cracks of the strengthened beam BS1I` of higher concrete strength was lower than it in the strengthened beam AS1I of lower concrete strength. However, the crack spacing and crack length in beam BS1I` were higher than them in beam AS1I. The NSM strengthening with A_f of 28 mm^2 in all cases (different concrete strengths or different steel reinforcement ratios) increased the number of cracks, decreased the crack spacing and decreased the crack length. Despite this, the increasing of A_f to 56 mm^2 in beam AD1I decreased the number of cracks, increased the crack spacing and increased the crack length compared to beam AS1I with A_f of 28 mm^2.

The un-strengthened and strengthened beams with higher steel reinforcement ratio, i.e. beams AR2I and AS2I, showed larger number of cracks, lower crack spacing and lower crack length than the corresponding beams with lower steel reinforcement ratio, i.e. beams AR1I and AS1I.

4.3.1.3 Variation of strains with load

The concrete strain at the top of RC section, ε_c, and tension steel strain, ε_s, at the mid-span of each beam were plotted on horizontal axis in $\mu\varepsilon$ versus load, P, in kN as shown in Figure 4.20 for groups A1 and B1.The concrete strains are presented in the left side with negative values and the steel strains are presented in the right side with positive values.

The CFRP strain at mid-span section, ε_{f1}, was plotted on horizontal axis in $\mu\varepsilon$ versus load, P, in kN as shown in Figure 4.21.

The values of ε_c, ε_s and ε_{f1} at mid-span section at service design load and their permanent values for each beam are summarized in Table 4.9 in $\mu\varepsilon$. Strain notations are tailed by $_D$ and $_{r,o}$ for strains at P_D and permanent strains, respectively.

The un-strengthened beams, AR1I and BR1I`, with different concrete strengths showed almost the same load-concrete strain response at the top of mid-span section as shown in Figure 4.20a. However, the strengthened ones, AS1I and BS1I`, showed different load-concrete strain response. As reported in Table 4.9, the values of $\varepsilon_{c,D}$ and $\varepsilon_{c,r,o}$ for the un-strengthened beams, AR1I and BR1I`, were almost the same. However, these values in the strengthened beam AS1I were higher than those in the strengthened beam BS1I` with higher concrete strength.

The un-strengthened beam AR1I with lower concrete strength showed higher steel strain with load compared to the un-strengthened beam BR1I`with higher concrete strength as shown in Figure 4.20a. Opposite trend was observed for strengthened beams, beam AS1I with lower concrete strength showed lower steel strain with load compared to the beam BS1I` with higher concrete strength, see Table 4.9. This happened despite the similarity between the crack widths of the two strengthened beams and although the un-strengthened beams showed larger crack width in beam BR1I` compared to beam AR1I. This may be due to a bit misalignment of the positions of strain gage and measured crack.

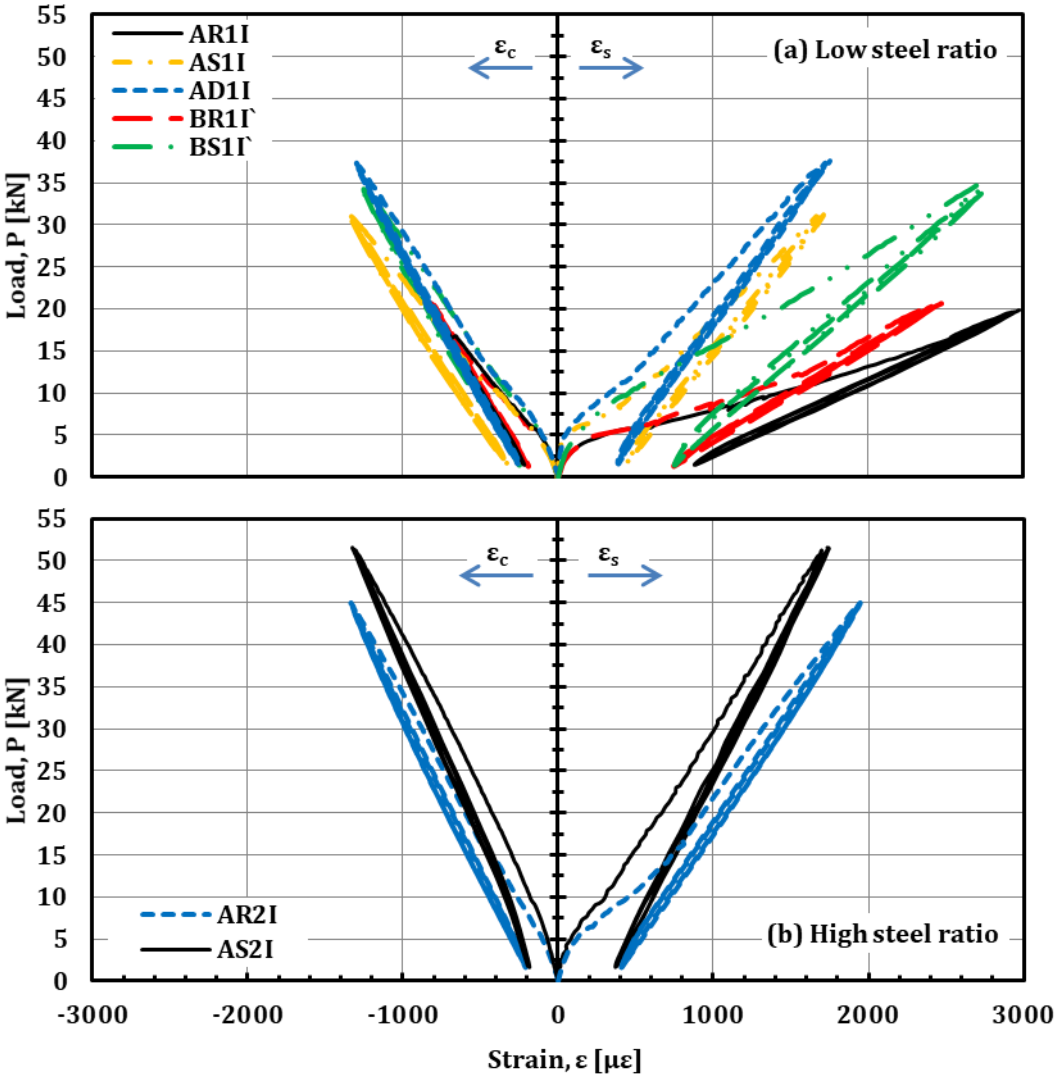

Figure 4.20 Strains of concrete and tensile steel at mid-span section for the tested beams under two loading/unloading cycles.

As shown in Figure 4.20a, the strengthened beam AS1I with A_f of 28 mm² in group A2 showed the same load- concrete strain response of the un-strengthened beam AR1I during the initial loading part. Then, it showed larger slope during the two loading/unloading cycles with higher concrete strains compared to the un-strengthened beam AR1I. On the other hand, the strengthened beam BS1I` with $A_f$ of 28 mm² in group B2 showed higher concrete strains with load compared to the un-strengthened beam BR1I`. By increasing A_f to 56 mm² in beam AD1I, the slope of the load-concrete strain curve was smaller with lower concrete strains compared to beam AS1I, see Table 4.9.

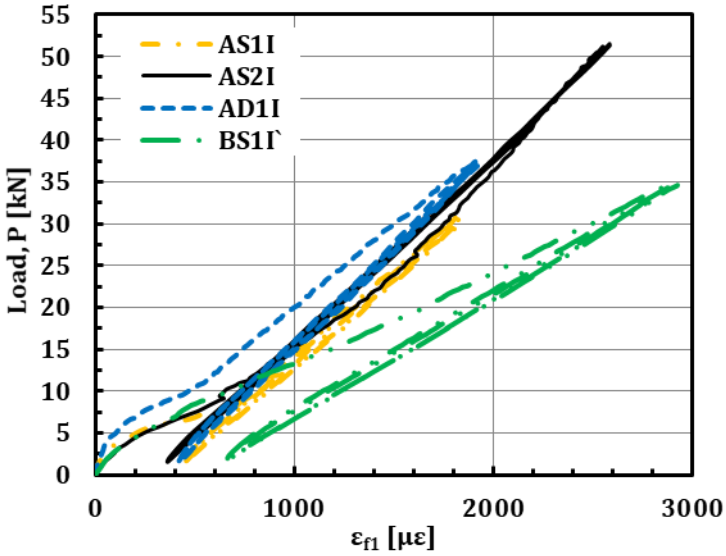

Figure 4.21 Strains of CFRP strip at mid-span section for the tested beams under two loading/unloading cycles.

Table 4.9 Strains of concrete, tension steel and CFRP strip at mid-span section for the tested beams under two loading/unloading cycles.

	Beam ID	P_D [kN]	$\varepsilon_{c,D}$ [με]	$\varepsilon_{s,D}$ [με]	$\varepsilon_{f1,D}$ [με]	$\varepsilon_{c,r,o}$ [με]	$\varepsilon_{s,r,o}$ [με]	$\varepsilon_{f1,r,o}$ [με]
Group A2	AR1I	19.87	804	2950	---	200	880	---
	AS1I	31.17	1340	1690	1840	320	450	450
	AD1I	37.67	1290	1720	1920	250	380	420
	AR2I	45.15	1340	1940	---	200	400	---
	AS2I	51.58	1310	1730	2570	180	370	360
Group B2	BR1I`	20.31	800	2410	---	190	740	---
	BS1I`	34.62	1250	2730	2900	240	750	650

As shown in Figure 4.20b for the beams with higher steel reinforcement ratio, the strengthened beam AS2I showed concrete and steel strains with load lower than those in the un-strengthened beam AR2I, see Table 4.9.

The increase in CFRP area decreased the steel strain with load. This can be seen from the comparison between the load-steel strain curves plotted in Figure 4.20a for the three beams with different A_f in group A2 (beam AR1I with A_f of 0 mm^2, beam AS1I with A_f of 28 mm^2 and beam AD1I with A_f of 56 mm^2), see Table 4.9.

On the variation of CFRP strain at mid-span section plotted in Figure 4.21, it can be seen that beam BS1I` with higher concrete strength produced higher ε_{f1} with load compared to beam AS1I with lower concrete strength. Beam AD1I with A_f of 56 mm^2

had load-CFRP strain response close to the load-CFRP strain response of AS1I with A_f of 28 mm^2. Beam AS2I with higher steel reinforcement ratio showed increasing in ε_{f1} with load larger than it in beam AS1I with lower steel reinforcement ratio.

In terms of ε_{f1} values presented in Table 4.9, the values of $\varepsilon_{f1,\,D}$ and $\varepsilon_{f1,\,r,o}$ increased in beam BS1I` with higher concrete strength compared to beam AS1I with lower concrete strength. This happened despite the similarity of their crack widths. This may be due to a bit misalignment of the positions of strain gage and measured crack.

Beam AD1I with A_f of 56 mm^2 had higher $\varepsilon_{f1,\,D}$ and lower $\varepsilon_{f1,\,r,o}$ compared to beam AS1I with A_f of 28 mm^2. Beam AS2I with higher steel reinforcement ratio had higher $\varepsilon_{f1,\,D}$ and lower $\varepsilon_{f1,\,r,o}$ compared to beam AS1I with lower steel reinforcement ratio.

4.3.1.4 Load- end slip of CFRP strip responses

The registered end slips of CFRP strip at its two ends, *S1* and *S2*, were just a noise. This means that the applied design load was unable to produce a significant slip at the ends of CFRP strips for all strengthened beams subjected to two loading/unloading cycles.

4.3.2 Flexural behavior under sustained loading

All beams, either preloaded or virgin, were sustained loaded with concrete stress at the top of mid-span section below 0.4f_c. This stress was the same in all beams of group A2 producing different sustained loads. while the strengthened beams of group B2 were sustained loaded with the same sustained load of their corresponding un-strengthened beams. It is worth noting that microcracks and permanent deflection, $\delta_{r,o}$, occurred due to the application of two loading/unloading cycles will be taken into consideration for the analysis of beams under sustained load. The maximum load of these cycles was chosen according to the applied service design load, which was varied from beam to beam.

4.3.2.1 Beams with different CFRP areas

The effect of CFRP area on the time dependent flexural behavior of NSM CFRP strengthened RC beams was investigated using beams AR1I, AS1I and AD1I from group A2, which had different CFRP areas of 0, 28 and 56 mm^2, respectively, and beams BR3II`, BS3II` and BT3II` from group B2, which had different CFRP areas of 0, 28 and 84 mm^2, respectively.

Table 4.10 presents the applied sustained load, P_s in kN and its ratio to failure load, P_s/P_u for the beams with different CFRP area. Moreover, it includes $\delta_{r,o}$, instantaneous deflection, δ_i, initial deflection, $\delta_o = \delta_{r,o} + \delta_i$, total deflection at the end of the loading period, $\delta_{T,e}$, and permanent deflection after removing the sustained load, δ_r, in mm.

Table 4.10 Sustained loads and their deflections of the beams with different CFRP area.

	Beam ID	Sustained loads		Deflections [mm]					
		P_s [kN]	P_s/P_u	$\delta_{r,o}$	δ_i	$\delta_o = \delta_{r,o} + \delta_i$	$\delta_{T,e}$	δ_r	$\delta_{r,e} = \delta_r - \delta_{r,o}$
Group A2	AR1I	12.40	0.359	2.70	3.93	6.63	10.06	6.01	3.31
	AS1I	13.62	0.233	3.00	3.65	6.65	9.96	5.62	2.62
	AD1I	14.71	0.201	2.80	3.45	6.25	9.34	6.06	3.26
Group B2	BR3II`	14.19	0.393	0.00	5.33	5.33	10.61	5.40	5.40
	BS3II`	14.19	0.215	0.00	3.40	3.40	8.94	4.73	4.73
	BT3II`	14.19	0.172	0.00	2.78	2.78	7.43	4.66	4.66

Also, the difference between δ_r and $\delta_{r,o}$ is listed in the last column of Table 4.10 as the permanent deflection due sustained loading, $\delta_{r,e}$. The total deflections, δ_T of beams with different CFRP area in group A2 were plotted on the vertical axis in mm versus loading time, t in days on the horizontal axis as shown in Figure 4.22.

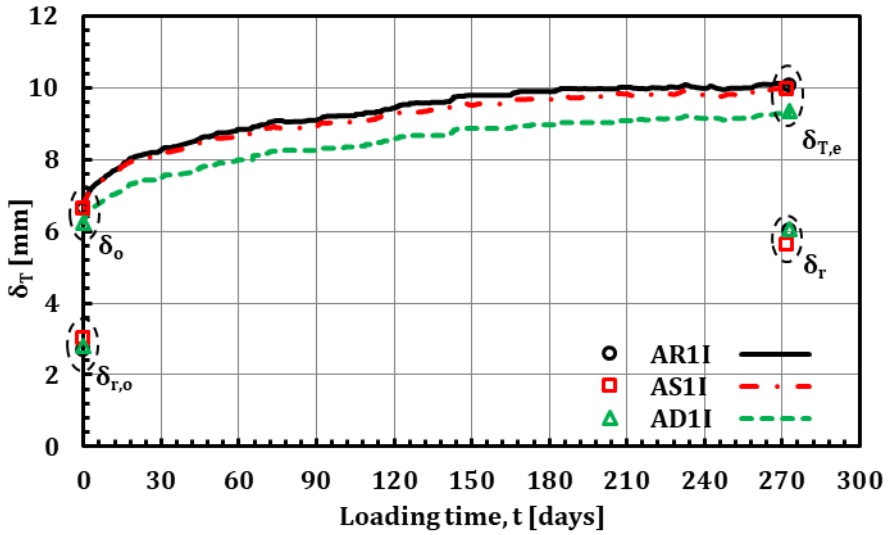

Figure 4.22 Total deflection with time for the beams of different CFRP area in group A2.

All beams have similar shape of their curves regardless of the CFRP strengthening areas. As can be seen in the steep slope at the beginning of the curves, the deflection increased considerably with time in the initial period. After 20 days the deflection

gained about 40% of the time dependent deflection at 270 days in all beams, while about 70% and 90% of time dependent deflection were achieved at 75 and 180 days, respectively.

It can be seen from Figure 4.22 that δ_T through the period of loading for the un-strengthened beam AR1I and the strengthened beam AS1I with A_f of 28 mm^2 were very close to each other. As presented in Table 4.10, the two beams had small differences in δ_o and $\delta_{T,e}$ of 0.02 mm and 0.1 mm, respectively. Not as expected the presence of NSM strengthening did not decrease δ_o and δ_T due to the increase in the RC section tensile stiffness. This may be due to higher cracking level (M_D/M_{cr}) of beam AS1I, which made more concrete in tension side out of work increasing the deflection. Furthermore, $\delta_{r,o}$ in beam AS1I is higher than that in beam AR1I. On the other hand, stored deformation in beam AS1I is higher than that in beam AR1I, i.e. δ_r in beam AR1I is higher than that in beam AS1I.

By increasing A_f to 56 mm^2 in beam AD1I, δ_T through the loading period decreased. This is presented in Table 4.10 as decreases in δ_o and $\delta_{T,e}$ compared to beam AS1I of 0.4 mm and 0.62 mm, respectively. This might be due to the nearby between the values of cracking level (M_D/M_{cr}) of the two strengthened beams AS1I and AD1I magnifying the decrease in δ_o by increasing A_f and therefore in δ_T. Furthermore, $\delta_{r,o}$ in beam AD1I is lower than that in beam AS1I.

As can be seen from Figure 4.22 and Table 4.10, the NSM strengthening reduced δ_r with 0.39 mm in beam AS1I of A_f = 28 mm^2 and increase it again with 0.44 mm in beam AD1I of A_f = 56 mm^2. On the comparison between the permanent deflection after the two loading/unloading cycles and after removing the sustained loads, the beam with lower A_f showed a higher decrease in $\delta_{r,e}$ than it in the beam with higher A_f. This trend was the opposite in permanent deflection after preloading, $\delta_{r,o}$ as mentioned before. This means that the larger CFRP area made the NSM strengthened beam retained more deflection from its time dependent deflection.

The ratio of the time dependent deflection ($\delta_{td}=\delta_T-\delta_o$) to the instantaneous deflection, δ_{td}/δ_i, of beams with different A_f from group A2 is plotted on the vertical axis versus loading time, t in days on the horizontal axis as shown in Figure 4.23.

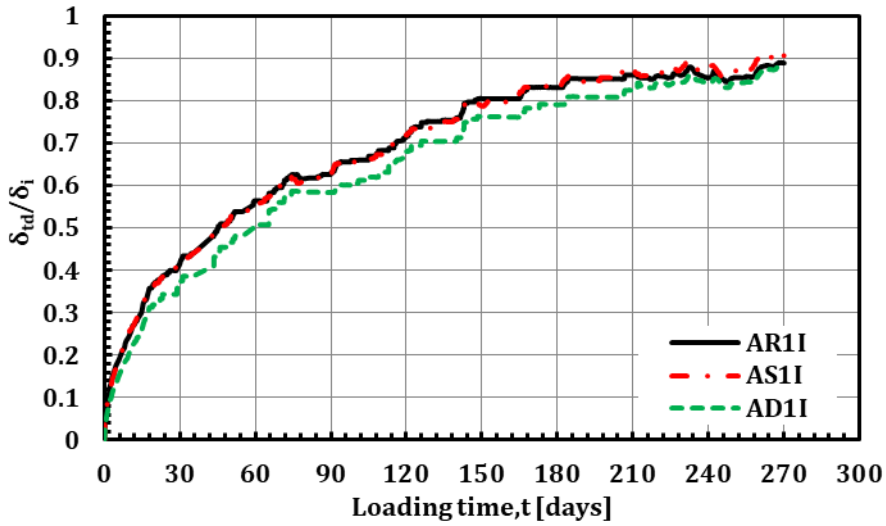

Figure 4.23 The ratio of time dependent deflection to instantaneous deflection of beams with different CFRP area from group A2.

All curves show a similar shape, regardless of values. δ_{td}/δ_i ratio was almost the same along the loading time for the un-strengthened beam AR1I and the strengthened beam As1I with A_f of 28 mm^2, while it was lower in the strengthened beam AD1I with A_f of 56 mm^2. This was at the odds of the fact that higher reinforcement ratios lead to higher neutral axis depth (larger compressed area of concrete), causing higher creep deformations, and therefore higher time-dependent deflections. This might be due to the preloading effect, which increased the cracking level (M_D/M_{cr}) of the strengthened beams specially the beam with higher A_f leading to lower neutral axis depth (smaller compressed area of concrete), causing lower creep deformations, and therefore lower time-dependent deflections than the expected. It is worth noting that the maximum load of preloading is higher than the sustained load. This may be one of the reasons to cause difficulty to make extensive creep damage, i.e. the instantaneous damage of the preloading is the main damage in the beam. Also, the presence of compression reinforcement decreases shrinkage curvature with increasing tensile reinforcement ratio for cracked section [122].

δ_T of the beams with different A_f in group B2 were plotted on the vertical axis in mm versus loading time, t in days on the horizontal axis as shown in Figure 4.24. All beams have the similar shape of their curves, regardless of the strengthening with different CFRP areas.

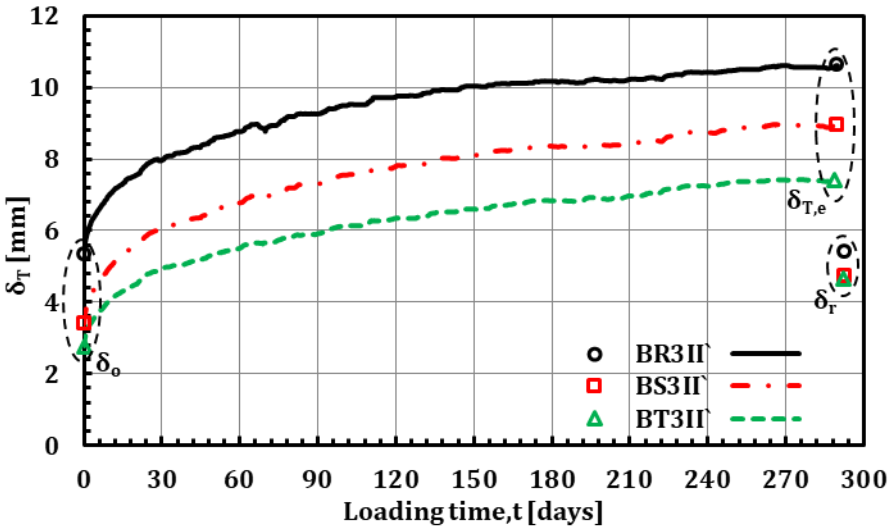

Figure 4.24 Total deflection with time for the beams of different CFRP area in group B2.

As can be seen in the steep slope at the beginning of the curves, the deflection increased considerably with time in the initial period. After 20 days the deflection gained about 47% of the time dependent deflection at 270 days, while about 90% of the time dependent deflection was achieved at 180 days. The time dependent deflection would be constant after 180 days but, suddenly, it started to increase again after 195 days to be almost constant after 270 days. This sudden change might be due to occurrence of new cracks as result of the concrete shrinkage with time reducing the tensile concrete strength around reinforcement adding more deflections and increasing the time dependent deflections. Also creep of tensioned part, as well as increment of curvature with time leading to some increment of tensile stresses, contributed to these possible new cracks.

As can be seen a reducing in δ_T by increasing CFRP area along the loading time with a higher reducing step between beam BS3II` strengthened with $A_f$ of 28 mm$^2$ and the reference beam BR3II` than it between beam BT3II` strengthened with $A_f$ of 84 mm$^2$ and beam BS3II`. As reported in Table 4.10, increasing A_f decreased $\delta_{T,e}$ 1.67 mm in beam BS3II` and 3.18 mm in beam BT3II`compared to beam BR3II`.

It can be seen from Figure 4.24 that, the initial deflection was reduced with decreased steps by increasing CFRP area. This can be seen in numbers in Table 4.10, δ_o decreased from 5.33 mm in beam BR3II` to 3.4 mm and 2.78 mm with steps of 1.93 mm and 0.62 mm by NSM strengthening with different $A_f$ of 28 and 84 mm$^2$ in beams BS3II`and BT3II`, respectively. This reflects the better efficiency of NSM strengthening to control

the beam deflection by increasing CFRP area. This also can illustrate the reducing in total deflection, which is a function of the initial deflection, by increasing the CFRP area.

The decrease in δ_o and δ_T by NSM strengthening with A_f of 28 mm^2 was very clear in group B2 because of keeping the same load, while it almost nothing in the preloaded beams in group A2 beams. Therefore, it can be concluded that, the preloading of NSM strengthened beam and probably also changing the sustained loads limited the decrease in initial deflection and consequently in total deflection by NSM strengthening with CFRP area of 28 mm^2.

The NSM strengthening reduced δ_r in group B2 with almost similar amounts for the beams with A_f of 28 mm^2 and 84 mm^2. The presented value of δ_r in Table 4.10 decreased from 5.40 mm in beam BR3II` to 4.73 mm and 4.66 in beams BS3II` and BT3II` with steps of 0.67 mm and 0.07 mm, respectively. In addition to the previous observation in group A2 that the beam with lower A_f showed a decrease in $\delta_{r,e}$ higher than it in the beam with higher A_f, it can be concluded that the larger CFRP area made the NSM strengthened beam retained more deflection from its time dependent deflection either the beams were virgin or preloaded.

The ratio of the time dependent deflection ($\delta_{td}=\delta_T-\delta_o$) to the instantaneous deflection (δ_i), δ_{td}/δ_i, of beams with different A_f from group B2 were plotted on the vertical axis versus loading time, t in days on the horizontal axis as shown in Figure 4.25. All curves show the same trend, regardless of values. δ_{td}/δ_i ratio had a significant increase by NSM strengthening with CFRP strips, where $\delta_{td}/\delta_i > 1$. This was in harmony with the fact that increasing tension side stiffness by NSM strengthening lead to higher neutral axis depth (larger compressed area of concrete), causing higher creep deformations, and therefore higher time-dependent deflections. This was in the opposite of the preloaded beams with different CFRP area in group A2, where $\delta_{td}/\delta_i < 1$. This reflects that the preloading of NSM strengthened beams before sustained loading decreased the time dependent deflection.

By increasing the CFRP area in beam BT3II` to three times of the area used in beam BS3II`, their δ_{td}/δ_i ratios were the same up to 195 days since loading. After, beam BT3II` started to produce a bit higher ratio up to the end of loading achieving 1.68,

while beams BR3II` and BS3II` reached 1 and 1.64, respectively. This made the observed changes in δ_{td}/δ_i ratios by increasing CFRP area in group B2 beams more compatible with the fact that higher reinforcement ratios cause higher creep deformations in the opposite the preloaded strengthened beams in group A2.

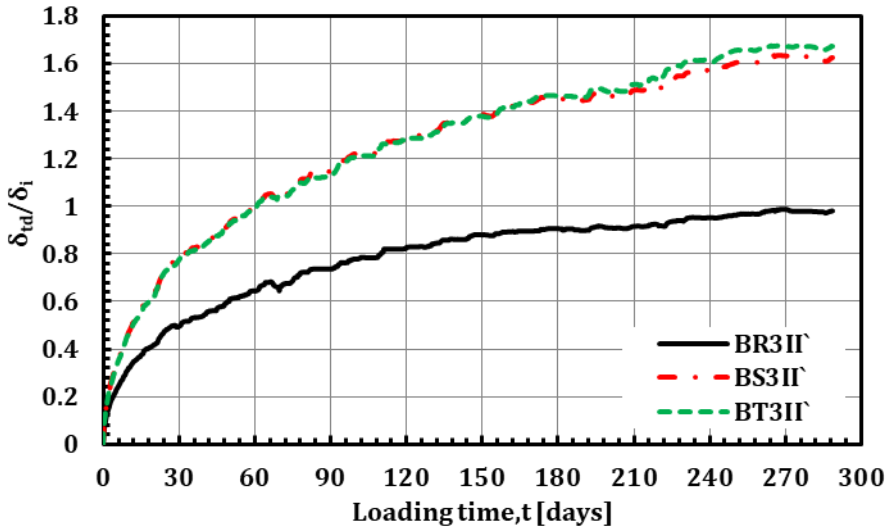

Figure 4.25 The ratio of time dependent deflection to instantaneous deflection of beams with different CFRP area from group B2.

4.3.2.2 Beams with different tension steel ratios

The effect of tension steel ratios, ρ on the time dependent flexural behavior of NSM CFRP strengthened RC beams was investigated in group A2 using beams AR1I and AS1I with ρ of 0.77% and beams AR2I and AS2I with ρ of 1.97%. δ_T at mid-span section were registered and plotted on the vertical axis in mm versus loading time, t in days on the horizontal axis as shown in Figure 4.26. All beams behaved with similar shape of their curves, regardless of values. Table 4.11 presents P_s in kN and its ratio to failure load, P_s/P_u for the beams with different tension steel ratios. Moreover, it includes $\delta_{r,o}$, δ_i, δ_o, $\delta_{T,e}$, δ_r and $\delta_{r,e}$ in mm.

For the strengthened and un-strengthened beams, the higher ratio of tension steel reinforcement produced larger tension side stiffness decreasing δ_o and therefore δ_T along the loading time as shown in Figure 4.26.

For the beams with higher ρ, the strengthened beam AS2I showed a bit lower values of δ_o and δ_T during the loading time compared to the un-strengthened beam AR2I. Whereas, the values of δ_o and $\delta_{T,e}$ in beam AS2I were lower than corresponding values in beam AR2I with amounts of 0.17 mm and 0.18 mm, respectively, as presented in

Table 4.11. On the side of the beams with lower ρ, it was not a noticeable difference in δ_o and δ_T during the loading time between the strengthened beam AS1I and the un-strengthened beam AR1I.

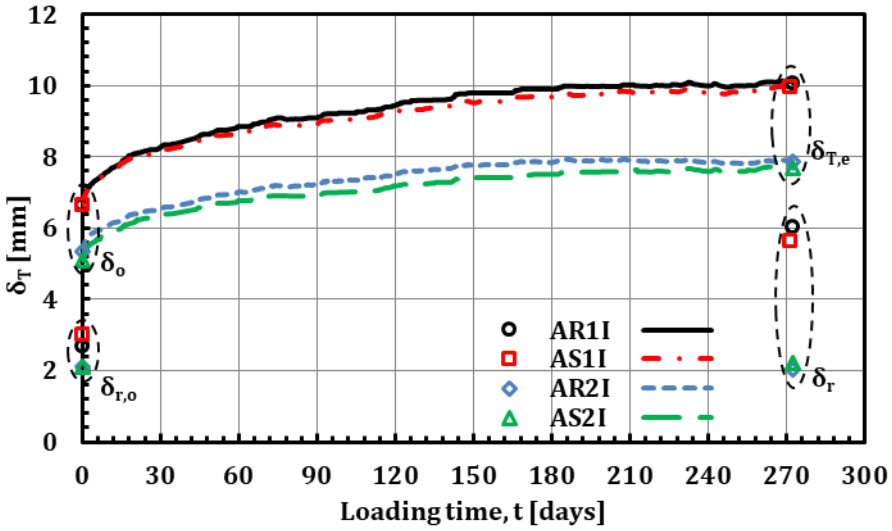

Figure 4.26 Total deflection with time for the beams of different tension steel ratios.

Table 4.11 Sustained loads and their deflections of the beams with different tension steel ratios.

Beam ID	Sustained loads		Deflections [mm]					
	P_s [kN]	P_s/P_u	$\delta_{r,o}$	δ_i	$\delta_o=\delta_{r,o}+\delta_i$	$\delta_{T,e}$	δ_r	$\delta_{r,e}=\delta_r-\delta_{r,o}$
AR1I	12.40	0.359	2.70	3.93	6.63	10.06	6.01	3.31
AS1I	13.62	0.233	3.00	3.65	6.65	9.96	5.62	2.62
AR2I	18.16	0.239	2.10	3.26	5.36	7.88	2.02	-0.08
AS2I	18.74	0.191	2.12	2.97	5.09	7.70	2.23	0.11

As can be seen in Figure 4.26, the beams with higher ρ almost recovered all the deflections induced during loading time after removing the sustained loads reaching values of δ_r around the values of $\delta_{r,o}$ with values of $\delta_{r,e}$ around zero as reported in Table 4.11. On the opposite, the beams with lower ρ retained higher values of δ_r with a small decrease by NSM strengthening. This reflects that the beams with higher ρ were able to behave as elastic elements after removing the sustained loading.

The ratio δ_{td}/δ_i of the beams with different tension steel ratios in group A2 was plotted versus loading time, as shown in Figure 4.27.

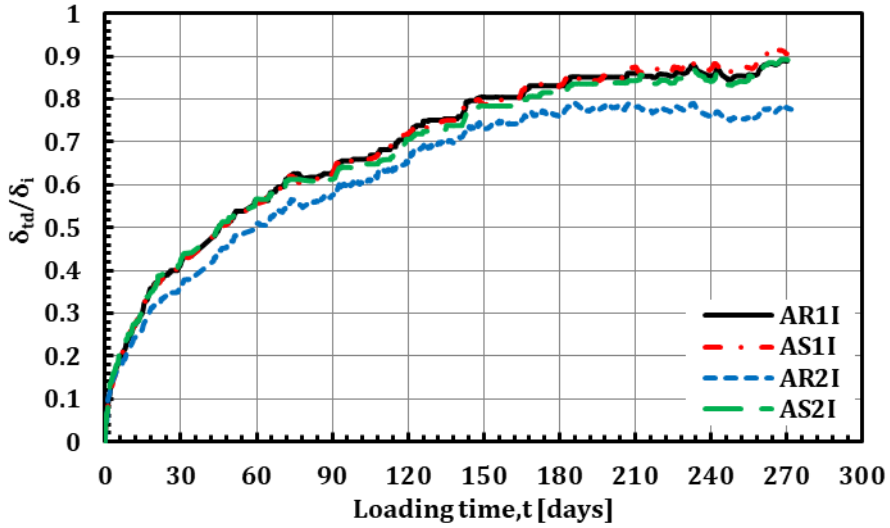

Figure 4.27 The ratio of time dependent deflection to instantaneous deflection of beams with different tension steel ratios.

As discussed above, there is a difficulty to make extensive creep damage due to the maximum load of preloading is higher than the sustained load. For the beams with lower ρ, δ_{td}/δ_i ratio did not change by NSM strengthening except the last ten days; the strengthened beam AS1I produced a slight increase. Comparing between the un-strengthened beams, beam AR2I with ρ of 1.97% produced lower values of δ_{td}/δ_i than those in beam AR1I with ρ of 0.77%. This was at the odds of the fact that higher reinforcement ratios lead to higher neutral axis depth (larger compressed area of concrete), causing higher creep deformations, and therefore higher time-dependent deflections. This might be due to higher level of previous and sustained cracking in beam AR2I, which had M_D/M_{cr} and M_s/M_{cr} of 10.38 and 4.18, while beam AR1I had 3.66 and 2.28, respectively. This might highly decrease the compressed area of concrete in beam R2A causing lower creep deformations, and therefore lower values of δ_{td}/δ_i. Also, the presence of compression reinforcement decreases shrinkage curvature with increasing tensile reinforcement ratio for cracked section [122].

On the other hand, in the beams with higher ρ, the δ_{td}/δ_i ratio had a significant increase by NSM strengthening with CFRP strips. This was in harmony with the fact that increasing tension side stiffness by NSM strengthening lead to higher neutral axis depth (larger compressed area of concrete), causing higher creep deformations, and therefore higher time-dependent deflections.

4.3.2.3 Beams with different concrete types

The effect of concrete type was studied using results of un-strengthened beam AR1I and strengthened beam AS1I from group A2 compared with results of un-strengthened beam BR1I` and strengthened beam BS1I` from group B2. All of these beams had same steel reinforcement and curing period of 12 days and the strengthened beams had same CFRP strengthening. All beams presented a similar shape in their curves of δ_T versus t regardless of values, as shown in Figure 4.28.

Table 4.12 presents P_s in kN for the beams with different concrete types. Moreover, it includes δ_i, δ_o, $\delta_{T,e}$, δ_r and $\delta_{r,e}$ in mm. As can be seen in Figure 4.28 after removing the sustained loads that, the strengthened beam of lower concrete strength recovered deflection more than it in the un-strengthened beam achieving δ_r of 5.62 mm and 6.01 mm in beams AS1I and AR1I, respectively as reported in Table 4.12. On the opposite, the strengthened beam of higher concrete strength recovered deflection less than it in the un-strengthened beam achieving δ_r of 6.06 mm and 2.22 mm in beams BS1I` and BR1I`, respectively.

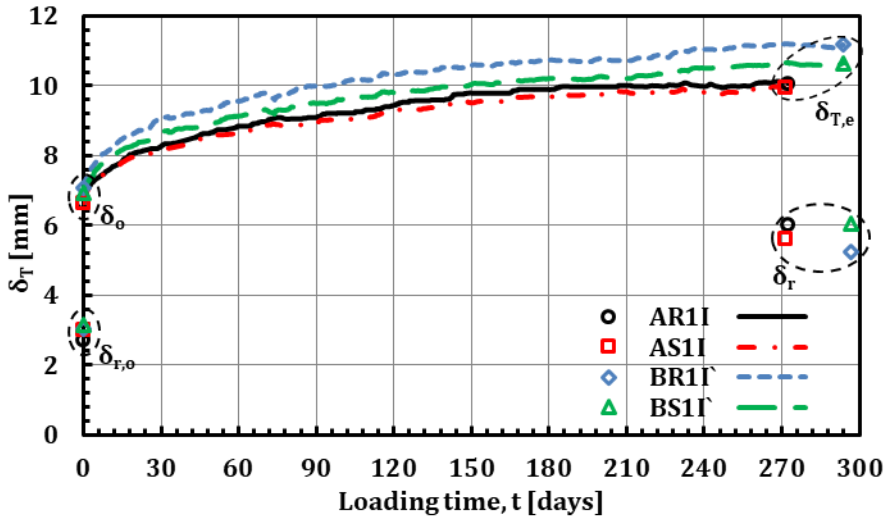

Figure 4.28 Total deflection with time for the beams of different concrete types.

Table 4.12 Sustained loads and their deflections of the beams with different concrete types.

Beam ID	Sustained loads	Deflections [mm]				
	P_s [kN]	δ_i	$\delta_o=\delta_{r,o}+\delta_i$	$\delta_{T,e}$	δ_r	$\delta_{r,e}=\delta_r-\delta_{r,o}$
AR1I	12.40	3.93	6.63	10.06	6.01	3.31
AS1I	13.62	3.65	6.65	9.96	5.62	2.62
BR1I`	14.19	4.05	7.07	11.18	5.22	2.20
BS1I`	14.19	3.78	6.92	10.66	6.06	2.92

For the higher concrete strength, the strengthened beam BS1I` showed a lower $\delta_o$ compared to the un-strengthened beam BR1I` with small difference of 0.15 mm as presented in Table 4.12. However, the strengthened and un-strengthened beams of lower concrete strength showed almost similar values of δ_o. The strengthened beam BS1I` of higher concrete strength showed lower $\delta_T$ with time compared to the un-strengthened beam BR1I` achieving a decrease at the end of loading equal 0.52 mm as presented in Table 4.12. However, the strengthened and un-strengthened beams of lower concrete strength showed almost similar values of δ_T with time.

The ratio δ_{td}/δ_i, of the beams with different concrete types was plotted versus loading time, as shown in Figure 4.29. It can be seen that δ_{td}/δ_i, increased by increasing concrete strength for the strengthened and un-strengthened beams. This might be due to the higher creep coefficients and shrinkage strains of the higher concrete strength (Figure 3.19) compared to the lower concrete strength (Figure 3.17).

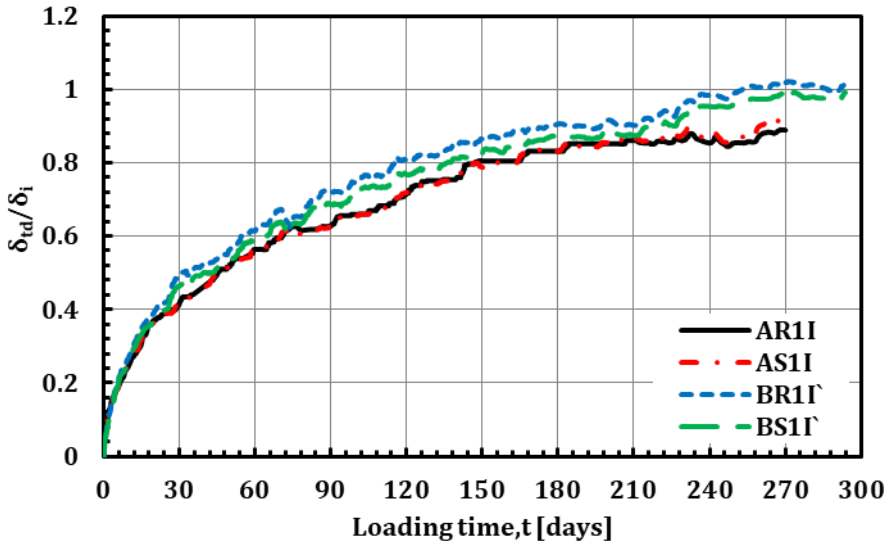

Figure 4.29 The ratio of time dependent deflection to instantaneous deflection of beams with different concrete types.

As observed in the beams with lower concrete strength, δ_{td}/δ_i ratio had no significant difference by NSM strengthening with CFRP strips, while it had a small decrease in the beams with higher concrete strength by NSM strengthening with CFRP strips.
Lack of increase in δ_{td}/δ_i ratio by NSM strengthening was at the odds of the fact that higher reinforcement ratios lead to higher neutral axis depth (larger compressed area

of concrete), causing higher creep deformations, and therefore higher time-dependent deflections. This might be due to higher level of previous cracking in strengthened beams AS1I and BS1I`, which had $M_D/M_{cr}$ of 5.50 and 5.09, respectively. While the un-strengthened beams AR1I and BR1I` had M_D/M_{cr} of 3.66 and 3.89, respectively. This might highly decrease the compressed area of concrete in the strengthened beams causing lower creep deformations, and therefore lower values of δ_{td}/δ_i. Therefore, it can be concluded that the preloading of the NSM strengthened beam with CFRP strips up to its design service load led to decrease its time dependent deflection under sustained loading compared to the un-strengthened beam at the odds of the beams sustained loaded directly without preloading.

4.3.2.4 Beams with different compression/tension steel ratios

The effect of compression/tension steel ratio, ρ'/ρ, on the time dependent flexural behavior of NSM CFRP strengthened RC beams was investigated in group B2 using beams BR3II` and BS3II`with compression steel (ρ'/ρ = 0.36) and beams BR4II` and BS4II` without compression steel (ρ'/ρ = 0). δ_T of these beams were plotted versus loading time, as shown in Figure 4.30. All beams behaved with similar shape of their curves, regardless of the different values of ρ'/ρ ratio. Table 4.13 presents P_s in kN for the beams with different ρ'/ρ ratios. Moreover, it includes δ_i, δ_o, $\delta_{T,e}$, δ_r and $\delta_{r,e}$ in mm.

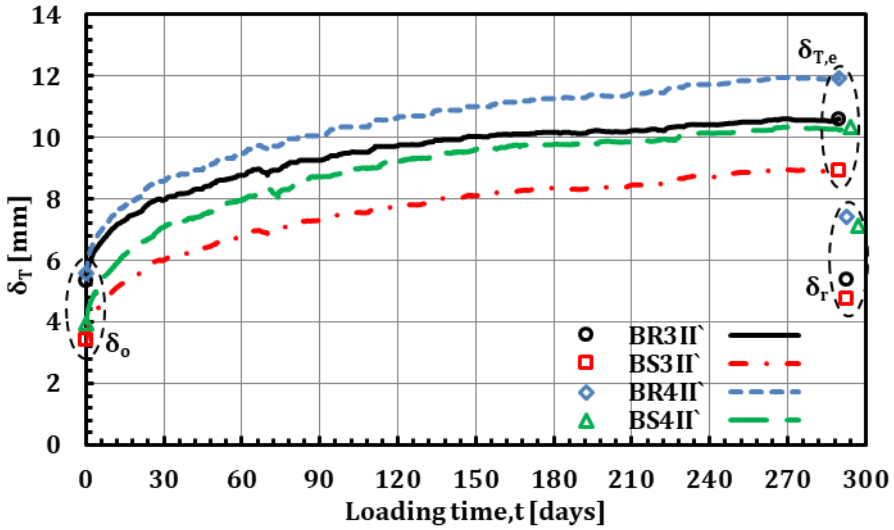

Figure 4.30 Total deflection with time for the beams of different compression/tension steel ratios.

Table 4.13 Sustained loads and their deflections of the beams with different ρ'/ρ.

Beam ID	Sustained loads	Deflections [mm]				
	P_s [kN]	δ_i	$\delta_o=\delta_{r,o}+\delta_i$	$\delta_{T,e}$	δ_r	$\delta_{r,e}=\delta_r-\delta_{r,o}$
BR3II`	14.19	5.33	5.33	10.61	5.40	5.40
BS3II`	14.19	3.40	3.40	8.94	4.73	4.73
BR4II`	13.87	5.59	5.59	11.93	7.40	7.40
BS4II`	13.87	3.96	3.96	10.35	7.12	7.12

The beams with compression steel showed lower initial deflections, δ_o than the beams without compression steel, which is logical. By NSM strengthening, δ_o decreased in the beams with compression steel with rate higher than it in the beams without compression steel. δ_o of beam BS3II`decreased with percentage of 36% compared to beam BR3II`, while δ_o of beam BS4II` decreased with percentage of 29% compared to beam BR4II`. This means that the presence of the compression steel magnified the benefit of NSM CFRP strengthening in the reduction of initial deflections.

Also, the beams with compression steel showed δ_T lower than it in the beams without compression steel along the loading time, which is in harmony with the decreasing in initial and time dependent deflections. By NSM strengthening, δ_o decreased in the beams with compression steel with rate higher than it in the beams without compression steel. $\delta_{T,e}$ of beam BS3II` decreased with 1.67 mm compared to beam BR3II`, while $\delta_{T,e}$ of beam BS4II` decreased with 1.55 mm compared to beam BR4II`. The difference between these decreases was near to the difference between the decreases in δ_o in the beams, which returned this trend to the change of the initial deflection trend.

The values of δ_r were near in strengthened and un-strengthened beams compared with the difference in δ_o. This might be due to that the permanent deflection included deflection induced based on concrete shrinkage, which is not recoverable and increases by increasing reinforcement ratio. Therefore, the increasing of reinforcement ratio by NSM strengthening increased the shrinkage deflection decreasing the difference between strengthened and un-strengthened beams. Also, this difference was very low in the beams without compression steel because this effect was higher by removing compression steel [122].

In terms of time dependent deflection, its ratio to the instantaneous deflection, δ_{td}/δ_i, for the beams with different ρ'/ρ were plotted on the vertical axis versus loading time, t in days on the horizontal axis as shown in Figure 4.31. All curves show the same manners, regardless of values. With respect to the decrease in the instantaneous deflection by strengthening, δ_{td}/δ_i increased by removing the compression steel in the compared un-strengthened beams. This was in harmony with the fact that removing compression steel releases the compressed concrete area from reinforcement restraint producing higher deformation with time due to creep and shrinkage.

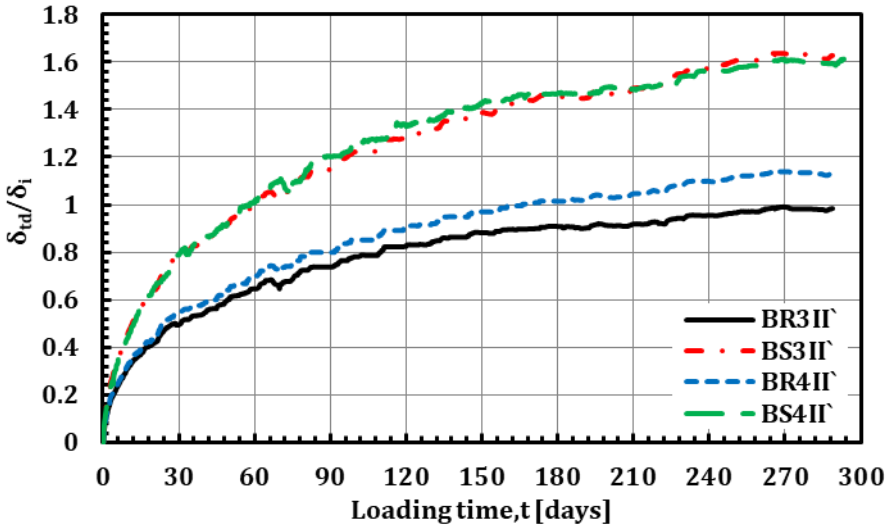

Figure 4.31 The ratio of time dependent deflection to instantaneous deflection of beams with different compression/tension steel ratios.

This also was compatible with the equations in literature, which consider the compression steel effect on the creep and shrinkage curvature of RC beams [97,122]. On the contrary of that fact, the strengthened beams, with and without compression steel, produced almost same values of δ_{td}/δ_i during the loading time. This might be due to the higher effect of previous concrete shrinkage on the instantaneous deflection by increasing the reinforcement ratio using NSM strengthening adding more deflection to the instantaneous deflection of the strengthened beam of zero compression steel, which decreased its δ_{td}/δ_i ratio to match the strengthened beam of compression steel. This can be detected in numbers from the decrease in instantaneous deflections by adding the compression steel. From Table 4.13, this decrease between un-strengthened beams was 0.26 mm, while it was 0.56 mm between strengthened beams supporting the explained reason.

4.3.2.5 Beams with different levels of sustained load

The effect of the sustained load level on the time dependent flexural behavior of NSM CFRP strengthened RC beams was investigated in group B2 using beams BR3II` and BS3II` with lower sustained load levels and beams BR3II and BS3II with higher sustained load levels. The initial concrete stresses of the un-strengthened beams BR3II` and BR3II were 12.83 MPa and 17.11 MPa, respectively. The total deflections, δ_T of these beams were plotted on the vertical axis in mm versus loading time, t in days on the horizontal axis as shown in Figure 4.32. All beams behaved with similar shape of their curves, regardless of the different levels of sustained loads.

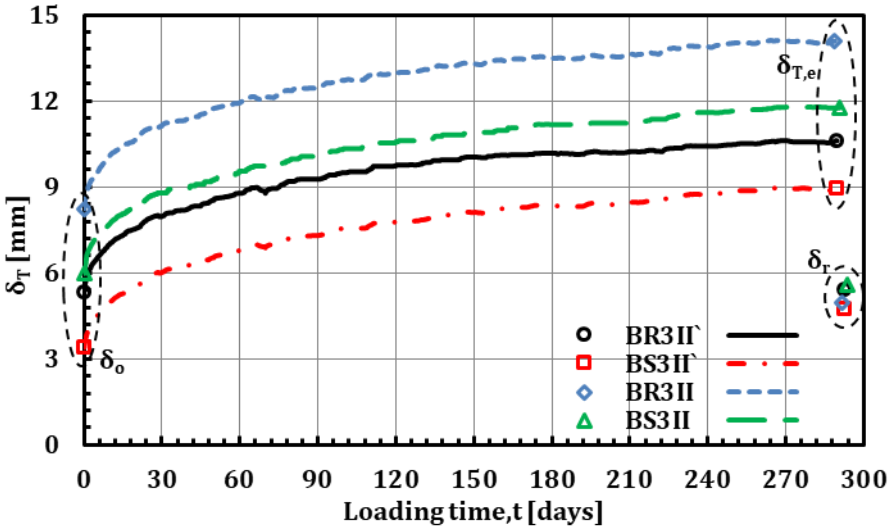

Figure 4.32 Total deflection with time for the beams of different sustained load levels.

The sustained loads and their deflections of these beams were summarized in Table 4.14. This table presents the sustained load, P_s in kN with its ratio to the ultimate load, P_s/P_u. Moreover, it includes δ_i, δ_o, $\delta_{T,e}$, δ_r and $\delta_{r,e}$ in mm.

Although, the load was increased with same value in the un-strengthened and strengthened beams, the increase in P_s/P_u ratio was lower in the strengthened beams. The increase was 0.132 in the un-strengthened beams, while it was 0.072 in the strengthened beams. On the other hand, the NSM strengthening with CFRP strips reduced this ratio with higher decrease in the beams of high load level. This decrease was 0.238 in the beams with high load level, while it was 0.178 in the beams with low load level.

Table 4.14 Sustained loads and their deflections of the beams with different sustained load levels.

Beam ID	Sustained loads		Deflections [mm]				
	P_s [kN]	P_s/P_u	δ_i	$\delta_o=\delta_{r,o}+\delta_i$	$\delta_{T,e}$	δ_r	$\delta_{r,e=}\delta_r-\delta_{r,o}$
BR3II`	14.19	0.393	5.33	5.33	10.61	5.40	5.40
BS3II`	14.19	0.215	3.40	3.40	8.94	4.73	4.73
BR3II	18.93	0.525	8.25	8.25	14.09	4.94	4.94
BS3II	18.93	0.287	5.98	5.98	11.76	5.61	5.61

The initial deflection, δ_o increased by increasing level of the sustained loads in the un-strengthened and strengthened beams but with higher ratio in the strengthened beams. Whereas δ_o increased from 5.33 mm in beam BR3II` to 8.25 mm in beam BR3II with percentage of 55%, while it increased from 3.4 mm in beam BS3II` to 5.98 mm in beam BS3II with percentage of 76%.

The NSM strengthening with CFRP strips reduced the initial deflections in both load levels but with higher ratio in the beams with lower load level. Whereas δ_o decreased from 5.33 mm in beam BR3II` to 3.4 mm in beam BS3II` with percentage of 36%, while it decreased from 8.25 mm in beam BR3IIto 5.98 mm in beam BS3IIwith percentage of 28%.

The un-strengthened and strengthened beams showed higher values of the total deflection, δ_T with time at high level of the sustained load as shown in Figure 4.32. NSM strengthening with CFRP strips decreased δ_T at both levels of the sustained load but with higher step in the beams with high load level. This can be seen as numbers from the values of $\delta_{T,e}$ reported in Table 4.14. At high load level, $\delta_{T,e}$ decreased by NSM strengthening with step of 2.33 mm, while the decrease was 1.67 mm at low load level. After removing the loads, δ_r decreased in the un-strengthened beams by increasing load level, while it increased in the strengthened beams. On the effect of NSM strengthening, δ_r decreased by NSM strengthening at low level load, while it increased at high load level. Despite these effects, the changes in δ_r were small by increasing level of the sustained load as shown in Figure 4.32.

In terms of the ratio of time dependent deflection to the instantaneous deflection, δ_{td}/δ_i of beams with different sustained load levels were plotted on the vertical axis versus loading time, t in days on the horizontal axis as shown in Figure 4.33. All curves show the same trend, regardless of values. It can be seen that δ_{td}/δ_i decreased by increasing

sustained load level for the un-strengthened and strengthened beams. Also, it is clear that the increase in this ratio by NSM strengthening was larger at the low load level compared with the increase at the high load level. Whereas at the end of loading, beam BS3II` achieved an increase percentage of 64% compared to beam BR3II`, while beam BS3II achieved an increase percentage of 40% compared to beam BR3II. Therefore, it can be concluded that the higher level of sustained load led to lower δ_{td}/δ_i ratio and limited its increase by NSM strengthening. This might be due to the larger M_s/M_{cr} applied in sequence II`, whereas the ratio between the applied sustained loads in sequence II` to sequence II was 1.33. This means that beam BR3II` was more cracked than beam BR3II, which would present a lower creep multiplier.

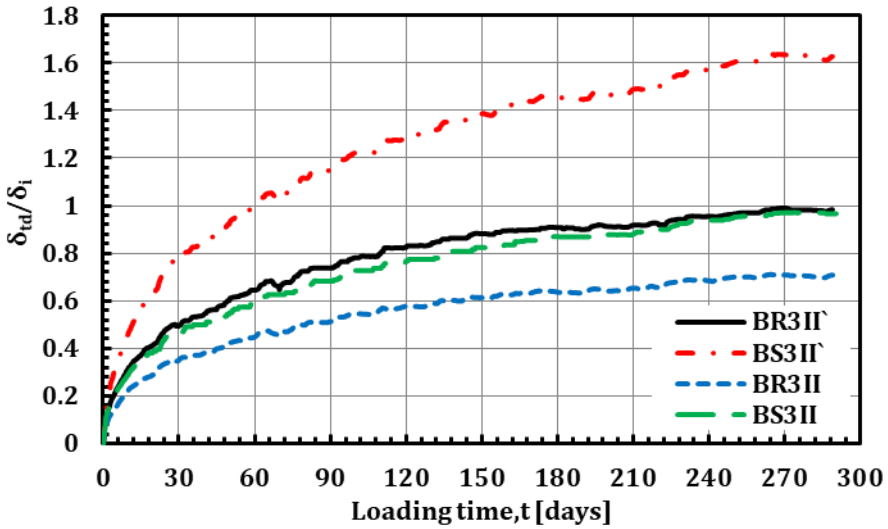

Figure 4.33 The ratio of time dependent deflection to instantaneous deflection of beams with different sustained load levels.

4.3.2.6 Beams with different loading sequences

Three different load sequences (I`, II` and II") were studied in group B2, detailed in Table 3-1 in CHAPTER 3. Beam BS3II` was tested under sustained loading without any preloading, while beam BS1I` was previously subject to monotonic short-term loading followed by two cycles of unloading/reloading up to service design load. Additionally, in beam BS3II", a third loading sequence consisted on NSM FRP strengthening after monotonic short-term loading followed by two cycles of unloading/reloading up to service design load of an un-strengthened beam before application of the sustained loading. All studied beams were loaded with the same load of the reference beam,

which was calculated to obtain concrete stresses of 12.83 MPa at the top of mid-span section lower than 40% of their concrete compressive strength.

The total deflections, δ_T of these beams were plotted on the vertical axis in mm versus loading time, t in days on the horizontal axis as shown in Figure 4.34. All beams behaved with similar shape of their curves, regardless of the different load sequences. The sustained loads and their deflections of these beams were summarized in Table 4.15. This table presents the sustained load, P_s in kN and δ_i, δ_o, $\delta_{T,e}$, δ_r and $\delta_{r,e}$ in mm.

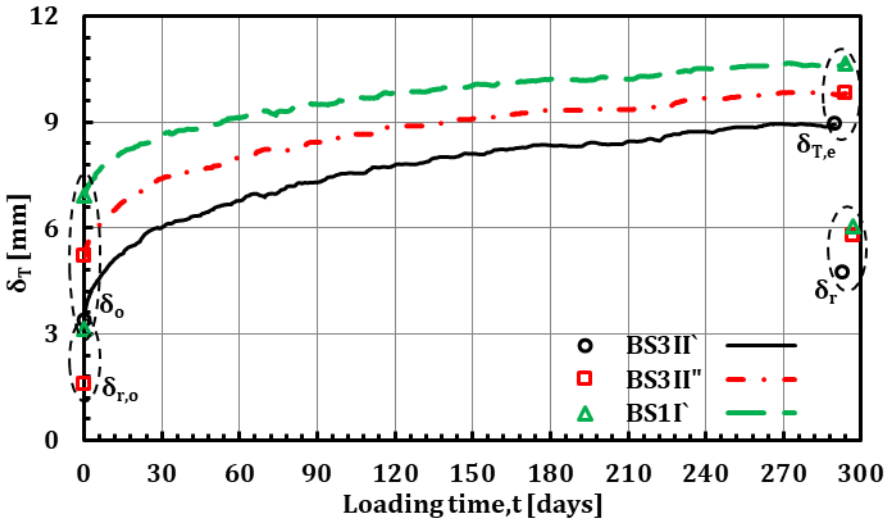

Figure 4.34 Total deflection with time for the beams of different loading sequences.

Table 4.15 Sustained loads and their deflections of the beams with different loading sequences.

Beam ID	Sustained loads	Deflections [mm]				
	P_s [kN]	δ_i	$\delta_o=\delta_{r,o}+\delta_i$	$\delta_{T,e}$	δ_r	$\delta_{r,e}=\delta_r-\delta_{r,o}$
BS3II`	14.19	3.40	3.40	8.94	4.73	4.73
BS3II"	14.19	3.61	5.21*	9.82	5.79	4.19
BS1I`	14.19	3.78	6.92	10.66	6.06	2.92

* $\delta_{r,o}$ of beam BS3II" was induced before its NSM strengthening due to previous two loading/unloading cycles.

The initial deflection, δ_o increased in the strengthened beams preloaded before sustained loading compared with the beams sustained loaded without any preloading. It is observed that strengthened beam BS3II", preloaded before strengthening, achieved initial deflection larger than strengthened beam BS3II`, without any preloading, and lower than strengthened beam BS1I`, preloaded before sustained loading. This might be due to the larger level of the previous cracking of beam BS1I`

compared with beam BS3II", while beam BS3II` did not have previous cracking. In terms of the total deflection with time, the strengthened beams behaved in the same trend of the initial deflections. Whereas, the ascending order of strengthened beams according to the total deflection with time was beam BS3II`, beam BS3II" then beam BS1I`. This can be clarified in numbers from the values of total deflection at the sustained loading end reported in Table 4.15. The values of $\delta_{T,e}$ increased from 8.94 mm in beam BS3II` to 9.82 mm in BS3II"and to 10.66 mm in beam BS1I` with almost equal steps.

After removing the sustained loading, the permanent deflections of the strengthened beams were in same ascending order of their total deflections but with higher step between beams BS3II` and BS3II" (1.06 mm) than it between beams BS3II" and BS1I` (0.27 mm).

In terms of the ratio of time dependent deflection to the instantaneous deflection, δ_{td}/δ_i of beams with different load sequences were plotted on the vertical axis versus loading time, t in days on the horizontal axis as shown in Figure 4.35. All curves show similar shapes, regardless of values.

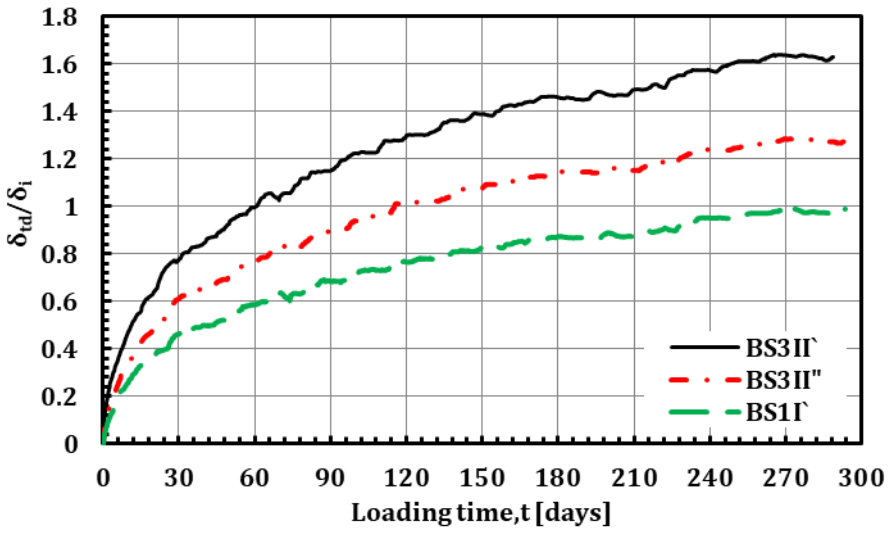

Figure 4.35 The ratio of time dependent deflection to instantaneous deflection of beams with different loading sequences.

The strengthened beams showed descending in δ_{td}/δ_i ratio by preloading before NSM strengthening in beam BS3II" and showed more descending by preloading before sustained loading in beam BS1I` achieving δ_{td}/δ_i ratios at the end of loading equal 1.64,

1.28 and 1 for beams BS3II`, BS3II" and BS1I`, respectively. Therefore, it can be concluded that the preloading of the NSM strengthened beams, either before strengthening or before sustained loading, reduced the creep and shrinkage effects on their time dependent behavior.

4.4 Residual Flexural Strength after Sustained Loading and Ageing

This section presents the experimental results and analysis the short-term tests carried out on the beams of group A2 and group B2 after removing the sustained loads and group B3 after ageing. The tested parameters and the full details of these beams were described in CHAPTER 3. The results of each series are presented and discussed in the following sections.

4.4.1 Beams of series A

After removing the sustained loads, the beams in group A2 are tested up to failure to measure their residual strength. The load-deflection curves of these beams are presented in Figure 4.36.

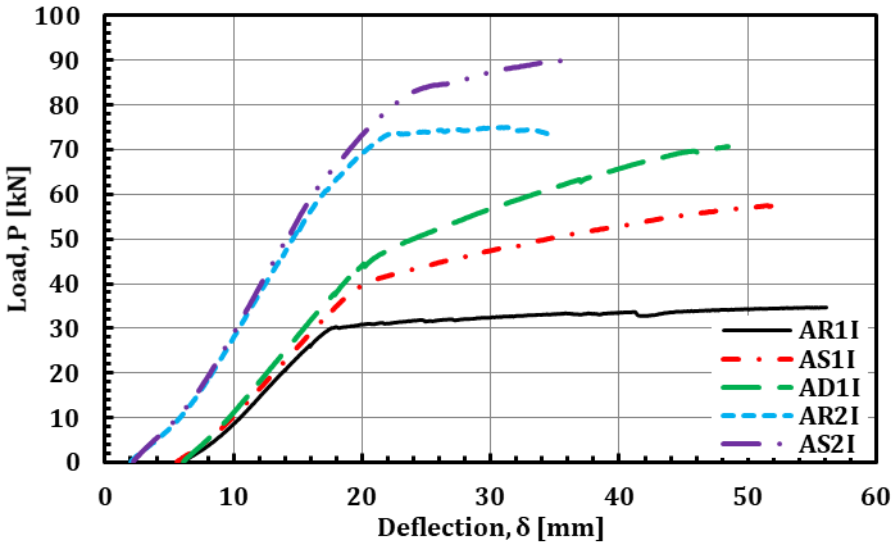

Figure 4.36 Load-deflection curves of group A2 beams tested after removing sustained loads.

The value of the permanent deflection induced after previous loading, δ_r, was added to each beam to describe its actual deflection. The load deflection curves of all previously cracked beams show two stages only defined at their ends by yield and failure points. The summary of the loads and deflections at the main points of each load deflection curve and the modes of failure are presented in Table 4.16. This table presents the values of yield load, P_y, in kN, corresponding deflection, δ_y, in mm, ultimate load, P_u, in kN, and the maximum deflection, δ_{max}, in mm. The failure modes of the studied beams are indicated in the last column in this table. Moreover, the sustained load, P_s in kN and remaining deflection after removing sustained load, δ_r in mm are listed in the same

table for each beam. Also, the applied design service loads, P_D, on beams before their sustained loading, are presented in kN.

Table 4.16 Load-deflection results of group A2 beams tested after removing sustained loads.

Beam ID	P_D [kN]	P_s [kN]	δ_r [mm]	P_y [kN]	δ_y [mm]	P_u [kN]	δ_{max} [mm]	Failure Mode
AR1I	19.87	12.40	6.01	29.98	17.61	34.60	56.10	CC
AS1I	31.17	13.62	5.62	40.24	20.49	57.55	51.84	FR+ICs
AD1I	37.67	14.71	6.06	45.28	20.86	70.66	48.51	ECs
AR2I	45.15	18.16	2.02	73.98	22.92	75.01	34.42	CC
AS2I	51.58	18.74	2.23	82.54	23.89	90.33	36.75	CC

The failure modes of group A2 beams are shown in Figure 4.37. The observed modes of failure were similar to the summarized failure modes in De Lorenzis and Teng [15] and Sena-Cruz et al. [81]. In group A2, Beam AS1I had failure mode of CFRP rupture followed by intermediate concrete cover separation, FR+ICs. Beam AD1I had failure mode of concrete cover separation at the end of CFRP strip, ECs. Beams AR1I, AR2I and AS2I had failure mode of concrete crushing at the top of beam, CC.

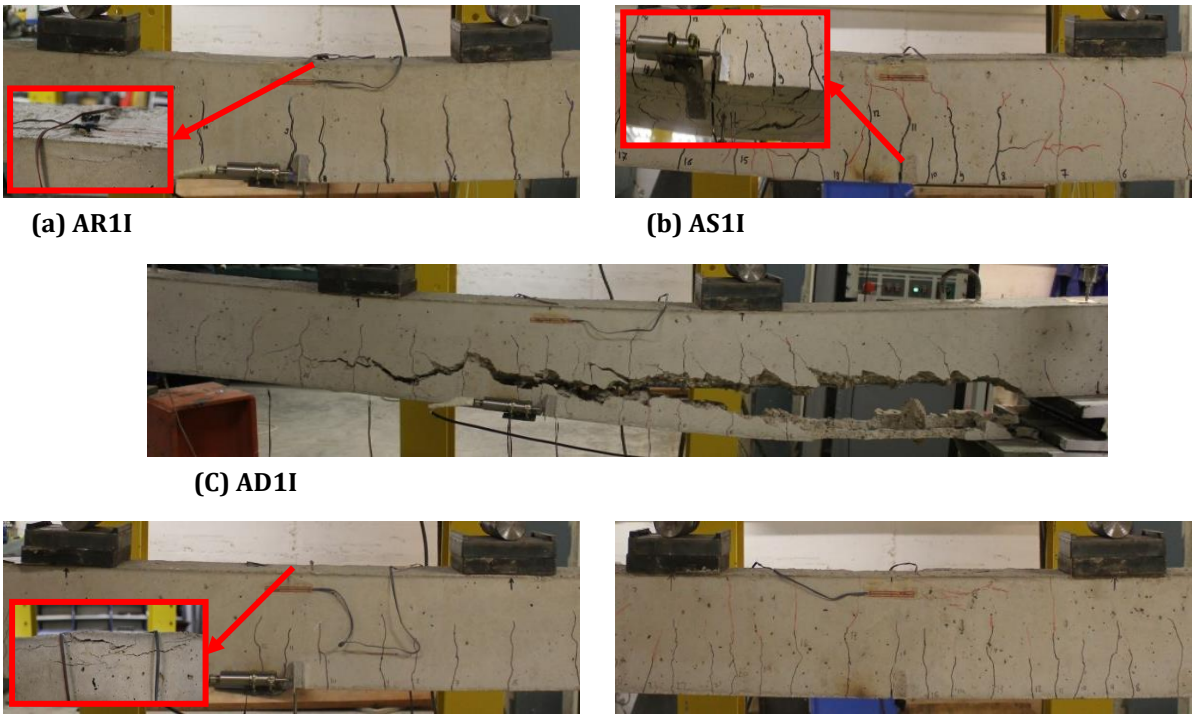

(a) AR1I **(b) AS1I**

(C) AD1I

(d) AR2I **(e) AS2I**

Figure 4.37 Failure modes of group A2 beams.

By NSM strengthening in beam AS1I using A_f of 28 mm^2, it showed increasing in load, deflection at yield point compared to beam AR1I. By doubling A_f to 56 mm^2 in beam AD1I, the load and deflection at yield also increased but with lower rate compared to beam AS1I. Compared to beam AR1I, P_y and δ_y of beam AS1I increased by 34% and 16%, respectively. However, their values in beam AD1I increased by 51% and 19%, respectively. The results at yield point were enhanced by increasing CFRP area due to the gained stiffness in the tension side growing the neutral axis depth especially at the cracked sections. Therefore, the yield of the tensile steel reinforcement was delayed enhancing the yield point position on load deflection curve. The same trends were observed in beams in group A1, which were tested before the sustained loading, regardless of the values. Therefore, it can be concluded that as CFRP area increased the load and deflection at yield increased with a decrement.

By increasing CFRP Area, the load carrying capacity increased compared to beam AR1I with percentage of 66% in beam AS1I and 104% in beam AD1I. However, the maximum deflection decreased with percentages of 8% and 14% in beams AS1I and AD1I, respectively. This decrease in the maximum deflection might be due to the change of failure mode from concrete crushing in beam AR1I to CFRP rupture gathered with intermediate concrete cover separation in beam AS1I and to the premature failure of concrete cover separation at strip end in beam AD1I. The same trends were observed in beams in group A1. Therefore, it can be concluded that as CFRP area increased the load carrying capacity enhanced, while the maximum deflection decreased.

It is clear from Figure 4.36 that like group A1 beams, the load and deflection at yield point increased by NSM strengthening with A_f of 28 mm^2 in beams with higher steel reinforcement ratio as in beams with lower tension steel ratio but with lower percentages. As reported in Table 4.16, P_y and δ_y increased in beam AS2I with percentage of 12% and 1%, respectively, compared to beam AR2I. However, these percentages between beams AS1I and AR1I of lower steel reinforcement ratio were 34% and 16%, respectively. Like group A1 beams, the ratio between strengthening CFRP stiffness to tension steel stiffness in beam S2A was larger than it in beam S1A. The percentage of gained stiffness was lower in beams with ρ of 1.97% than those with ρ of 0.77% reducing the enhancement of the yield point position on load deflection

curve in the beams with ρ of 1.97%. Therefore, it can be concluded that as the tension steel ratio increased the enhancement in yield load and deflection decreased for NSM strengthened beams with the same CFRP area whether the beams subjected to sustained loads before or not.

It is clear from Figure 4.36 that, CFRP NSM strengthening of the beams with high steel reinforcement ratio increased the load carrying capacity and the maximum deflection. However, CFRP NSM strengthening of the beams with low steel reinforcement ratio increased the load carrying capacity and decreased the maximum deflection. As reported in Table 4.16, P_u and δ_{max} increased in beam AS2I compared to beam AR2I with percentages of 20%and 8%, respectively. However, P_u increased in beam AS1I compared to beam AR1I with percentage of 66% and δ_{max} decreased with percentage of 8%.

It is worth noting that beams AR2I and AS2I were failed with the same failure mode of concrete crushing as shown in Figure 4.37d and Figure 4.37e, respectively. Therefore, it can be concluded that as the steel reinforcement ratio increased the enhancement in the load carrying capacity and the maximum deflection increased for NSM strengthened beams with the same CFRP area, if the un-strengthened and strengthened beams had the same mode of failure of concrete crushing, whether the beams subjected to sustained loads before or not.

On the effect of sustained loading, the load-deflection responses of group A2 beams, which tested after removing their sustained loads, were compared with the load-deflection responses of group A1 beams, which tested before the sustained loading. These comparisons are presented in Figure 4.38 for the un-strengthened beams and Figure 4.39 for the strengthened beams. The values of permanent deflection induced after previous loading, δ_r, was added to each beam of group A2 to describe the its actual deformation.

For the un-strengthened beams, Figure 4.38 shows that beams AR1I and AR2I showed flexural behavior, after reaching the yield, identical to the flexural behavior of beams AR1sh and AR2sh regardless their deflections at the failure. As shown in Figure 4.38b, beam AR2I showed lower maximum deflection at failure compared to it in beam AR2sh. This may be due to the failure by concrete crushing of both beams and this

mode of failure depends on the concrete compressive strain at failure, which may decrease by ageing.

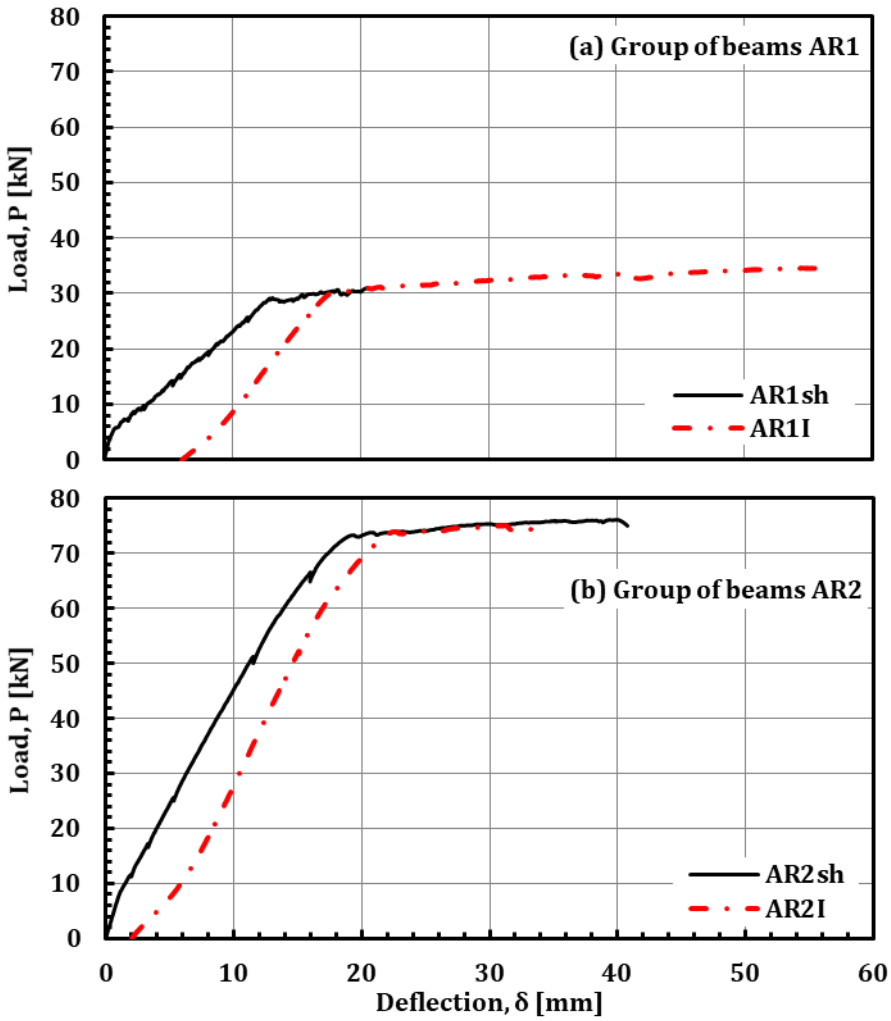

Figure 4.38 Load-deflection curves of the un-strengthened beams in series A before and after sustained loading.

For the strengthened beams, Figure 4.39a shows that beam AS1I showed flexural behavior, after reaching its yield, identical to the flexural behavior of beam AS1sh with a bit lower values of load and deflection at failure. The same behavior was found for beams AD1I and AD1sh as shown in Figure 4.39b. This small decrease may be due to the final failure of these beams is not concrete crushing in compression zone.

For the strengthened beams of high steel reinforcement ratio presented in Figure 4.39c, beam AS2I showed, after yielding, similar response to beam AS2sh with lower load and deflection at failure. This might be due to the failure with concrete crushing

in both beams and this mode depends on the concrete compressive strain at failure, which decreased by ageing as mentioned before.

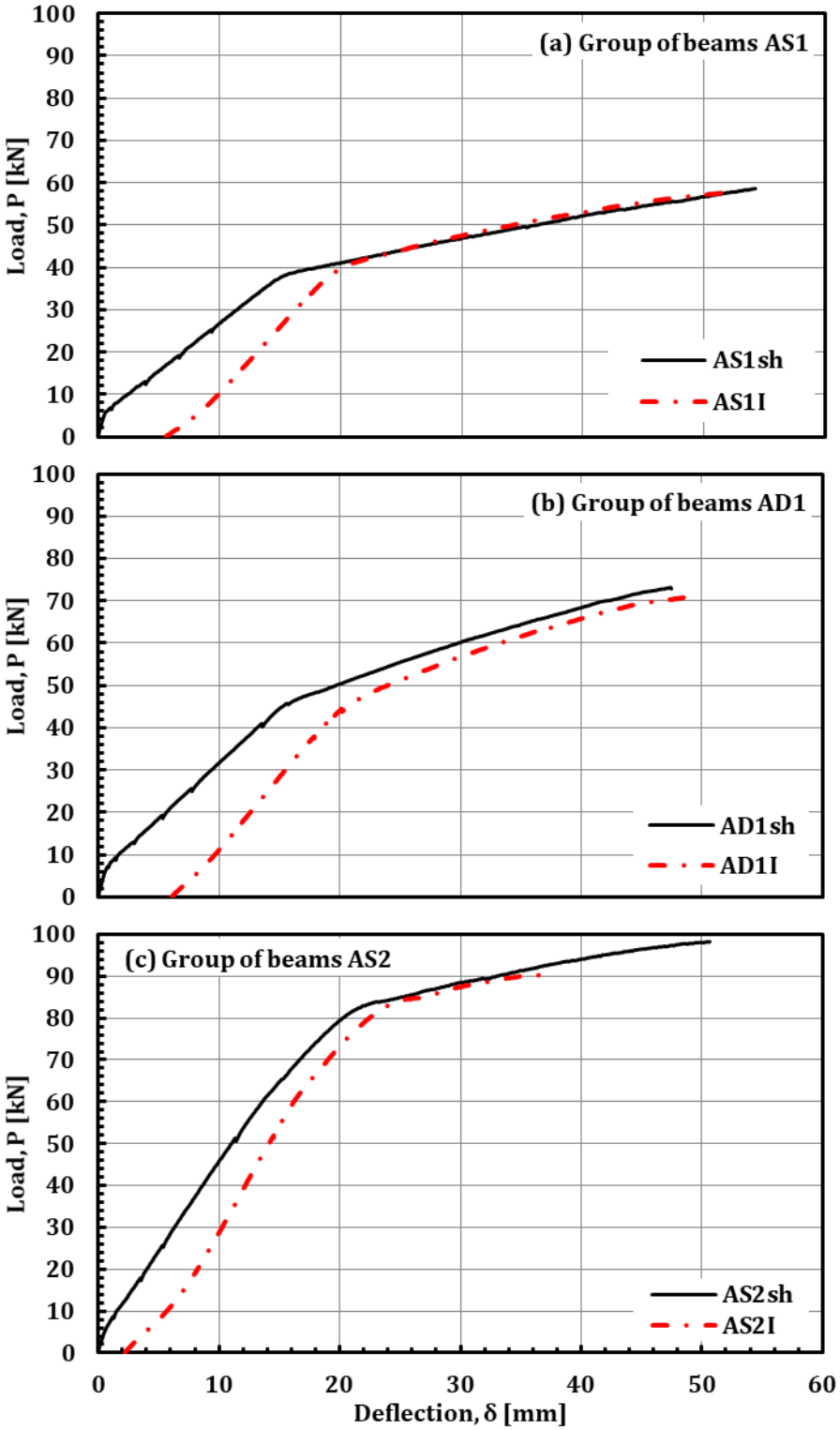

Figure 4.39 Load-deflection curves of the strengthened beams in series A before and after sustained loading.

The registered values of strains at failure in concrete at the top of mid-span sections, $\varepsilon_{c,u}$, reflects this discussion. Whereas, $\varepsilon_{c,u}$ was 2952 $\mu\varepsilon$ in beam AS2I after sustained loading and 5650 $\mu\varepsilon$ in its counterpart beam AS2sh before the sustained loading. Therefore, it can be concluded that the change of the load carrying capacity was mainly affected by time-dependent behavior of the failed constitutive material.

In terms of the strain variation with load, ε_c and ε_s at the mid-span section were plotted versus P for each beam in group A2 compared with its corresponding beam in group A1 in the same figure; Figure 4.40 and Figure 4.41. Figure 4.40 plotted for the un-strengthened beams and Figure 4.41 for the strengthened beams.

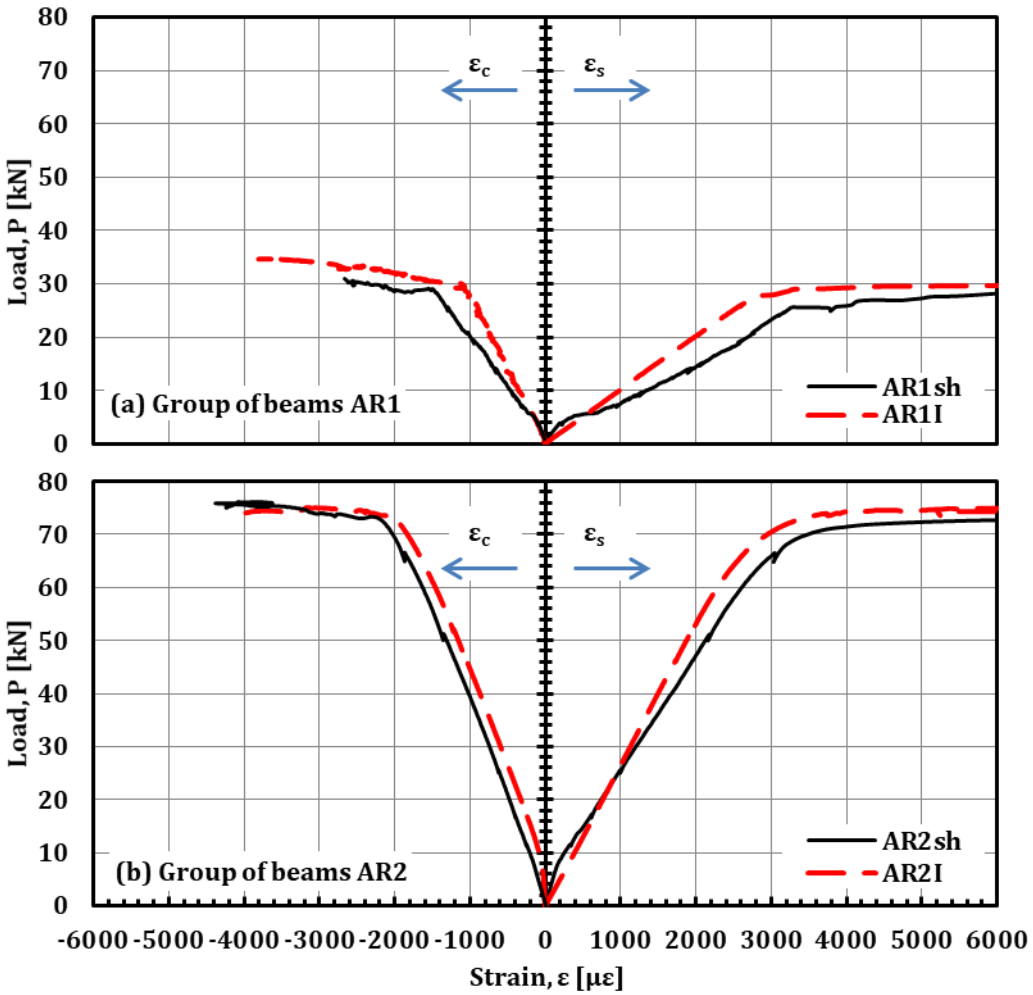

Figure 4.40 Strains of concrete and tensile steel at mid-span section for the un-strengthened beams in series A before and after sustained loading.

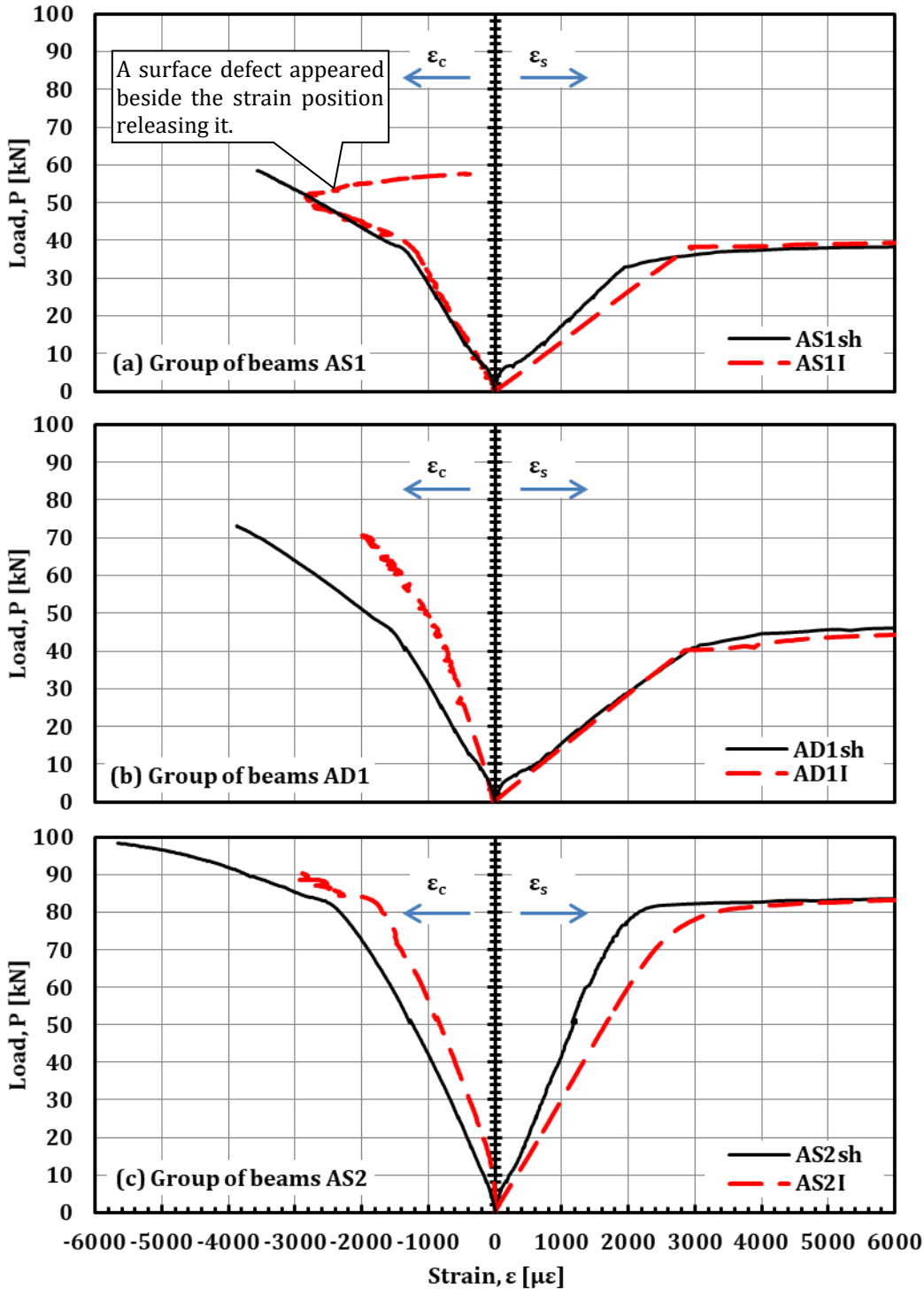

Figure 4.41 Strains of concrete and tensile steel at mid-span section for the strengthened beams in series A before and after sustained loading.

The concrete strains are presented in the left side with negative values and the steel strains are presented in the right side with positive values. All steel strain gages were failed after yielding. Therefore, only the first 6000 $\mu\varepsilon$ of steel strain are presented. As shown in Figure 4.41a, the registered concrete strain in beam AS1I decreased beyond

a load of 50 kN and up to failure. This happened because a defect on the concrete surface appeared beside the position of the concrete strain gage releasing it.

The longitudinal strain distributions along CFRP strip at different loads for the strengthened beams in series A before and after sustained loading are presented in Figure 4.42. Some of CFRP strain gages were cut before the test, and therefore their results are not presented. It is worth noting that the previous strains before the residual strength test were not recorded. This can explain the difference between the strains in beams subjected to short term loading (beams sh) and those subjected to residual strength test after removing the sustained load (beams I). At the same applied load, the compressive strain in concrete for beams sh is lower than that in beams I. This trend is similar to tensile strain in steel reinforcement for un-strengthened beams, while opposite trend was observed in the case of strengthened beams.

4.4.2 Beams of series B

The load-deflection curves of the tested beams after removing their sustained loads in group B2 are presented in Figure 4.43. The value of the permanent deflection induced after previous loading, δ_r, was added to each beam to describe the its actual deflection. The load deflection curves of all beams show the stages defined at their ends by yield and failure points, while the previous loading before these short-term tests prevented the appearance of un-cracked stages.

The summary of the loads and deflections at the main points of each load deflection curve and the modes of failure are presented in Table 4.17. This table presented the values of yield load, P_y, in kN, yield deflection, δ_y, in mm, ultimate load, P_u, in kN, and the maximum deflection, δ_{max}, in mm. The failure modes of the studied beams are indicated in the last column in this table. Moreover, the sustained load, P_s in kN and remaining deflection after removing sustained load, δ_r in mm are listed in the same table for each beam. Also, the applied design service loads, P_D, on beams before their sustained loading, are presented in kN.

The failure modes of group B2 beams are shown in Figure 4.44. The observed modes of failure were similar to the summarized failure modes in De Lorenzis and Teng [15] and Sena-Cruz et al. [81]. BeamsBS3II` and BS3II had failure mode of CFRP rupture followed by intermediate concrete cover separation, FR+ICs. Beam BT3II` had failure

mode of concrete cover separation at the end of CFRP strip, ECs. Beams BR3II`, BR3IIand BS3II"had failure mode of concrete crushing at the top of beam, CC.

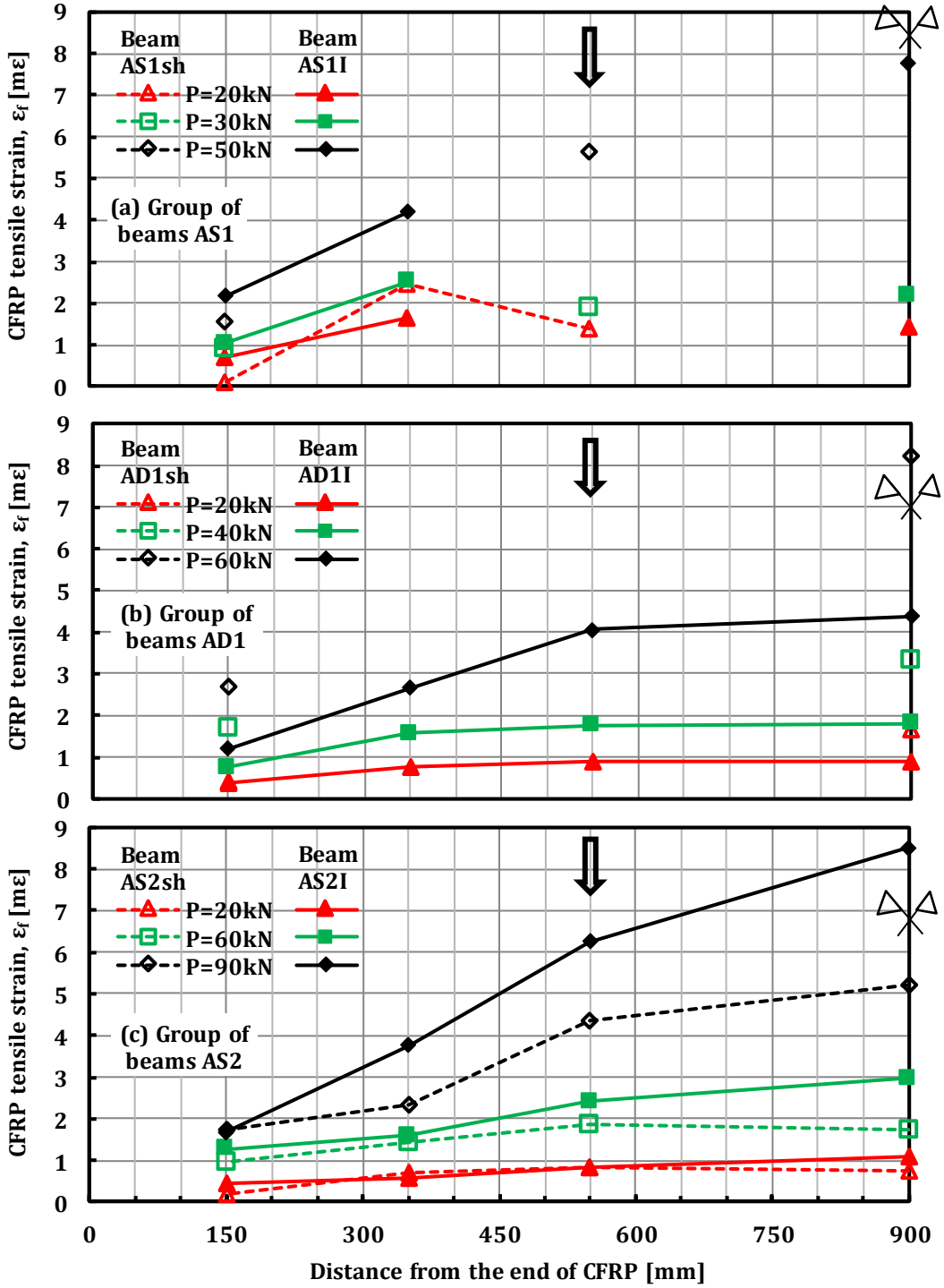

Figure 4.42 Longitudinal strain distribution along CFRP strip at different loads for the strengthened beams in series A before and after sustained loading.

As shown in Figure 4.43 the load and deflection at yield point were increased by increasing CFRP area. As presented in Table 4.17 compared to the un-strengthened

beam BR3II`, $P_y$ and $\delta_y$ increased with percentages of 33% and 5% in beam BS3II`, and 89% and 19% in beam BT3II`, respectively. This support the conclusion of the studied beams in group A2 that the load and deflection at yield increased by increasing CFRP area.

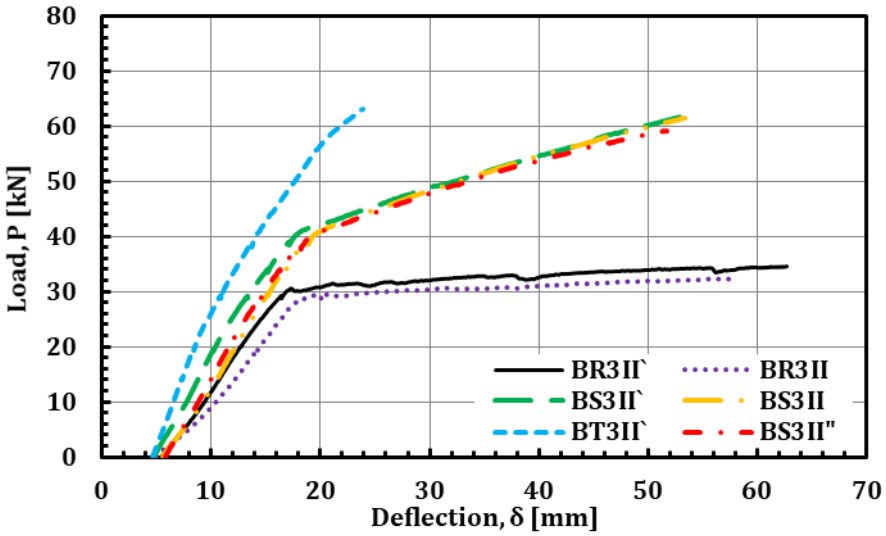

Figure 4.43 Load-deflection curves of group B2 beams tested after removing the sustained loads.

Table 4.17 Load-deflection results of group B2 beams tested after removing sustained loads.

Beam ID	P_D [kN]	P_s [kN]	δ_r [mm]	P_y [kN]	δ_y [mm]	P_u [kN]	δ_{max} [mm]	Failure Mode
BR3II`	---	14.19	5.40	30.66	17.34	34.64	62.64	CC
BS3II`	---	14.19	4.73	40.81	18.11	62.13	54.14	FR+ICs
BT3II`	---	14.19	4.66	58.06	20.70	63.09	23.87	ECs
BS3II"	20.30*	14.19	5.79	39.49	18.87	59.04	51.72	CC
BR3II	---	18.93	4.94	28.53	18.01	32.13	57.76	CC
BS3II	---	18.93	5.61	40.13	19.35	61.44	53.32	FR+ICs

* This beam subjected to two loading/unloading cycles before NSM strengthening of it.

The effect CFRP area on yielding after sustained loading of this group beams was clearer than group A2 beams. In addition to high CFRP area in beam BT3II`compared to AD1I, this might be due to the preloading of group A2 before its sustained loading with design service loads proportion the reinforcement of each beam increasing the cracking level of NSM strengthened beams with lager CFRP area. Therefore, the whole beam stiffness decreased in the beams with higher CFRP area against the increasing in its cracked and un-cracked sections compared to the beam with lower reinforcement. On the contrary, group B2 beams, BR3II`, BS3II`and BT3II`, were not preloaded

previous to their sustained loading. Moreover, these beams were loaded with the same value of sustained load achieving convergent levels of cracking.

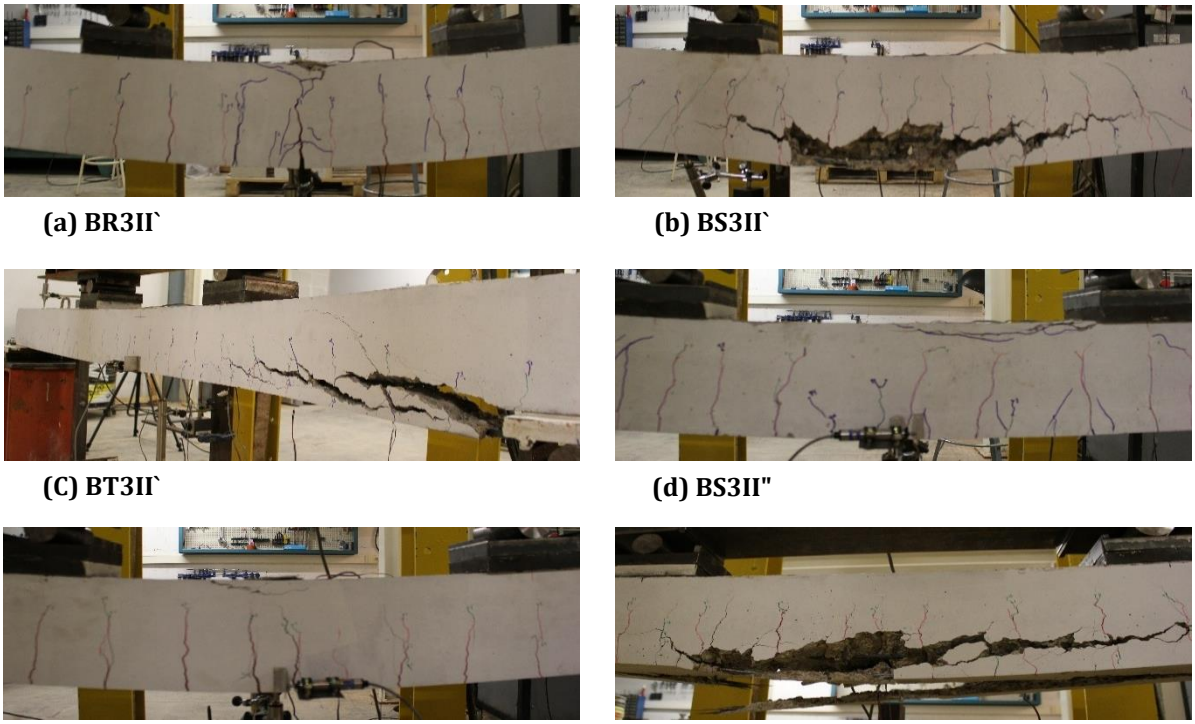

(a) BR3II`** **(b) BS3II`

(C) BT3II` **(d) BS3II"**

(e) BR3II **(f) BS3II**

Figure 4.44 Failure modes of group B2 beams.

As observed in group A2, the studied beams in group B2 showed decreasing in the maximum deflection and increasing in the load carrying capacity by increasing CFRP area. By increasing CFRP Area, the values of P_u, increased compared to the un-strengthened beam BR3II` with percentages of 79% and 82%, While $\delta_{max}$ decreased with percentages of 14% and 62% in beams BS3II`and BT3II`, respectively.

It's noticeable that the increasing percentage of load carrying capacity in beam BT3II`compared to its un-strengthened beam was lower than it in beam AD1I compared to its un-strengthened beam. This happened although both beams were failed with same premature failure of concrete cover separation at strip end and CFRP area of beam BT3II`equal 150% of it in beam AD1I. This might be due to the dependency of this failure mode on the shear stresses at the end of strips, which increased by increasing CFRP area transferring larger shear forces at cut off points of strips act on the same beam width. Therefore, it can be concluded that although the increasing CFRP area enhanced the load carrying capacity in NSM strengthened beams,

it increased the occurrence chance of premature failure of concrete cover separation at strip end, decreasing the enhancement in the load carrying capacity. This means that there is a value of CFRP percentage after which the increasing in CFRP will decrease the load carrying capacity.

On the effect of the higher level of the previous sustained loading, the un-strengthened beam BR3II showed a bit lower load-deflection curve with small shift compared to the un-strengthened beam BR3II`. While, the strengthened beam BS3II showed, after yielding, flexural behavior similar to the strengthened beamBS3II`. As presented in Table 4.17, the differences in the values of P_y, δ_y, P_u and δ_{max} between beam BS3II`and beam BS3II were very small.

On the effect of the preloading before NSM strengthening, beam BS3II" showed flexural behavior near to it in beam BS3II`. As presented in Table 4.17, the differences in the values of $P_y$, $\delta_y$, $P_u$ and $\delta_{max}$ between beam BS3II`and beam BS3II" were 3%, 4%, 5% and 4%, respectively. Despite this slight change, the failure modes were different in these two beams at variance of the two beams tested before the sustained loading.

The load-deflection curves of the tested beams after ageing in group B3 are presented in Figure 4.45. The load deflection curves of all beams show the stages defined at their ends by cracking, yield and failure points except beam BS3III`, which preloaded before NSM strengthening preventing the appearance of un-cracked stage here. The summary of the loads and deflections at the main points of each load deflection curve and the modes of failure are presented in Table 4.18.This table presented the values of yield load, P_y, in kN, yield deflection, δ_y, in mm, ultimate load, P_u, in kN, and the maximum deflection, δ_{max}, in mm. The failure modes of the studied beams are indicated in the last column in this table.

The failure modes of group B3 beams are shown in Figure 4.46. The observed modes of failure were similar to the summarized failure modes in De Lorenzis and Teng [15] and Sena-Cruz et al. [81]. Beams BS3III and BS3III` had failure mode of CFRP rupture followed by intermediate concrete cover separation, FR+ICs. Beam BT3III had failure mode of concrete cover separation at the end of CFRP strip, ECs. Beam BR3III had failure mode of concrete crushing at the top of beam, CC.

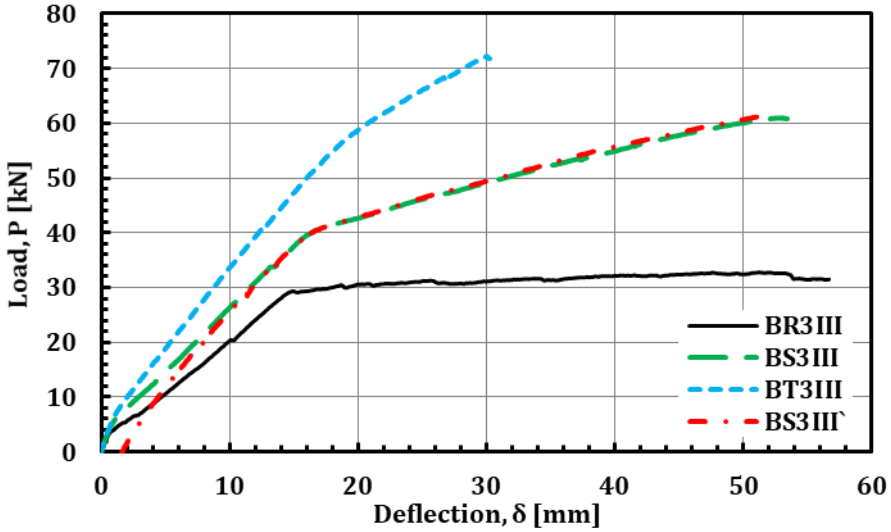

Figure 4.45 Load-deflection curves of group B3 beams tested after ageing.

Table 4.18 Load-deflection results of group B3 beams tested after ageing.

Beam ID	P_y [kN]	δ_y [mm]	P_u [kN]	δ_{max} [mm]	Failure Mode
BR3III	29.46	14.90	32.90	56.62	CC
BS3III	40.60	16.90	60.99	53.43	FR+ICs
BT3III	56.65	18.84	72.22	30.25	ECs
BS3III`	40.60	16.90	61.74	50.92	FR+ICs

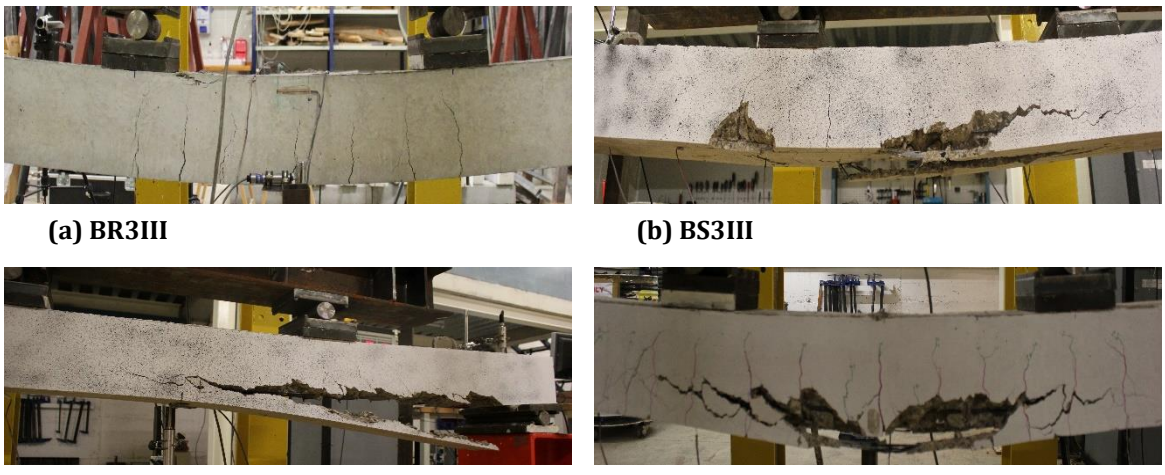

(a) BR3III **(b) BS3III**

(C) BT3III **(d) BS3III`**

Figure 4.46 Failure modes of group B3 beams.

As shown in Figure 4.45, the pre-cracked beam BS3III` showed load-deflection response lower than it in the virgin beam BS3III up to almost the pre-cracking load. After this load, it was observed that the behavior of the pre-cracked beam BS3III`was identical to that of virgin beam BS3III up to failure. This means that this matching

happened when the generated cracks in the virgin beam reached to equal lengths as those of the virgin one at almost the pre-cracking load. Even this was after ageing period, it was like what happened early between the pre-cracked beam BS3sh` and the virgin beam BS3sh in group B1. A similar finding was reported for pre-cracked RC beams under mode I (tensile crack) by Sallam et al. [159] regarding rectangle beams and Yehia and Wahab[160] regarding T-flanged beams and reported by Abou El-Mal et al. [161] for pre-cracked RC beams under mode II (shear crack). This also can be seen in Table 4.18 from the closeness between the reported values of load and deflection at yield and failure points.

On the effect of CFRP area, the aged beams in group B3 showed a trend similar to that observed in groups B1 and B2 as shown in Figure 4.45. The load and deflection at yield point were increased by increasing CFRP area. As presented in Table 4.18 compared to the un-strengthened beam BR3III, P_y and δ_y increased with percentages of 38% and 13% in beam BS3III, and 92% and 26% in beam BT3III, respectively.

The beams of group B2 showed decreasing in the ultimate deflection and increasing in the load carrying capacity by increasing CFRP area. By increasing CFRP Area, the values of P_u, increased compared to the un-strengthened beam BR3III with percentages of 85% and 120%, While δ_{max} decreased with percentages of 6% and 47% in beams BS3III and BT3III, respectively.

On the effect of sustained loading and ageing, the load-deflection responses of group B2 beams, which tested after removing their sustained loads, and group B3 beams, which kept without loading, were compared with the load-deflection responses of group B1 beams, which tested before the sustained loading. These comparisons are presented in Figure 4.47 for the un-strengthened beams and Figure 4.48 for the strengthened beams. The values of permanent deflection induced after previous loading, δ_r, was added to each beam to describe the its actual deformation.

It is clear that there is an obvious effect of both age and load history on the load bearing capacity and maximum deflection of RC beams failed due to concrete crushing in compressive zone, see Figure 4.38, Figure 4.39c, and Figure 4.47. In the case of strengthened beams failed due to debonding of CFRP, the effect of age and load history

is marginal. Furthermore, there is two opposite trends were observed in the case of strengthened beams failed due to debonding of CFRP as follow: beams BT3II' and BT3III show large degradation compared to BT3sh, see Figure 4.48b, while this observation was not realized in the case of beams AD1sh and AD1I.

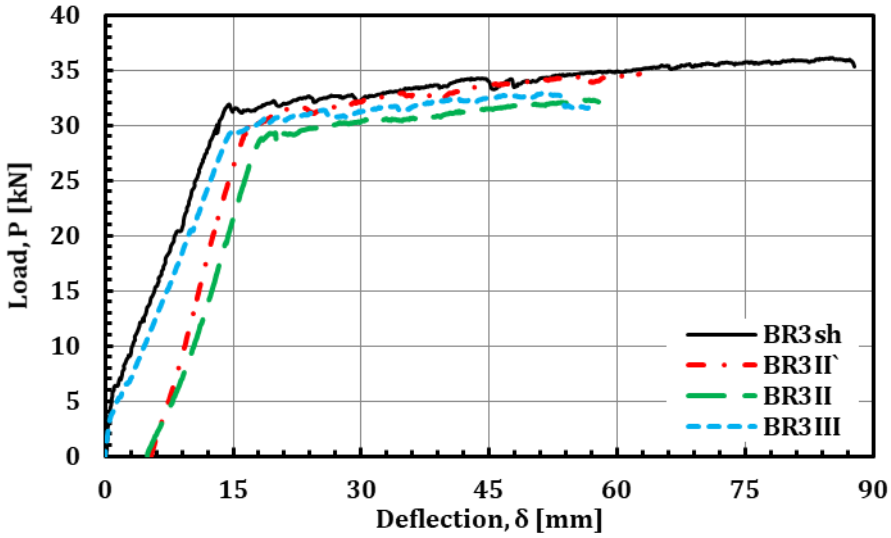

Figure 4.47 Load-deflection curves for the un-strengthened group of beams BR3 in series B before and after sustained loading and after ageing.

On the effect of ageing, the un-strengthened and strengthened beams in group B3, except beam BS3III, showed a shift in their load-deflection curves with decrease in loads compared to their corresponding beams in group B1. This was due to the effect of the concrete shrinkage previous to loading of group B3 beams along their ageing. Beam BS3III` did not show this shift because it was subjected to two loading/unloading cycles before its NSM strengthening and subjected to ageing in cracked status, which eliminate the effect of the previous concrete shrinkage.

All aged beams of group B3 showed decreases in the load carrying capacity and the maximum deflection compared to their corresponding beams in group B1, despite the similarity of their failure modes. For the un-strengthened beams, this might be due to the decreasing of the concrete strain at failure by concrete ageing accelerating the concrete crushing in beam BR3III compared to beam BR3sh. For the strengthened beams with A_f of 84 mm^2, this might be due to the decreasing in tensile strength of concrete cover as a result of the combined effect of the previous concrete shrinkage and presence of steel reinforcement, which accelerated the concrete cover separation at the end of CFRP strip in beam BT3III compared to beam BT3sh.

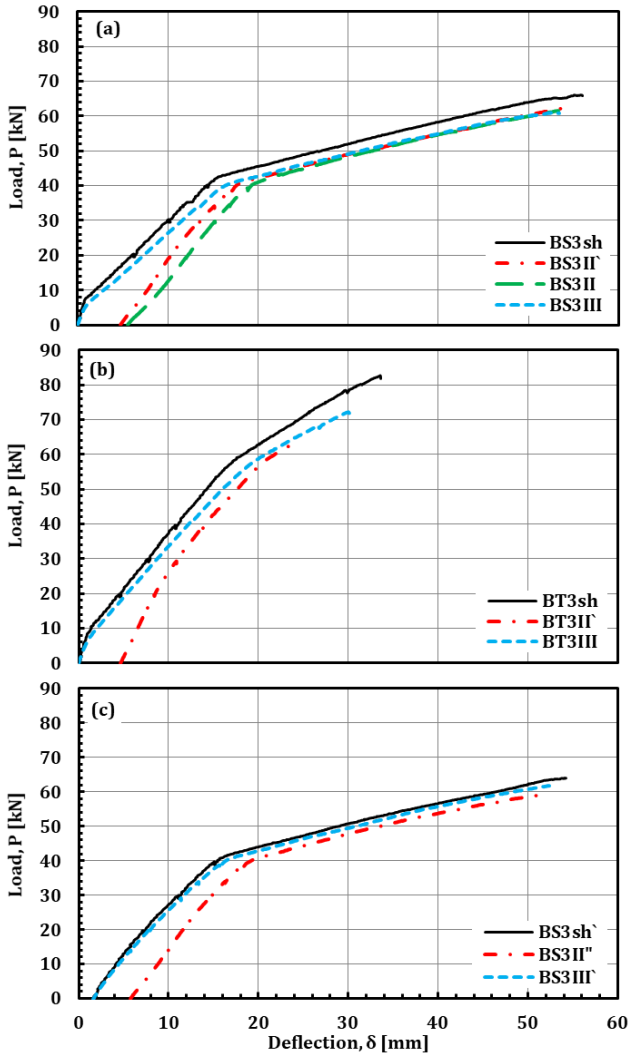

Figure 4.48 Load-deflection curves of the strengthened beams in series B before and after sustained loading and after ageing.

On the effect of the previous sustained loading, group B2 beams showed, after yielding, flexural behavior similar or near to the flexural behavior of their corresponding aged beams in group B3, regardless their load carrying capacities and their ultimate deflections.

As shown in Figure 4.47, the un-strengthened beams BR3II` and BR3II with previous lower and higher levels of sustained load showed, after yielding, flexural behaviors around the flexural behavior of the aged beam BR3III with same failure mode of concrete crushing and very close load carrying capacities and ultimate deflections. As shown in Figure 4.48a, the strengthened beams BS3II` and BS3II with lower and higher levels of sustained load showed, after yielding, the same flexural behavior of the aged beam BS3III with the same failure mode of FR+ICs and almost the same load carrying capacities and ultimate deflections. As shown in Figure 4.48c, beam BS3II" showed,

after yielding, flexural behavior near to the flexural behavior of the aged beam BS3III` with very close load carrying capacities and ultimate deflections, while it had different failure mode of concrete crushing.

Therefore, it can be concluded that the previous sustained loading did not change the flexural behavior after yielding, the load carrying capacity and the ultimate deflection of the un-strengthened and NSM strengthened beams failed with concrete crushing or CFRP rupture, whether these beams preloaded before strengthening or not.

As shown in Figure 4.48b, the strengthened beam BT3II` with A_f of 84 mm^2 showed, after yielding, the same flexural behavior of the aged beam BT3III with the same failure mode of ECs, but with very low load carrying capacities and ultimate deflections. This reflects that the previous sustained loading increased the tensile stresses induced in the concrete cover at the end of CFRP strip accelerating the concrete cover separation at this end in beam BT3II` compared to beam BT3III.

In terms of the strain variation with load, ε_c and ε_s at the mid-span section were plotted versus P for each beam in group B1 compared with its corresponding beams in groups B2 and B3 in the same figure. Figure 4.49 plotted for the un-strengthened beams and Figure 4.50 for the strengthened beams.

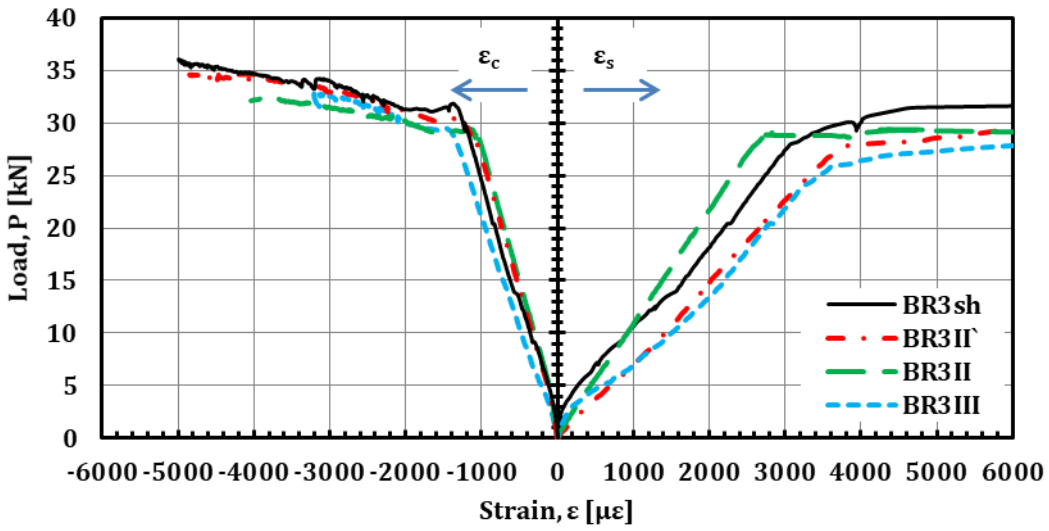

Figure 4.49 Strains of concrete and tensile steel at mid-span section for the un-strengthened group of beams BR3 in series B before and after sustained loading and after ageing.

The concrete strains are presented in the left side with negative values and the steel strains are presented in the right side with positive values. All steel strain gages were failed after yielding. Therefore, only the first 6000 $\mu\varepsilon$ of steel strain are presented.

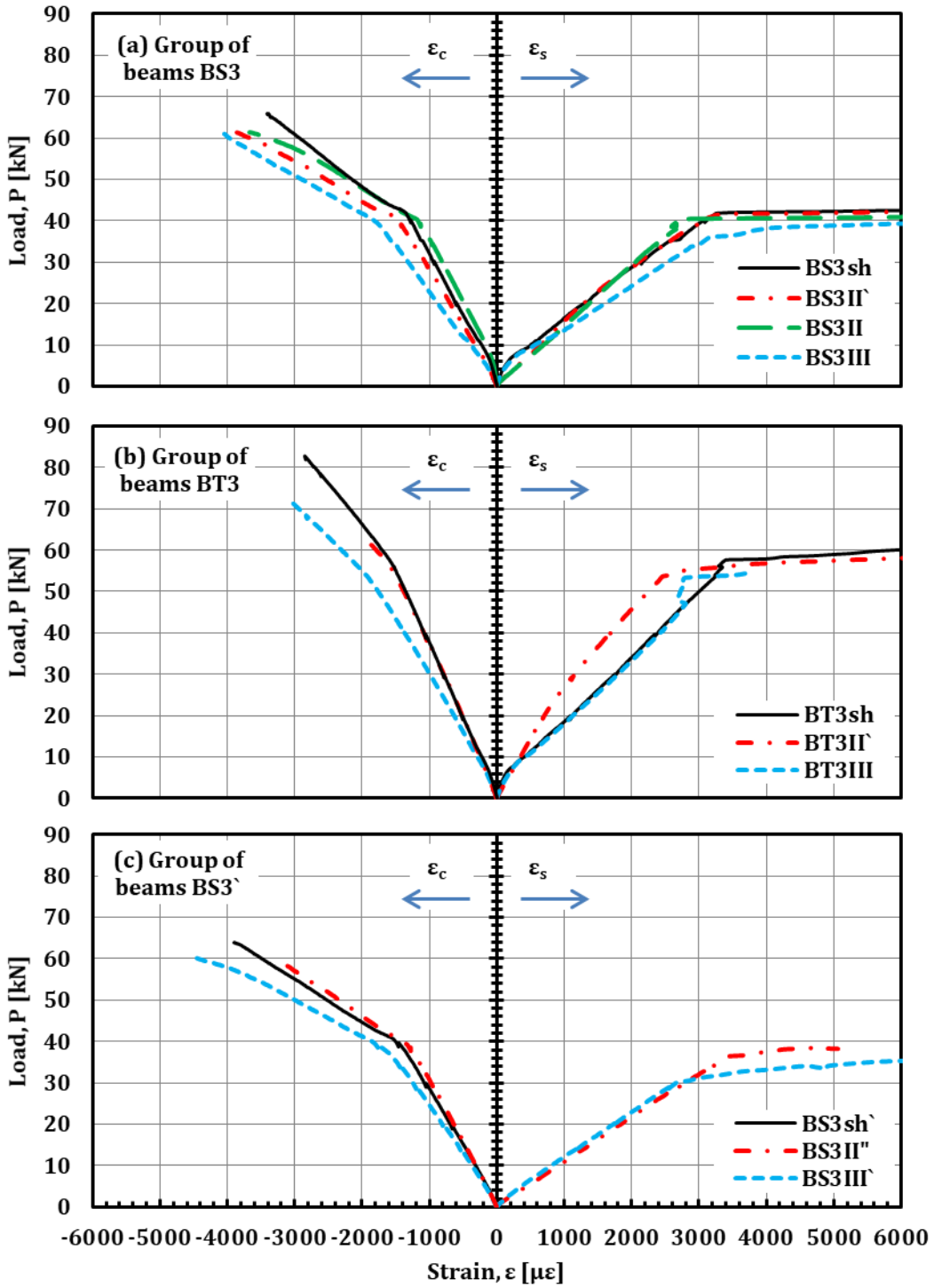

Figure 4.50 Strains of concrete and tensile steel at mid-span section for the strengthened beams in series B before and after sustained loading and after ageing.

The steel strain gage of beam BR3sh` failed before the test, therefore its results are not presented. The tensile steel of aged beams started to yield at lower loads compared to the beams tested at early age, either these beams were strengthened or not. For the

un-strengthened beams, the tensile steel yielded at 28 kN in beam BR3sh, while it yielded at 26 kN in beam BR3III as shown in Figure 4.49. For strengthened beams with CFRP area of 28 mm^2, the tensile steel yielded at 42 kN in beam BS3sh, while it yielded at 37 kN in beam BS3III as shown in Figure 4.50a. For strengthened beams with CFRP area of 84 mm^2, the tensile steel yielded at 57 kN in beam BT3sh, while it yielded at 53 kN in beam BT3III as shown in Figure 4.50b. In general, at the same load the concrete compressive strain was higher in aged beams than it in the beams tested at early age and this difference was more pronounced after the yielding of tensile steel.

The longitudinal strain distributions along CFRP strip at different loads for the strengthened beams in series B before and after sustained loading and after ageing are presented in Figure 4.51. The strain should be constant along the constant moment region (the middle third of beam) and decreases along the rest of CFRP strip up to its ends. this occurred in beam BT3II` before and after the beam yielding as shown in Figure 4.51b. On the contrary, the measured strain patterns after yielding for all presented beams except this beam displayed irregular activity. This could be linked to improper strain gauge bonding. It could also be attributed to the instability of strain gauge measurements during yielding and cracking [167,168] which could be influencing the measured strains during testing to the first load drop [169].

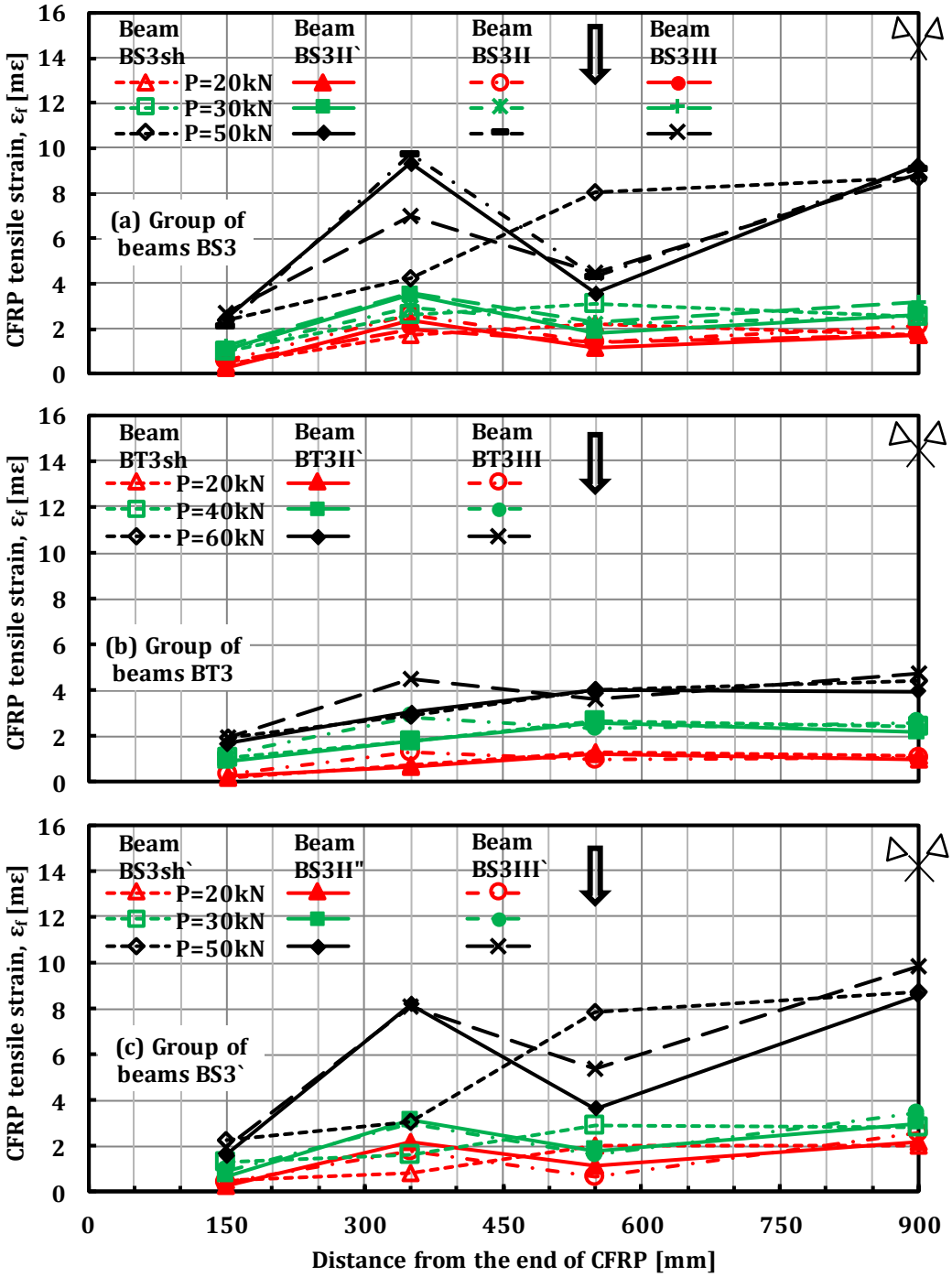

Figure 4.51 Longitudinal strain distribution along CFRP strip at different loads for the strengthened beams in series B before and after sustained loading and after ageing.

CHAPTER 5 CONCLUSIONS

5.1 Summary

The effect of sustained loading on the NSM FRP strengthened RC structures during the life-span of the structure is observed as an area of incomplete knowledge. Understanding and clarifying how the structure is affected by this type of external actions is a main requirement for an improved design of FRP strengthened members. In the present work, an extensive experimental program was carried out to study the long-term and residual flexural strength of NSM strengthened RC beams with carbon FRP (CFRP) strips when subjected to sustained loading.

In order to achieve the aim of this work, two series of un-strengthened and CFRP NSM strengthened beams were tested and studied in three main stages:

Firstly, the short-term flexural behavior was experimentally investigated at age of 55 days. The studied beams in this stage included different CFRP areas, tensile reinforcement ratios, concrete types and strengthening sequences. The experimental results were presented and discussed in terms of load-deflection response, mode of failure, deformability and ductility indices, cracking behavior with load, strains variation of constitutive materials (steel, concrete and CFRP strips) and slip of CFRP strips with load of strengthened beams.

Secondly, the long-term flexural behavior was experimentally investigated under sustained loading up to age of 345 days. The studied beams in this stage included different CFRP areas, tensile and compression reinforcement ratios, loading sequences, concrete types and load levels. The experimental results of each studied parameter were presented and discussed in terms of initial deflection, total deflection with time, the ratio of time dependent deflection to instantaneous deflection and permanent deflection after removing loads.

Finally, the residual flexural strength was experimentally investigated at age of 365 days, either after removing the sustained loads or after ageing. The experimental results were presented and discussed in terms of load-deflection response, mode of failure and strains variation of constitutive materials (steel, concrete and CFRP strips).

5.2 Concluding Remarks

The most relevant conclusions from the experimental investigation of the short-term flexural behavior can be summarized as follows:

- Increasing the CFRP area increased the yield load and the load carrying capacity, magnified the slips of CFRP strip at its both ends and decreased the ductility and crack width of strengthened beams. The RC beam NSM strengthened with three CFRP strips of 2.8 mm thickness each achieved an increase of 79% and 129% in the yield load and the load carrying capacity, respectively, and a decrease 61% and of 68% in the maximum deflection and the ductility, respectively.

- Failure mode of concrete cover separation at the cut-off point of CFRP strip, controlled the increase in the load carrying capacity of strengthened by increasing CFRP area.

- Despite the decrease in the crack width at the same applied load by increasing steel reinforcement or concrete strength, these parameters had a little influence on the crack pattern of the studied un-strengthened beams.

- The behavior of the pre-cracked beam was identical to that of virgin beam after the pre-cracking load and up to failure. This means that this matching happened when the main crack in the virgin beam reached to the length of the pre-crack in the cracked beam.

- The increase in the concrete strength did not achieve a noticeable effect on the flexural behavior of the un-strengthened RC beams due to the failure being mainly governed by the effect of steel yielding.

- The increase of concrete cover strength increased the load transfer efficiency of NSM strengthened RC sections leading to higher stiffness of whole strengthened beam enhancing its flexural behavior and increasing load carrying capacity up to 13%. While, it was unable to resist the stress concentration at the end of CFRP strips due to the failure mode of concrete cover separation at the cut-off point of CFRP strip.

- In the beams with higher steel reinforcement ratio, the ratio between CFRP and steel reinforcement was low. Therefore, the failure mode of the strengthened beam was identical to the un-strengthened one (concrete crushing after steel yielding). This made the NSM CFRP strengthening improve the ultimate deflection like the ultimate load and the effective stiffness.

The most relevant conclusions from the experimental investigation of the time dependent flexural behavior under sustained loading can be summarized as follows:

- Increasing of CFRP area enhanced the efficiency of NSM strengthening to control initial deflection, δ_o.

- Increasing of CFRP area aided the NSM strengthened beam to retain more deflection from its time dependent deflection, δ_{td}, either the beams were virgin or preloaded.

- The preloading of NSM strengthened beam limited the decrease in initial deflection, δ_o, and consequently in total deflection, δ_T, and decreased the time dependent deflection, δ_{td}.

- The beams with higher reinforcement ratios were able to retain all of the time dependent deflection, δ_{td}, after removing the sustained loading, despite their higher creep deformations during sustained loading.

- Increasing the tensile reinforcement by adding NSM strips lead to moving of the neutral axis toward the bottom surface and subsequently increase the compressive strain at the upper surface for the same tensile strain at the bottom surface, i.e. causing higher creep deformations.

- The preloading of the NSM strengthened beam with CFRP strips up to its design service load led to decrease its time dependent deflection under sustained loading compared to the un-strengthened beam at the odds of the beams sustained loaded directly without preloading. The ratio of time dependent deflection to instantaneous deflection was < 1 for the preloaded beams with different CFRP areas, while it was > 1 for the others loaded directly without preloading.

- The ratio of time dependent deflection to instantaneous deflection increased by increasing concrete strength for the strengthened and un-strengthened beams.

- The presence of the compression steel magnified the benefit of NSM CFRP strengthening in the reduction of initial deflections of the strengthened beams. This reduction was 29% for the beams without compression steel and 36% for the beams with compression steel.

- The ratio of time dependent deflection to instantaneous deflection increased by removing the compression steel in the compared un-strengthened beams. This increase reached 12% at the end of the sustained loading. However, the strengthened beams, with and without compression steel, produced almost same values of this ratio during the loading time.

- The higher level of sustained load limited the increase by NSM strengthening in the ratio of time dependent deflection to instantaneous deflection. This increase was 64% at lower level of sustained load, while it was 40% at higher level of sustained load.

- The permanent deflection in beams after removing loads decreased 12% by NSM strengthening at low level load, while It increased 14% at high load level.

The most relevant conclusions from the experimental investigation of the residual flexural strength, either after sustained loading or ageing can be summarized as follows:

- The aged un-strengthened and strengthened beams showed decreases in the load carrying capacity and the maximum deflection compared to their corresponding control beams, despite the similarity of their failure modes.

- The un-strengthened and strengthened beams subjected to sustained loading without preloading showed flexural behavior after yielding almost similar to the flexural behavior of their corresponding aged beams. On the other hand, the beams with preloading showed flexural behavior after yielding almost similar to the flexural behavior of their corresponding control beams.

- The sustained loading increased the tensile stresses in the concrete cover at the end of CFRP strip accelerating its separation for the beams. Therefore, the sustained loading did not change the load carrying capacity and the maximum deflection of either the un-strengthened beam and NSM strengthened beam failed due to concrete crushing or CFRP rupture.

5.3 Future Work

Based on the results of this research and the conducted literature review, the following topics are proposed as future work:

- To obtain a methodology that could be used in design to determine the long-term curvatures and deflections due to creep and shrinkage phenomena for the FRP NSM strengthened RC beams. A parametric study and further experimental tests should be carried out for its validation.

- To provide a convenient design methodology for the assessment of long-term deflections of the FRP NSM strengthened RC beams.

- To extend the experimental work regarding the long-term flexural behavior of NSM CFRP RC beams under different levels of sustained loading and/or fatigue loading corresponding to serviceability conditions.

- To extend the experimental work to the long-term flexural behavior of NSM CFRP RC beams under environmental adversities such as freeze-thaw cycles and elevated temperatures.

- To carry out a numerical investigation using finite element simulation in order to study the long-term effects for different combinations of influencing parameters. Various bond-slip models, together with nonlinear material modeling of materials and time-dependent analysis shall be considered.

Bibliography

[1] J. Aidoo, K.A. Harries, M.F. Petrou, Full-scale experimental investigation of repair of reinforced concrete interstate bridge using CFRP materials, Journal of Bridge Engineering. 11 (2006) 350–358.

[2] J.F. Bonacci, M. Maalej, Externally bonded FRP for service-life extension of RC infrastructure, Journal of Infrastructure Systems. 6 (2000) 41–51.

[3] K. Neale, FRPs for structural rehabilitation: a survey of recent progress, Structural Engineering and Materials. 2 (2000) 133–138.

[4] N.T.K. Al-Saadi, A. Mohammed, R. Al-Mahaidi, J. Sanjayan, A state-of-the-art review: Near-surface mounted FRP composites for reinforced concrete structures, Construction and Building Materials. 209 (2019) 748–769.

[5] L.C. Bank, Composites for Construction: Structural Design with FRP Materials, John Wiley & Sons, 2007.

[6] J.G. Teng, J.F. Chen, S.T. Smith, L. Lam, FRP : Strengthened RC Structures, John Wiley & Sons, 2002.

[7] H.V.S. GangaRao, N. Taly, P. V. Vijay, Reinforced Concrete Design with FRP Composites, CRC Press, 2006.

[8] L.C. Hollaway, J.G. Teng, Strengthening and rehabilitation of civil infrastructures using fibre-reinforced polymer (FRP) composites, Woodhead Pubishing, 2008.

[9] P.N. Balaguru, A. Nanni, J. Giancaspro, FRP composites for reinforced and prestressed concrete structures : a guide to fundamentals and design for repair and retrofit, CRC Press, 2009.

[10] ISIS Canada, Reinforcing Concrete Structures with Fibre Reinforced Polymers Reinforcing, ISIS Canada Corporation, 2001.

[11] N. Banthia, L. Bisby, R. Cheng, G. Fallis, R. Hutchinson, a Mufti, K.W. Neale, J. Newhook, K. Soudki, L. Wegner, An Introduction to FRP Composites for Construction, ISIS Canada Educational Module No. 2: FRP Composites for Construction. (2006) 25.

[12] Fédération Internationale du Béton (fib), Externally bonded FRP reinforcement for RC structures, Task Group 9.3, Bulletin No. 14, 2001.

[13] L. De Lorenzis, A. Nanni, Characterization of FRP rods as near-surface mounted reinforcement, Journal of Composites for Construction. 5 (2001) 114–121.

[14] R. Parretti, A. Nanni, Strengthening of RC members using near-surface mounted FRP composites: Design overview, Advances in Structural Engineering. 7 (2004)

469–483.

[15] L. De Lorenzis, J.G. Teng, Near-surface mounted FRP reinforcement: An emerging technique for strengthening structures, Composites Part B: Engineering. 38 (2007) 119–143.

[16] J.A.O. Barros, S.J.E. Dias, J.L.T. Lima, Efficacy of CFRP-based techniques for the flexural and shear strengthening of concrete beams, Cement and Concrete Composites. 29 (2007) 203–217.

[17] A. Bilotta, F. Ceroni, M. Di Ludovico, E. Nigro, M. Pecce, G. Manfredi, Bond efficiency of EBR and NSM FRP systems for strengthening concrete members, Journal of Composites for Construction. 15 (2011) 757–772.

[18] D. Lee, L. Cheng, J. Yan-Gee Hui, Bond characteristics of various NSM FRP reinforcements in concrete, Journal of Composites for Construction. 17 (2013) 117–129.

[19] R. Kotynia, Bond between FRP and concrete in reinforced concrete beams strengthened with near surface mounted and externally bonded reinforcement, Construction and Building Materials. 32 (2012) 41–54.

[20] S.S. Zhang, J.G. Teng, T. Yu, Bond strength model for CFRP strips near-surface mounted to concrete, Journal of Composites for Construction. 18 (2014) A4014003.

[21] M. Rezazadeh, S. Cholostiakow, R. Kotynia, J. Barros, Exploring new NSM reinforcements for the flexural strengthening of RC beams: Experimental and numerical research, Composite Structures. 141 (2016) 132–145.

[22] G.M. Dalfré, J.A.O. Barros, NSM technique to increase the load carrying capacity of continuous RC slabs, Engineering Structures. 56 (2013) 137–153.

[23] E. Hamed, M.A. Bradford, Creep in concrete beams strengthened with composite materials, European Journal of Mechanics, A/Solids. 29 (2010) 951–965.

[24] E. Hamed, Effect of Adhesive Viscoelasticity on the Creep Behaviour of FRP Strengthened Concrete Beams, Composites Science and Technology. 74 (2012) 186–193.

[25] E. Hamed, M.A. Bradford, Flexural time-dependent cracking and post-cracking behaviour of FRP strengthened concrete beams, International Journal of Solids and Structures. 49 (2012) 1595–1607.

[26] M.M. Reda Taha, M.J. Masia, K.K. Choi, P.L. Shrive, N.G. Shrive, Creep effects in plain and fiber-reinforced polymer-strengthened reinforced concrete beams, ACI Structural Journal. 107 (2010) 627–635.

[27] I.A. Sharaky, A study of the bond and flexural behaviour of reinforced concrete elements strengthened with near surface mounted (NSM) FRP reinforcement,

Universitat de Girona, Spain, 2013.

[28] D. Foti, Preliminary analysis of concrete reinforced with waste bottles PET fibers, Construction and Building Materials. 25 (2011) 1906–1915.

[29] D. Foti, Use of recycled waste pet bottles fibers for the reinforcement of concrete, Composite Structures. 96 (2013) 396–404.

[30] D. Foti, S. Vacca, Comportamiento mecánico de columnas de hormigón armado reforzadas con mortero reoplástico, Materiales de Construccion. 63 (2013) 267–282.

[31] Fédération Internationale du Béton (fib), Bond of Reinforcement in Concrete: State-of-the-art report, 2000.

[32] A. Nanni, Guide for the design and construction of concrete reinforced with FRP bars (ACI 440.1R-03), in: Proceedings of the Structures Congress and Exposition, 2005: pp. 1621–1626.

[33] M.R.A.E. Emara, Bond behavior of NSM FRP strips in concrete under sustained loading, Universitat de Girona, Spain, 2018.

[34] R. El-Hacha, S.H. Rizkalla, Near-surface-mounted fiber-reinforced polymer reinforcements for flexural strengthening of concrete structures, ACI Structural Journal. 101 (2004) 717–726.

[35] M. Blaschko, Bond behaviour of CFRP strips glued into slits, in: K.H. Tan (Ed.), Sixth Int. Symposium on FRP Reinforcement for Concrete Structures (FRPRCS-6), World Scientific, Singapore, 2003: pp. 205–214.

[36] L. De Lorenzis, Anchorage length of near-surface mounted fiber-reinforced polymer rods for concrete strengthening - Analytical modeling, ACI Structural Journal. 101 (2004) 375–386.

[37] J.G. Teng, L. De Lorenzis, B. Wang, R. Li, T.N. Wong, L. Lam, Debonding failures of RC beams strengthened with near surface mounted CFRP strips, Journal of Composites for Construction. 10 (2006) 92–105.

[38] J.M. De Sena Cruz, J.A.O. De Barros, Bond between near-surface mounted carbon-fiber-reinforced polymer laminate strips and concrete, Journal of Composites for Construction. 8 (2004) 519–527.

[39] M.B. Muñoz, Study of bond behaviour between FRP reinforcement and concrete, Universitat de Girona, Spain, 2010.

[40] N.A.A. Mohamed, Strength and drift capacity of GFRP-reinforced concrete shear walls, Université de Sherbrooke, 2013.

[41] B. Täljsten, The importance of bonding - A historic overview and future possibilities, in: Advances in Structural Engineering, 2006: pp. 721–736.

[42] S. Ebnesajjad, A.H. Landrock, Adhesives Technology Handbook, William Andrew, 2008.

[43] A. Pizzi, K. Mittal, C. Pearson, Animal Glues and Adhesives, in: Handbook of Adhesive Technology, Revised and Expanded, CRC Press, 2003: pp. 479–494.

[44] L. De Lorenzis, A. Rizzo, A. La Tegola, A modified pull-out test for bond of near-surface mounted FRP rods in concrete, Composites Part B: Engineering. 33 (2002) 589–603.

[45] D.S. Yang, S.K. Park, K.W. Neale, Flexural behaviour of reinforced concrete beams strengthened with prestressed carbon composites, Composite Structures. 88 (2009) 497–508.

[46] S.O. Asplun, Strengthening Bridge Slabs with Grouted Reinforcement, ACI Journal Proceedings. 45 (1949) 397–406.

[47] R. Capozucca, Damage to reinforced concrete due to reinforcement corrosion, Construction and Building Materials. 9 (1995) 295–303.

[48] M. Tavakkolizadeh, H. Saadatmanesh, Strengthening of steel-concrete composite girders using carbon fiber reinforced polymers sheets, Journal of Structural Engineering. 129 (2003) 30–40.

[49] M. Tavakkolizadeh, Strengthening and repair of steel-concrete composite girders using CFRP laminates, University of Arizona, 2001.

[50] J.F. Chen, J.G. Teng, Anchorage strength models for FRP and steel plates bonded to concrete, Journal of Structural Engineering. 127 (2001) 784–791.

[51] M.S. Mohamed Ali, D.J. Oehlers, M.C. Griffith, R. Seracino, Interfacial stress transfer of near surface-mounted FRP-to-concrete joints, Engineering Structures. 30 (2008) 1861–1868.

[52] X.Z. Lu, J.G. Teng, L.P. Ye, J.J. Jiang, Bond-slip models for FRP sheets/plates bonded to concrete, Engineering Structures. 27 (2005) 920–937.

[53] S.K. Sharma, M.S.M. Ali, D. Goldar, P.K. Sikdar, Plate-concrete interfacial bond strength of FRP and metallic plated concrete specimens, Composites Part B: Engineering. 37 (2006) 54–63.

[54] J.F. Chen, H. Yuan, J.G. Teng, Debonding failure along a softening FRP-to-concrete interface between two adjacent cracks in concrete members, Engineering Structures. 29 (2007) 259–270.

[55] J. Yao, J.G. Teng, Plate end debonding in FRP-plated RC beams-I: Experiments, Engineering Structures. 29 (2007) 2457–2471.

[56] H. Yuan, J.G. Teng, R. Seracino, Z.S. Wu, J. Yao, Full-range behavior of FRP-to-concrete bonded joints, Engineering Structures. 26 (2004) 553–565.

[57] U. Ebead, H. Saeed, Hybrid shear strengthening system for reinforced concrete beams: An experimental study, Engineering Structures. 49 (2013) 421–433.

[58] K.C. Panda, S.K. Bhattacharyya, S. V. Barai, Shear strengthening of RC T-beams with externally side bonded GFRP sheet, Journal of Reinforced Plastics and Composites. 30 (2011) 1139–1154.

[59] N.A. Siddiqui, Experimental investigation of RC beams strengthened with externally bonded FRP composites, Latin American Journal of Solids and Structures. 6 (2009) 343–362.

[60] B. Täljsten, A. Carolin, H. Nordin, Concrete beams strengthened with near surface mounted CFRP laminates, in: Proceedings FRPRCS, 2001: pp. 107–116.

[61] B. Täljsten, A. Carolin, H. Nordin, Concrete structures strengthened with near surface mounted reinforcement of CFRP, Advances in Structural Engineering. 6 (2003) 201–213.

[62] A. Prota, A.; Parretti, R.; Nanni, Upgrade of RC silos using near surface mounted FRP composites, L'Industria Italiana Del Cemento. 73 (2003) 170–183.

[63] ACI 440.2R-08, Guide for the design and construction of externally bonded FRP systems for strengthening existing structures, 2008.

[64] Fédération Internationale du Béton (fib), Externally bonded FRP reinforcement for RC structures, Task Group 9.3, Bulletin No. 14, 2001.

[65] CSA (Canadian Standards Association), Design and Construction of Building Components with Fibre-Reinforced Polymers (Reaffirmed 2007), 2009.

[66] W.C. Tang, R. V. Balendran, A. Nadeem, H.Y. Leung, Flexural strengthening of reinforced lightweight polystyrene aggregate concrete beams with near-surface mounted GFRP bars, Building and Environment. 41 (2006) 1381–1393.

[67] I.S.T. Liu, D.J. Oehlers, R. Seracino, Tests on the ductility of reinforced concrete beams retrofitted with FRP and steel near-surface mounted plates, Journal of Composites for Construction. 10 (2006) 106–114.

[68] I.A. Sharaky, L. Torres, M. Baena, C. Miàs, An experimental study of different factors affecting the bond of NSM FRP bars in concrete, Composite Structures. 99 (2013) 350–365.

[69] J.A.O. Barros, A.S. Fortes, Flexural strengthening of concrete beams with CFRP laminates bonded into slits, Cement and Concrete Composites. 27 (2005) 471–480.

[70] H. Nordin, B. Täljsten, Concrete Beams Strengthened With Pre-Stressed Near Surface Mounted Reinforcement, Fibre-Reinforced Polymer Reinforcement for Concrete Structures. 2 (2003) 1077–1086.

[71] R. Seracino, N.M. Jones, M.S.M. Ali, M.W. Page, D.J. Oehlers, Bond strength of near-

surface mounted FRP strip-to-concrete joints, Journal of Composites for Construction. 11 (2007) 401–409.

[72] Y. Yun, Y.F. Wu, W.C. Tang, Performance of FRP bonding systems under fatigue loading, Engineering Structures. 30 (2008) 3129–3140.

[73] J.M. Sena Cruz, J.A.O. Barros, R. Gettu, Á.F.M. Azevedo, Bond behavior of near-surface mounted CFRP laminate strips under monotonic and cyclic loading, Journal of Composites for Construction. 10 (2006) 295–303.

[74] X. Yan, B. Miller, A. Nanni, C.E. Bakis, Characterization of CFRP rods used as near surface mounted reinforcement, in: 8th International Conference on Structural Faults and Repair, 1999: pp. 1–12.

[75] D. Galati, L. De Lorenzis, Effect of construction details on the bond performance of NSM FRP bars in concrete, in: Advances in Structural Engineering, 2009: pp. 683–700.

[76] S.M. Soliman, E. El-Salakawy, B. Benmokrane, Bond performance of near-surface-mounted FRP bars, Journal of Composites for Construction. 15 (2011) 103–111.

[77] J.M.S. Cruz, J. a O. Barros, Bond Behavior of Carbon Laminate Strips Into Concrete By Pullout-Bending Tests, in: Bond in Concrete – from Research to Standards, Budapest, 2002: pp. 1–8.

[78] D. Novidis, S.J. Pantazopoulou, E. Tentolouris, Experimental study of bond of NSM-FRP reinforcement, Construction and Building Materials. 21 (2007) 1760–1770.

[79] F. Al-Mahmoud, A. Castel, R. François, C. Tourneur, Anchorage and tension-stiffening effect between near-surface-mounted CFRP rods and concrete, Cement and Concrete Composites. 33 (2011) 346–352.

[80] A. Al-Abdwais, R. Al-Mahaidi, Modified cement-based adhesive for near-surface mounted CFRP strengthening system, Construction and Building Materials. 124 (2016) 794–800.

[81] J. Sena-Cruz, J. Barros, V. Bianco, A. Bilotta, D. Bournas, F. Ceroni, G. Dalfré, R. Kotynia, G. Monti, E. Nigro, T. Triantafillou, NSM systems, in: RILEM State-of-the-Art Reports, 2016: pp. 303–348.

[82] L. De Lorenzis, a Nanni, Strengthening of Reinforced Concrete Structures with Near Surface Mounted FRP Rods Previous Work on NSM Rods, ACI Structural Journal. 1948 (2002) 1–8.

[83] T. Hassan, S. Rizkalla, Investigation of bond in concrete structures strengthened with near surface mounted carbon fiber reinforced polymer strips, Journal of Composites for Construction. 7 (2003) 248–257.

[84] E.K. Castro, G.S. Melo, Flexural Strengthening of Rc "T" Beams With Near Surface Mounted (NSM) FRP Reinforcements, in: Proceedings of the 8th International

Symposium on Fiber Reinforced Polymer Reinforcement for Concrete Structures (FRPRCS-8), Patras, Greece, 2007: pp. 16–18.

[85] D.G. Novidis, S.J. Pantazopoulou, Beam tests of NSM-FRP laminates in concrete, in: FRPRSCS-8, In Proceedings of the eight international conference on fibre-reinforced plastics for reinforced concrete structures (FRPRSCS-8), Patras, Greece, 2007: pp. 1–10.

[86] R. Kotynia, Analysis of the Flexural Response of Nsm Frp-Strengthened Concrete Beams, in: Proceedings of the Eight International Conference on Fibre-Reinforced Plastics for Reinforced Concrete Structures (FRPRSCS-8), Patras, Greece, 2007: pp. 1–10.

[87] A.S. Kalayci, Development of Surface Flaw Thresholds for Pre- Cured Fiber Reinforced Polymer and Groove Size Tolerance for Near Surface Mounted Fiber Reinforced Polymer Retrofit Systems, Florida International University, 2008.

[88] I.A. Sharaky, R.M. Reda, M. Ghanem, M.H. Seleem, H.E.M. Sallam, Experimental and numerical study of RC beams strengthened with bottom and side NSM GFRP bars having different end conditions, Construction and Building Materials. 149 (2017) 882–903.

[89] I.A. Sharaky, M. Baena, C. Barris, H.E.M. Sallam, L. Torres, Effect of axial stiffness of NSM FRP reinforcement and concrete cover confinement on flexural behaviour of strengthened RC beams: Experimental and numerical study, Engineering Structures. 173 (2018) 987–1001.

[90] I.A. Sharaky, S.A.I. Selmy, M.M. El-Attar, H.E.M. Sallam, The influence of interaction between NSM and internal reinforcements on the structural behavior of upgrading RC beams, Composite Structures. 234 (2020) 111751.

[91] M.R.F. Coelho, J.M. Sena-Cruz, L.A.C. Neves, A review on the bond behavior of FRP NSM systems in concrete, Construction and Building Materials. 93 (2015) 1157–1169.

[92] E. Bonaldo, J.A.O. De Barros, P.B. Loureņo, Efficient strengthening technique to increase the flexural resistance of existing RC slabs, Journal of Composites for Construction. 12 (2008) 149–159.

[93] F. Al-Mahmoud, A. Castel, R. François, C. Tourneur, Strengthening of RC members with near-surface mounted CFRP rods, Composite Structures. 91 (2009) 138–147.

[94] I.G. Costa, J.A.O. Barros, Flexural and shear strengthening of RC beams with composite materials - The influence of cutting steel stirrups to install CFRP strips, Cement and Concrete Composites. 32 (2010) 544–553.

[95] K. Naumenko, H. Altenbach, Modeling of creep for structural analysis. Foundations of Engineering Mechanics., Springer, 2007.

[96] P. Majda, J. Skrodzewicz, A modified creep model of epoxy adhesive at ambient

temperature, International Journal of Adhesion and Adhesives. 29 (2009) 396–404.

[97] R.I. Gilbert, G. Ranzi, Time-Dependent Behaviour of Concrete Structures, CRC Press, 2010.

[98] A. Neville, Properties of Concrete - 5th Edition, Pearson Education Limited, 2012.

[99] CEB - Comité Euro-international du Béton, CEB-FIP Model Code for Concrete Structures 2010, Lausanne, Switzerland, 2012.

[100] British Standards Institution, Eurocode2: Design of Concrete Structures: Part 1-1: General Rules and Rules for Buildings, 2004.

[101] Z.P. Bazant, Creep and shrinkage of concrete: mathematical modelling, Wiley, Chichester, New York, 1987.

[102] R.I. Gilbert, Time effects in concrete structures, Elsevier Sience Publishers, Amsterdam, 1989.

[103] K.T. Chong, S.J. Foster, R.I. Gilbert, Time-dependent modelling of RC structures using the cracked membrane model and solidification theory, Computers and Structures. 86 (2008) 1305–1317.

[104] ACI committee 318, Building Code Requirements for Structural Concrete and Commentary (ACI 318M-11), 2011.

[105] ACI Committee 209, 209R-92: Prediction of Creep, Shrinkage, and Temperature Effects in Concrete Structures, 2008.

[106] ACI 440R-07, Report on Fiber-Reinforced Polymer (FRP) Reinforcement for Concrete Structures, 2007.

[107] L.J. Malvar, Durability of Composites in Reinforced Concrete, in: First International Conference on Durability of Composites for Construction, Sherbrooke(Québec),Canada, 1998: pp. 1–12.

[108] W.K. Goertzen, M.R. Kessler, Creep behavior of carbon fiber/epoxy matrix composites, Materials Science and Engineering A. 421 (2006) 217–225.

[109] W.N. Findley, Mechanism and mechanics of creep of plastics, SPE Journal. 16 (1960) 57–65.

[110] D.J. Holmes, M.; Just, GRP in structural Engineering, Applied Science, London, 1983.

[111] C.W. Feng, C.W. Keong, Y.P. Hsueh, Y.Y. Wang, H.J. Sue, Modeling of long-term creep behavior of structural epoxy adhesives, International Journal of Adhesion and Adhesives. 25 (2005) 427–436.

[112] R.D. Maksimov, E. Plume, Long-term creep of hybrid aramid/glass-fiber-reinforced plastics, Mechanics of Composite Materials. 37 (2001) 271–280.

[113] M. Miravalles, I.I.P. Dharmawan, The creep behaviour of adhesives A numerical and experimental investigation, Chalmers University of Technology, Göteborg, Sweden, 2007.

[114] H.F. Brinson, L.C. Brinson, Polymer engineering science and viscoelasticity: An introduction, Springer, 2008.

[115] I. Costa, J. Barros, Tensile creep of a structural epoxy adhesive: Experimental and analytical characterization, International Journal of Adhesion and Adhesives. 59 (2015) 115–124.

[116] K. Borchert, K. Zilch, Bond behaviour of NSM FRP strips in service, Structural Concrete. 9 (2008) 127–142.

[117] P. Silva, P. Fernandes, J. Sena-Cruz, M. Azenha, J. Barros, Creep behavior and durability of concrete elements strengthened with NSM CFRP strips, in: Proceedings of the 7th International Conference on FRP Composites in Civil Engineering, CICE 2014, Vancouver, Canada, 2014: pp. 1–6.

[118] M. Derias, R. El-Hacha, S. Rizkalla, Durability of NSM FRP strengthening systems for RC flexural members, in: CICE 2008, 4th International Conference on Fiber Reinforced Polymer (FRP) Composites in Civil Engineering, Zurich, Switzerland, 2008.

[119] M. Emara, C. Barris, M. Baena, L. Torres, J. Barros, Bond behavior of NSM CFRP laminates in concrete under sustained loading, Construction and Building Materials. 177 (2018) 237–246.

[120] M. Emara, L. Torres, M. Baena, C. Barris, X. Cahís, Bond response of NSM CFRP strips in concrete under sustained loading and different temperature and humidity conditions, Composite Structures. 192 (2018) 1–7.

[121] K.H. Tan, M.K. Saha, Long-term deflections of reinforced concrete beams externally bonded with FRP system, Journal of Composites for Construction. 10 (2006) 474–482.

[122] A. Ghali, R. Favre, M. Elbadry, Concrete Structures: Stresses and Deformations: Analysis and Design for Serviceability, Third Edition, CRC Press, 2002.

[123] K.H. Tan, M.K. Saha, Y.S. Liew, FRP-strengthened RC beams under sustained loads and weathering, Cement and Concrete Composites. 31 (2009) 290–300.

[124] S.H. Kim, K.B. Han, K.S. Kim, S.K. Park, Stress-strain and deflection relationships of RC beam bonded with FRPs under sustained load, Composites Part B: Engineering. 40 (2009) 292–304.

[125] C. Zhang, J. Wang, Viscoelastic analysis of FRP strengthened reinforced concrete beams, Composite Structures. 93 (2011) 3200–3208.

[126] H.S. Kim, Y.S. Shin, Flexural behavior of reinforced concrete (RC) beams retrofitted

with hybrid fiber reinforced polymers (FRPs) under sustaining loads, Composite Structures. 93 (2011) 802–811.

[127] B. Fahsi, K.H. Benrahou, B. Krour, A. Tounsi, S. Benyoucef, E.A.A. Bedia, On the effect of time-dependent deformations on the interface behaviour of RC beams strengthened by FRP plates, Journal of Adhesion Science and Technology. 25 (2011) 1909–1924.

[128] C. Zhang, J. Wang, Interface stress redistribution in FRP-strengthened reinforced concrete beams using a three-parameter viscoelastic foundation model, Composites Part B: Engineering. 43 (2012) 3009–3019.

[129] H.R. Sobuz, E. Ahmed, N.M. Sutan, N.M. Sadiqul Hasan, M.A. Uddin, M. Jahir Uddin, Bending and time-dependent responses of RC beams strengthened with bonded carbon fiber composite laminates, Construction and Building Materials. 29 (2012) 597–611.

[130] X. Li, X. Gu, Y. Ouyang, X. Song, Long-term behavior of existing low-strength reinforced concrete beams strengthened with carbon fiber composite sheets, Composites Part B: Engineering. 43 (2012) 1637–1644.

[131] E. Oller, A.R. Marí, Long-term bond stresses and debonding failure of FRP-strengthened RC cracked members, Composites Part B: Engineering. 52 (2013) 30–39.

[132] A.R. Marí, E. Oller, J.M. Bairán, N. Duarte, Simplified method for the calculation of long-term deflections in FRP-strengthened reinforced concrete beams, Composites Part B: Engineering. 45 (2013) 1368–1376.

[133] E. Hamed, Z.T. Chang, Effect of creep on the edge debonding failure of FRP strengthened RC beams - A theoretical and experimental study, Composites Science and Technology. 74 (2013) 186–193.

[134] A.K. El-Sayed, R.A. Al-Zaid, A.I. Al-Negheimish, A.B. Shuraim, A.M. Alhozaimy, Long-term behavior of wide shallow RC beams strengthened with externally bonded CFRP plates, Construction and Building Materials. 51 (2014) 473–483.

[135] S. Hong, S.K. Park, Long-term behavior of fiber-reinforced-polymer-plated concrete beams under sustained loading: Analytical and experimental study, Composite Structures. 152 (2016) 140–157.

[136] S. Jiang, W. Yao, J. Chen, S. Tao, Time dependent behavior of FRP-strengthened RC beams subjected to preload: Experimental study and finite element modeling, Composite Structures. 200 (2018) 599–613.

[137] F. Bouziadi, B. Boulekbache, A. Haddi, M. Hamrat, C. Djelal, Finite element modeling of creep behavior of FRP-externally strengthened reinforced concrete beams, Engineering Structures. 204 (2020) 109908.

[138] N. Plevris, T.C. Triantafillou, Time-dependent behavior of RC members

strengthened with FRP laminates, Journal of Structural Engineering (United States). 120 (1994) 1016–1042.

[139] M. Mazzotti, C.; Savoia, Long-term behaviour of FRP-strengthened beams, in: Proceedings of the Eight International Conference on Fibre-Reinforced Plastics for Reinforced Concrete Structures (FRPRSCS-8), Patras, Greece, 2007.

[140] S. Benyoucef, A. Tounsi, E.A. Adda Bedia, S.A. Meftah, Creep and shrinkage effect on adhesive stresses in RC beams strengthened with composite laminates, Composites Science and Technology. 67 (2007) 933–942.

[141] A. Tounsi, S. Benyoucef, Interfacial stresses in externally FRP-plated concrete beams, International Journal of Adhesion and Adhesives. 27 (2007) 207–215.

[142] G. Al Chami, M. Thériault, K.W. Neale, Creep behaviour of CFRP-strengthened reinforced concrete beams, Construction and Building Materials. 23 (2009) 1640–1652.

[143] CEB-FIP (Comite Euro-International du Beton), CEB-FIP Model Code 1990, 1993.

[144] J. Sena-cruz, P. Silva, P. Fernandes, M. Azenha, J. Barros, Creep behavior of RC slabs strengthened NSM CFRP laminate strips under different environmental conditions, in: Smar 2013, 2013: pp. 4–11.

[145] Y.J. Kim, F. Khan, Creep-induced distress on flexural behavior of reinforced concrete beams retrofitted with near-surface-mounted carbon fiber-reinforced polymer, ACI Structural Journal. 112 (2015) 493–504.

[146] S&P, S&P CFRP – laminates and slot-applied laminates, (2014) 6.

[147] BS EN 12390-3:2009, Testing hardened concrete, Part 3: Compressive strength of test specimens, 2009.

[148] ASTM, ASTM C469/C469M-14 Standard Test Method for Static Modulus of Elasticity and Poisson's Ratio of Concrete in Compression, ASTM International. (2014) 1–5.

[149] A. Scanlon, P.H. Bischoff, Shrinkage restraint and loading history effects on deflections of flexural members, ACI Structural Journal. 105 (2008) 498–506.

[150] BS EN 12390-6:2009, Testing hardened concrete. Tensile splitting strength of test specimens, 2009.

[151] ASTM, ASTM C512 - Standard Test Method for Creep of Concrete in Compression, ASTM International, West Conshohocken, 2010.

[152] ISO 15630-1:2019, Steel for the reinforcement and prestressing of concrete - Test methods - Part 1: Reinforcing bars, rods and wire, UNE Asociacion Espanola de Normalizacion, 2019.

[153] ASTM D7565-10, Standard Test Method for Determining Tensile Properties of Fiber Reinforced Polymer Matrix Composites Used for Strengthening of Civil Structures, 2010.

[154] S&P220, Two-component epoxy resin-based adhesive for S&P FRP Systems, Technical Data Sheet. (2013).

[155] ISO 527-2, Plastics: determination of tensile properties, 2012.

[156] BS ISO 527-1, Plastics — Determination of tensile properties — Part 1 : General principles, 2012.

[157] P. Silva, T. Valente, M. Azenha, J. Sena-Cruz, J. Barros, Viscoelastic response of an epoxy adhesive for construction since its early ages: Experiments and modelling, Composites Part B: Engineering. 116 (2017) 266–277.

[158] M. Emara, L. Torres, M. Baena, C. Barris, M. Moawad, Effect of sustained loading and environmental conditions on the creep behavior of an epoxy adhesive for concrete structures strengthened with CFRP laminates, Composites Part B: Engineering. 129 (2017) 88–96.

[159] H.E.D.M. Sallam, A.A.M. Saba, H.H. Shahin, H. Abdel-Raouf, Prevention of peeling failure in plated beams, Journal of Advanced Concrete Technology. 2 (2004) 419–429.

[160] N.A.B. Yehia, N.M. Wahab, Fracture mechanics of flanged reinforced concrete sections, Engineering Structures. 29 (2007) 2334–2343.

[161] H.S.S. Abou El-Mala, A.S. Sherbini, H.E.M. Sallam, Structural Behavior of RC Beams Containing a Pre- Diagonal Tension Crack, Latin American Journal of Solids and Structures. 15 (2018) e82.

[162] R.I. Gilbert, Deflection calculation for reinforced concrete structures - Why we sometimes get it wrong, ACI Structural Journal. 96 (1999) 1027–1032.

[163] V. Gribniak, G. Kaklauskas, Improving the deflection prediction model from ACI 318, ACI Structural Journal. 111 (2014) 1491–1496.

[164] V. V. Bertero, State-of-the art report: ductility based structural design, in: 9th Word Conference on Earthquake Engineering, Tokyo-Kyoto, Japan, 1988: p. Volume VIII: 673-686.

[165] A.E. Naaman, S.M. Jeong, Structural ductility of concrete beams prestressed with FRP tendons, in: 2th International Symposium on Non-Metallic Fiber Reinforced Polymer Reinforcement for Reinforced Concrete Structures (FRPRCS-2), Ghent, Belgium, 1995: pp. 379–386.

[166] L. Jaeger, A. Mufti, G. Tadros, The Concept of the Overall Performance Factor in Rectangular-Section Reinforced Concrete Beams, in: Proceedings of the 3rd International Symposium on Non-Metallic (FRP) Reinforcement for Concrete

Structures, Sapporo, Japan, 1997: pp. 551–558.

[167] H.E.M. Sallam, A.A.M. Badawy, A.M. Saba, F.A. Mikhail, Flexural behavior of strengthened steel-concrete composite beams by various plating methods, Journal of Constructional Steel Research. 66 (2010) 1081–1087.

[168] H.E.M. Sallam, Discussion of "flexural strengthening of steel bridges with high modulus CFRP strips" by David Schnerch and Sami Rizkalla, Journal of Bridge Engineering. 15 (2010) 117–118.

[169] B.R. Murray, K.A. Kalteremidou, D. Carrella-Payan, A. Cernescu, D. Van Hemelrijck, L. Pyl, Failure characterisation of CF/epoxy V-shape components using digital image correlation and acoustic emission analyses, Composite Structures. 236 (2020) 111797.